NATIONAL TRANSPORTATION SAFETY BOARD

Office of Research and Engineering
Materials Laboratory Division
Washington, D.C. 20594

November 12, 2008

MODELING GROUP CHAIRMAN FINAL REPORT   Report No. 08-119

A. ACCIDENT

    Place   : Minneapolis, Minnesota
    Date   : August 1, 2007
    Vehicle   : I-35W Bridge
    NTSB No.   : HWY07MH024
    Investigator : Mark Bagnard

B. MODELING GROUP

Carl R. Schultheisz, Group Chairman
National Transportation Safety Board
490 L'Enfant Plaza East, SW
Washington, DC 20594

Alan S. Kushner
National Transportation Safety Board
490 L'Enfant Plaza East, SW
Washington, DC 20594

Justin M. Ocel
Federal Highway Administration
Turner-Fairbank Highway Research Center
6300 Georgetown Pike
McLean, VA 22101

William J. Wright
Federal Highway Administration
Turner-Fairbank Highway Research Center
6300 Georgetown Pike
McLean, VA 22101

John Finke
Jacobs Engineering Group
501 North Broadway
St. Louis, Missouri 63102

Carlos Matos
Jacobs Engineering Group
501 North Broadway
St. Louis, Missouri 63102

Jihshya Lin
Minnesota Department of Transportation
Bridge Office
3485 Hadley Avenue
Oakdale, MN 55128

C. SYNOPSIS

This report documents finite element analyses performed for the I-35W bridge investigation. These analyses were carried out under the direction of the Modeling Group with the participation of Professor Toshio Nakamura through an external contract with the State University of New York at Stony Brook and with added resources and expertise acquired through a subcontract with Dassault Systemes Simulia Corporation (developers of the Abaqus finite element software used for all of the analyses). Parallel investigations undertaken by the Federal Highway Administration (FHWA) Turner-Fairbank Highway Research Center (TFHRC) in collaboration with this effort are documented in a separate report. The finite element analyses in this report relied heavily on global models of the bridge that were constructed at the FHWA TFHRC and made available to the Modeling Group.

The 0.5-inch-thick gusset plates at the U10 and L11 nodes were the focus of the investigation, and these nodes were studied with detailed finite element models that were integrated into the global model. A large number of analyses were undertaken during the course of the investigation, studying the effects of a variety of parameters and evaluating different aspects of the models to ensure that the results were valid. Many aspects of the models evolved over time, and some parameters were studied with models that were later superseded. The schedule of the investigation made it impossible to revisit all of the early parameter studies to match the conditions with later models, so in general, each parameter study is placed in a separate section of the report, with two otherwise identical models used to assess the effect of that parameter. Most of the parameters were investigated using models with an in-plane mesh dimension of 0.5 inch in the highly stressed areas of the gusset plates. The final analyses of the investigation used a more refined in-plane mesh dimension of 0.2 inch in the highly stressed areas of the gusset plates; these results are actually presented first in the report, with the results from studies with the coarser mesh following.

The following list highlights some of the results from the analyses:
- Failure initiates through a bending instability in the U10W gusset plates and a lateral shift of the upper end of the L9/U10W compression diagonal.
- The instability occurs at a critical value of the axial compressive force in the L9/U10W diagonal coupled with a critical value of the out-of-plane displacement of the upper end of that diagonal.
- The bending instability is allowed to occur as a result of the widespread yielding of the U10 gusset plates around the upper ends of the L9/U10 diagonals.
- This failure initiation mechanism was confirmed by static load-controlled analyses, Riks analyses and static displacement-controlled analyses.
- Beyond the instability, bending induces large stresses and strains in the gusset plates, which would be expected to lead to material failure; the high stresses and strains occur in locations consistent with fractures observed in the collapsed bridge components; a dynamic solution method would be required to more accurately capture the behavior beyond the point of instability.
- Some increase in the estimated load on the bridge at the time of the accident is necessary to trigger instability, but the instability at node U10W is predicted to occur before any other failure mechanism.

- In particular, the instability at U10W occurs before local material failure.
- Stresses at U10W are higher than at U10E as a result of the placement of the construction materials on the west side of the bridge.
- Instability is predicted to occur at U10W before U10E.
- Decreasing the in-plane mesh dimension from 0.5 inch to 0.2 inch reduces the loads necessary to trigger instability.
- Forces in the U10W members under the accident loading conditions are similar to their original design forces (from dead load + live load + impact); under those forces, properly designed gusset plates should be in the vicinity of 55 percent of their yield stress.
- Stresses in the U10 and L11 gusset plates exceed the yield stress even under the dead load of the original bridge design, confirming their inadequacy with respect to their design requirements.
- Stresses in 1-inch-thick U10 gusset plates under the accident loads were consistent with expected stress levels for properly designed gusset plates.
- 1-inch-thick U10 gusset plates would have supported much higher loads than those that triggered the instability in 0.5-inch-thick gusset plates.
- Section loss resulting from corrosion in the models of the L11 gusset plates increased and localized the stresses in those gusset plates, but even with corrosion in the model, the L11 nodes supported much higher loads than those that triggered instability at U10W.
- Including the photographically documented bowing distortion of the U10 gusset plates in the model reduces the load required to trigger instability.
- With the U10W gusset plates bowed in the directions shown in the photographs, the upper end of the L9/U10W diagonal shifts to the outside of the bridge at instability, consistent with the physical observations of the collapsed bridge structure.
- With flat U10 gusset plates, the upper end of the L9/U10W diagonal shifts toward the inside of the bridge at instability.
- Bowing distortion was input to the gusset plates in the models as an initial stress-free imperfection; incorporating the stress that caused the bowing would likely reduce the load necessary to trigger instability.
- The source of the bowing distortion could not be identified, but a relatively large initial imperfection was required to match the deformation under the loading conditions at the time when the photographs were taken.
- The choice of the shape of the initial imperfection for the bowing distortion has an effect on the results.
- An increase in temperature with restrained bearings leads to a decrease in the force in the L9/U10W diagonal, which increases the applied load necessary to trigger instability.
- The beam elements representing the truss members in the global model indicated that no yielding occurs as a result of their direct axial stress under the loads that trigger instability at node U10W.

STRUCTURAL AND LOCAL FAILURE STUDY OF GUSSET PLATE IN MINNEAPOLIS BRIDGE COLLAPSE

Final Report - NTSBC070010

November 12, 2008

Submitted to
National Transportation Safety Board
Washington D.C. 20594

Toshio Nakamura, Professor
Department of Mechanical Engineering
State University of New York at Stony Brook
Stony Brook, NY 11794

Dassault Systemes Simulia Corp.
SIMULIA Central
1440 Innovation Place
West Lafayette, IN 47906

Table of Contents

Executive Summary

This report summarizes the results of a study performed to define the magnitude and distribution of the stresses and deformations in the gusset plates of the U10W joints in the I-35W highway bridge in Minneapolis, MN that collapsed on August 1, 2007. NTSB investigators at the accident site identified this bridge truss node as a likely initiation site for the bridge collapse. The finite element computations indicated the bridge failure was initiated by a local structural instability before any localized material failure occurred. Additionally, the computations indicate that the structural instability that triggered the bridge collapse was a local bending instability in the U10W gusset plates.

As part of the investigation, the Federal Highway Administration (FHWA) undertook a design study to check the gusset plates according to the design methodology believed to have been used at the time the bridge was designed. The results of this study indicated that the gusset plates at the U10, U10′, L11 and L11′ truss nodes were inadequate when compared to the design criteria. The gusset plates at these deficient nodes were all 0.5 inch thick, and all of these gusset plates were found fractured after the collapse. The design calculations indicated these gusset plates should have been approximately 1.0 inch thick. An additional concern identified for the U10 and U10′ gusset plates was that they had a bowing distortion with a peak out-of-plane displacement of approximately 0.6 inch. Under compressive loading, such deformations can significantly lower the load carrying capacity of structural members and connections.

All finite element computations discussed in this report employed a detailed model of one or two U10 or L11 truss nodes embedded in the global bridge finite element model created by the FHWA. The study progressed simultaneously with the other activities in the investigation and a large number of analyses were run to both investigate the behavior of the bridge and to evaluate the sensitivity of the results to various parameters that were thought to influence the predicted collapse load. Separate parametric studies are covered in the subsequent sections of this report. Different parameters were investigated at different times during the investigation as the models were evolving, so different load case or modeling choices appear in different sections. In general, the parametric studies involved comparisons between equivalent models with only a single parameter being varied. Unless noted otherwise, the results discussed in this Executive Summary came from a finite element model that had a 0.5 inch in-plane mesh size in the highly stressed regions of the gusset plates.

Estimates of the traffic load on the bridge at the time of the accident and the loads due to the construction equipment and supplies on the bridge came from NTSB reports. Loads due to the weight of the bridge were calculated by the FHWA, and defined by the FHWA global model. The estimated total load on the deck truss portion of the bridge at the time of collapse was 24,482 kips[1], including the bridge weight of 21,956 kips, the approach span reaction force of 1,571.3 kips, the traffic load of 376.7 kips, and the construction load of 578.5 kips.

In defining inputs that could have an influence on the collapse load computations, attempts were made to be conservative. For example the piles of sand and gravel on the bridge were assumed

---

[1] A kip is defined as 1,000 pounds.

to be uniformly distributed over their bridge deck areas as determined by pre-collapse photographs of the bridge. Assuming a mound profile would have given a more concentrated loading profile that could have lowered the collapse load. Additionally, the bowing profile of the initial imperfection input to the U10 gusset plates was in most models assumed to follow a sinusoidal curve between the edges of the truss members. While the conditions causing the bowing are unknown, load transfer to/through the gusset plates occurs through the rivets. Hence, all deformations are associated with loads applied along the rivet lines. Because the photographic evidence could not discern the bowing with enough resolution to verify this, most analyses were run with the bowing between the truss member edges. As part of a sensitivity analysis, one analysis was run with the initial imperfection input of the bowing between the rivet lines. It showed a reduction of the predicted construction load to cause collapse of 13% of the estimated construction load.

The steel in the gusset plates at the U10 joint was specified to have a minimum yield stress of 50 ksi. To corroborate that the material met the specification, test sections were cut from the gusset plate in an undeformed region between two rows of rivets. Test data from a representative sample were used in the model. This sample had a yield stress of 51.5 ksi, and the ultimate tensile strength (maximum engineering stress) was achieved at an engineering strain of approximately 12%. Beyond this point, the material cannot sustain additional uniform tensile loading and stretches until it ruptures.

Analyses performed using an embedded model of the U10W joint with the 0.2 inch mesh subjected to the baseline estimation of loads on the bridge at the time of the accident indicated that stresses in a region of the U10W gusset plates were slightly above yield stress under only the dead load of the original bridge design. When the weight from modifications and the estimated construction loads were applied, the maximum plastic strain was found to be 2.2%, well below the 12% value required to initiate material failure. It was found (see Figure 3.25) that a significant region of the U10W gusset plates is above yield when the construction loads were applied. The pattern of this region is consistent with the observed fracture patterns in the U10W gusset plates. The estimated construction loads were increased in the analysis until the solution would not converge. The analysis diverged, indicating an instability, when the total load on the bridge had increased from 24,482 kips to 24,809 kips. To understand the nature and drivers of the collapse process, the finite element computations were extended beyond the collapse point by utilizing a Riks analysis. The Riks method allows static structural computations to be extended beyond the point of maximum load by parameterizing the collapse deformation mode and using it to define the nature of the load drop necessary to maintain equilibrium after the collapse begins. Such solutions do not in general represent the actual collapse process, but they do give significant insight into the behavior of the structure around the collapse initiation point. Evaluating these characteristics for the U10W joint can provide insight into the collapse process. The Riks analysis predicted unstable behavior at 24,818 kips, confirming the results of the original analysis.

The analyses indicated that the collapse occurred due to a bending instability in the U10W gusset plates. Such an instability would be accentuated by both the observed bowing of the gusset plates and the inadequate thickness of the gusset plates as shown in Figure E.1. The diagonal U10_L9W truss member is one of the most heavily loaded in the bridge, carrying a compressive

force of nearly 2.3 million pounds under the bridge weight and traffic live loads specified for the design. Figure E.2 reproduces Figure 3.33(a) from the report and shows that the westward displacement of the upper end of this member (at the U10W node) out of the plane of the truss grows rapidly when the construction loads are applied to the model. As the member displaces outward bending the gusset plate, the increased displacement creates an increasing bending moment to be applied to the gusset plate.
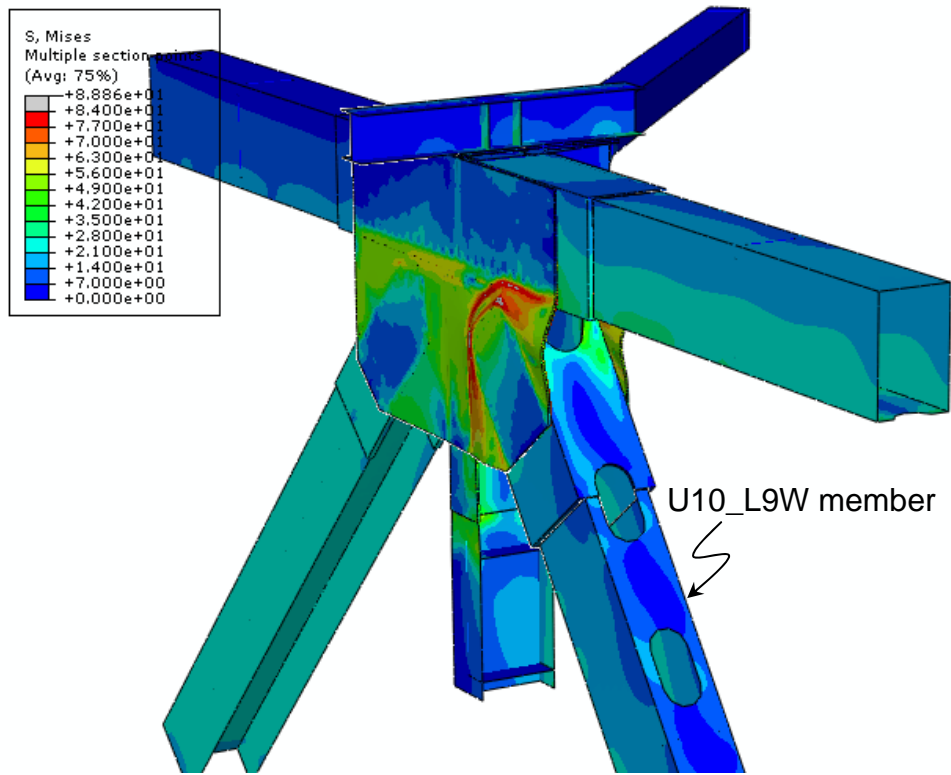
Figure E.1: Mises stress and deformation of U10W node region showing
out-of-plane tilting of U10_L9W member
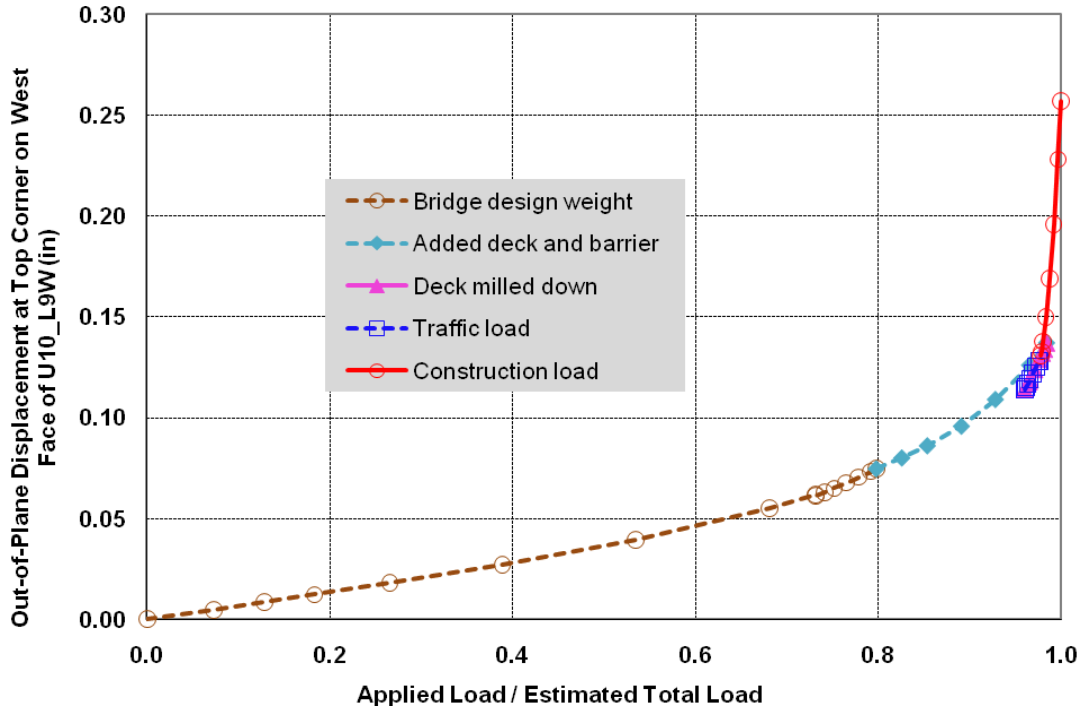
Figure E.2: Normalized load versus displacement for load condition A1 and
0.2 inch mesh

Because a 1-inch-thick gusset plate would have eight times the bending stiffness of a 0.5-inch-thick gusset plate, an analysis was run to compare the behavior of the two. The analysis with a 1-inch-thick gusset plate was carried to a total load of 26,504 kips without any instability occurring. At this load level, minimal levels of plastic deformation were predicted by the analysis. The load displacement behavior of the gusset plates was found to be essentially linear over the entire loading regime. In addition, ignoring the initial bowing in a 0.5-inch-thick gusset plate gave an increase in construction load at the point of instability equal to 280 kips. Since the estimation of the construction loads was 578 kips, the bowing reduced the predicted construction load at collapse by about 30%. While significant, this is inconsequential relative to the increased load carrying capacity associated with a properly designed 1-inch-thick gusset plate. These results together with the previously mentioned result drop equal to 13% of the estimated construction load in the construction load at collapse when the gusset plate bowing was modeled between rivet lines shows that gusset plate geometry plays a significant role in determining the magnitude of the predicted bridge collapse load. It is important to recognize that the gusset plate bowing was input into the model as a stress free initial imperfection. The bowing obviously is the result of an undetermined loading condition applied to the bridge and/or gusset plates. No sound procedure was identified for defining a loading scenario responsible for creating the gusset plate bowing. It is felt that including the stresses in the gusset plate from the loading that caused the existing bowing would further decrease the load necessary to trigger the instability that led to the collapse.

For all analyses, the maximum stress and strain at the predicted collapse load were below that associated with material failure. Comparing the results from the 0.5 inch mesh and the 0.2 inch

mesh, it was found that the mesh refinement led to a 27% drop relative to the estimated construction load in the predicted construction load at collapse and the peak stress at this reduced load was approximately 5% higher at collapse. At the predicted collapse load, the maximum von Mises stress for the 0.2 inch mesh was 81 ksi, while the 0.5 inch mesh predicted a 68 ksi maximum at the same load level. The measured ultimate stress for the gusset plate was 89 ksi. The predicted construction load at collapse using the 0.2 inch mesh was 58% above the estimated construction load.

As was previously discussed, the results were shown to be sensitive to the shape of the gusset plate bowing and the mesh density. These sensitivities were evaluated as a function of varying construction load. The construction load accounts for only 2.4% of the estimated total load on the bridge at the time of collapse. To evaluate the sensitivity of the collapse predictions to uncertainty in bridge and traffic weight, some of the analyses were rerun with the bridge and traffic weight increased by 5%. Using the 0.5 inch mesh, the predicted reduction in construction load at collapse was 22%. The maximum stress in the gusset plates at collapse was the same for the two cases.

All of the simulations predicted failure by a localized structural instability in the U10W gusset plates. A common feature of all of the predictions was a horizontal displacement of the upper U10 end of the U10_L9W diagonal truss member of approximately 0.5 inch at collapse. Figure E.3 shows a plot of data for two load cases A1 and A2. A1 is the estimated loads on the bridge at the collapse and A2 is the load case representing a 5% increase in bridge and traffic weight. It is observed that the compressive force in the U10_L9W diagonal for the two load cases is almost identical as a function of the out-of-plane displacement. The detailed finite element results all showed the gusset plate instability to be driven by the large stresses and plastic strains in the region between this member and the U10_U9W horizontal upper chord member. The combination of a critical diagonal member compressive force of approximately 2,550 kips and an out-of-plane displacement of approximately 0.55 inch is a common feature of all of the analyses run. The critical out-of-plane displacement of approximately 0.55 inch is extremely small compared to the dimensions of the bridge truss members and is indicative of a collapse driven by a local gusset plate instability rather than one driven by a global bridge collapse mechanism. This is consistent with the analysis results that showed embedding detailed models of the U10E joint or the L11W joint did not significantly change the predicted bridge behavior or collapse mechanism and load.
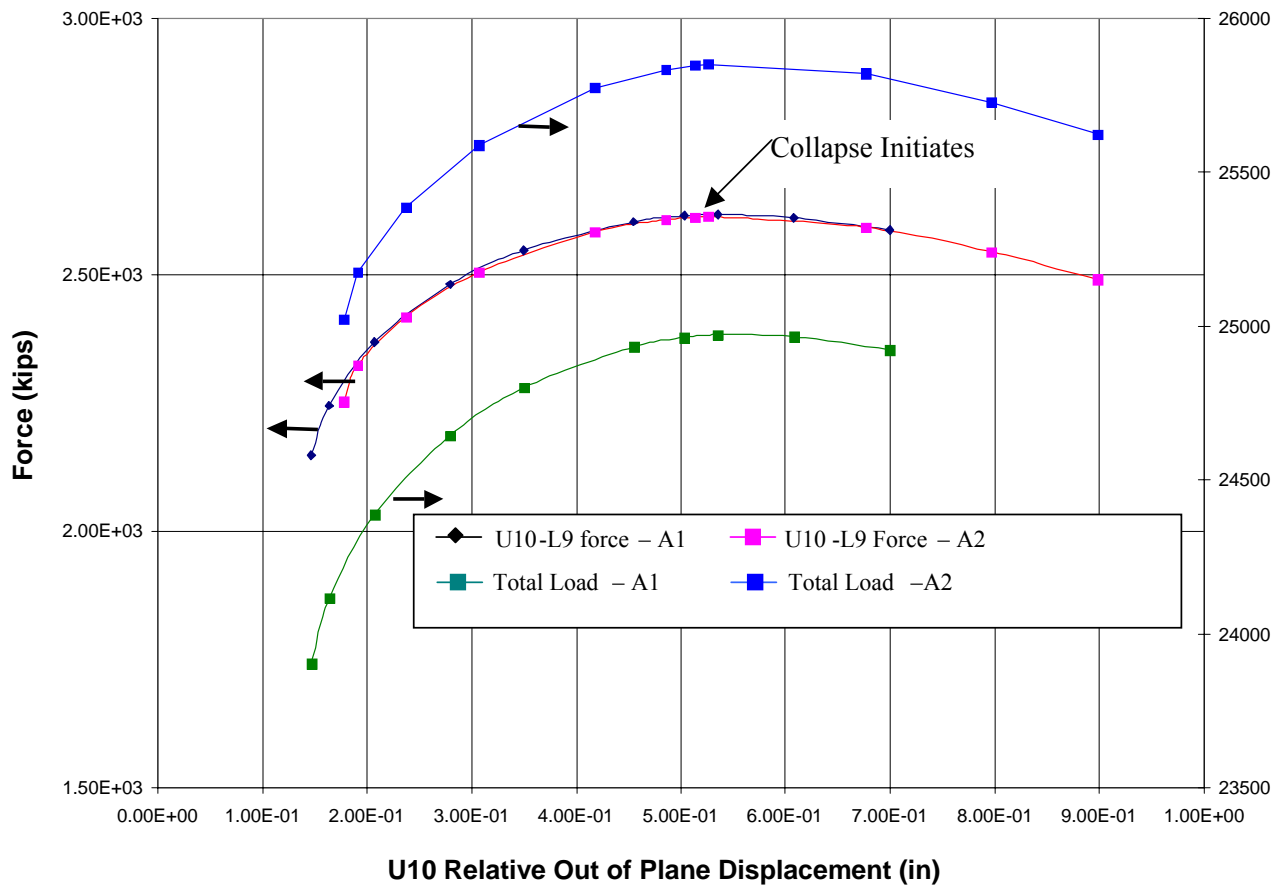
Figure E.3: Load and diagonal member compressive force shown as functions of out-of-plane displacement

While the predicted collapse load is higher for the A2 load case, the critical truss member force is seen to be more sensitive to construction loads than the total load. At failure, the A2 total load is 881 kips higher than the A1 total load. The force in the U10_L9W diagonal and the construction loads are plotted in Figure E.4 as a function of the out-of-plane displacement of the upper end of the U10_L9W diagonal for the two load cases. It is seen that the construction load at collapse is 240 kips higher in load case A1 in comparison to load case A2, whereas the total load for A2 is 881 kips higher than A1. This result demonstrates that it is the location of the construction loads in the vicinity of the U10W node that is the primary driver for the collapse. The previous discussion demonstrated that collapse was associated with a critical combination of compressive force and out-of-plane displacement in the U10_L9W truss member driving a bending instability in the U10W gusset plates. In addition, the concentration of the construction loads on the bridge deck near the U10W node causes the critical member force and displacement to be far more sensitive to the magnitude of the construction loads than to the magnitude of the total load on the bridge. Issues ignored in the study such as non-uniform distribution of the sand and gravel loads from the construction operation could cause further reductions in the magnitude of construction loads needed to cause collapse. Also, any initial eccentricity of the U10_L9W member in conjunction with the gusset plate bowing at the U10W joint would likely have caused

further lowering of the critical/collapse load, but such an eccentricity could not be conclusively identified in the photographs and was not included in the models.

U10-L9 force vs Out of Plane Displacement and Construction Load
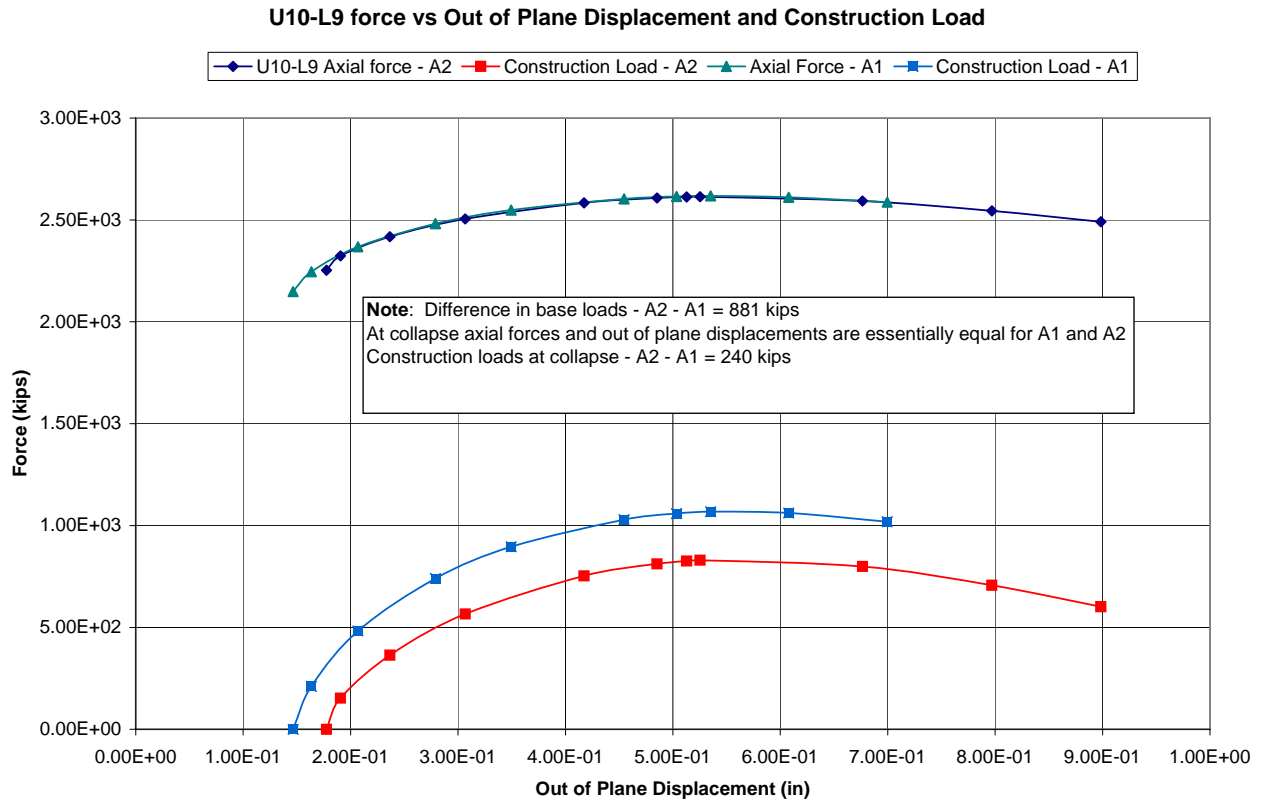
Figure E4: Construction load and diagonal member compressive force versus out-of-plane displacement

Additional analyses run that include more localized detail in the bridge model gave results consistent with those discussed. Examples include the inclusion of a detailed model of the L11W joint with the observed material loss from corrosion included and a detailed model of the U10E joint.

All of the calculations predicted collapse from a localized structural instability that developed prior to any material failure in the U10W gusset plate. The Riks solutions gave insight into the behavior near collapse. To evaluate behavior after collapse, an alternate procedure that replaces load incrementation with displacement incrementation at the construction load application points was utilized. The downward displacement associated with the initial increment of construction loads was used to create a displacement boundary condition that was applied in place of the force boundary conditions arising from the construction loads. Figure E.5 shows the results of such an analysis. Here the total vertical reaction force at the piers is shown as a function of the applied displacement amplitude. Point T1 corresponds to the predicted collapse load of the bridge. At T1, if loading continued to increase, one would expect to see a sudden jump via a dynamic behavior to a state corresponding to T3 at the same load level. Figure E.6 shows the evolution of the plastic strain in the U10W gusset plates for the stages going from T1 through T2 to T3. From uniaxial tests on actual samples of the gusset plate steel, it was observed that for strain levels

above approximately 12%, material flow and deformation localization initiates. It is shown in Figure E.6 that while the peak strain at collapse, point T1, is below failure, as the solution evolves to an identical load state at T3, continuously increasing areas of the gusset plate are at strains where failure could be expected to occur.
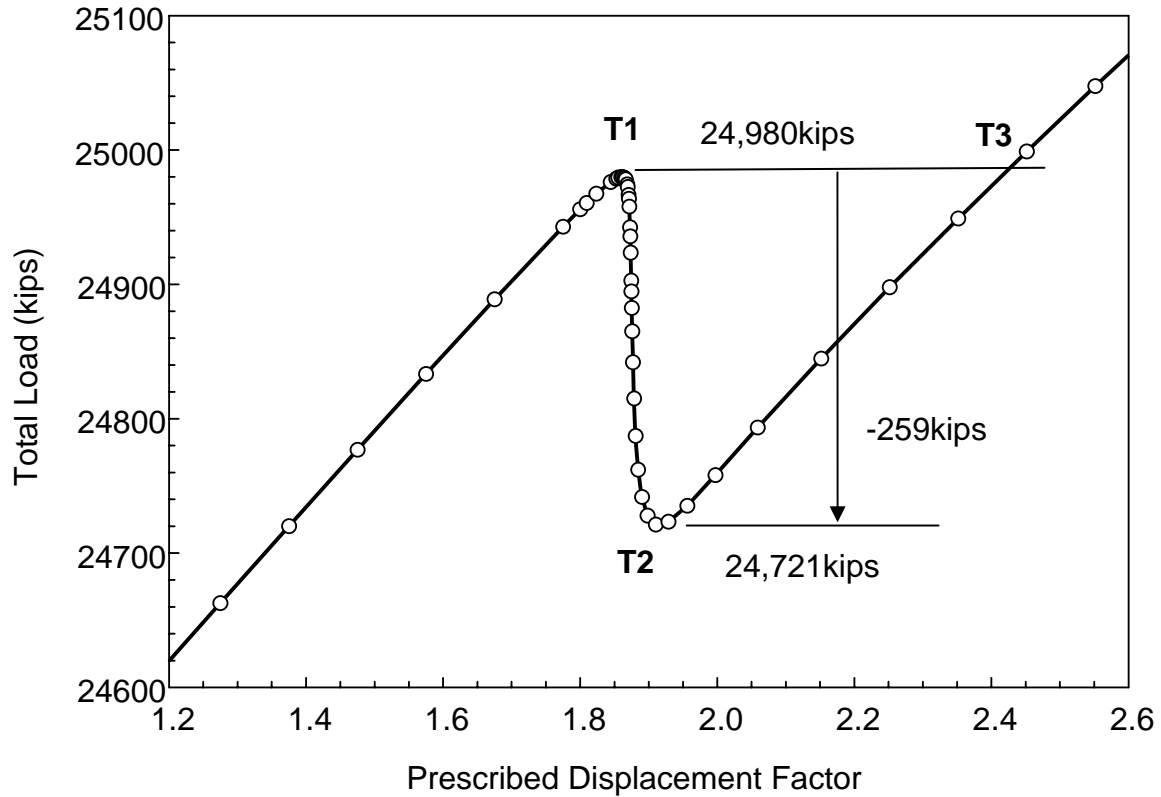
Figure E.5: Total load behavior under increasing construction load prescribed via displacement increments near the collapse point
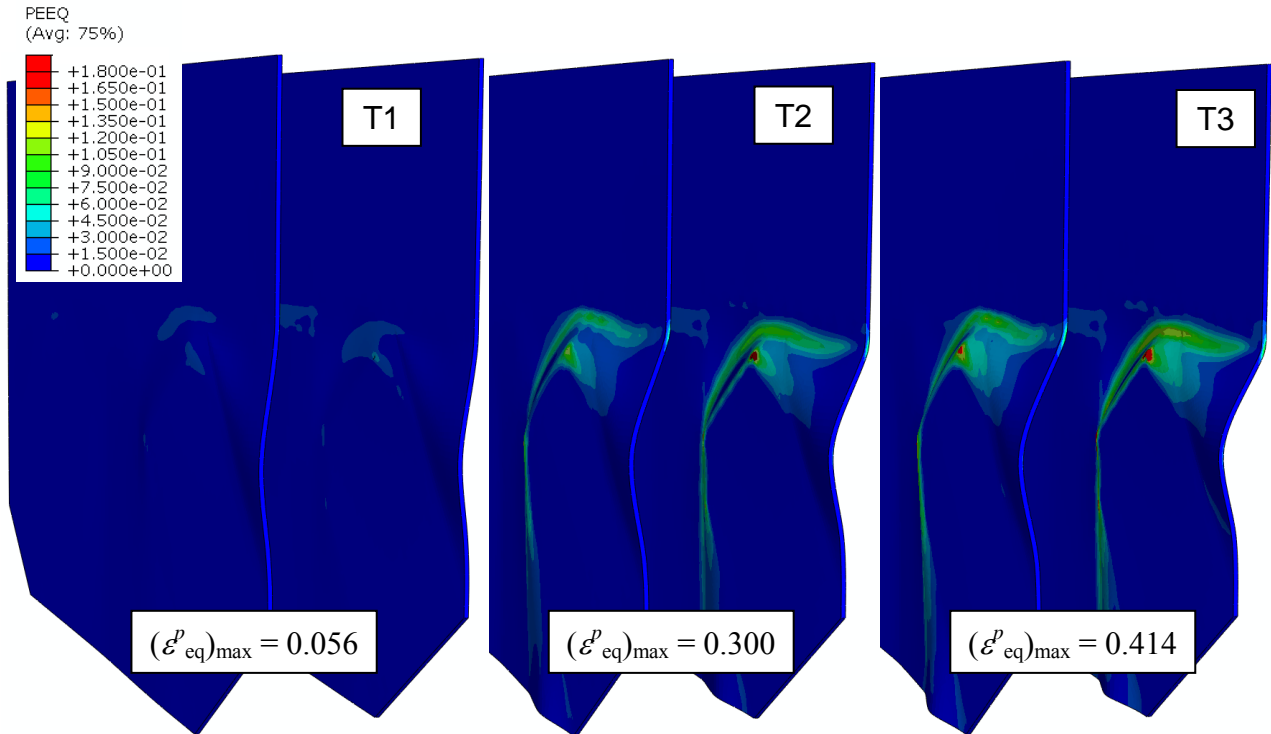
Figure E.6: Evolution of equivalent plastic strain of two gusset plates (east and west faces) at U10W joint

Figure E.7 shows a comparison of the observed fracture pattern in the east face of the U10W gusset plates and the computed maximum principal stress contours at state T2. Due to the bending nature of deformation, the regions of high tensile stress in the two surfaces are very different. In the figure, regions of red and gray represent material under very high tensile stress. The domains of high stress predicted in the gusset plate region between the U10_L9W diagonal and the U10_U9W are seen to correlate very well with the actual fracture pattern observed in this region.
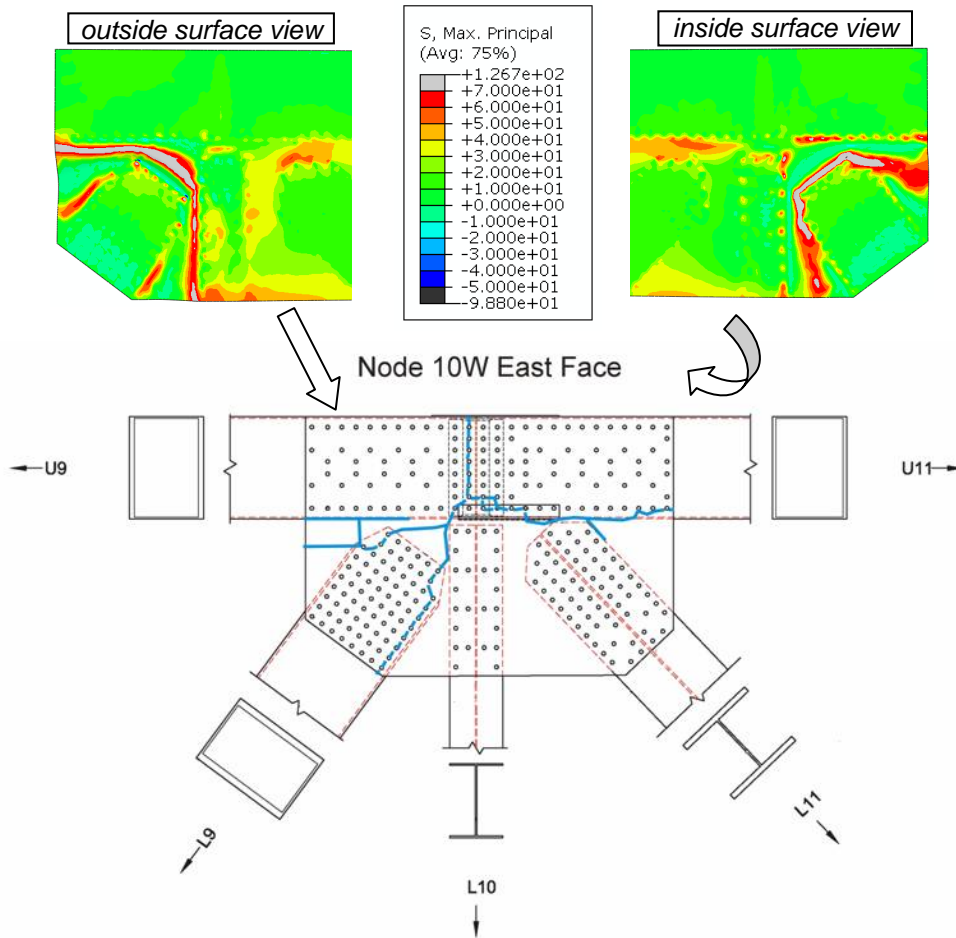
Figure E.7: Comparison of predicted maximum principal stresses of east face plate of U10W gusset at state T2. Note the two surfaces of the plate are shown from outside and inside. They are compared with observed fractures in the plate (view from outside)

In summary, it has been shown that the finite element analyses predict failure to initiate through a bending instability in the U10W gusset plates, driven by the high compression forces in the U10_L9W diagonal member coupled with the deformation of the gusset plates, which was exacerbated by the observed bowing distortion. The upper end of the U10_L9W diagonal member was shown by the analysis to translate to the west, consistent with the physical observations of the collapsed bridge structure. In addition, the peak stresses and strains correlate with the observed fracture pattern at this location. The results with a 0.5 inch in-plane mesh dimension predict a construction load at failure approximately 85% above the estimated value. Various modeling and geometry variations demonstrate that the predicted load is a conservative upper bound to the load required for failure. For example, analyses using a refined mesh and alternate gusset plate bowing geometry consistent with the loading mechanisms in the gusset plates reduced the predicted collapse load by 27% and 13% of the estimated construction loads. Allowing for uncertainty in the bridge dead weight also affects the predicted construction load at collapse.

Analysis Summary

SIMULIA Central performed nonlinear finite element analyses on the Minneapolis I-35W bridge. The analyses focused on the gusset joints at the U10W, U10E, and L11W bridge nodes and detailed three dimensional (3D) local models of these joints were created. In each analysis, one or two of these detailed local models were embedded into the structural element bridge model provided by FHWA to evaluate in more detail the stress and strain in the gusset plates and investigate potential instability in the bridge structure. The model was analyzed using the original bridge design weight, additional concrete weight from increased deck thickness and modifications to the barriers, and the traffic load and the construction load determined at the time of collapse. The estimated total load was 24,482 kips, including the bridge weight of 21,956 kips, the approach span reaction force of 1,571.3 kips, the traffic load of 376.7 kips, and the construction load of 578.5 kips. These loads were applied using a combination of gravity loads, line loads, concentrated loads, and pressure. A load-deflection (Riks) analysis was conducted to explore the observed instability in the gusset plates at node U10W.

Each 3D local model consisted of two gusset plates, five main truss members, one lateral brace, one floor truss at the U10W and U10E joints or one strut at the L11W joint, and other connecting components. Bowed gusset plates at the U10W and U10E joints and corroded gusset plates at the L11W joint were observed in the field and included in the models. The bowing geometry was included in the U10W and U10E local models and the corrosion geometry was included in the L11W local model. The gusset plates and the portions of the main truss members in contact with the gusset plates were represented with solid hexahedron elements while all other components in the local models were represented with shell elements. Isotropic elasto-plasticity was assumed for all components.

For most of the analyses, the rivets connecting the gusset plates to the five main truss members in the joint were represented with the "fastener" feature available in the Abaqus finite element software. Stresses associated with the rivets were explored with submodels, as discussed below. All of the other connections between components were represented with tie or fastener constraints. Two contact scenarios were examined: one with contact defined between components connected with fasteners, and one without contact defined wherever the fasteners were used to connect the components. No other boundary conditions were defined in the local models. The five main truss members, lateral brace, floor truss and stringer offset in the U10W and U10E local models or strut in the L11W local model were cut at about mid-span of the members in the FHWA structural element model. Tie and coupling constraints were introduced at the cut planes to connect the local models to the FHWA structural element bridge model.

Maximum Stresses and Plastic Deformation

The nonlinear analyses predicted no apparent plastic deformation in any of the bridge truss members when subjected to the estimated traffic and construction load. Plastic deformation occurred mainly in the central region of the two gusset plates between the truss members at the three joints of interest. The plastic deformation was apparent from the initial steps of the analyses, when subjected to the self-weight of the bridge as originally designed. Note that only a few elements yielded through the entire gusset thickness under this condition. With the application of

additional concrete weight from the increased deck thickness and modified barriers, traffic load, and construction load, additional elements yielded through the entire gusset thickness.

The maximum predicted von Mises stress due to the construction load occurred in the east gusset plate at the U10W joint and on the edge of the upper fastener connecting the east gusset plate and the diagonal truss member U10_L9W. The detailed stress distribution in the highly stressed region of the east gusset plate was analyzed using a submodel with a mesh density seed of 0.03 inches and two model rivets to replace the two upper fastener constraints. The submodel used an extrapolated stress strain curve for the gusset plates to prevent potential divergence of the analysis. In the submodel, the maximum predicted von Mises stress due to the construction load was 82 ksi, which corresponded to a predicted equivalent plastic strain of 6.3%. This maximum von Mises stress was smaller than the maximum measured true tensile stress from samples of the gusset plates, 89 ksi.

Instability

The Riks analysis method predicted that structural instability occurred at the U10W joint under a total load of 24,818 kips corresponding to a construction load of 914 kips, where a mesh density seed of 0.2 inches was used and the initial maximum out-of-plane deflection of the gusset bowing was defined to be 0.5 inches. The instability was driven by the significant increase in the out-of-plane displacement at the top corner on the west face of the diagonal truss member U10_L9W as additional construction load was applied. In the submodel, the maximum von Mises stress in the east gusset plate under the predicted maximum load at instability was predicted to be 90 ksi, which corresponded to an equivalent plastic strain of 13.5%. All three principal stresses of the maximum von Mises stress were compressive stresses. When the U10W and the U10E local models or the U10W and the L11W local models were incorporated into the FHWA structural element bridge model, the instability remained at the U10W joint, with a similar predicted maximum load at instability.

Results Allowing for Uncertainty in the Dead Load and Traffic Load Magnitude

A five percent increase in the deadweight of the bridge and the traffic load was introduced to investigate the effect of the uncertainty of these load magnitudes. The five percent increase resulted in an estimated total load of 25,600 kips. Using a gusset mesh density seed of 0.2 inches with the increased dead load and traffic load, the Riks analyses predicted an instability at U10W at a total load close to 25,702 kips, which corresponded to a construction load close to 680 kips.

Investigation of the Finite Element Model Mesh Density

Two in-plane mesh density seeds were used in the highly stressed region of the gusset plates in this report, 0.2 inches and 0.5 inches. For both choices of mesh density, a structural instability at U10W was observed. Analyses indicated that the predicted maximum total load for the instability to occur was significantly increased, in terms of construction load, from 24,818 kips to 24,973 kips if the 0.5-inch mesh instead of the 0.2-inch mesh was used. The model with a finer mesh in the gusset plates predicted a larger von Mises stress than that with a coarser mesh when a similar construction load was applied. The model with the 0.2-inch mesh predicted a maximum von Mises stress of 81 ksi under a total load of 24,812 kips. The model with the 0.5-inch mesh

predicted a maximum stress of 68 ksi under approximately the same load. The model with the 0.2-inch mesh also predicted a significantly larger bending moment at the lower end of the diagonal truss member U10_L9W. The difference in the bending moment was predicted to be 275 kip-inch. The larger bending moment introduced a larger out-of-plane displacement at the top corner on the west face of the diagonal truss member and an earlier occurrence of the instability.

Flat Gussets Compared to Initially Bowed Gussets

In order to match the bowed geometry of the U10W (and U10E) gusset plates observed in photographs, a bow had to be introduced to the gusset plates as a stress-free initial imperfection. Initially flat gusset plates at the U10W joint were also modeled to investigate the effect of the initially bowed gusset plates on the predicted maximum load at instability, where a gusset mesh density seed of 0.5 inches was used. The predicted maximum total load at instability increased from 24,973 kips to 25,253 kips when the initially flat gusset plates were used instead of initially bowed gusset plates. The analyses also predicted that the two initially flat gusset plates bowed towards the east when the total load was more than 101 percent of the estimated value, which was opposite to the westward bowing observed in the field. The eastward bowing changed the ratio of the two bending moment components at the lower end of the diagonal truss member U10_L9W. The change of the bending moment ratio shifted the movement direction of the west corner of the diagonal truss from moving westwards to moving eastwards.

Corrosion Investigation

Corrosion in the gusset plates at node L11W was introduced by removing material from the east and west gusset plates in the area where corrosion was observed in the field, along the top edges of the lower chord box members. The depth of the material removed was based on the field measurements of the section loss. The corrosion in the gusset plates at the L11W joint raised the von Mises stress in the corroded region. But the maximum von Mises stress at the L11W joint under the predicted maximum load at instability was predicted to be significantly smaller than that at the U10W joint when both local models were embedded into the FHWA structural element bridge model.

Comparison of One Inch and One-Half Inch Thick Gussets

Two bowed gusset plates, each 1-inch thick, were incorporated at the U10W joint to investigate the effect of gusset plate thickness on predicted maximum load. Analyses predicted that the bowed 1-inch thick gusset plates would support loads well above the maximum load at instability predicted when using the 0.5-inch thick gusset plates. When the 0.5-inch thick gusset plates were used, the Riks analyses predicted a maximum total load at instability of 24,641 kips. When the 1-inch thick gusset plates were used, no instability was predicted before the Riks analysis was terminated at a total load of 26,504 kips. Note that contact was not defined between gusset plates and truss members in the local models.

Comparison of Two Gusset Plate Bowing Geometries

Two types of stress-free initial bowing geometry in the gusset plates at the U10W joint were used to investigate the effect of the initial bowing geometry on the predicted maximum load at

instability. One model had the bowing initiate along the outer edges of the truss members, and the other model had the bowing initiate along the rivet lines that fasten the gussets to the truss members. Analyses predicted that the maximum total load at instability decreased by 0.3 percent, or 74 kips, approximately 13 percent of the estimated construction load, when the gusset plates bowed along the rivet lines. This decrease in the predicted maximum load at instability could be induced by the larger initial bowing region and easier bowing development when the gusset plates bowed along the rivet lines.

Effect of Temperature Increase on Analysis Results

A uniform temperature increase of 20°F was introduced in the traffic loading step to investigate the effect of the temperature increase on the predicted maximum load at instability. With the 20°F temperature increase, the predicted maximum total load at instability increased from 24,973 kips to 25,051 kips.

Effects of bearing functioning were addressed in the report of FHWA [1].

1   Introduction

Following the collapse of the I-35W bridge in Minneapolis, finite element modeling of the bridge was undertaken to investigate potential mechanisms of failure initiation as a function of the loading on the bridge [1, 2]. Information from the wreckage has been used to help guide the modeling effort and evaluate the results. Based on the initial information from the wreckage, the modeling was first focused on nodes U10 West and East. The focus of the modeling effort was expanded to include nodes L11 West following an assessment of the original design of the bridge by the Federal Highway Administration (FHWA), which showed that the gusset plates at both the U10 and L11 nodes were undersized [1], coupled with areas of corrosion found on the L11 gusset plates [3, 4].

The finite element modeling described in this report was performed in close collaboration with the FHWA, who created a global beam and shell model of the deck truss portion of the bridge [1]. This report documents investigations performed using detailed local models of nodes U10 and L11, which were built with solid and shell elements and embedded into the global model of the bridge created by the FHWA [2]. The work in this report was accomplished through a National Transportation Safety Board (NTSB) contract with the State University of New York at Stony Brook and SIMULIA. The FHWA modeling work is described in a separate report, including the global model and detailed models of nodes U10 and L11 built with shell elements [1].

The models were based on the original Sverdrup and Parcel construction plans and the Allied Structural Steel shop drawings, which were obtained by the NTSB from the Minnesota Department of Transportation. Along with post-accident cores from the concrete deck, the plans and drawings were used to calculate the dead load of the weight of the bridge structure itself, beginning with the as-designed bridge, and including changes in the weight from a 1977 increase in deck thickness, a 1998 change in the outside and median barriers, and a removal of part of the deck as part of the repaving operation underway on the day of the collapse. A post-accident survey of vehicles and construction materials was used to determine the additional loads on the bridge at the time of the collapse [5]; weather data was also collected for the day of the collapse. Results from tensile tests of gusset plate samples from nodes U10 East and West were used to define the mechanical properties used for the U10 and L11 gusset plates in the models [6, 7]. Hardness measurements of rivets and U10 gusset plates were used by NTSB to scale rivet material properties from the gusset plate tensile tests [8, 9]. Photographs from 1999 and 2003 were used by NTSB to estimate the magnitude and direction of the bowing of the U10W and U10E gusset plates for input to the models [10]. Section loss in the L11W and L11E gusset plates measured by NTSB in the field was used to incorporate the effects of corrosion into the model of node L11W [3, 4].

2   Summary of Structural Element Bridge Models Provided by FHWA

For convenience, the global beam and shell models of the bridge provided by FHWA will be called "FHWA structural element bridge models" hereafter. Eight structural element bridge models of the whole I-35W bridge were provided by FHWA throughout the investigation process, as shown in Table 2.1. Each model iteration was slightly modified by FHWA as more information was available, better techniques were incorporated, and different local models and their combinations were embedded. SIMULIA Central reviewed the models and used six of the

models to drive three-dimensional (3D) local models representing the gusset joints at the U10W, U10E, and L11W nodes. Most results reported here about the U10W and U10E joints came from the sixth FHWA bridge model. Results involving the L11W joint came from the seventh and eighth FHWA bridge models.

Table 2.1
Structural Element Bridge Models Provided by FHWA

File Number	File Type	File Name	Date Received
1	Abaqus input file	i35w_asdesigned.inp	10-19-07
2	Abaqus input file	i35w_asdesigned.inp	11-09-07
3	Abaqus input file	I35W_AsBuilt_forABAQUS_complete.inp	12-12-07
4	Abaqus input file	I35W_AsBuilt_forABAQUS_complete_New Densities.inp	01-17-08
5	Abaqus input file	BaseModel_ver2_forABAQUS_021508.INP	02-15-08
6	Abaqus input file	I35W_AsBuilt_forAbaqus_04072008.INP	04-07-08
7	Abaqus input file	Abaqus_Model_1_05142008.inp	05-14-08
8	Abaqus input file	Abaqus_Model_2_05142008.inp	05-14-08

The sixth FHWA model [1] consisted of Abaqus element types B31, B33, S4R, CONN3D2, SPRING1, and SPRINGA, as shown in Figure 2.1 and described in Table 2.2.

Table 2.2
Elements in the Sixth FHWA Model

Element	Description	Represents
B31	Two-node linear beam element using Timoshenko beam theory	Stringers, stringer offsets, and pier columns
B33	Two-node cubic beam element using Euler-Bernoulli beam theory	Trusses
S4R	Four-node doubly curved general-purpose shell and reduced integration element	Concrete decks and piers
CONN3D2	Two-node connector element	Expansion joints
SPRING1	Spring element between a node and ground	Effect of approach spans on the main trusses
SPRINGA	Spring element between two nodes	Expansion joints

The following seven loading steps were included in the sixth model:

1. Original bridge weight (wet concrete was represented by forces)
2. Deck weight to replace the forces representing the wet concrete (model change)
3. Original barrier weight
4. Additional concrete weight (increased deck and barriers)
5. Reduced concrete weight (concrete removed for repaving on the day of the accident) [1]
6. Traffic load at collapse
7. Construction load at collapse

Details on the loading conditions are provided in Section 3.1.6 of this report.

Boundary conditions were modified throughout the analysis to reflect the difference between the long-term effect of the bridge deadweight and the short-term effect of the reduced concrete weight, the traffic load and the construction load at the time of the collapse [1]. In the first step, five degrees of freedom (DOFs) of the foundation levels of the piers were fixed, except the translational DOF along the X-direction, which is the longitudinal direction of the bridge, as shown in the coordinate system of Figure 2.1. All three translational DOFs were fixed at the tops of pier 7, and two translational DOFs were also fixed at the tops of piers 5, 6, and 8, as shown in Figure 2.2. In the fifth step, all six DOFs of the foundation level of the piers were fixed, and the boundary conditions at the tops of the piers were removed.

The seventh and eighth FHWA models were used to analyze the L11 joint. They were the same as the sixth model, except that the beam elements around the U10W and L11W joints had different mesh sizes. Finer meshes around the local models were used to assist the convergence of the analyses.
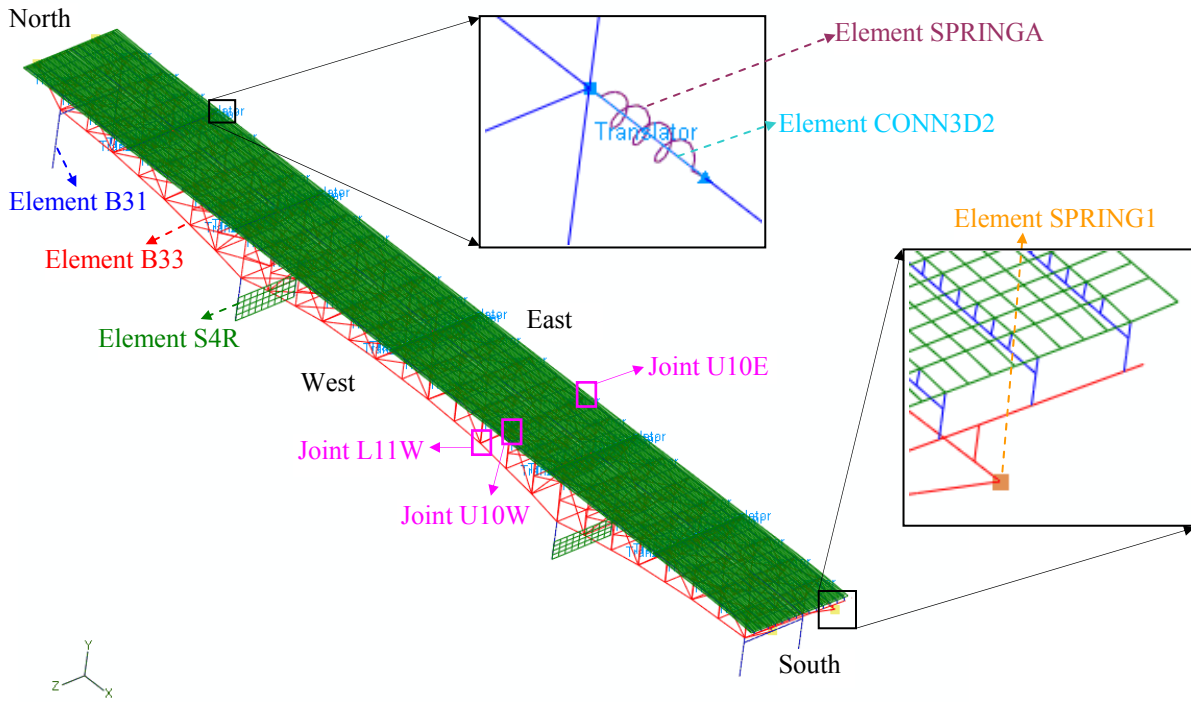
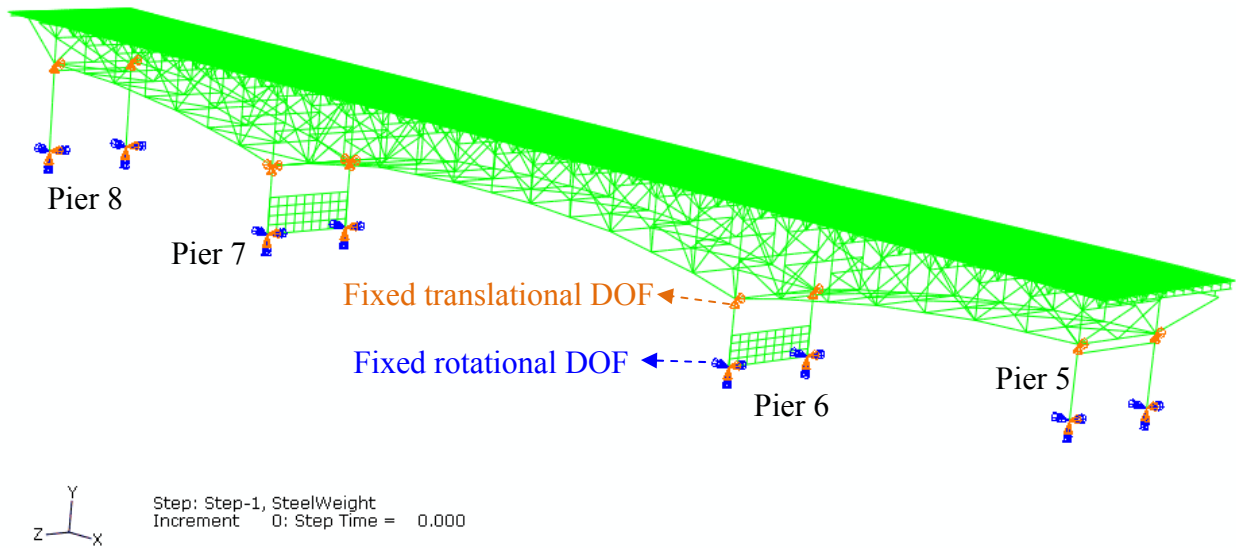Figure 2.1: The sixth structural element bridge model provided by FHWA in April 2008

Figure 2.2: Boundary conditions in the first step of the sixth FHWA structural element bridge model [1]

3 Embedding a U10W 3D Local Model into the FHWA Structural Element Bridge Model

3.1 Description of U10W 3D Local Model

3.1.1 Regular Static Analysis and Riks Method

Abaqus/Standard version 6.7 was used to perform nonlinear static finite element analyses to predict the distribution of stress and strain in the gusset plates at the U10W joint. The U10W 3D local model was embedded into the sixth FHWA structural element bridge model supplied by FHWA. This combined FHWA structural element-local model will be called a "mixed model" hereafter.

The Riks analysis, as implemented within Abaqus, was conducted to explore the local U10 gusset instability associated with nonconvergence in static analyses [11]. In a typical geometrically nonlinear static analysis, it is common for the analysis to diverge at the stability limit of the structure, due to the negative stiffness in the load-displacement response. To model such behavior, other analysis methods can be employed, such as a dynamic analysis procedure, a method that uses displacement control for simple problems instead of load control, or a modified Riks method. The Riks method was chosen for these analysis investigations since it was straightforward to extend the static FHWA structural element model and mixed model to the Riks analysis method. This method allowed material nonlinearity, geometric nonlinearity including contact, and could predict complex, unstable responses. Loading was applied proportionally in the Riks method, in which one scalar parameter was used to determine the magnitude of the load. The load magnitude and displacements were unknown variables and were solved together. The load could increase or decrease, depending on the structure stiffness.

3.1.2 Geometry and Meshing at the U10W Joint

NTSB provided original and reproduced drawings of gusset plates, truss members, lateral braces, floor trusses, fasteners and their positions, and additional details as summarized in Table 3.1. Also provided was one CAD model, in Abaqus/CAE format, of the gusset joint at the U10W node. Bowed gusset plates at the U10W joint were observed in the field, and the bowing geometry was provided by NTSB [10].

Table 3.1
Details on Gusset Joints Provided by NTSB

File Type	File Name	Note	Date
Drawing	Minnosota.pdf	---	10-09-07
Drawing	BR9340 Construction Plan (1965).pdf	---	10-25-07
Drawing	BR9340 Steel Details (1965).pdf	U10	10-25-07
Abaqus/CAE model	U10_west.cae	U10W	10-25-07
Drawing	U10 WEST bowing.pdf	Bowed gusset plates at U10	02-21-08

Figure 3.1 and Figure 3.2 show the CAD models of the gusset joint at the U10W node. The CAD model consisted of two identical gusset plates, two main truss upper chord members, two main truss diagonal members, one main truss vertical member, one lateral brace, one floor truss upper chord section, and other secondary structure, including filler plates, splice plates, plates supporting the lateral brace and floor truss, I-stiffener, and diaphragms. Table 3.2 summarizes these components.

Table 3.2
Components in U10_west.cae

Type	Component 1	Component 2	Component 3
Gusset plate (0.5 inches thick)	U10W_Gusset_W	U10W_Gusset_E	---
Main truss upper chord	U10_U9W	U10_U11W	---
Main truss diagonal member	U10_L9W	U10_L11W	---
Main truss vertical member	U10_L10W	---	---
Lateral brace	U10W_CU11	---	---
Floor truss upper chord section	U10W_FT	---	---
Internal filler plate	U10W_fill_W	U10W_fill_E	---
Internal splice plate	U10W_splice_W	U10W_splice_E	---
External splice plate	U10W_splice_top	U10W_splice_bottom	---
Plate supporting lateral brace	U10W_lateral_top	U10W_lateral_bottom	U10W_lateral_angle
Plate supporting floor truss	U10W_FT_support	---	---
Diaphragm A	U10W_diaphragmA	---	---
I-stiffener for lateral brace	U10W_I_stiffener	---	---

The 3D local model of the gusset joint at the U10W node included all the components listed in Table 3.2 and shown in Figure 3.3 and Figure 3.4. The five main truss members, lateral brace, floor truss upper chord section, and stringer offset in the local model were cut through the members in the FHWA structural element bridge model, as shown in Figure 3.3. The distances from these cutting planes to the U10W node were two fifths of the lengths of their bridge members. The gusset plates were represented with C3D8R solid elements, which are eight-node linear brick elements using reduced integration and hourglass control. Enhanced hourglass control [11] was used for the gusset plates. An in-plane mesh size of 0.2 inches was typical in the highly stressed region of the gusset plates. The largest in-plane element size was about 0.6 inches. Six elements were used through the thickness of the gusset plates. Each gusset plate had 288,672 elements.

The five main truss members were represented with the C3D8R solid and S4R shell elements, where the C3D8R elements were used in the portions of the truss members in contact with the

gusset plates. Four C3D8R elements were used through the thickness of the main truss members. The solid elements representing each member were transitioned to shell elements using a shell-to-solid coupling constraint, described more in Section 3.1.5. The in-plane mesh size of the solid representation of the truss members ranged from 0.3 inches to 1.0 inch. Mesh size of the truss member shell representation ranged from 1.0 inch to 2.0 inches. All other parts in the 3D local model were represented with the S4R elements. All secondary structure had average element size of 0.6 inches.

3.1.3   Bowing of the Gusset Plates at the U10W Joint

Both gusset plates at the U10W joint bowed towards the west [10], as shown in Figure 3.5. The initial bowed region defined in the 3D local model is indicated by the red triangle in Figure 3.6. The red triangle was assumed to follow the outer edges of the two truss members U10_U9W and U10_L9W. It was assumed that both plates initially had the same bowing geometry, and the plates were allowed to deflect naturally as load was applied. It was also assumed that the out-of-plane bowing deflection along the vertical edge AB followed a cosine curve, as shown in Figure 3.7. The deflection tapered to zero at the upper left corner of the triangle; this decay to zero was assumed to be linear.

Various initial maximum deflections were examined. An initial deflection of 0.5 inches was chosen since it matched the observed maximum deflection reported by the NTSB of 0.6 ± 0.15 inches after applying bridge dead weight and traffic load but prior to applying construction load. The initial bowing of the gusset plates was implemented by using a geometric imperfection defined in Abaqus. The geometric imperfection was specified directly as a table of node numbers and coordinate perturbations in the global coordinate system. Figure 3.8 shows the contour plot of the initial relative Z-coordinates (out-of-plane coordinates) of the bowed region of the west gusset plate at the U10W joint.

The initial bowing was introduced by ignoring pre-stress in the bowed gusset plates. This was a conservative assumption and would likely raise the load necessary to trigger the instability.

3.1.4   Material Properties

Two types of steel materials, 50 ksi steel and 36 ksi steel, were used for the components in the 3D local model. The steel was represented as an isotropic elasto-plastic material with the material properties shown in Table 3.3 and the true stress-plastic strain curves shown in Figure 3.9. The stiffness, Poisson's ratio, coefficient of thermal expansion and elasto-plastic properties of the steel were provided by NTSB and FHWA [1, 6]. The 50 ksi steel properties provided were measured from tensile tests of steel specimens cut from the actual bridge gusset plates; data from one sample considered to be typical was used for input to the models. For the 50 ksi steel, the true yield stress was measured to be 51.5 ksi. The entire stress-strain behavior to failure was not measured; the extent of the stress and strain measurements was limited by the range of the extensometer used, and by the onset of necking. The maximum measured engineering stress was 79.34 ksi at an engineering strain of 11.1 percent. The measured total elongation (in 8 inches) was 23 percent, and the measured reduction in area was 59 percent. The maximum true stress calculated from the (limited) measurements of the engineering stress and strain was 88.86 ksi at a true plastic strain of 0.114 [1]. These values are indicated in Figure 3.9. Assuming that the true stress-true strain curve would show additional strain hardening as is typical of steel [7], the true stress-plastic strain curve of the 50 ksi steel was extrapolated to a plastic strain of 20 percent, as

shown in Figure 3.9. The extrapolation was used to avoid potential divergence issues which might occur if the von Mises stress in the model reached the largest value provided. The properties of the 36 ksi steel were scaled from the measured 50 ksi steel by the ratio of the yield stresses. For the 36 ksi steel, the true yield stress was 36 ksi; the maximum true stress input was 62.1 ksi; and the maximum plastic strain input was 0.114. The 36 ksi steel was used for the U10_U11W main truss upper chord member, and the 50 ksi steel was used for all other components in the local model. Beyond the maximum input plastic strain, the material behavior would be assumed to be perfectly plastic.

Table 3.3
Material Properties of the Steel Used in the 3D Local Model

Material	Elastic Modulus (ksi)	Poisson's Ratio	Density (kip-sec^2/in^4)	Yield Strength (ksi)	Maximum True Tensile Stress (ksi)	Maximum Tensile Strain	CTE* {in/(in-°F)}
50 ksi steel	2.9×10^4	0.3	7.298×10^{-7}	51.5	88.9	0.114	6.5×10^{-6}
36 ksi steel (calculated from 50 ksi data through a ratio of yield stresses)	2.9×10^4	0.3	7.298×10^{-7}	36.0	62.1	0.114	6.5×10^{-6}

CTE*: Linear coefficients of thermal expansion [1]

3.1.5   Constraints, Rivets, Contacts, and Boundary Conditions

The cut planes of the five main truss members, lateral brace, floor truss upper chord section, and stringer offset passed through nine member nodes in the FHWA structural element bridge model. Nine reference points coincident with these nodes were created. Nine tie constraints were employed to tie the reference points and the nodes respectively, as shown in Figure 3.10. These reference points were then coupled to the cut planes of the shell truss representations, as shown in Figure 3.11. All nine couplings were surface-based kinematic couplings in which the shell nodes on each cut plane were coupled to the rigid body motion of corresponding reference points. As modeled, the entire 3D local model was embedded into and driven by the FHWA structural element bridge model.

As stated previously, the five main truss members in the local 3D model were represented with both solid elements and shell elements. The transition from the shell element modeling to the solid element modeling was implemented using surface-based shell-to-solid coupling constraints, as shown in Figure 3.12. The shell's midsurface was the reference surface of the shell representation for U10_L10W and U10_L11W truss members. The shell's inner surface was the reference surface of the shell representation for the other three truss members. In a shell-to-solid

coupling, the motion of the nodes along the shell edge is coupled to the motion of a set of nodes on the solid surface, using a set of distributing coupling constraints internally defined in Abaqus.

In the actual bridge, steel rivets were used for the connections at the U10W joint. In the connections of the main truss members, the shanks of the rivets had a radius of 0.5 inches, and the heads of the rivets were approximately hemispherical with a radius of 0.8 inches. All rivets connecting the gusset plates, the five main truss members, and the secondary structure were represented by Abaqus fasteners. Figure 3.13 shows the locations of the fasteners related to the vertical faces, and Figure 3.14 shows the locations of the fasteners related to the horizontal faces. Abaqus fasteners provide a simplified method to connect several components without having to model the actual fasteners in detail. With Abaqus fasteners, nodes within a specified radius of influence on one component are automatically coupled to nodes within the specified radius of influence on another component, thereby fastening the components together. In the local 3D model, the fasteners were defined to have a radius of influence of 0.5 inches. Both surfaces normal to the rivet axis of a solid component were involved in the fastener definition. The red regions in Figure 3.15 indicate the fastened nodes in the west gusset plate.

All other connections between the components in Table 3.2 were represented by surface-based tie constraints, as shown in Figure 3.16. The tie constraints connected the floor truss upper chord section to its support and the support to the top lateral plate and top splice plate. The tie constraints also connected the lateral brace to the top lateral plate and bottom lateral plate.

Contact pairs were defined between the components wherever the fasteners were employed to connect them. Figure 3.17 shows the contact regions defined between the gusset plates and the five main truss members. A Coulomb friction model with a friction coefficient of 0.1 was used to define the contact pairs.

No translational or rotational boundary conditions were defined in the local 3D model since the local model was fully constrained with the connections described above.

Figure 3.18 shows the embedded U10W joint that incorporates the bowed gusset plates, fasteners, constraints, and contact conditions described above.

3.1.6 Load Conditions

The local 3D model representing the U10W joint was embedded into the sixth FHWA structural element bridge model provided in April 2008 [1] and was driven by the bridge model loads transferred through the tie and coupling constraints defined above. As described previously, there were seven load steps in the mixed model. In the first step, decks and expansion joint springs were removed from the model to represent an initial state of the bridge during construction. The weight of steel and walkways, the forces representing wet deck concrete, and approach span reaction forces were then applied. The approach span reaction forces represented the loads applied by approach spans of the bridge [1]. In the second step, the deck elements were activated and the forces representing the wet concrete were deactivated. In the third step, the weight of the original barriers was applied. In the fourth step, the weight of the additional deck and barriers were included to represent changes that were made to the bridge during its lifespan. A corresponding approach span force increment was applied, as the approach span reaction forces increased as the weight of the approach spans increased [1]. In the fifth step, expansion joint

springs were added [1], and the weight of deck concrete was reduced to reflect the deck concrete that was milled down as part of the repaving process that was underway on the day of the collapse. In the sixth step, the traffic loads estimated at the time of collapse and the corresponding approach span force increment were applied. In the seventh step, the estimated construction load at the time of collapse was applied. Note that the traffic and construction loads used at the time of collapse were provided by the NTSB [5].

Table 3.4 summarizes the mixed model load steps described above. The combination of these load steps was called load condition A1. The first six steps were regular static analysis steps. The last step used the Riks method to proportionally increase the construction load while keeping the other loads constant.

Table 3.4
Load Steps in the Mixed Model, Load Condition A1

Step	Load Description	Model Change	Load Increment (kip)	Total Load (kip)	Normalized Total Load (kip)
1	Weight of steel and walkways, forces representing wet deck concrete, and approach span reaction forces	Remove decks and expansion joint springs	17,900	17,900	0.731
2	Weight of decks to replace the forces representing the wet concrete	Add decks	0	17,900	0.731
3	Weight of original barriers	---	1,629	19,529	0.798
4	Weight of added deck and barriers through the life of the bridge and approach span reaction force increment	---	4,554	24,083	0.984
5	Reduce weight of deck concrete due to milling	Add expansion joint springs	-585	23,498	0.960
6	Traffic load at collapse and approach span reaction force increment	---	406 (traffic 377, approach span force inc 29)	23,904	0.976
7	Construction material and vehicles at collapse	---	578	24,482	1.000

The estimated total load along the vertical direction (Y-direction) was 24,482 kip, including the bridge weight of 21,956 kip, the approach span reaction force of 1,571.3 kip, the traffic load of 376.7 kip, and the construction load of 578.5 kip. These loads were applied using a combination of gravity loads, line loads, concentrated loads, and pressure. Figure 3.19 shows the location of

the traffic load at the time of collapse, and Figure 3.20 shows the location of the construction materials and vehicles at the time of collapse.

To investigate the effect of uncertainty in the bridge deadweight and the traffic load, another load condition, A2, was analyzed. This load condition was similar to initial load condition A1, but increased the bridge deadweight and traffic load five percent. Table 3.5 summarizes load condition A2. Note that approach span reaction forces in load condition A2 were assumed to be the same as in load condition A1.

Table 3.5
Load Steps in the Mixed Model, Load Condition A2

Step	Load Conditions	Model Change	Load Increment (kip)	Total Load (kip)	Normalized Total Load (kip)
1	105% of weight of steel and walkways and forces representing wet deck concrete and 100% of approach span reaction forces	Remove decks and expansion joint springs	18,733	18,733	0.732
2	105% of weight of decks to replace the forces representing the wet concrete	Add decks	0	18,733	0.732
3	105% of weight of original barriers	---	1,710	20,443	0.799
4	105% of weight of added deck and barriers through the life of the bridge and 100% of approach span reaction force increment	---	4,769	25,212	0.985
5	Reduce 105% of the weight of deck concrete due to milling	Add expansion joint springs	-615	24,597	0.961
6	105% of traffic load at collapse and 100% of approach span reaction force increment	---	425 (traffic 396, approach span force inc 29)	25,022	0.977
7	Construction material and vehicles at collapse	---	578	25,600	1.000

3.2   Analysis Results When Embedding U10W 3D Local Model with Load Condition A1

3.2.1   Deformed Shape of Bowed Gusset Plates Prior to Applying Construction Load

Figure 3.21 is a visual comparison between the bowed gusset plates observed on the bridge and the shape of the gusset plates developed in the model. The model shape was obtained after the

bridge dead weight and the traffic load were applied but before the construction load was applied. Figure 3.22 shows the shape of the bowed vertical edge AB on both plates in the beginning of the analysis and before the construction load was applied. The initial maximum out-of-plane deflection was defined to be 0.5 inches in both gusset plates. The deformed maximum out-of-plane deflection was 0.676 inches in the east gusset plate and 0.684 inches in the west gusset plate. These values were in the range of the observed deflection that was provided by the NTSB, 0.6 ± 0.15 inches [10].

3.2.2 Stress and Strain Distribution Under the Estimated Construction Load

To obtain the stress and strain distribution at 100 percent of the estimated construction load, a regular static analysis was performed to apply the construction load. The analysis predicted that when subjected to the estimated construction load, no apparent plastic deformation occurred in any bridge truss members, as shown in Figure 3.23 and Figure 3.24. Note that Figure 3.23 includes only membrane stresses for all truss members and all the stresses were below yield stress. Figure 3.24 shows that only a few spots in the vicinity of the fasteners in the truss members of the U10W 3D local model were predicted to have von Mises stress slightly greater than the allowable yield strength of the material, 36 ksi for the U10_U11W main truss upper chord member and 51.5 ksi for other truss members and gusset plates.

Plastic deformation occurred mainly in the two gusset plates at the U10W joint, as shown in Figure 3.25, Figure 3.26, Figure 3.27, and Figure 3.28. The deformation scale factor in Figure 3.25 is five. The maximum von Mises stress predicted, 66 ksi, occurred on the east face of both gusset plates, which corresponded to an equivalent plastic strain (PEEQ) of 2.2 percent. The maximum stress under the estimated construction load was predicted to be much less than the maximum measured tensile stress of the material, 88.86 ksi. Note that the typical mesh size in the highly stressed region of the gusset plates was about 0.2 inches, as shown in Figure 3.3. The maximum stress predicted would increase with decreasing element size in the highly stressed region, as discussed later in Section 4 and Section 5 of this report.

Figure 3.29 shows the distribution of the von Mises stress on the east face of the east gusset at the end of three load steps: as-designed bridge weight, traffic load, and construction load. The maximum stress in the east gusset always occurred on the edge of the upper fastener connecting the east gusset and the diagonal truss member U10_L9W. The maximum stresses in the east gusset plate at the end of each load step were predicted to be 54 ksi, 56 ksi, and 66 ksi. The gusset material between the horizontal truss member U10_U9W and the upper edge of the diagonal truss member U10_L9W was predicted to yield under the bridge design weight. However, only a few elements yielded through the entire thickness. With the application of the weight of added deck and barriers through the life of the bridge and the corresponding approach span reaction force increment, more elements yielded through the entire gusset thickness, as shown in Figure 3.30.

3.2.3 Deformation of Diagonal Truss Member U10_L9W and Gusset Plates Under Estimated Construction Load

Figure 3.31 shows the contour plot of the out-of-plane displacement of the diagonal truss member U10_L9W under the estimated construction load. Figure 3.32 shows the deformed shape of the two gusset plates under the construction load. The deformation scale factor in both figures is 15. The contour plot and the deformed shape indicated that most regions of the diagonal truss

member moved transversely outward from the bridge, while the upper edge of the east face of the diagonal truss member moved transversely towards the bridge.

3.2.4 Force and Moment in Diagonal Truss Member U10_L9W in the Regular Static Analysis

Table 3.6 summarizes the axial force and bending moment at the lower end of the diagonal truss member U10_L9W when the approach span force increment, traffic load, and construction load were increased in the regular static analysis of the mixed model. The total load, traffic load, and construction load are normalized with respect to their values at the end of the construction loading step. Under the deadweight of the bridge, the axial force was calculated to be -2,106 kip, and the bending moment was predicted to be 449 kip-inch. After applying the traffic load with a value of 376.7 kip and the approach span force increment with a value of 29.4 kip, the axial force was -2,148 kip and the bending moment was 475 kip-inch. The percentage increase in the axial force and bending moment due to the traffic load and the approach span force increment is comparable to the percentage increase in the total load: 2 percent for the axial force and 3 percent for the bending moment versus 1.6 percent for the total load. This could be explained by the approximately uniform distribution of the traffic load on the bridge decks.

Under the estimated construction load, the axial force was predicted to be -2,410 kip, and the bending moment was predicted to be 943 kip-inch. They increased 11 percent and 50 percent respectively when the construction load increased from 0 percent to 100 percent of its estimated value and the total load increased from 97.6 percent to 100 percent of its estimated value. The percentage increase in the axial force due to the construction load is larger than the percentage increase in the total load: 11 percent for the axial force versus 2.4 percent for the total load. The most significant increase due to the application of the construction load is the increase in the bending moment: 50 percent for the bending moment versus 2.4 percent for the total load.

Table 3.6
Force and Moment at the Lower End of the Diagonal Truss Member U10_L9W with Load Condition A1 in the Mixed Model

Normalized Total Load	Normalized Traffic Load and Approach Span Force Increment	Normalized Construction Load	Axial Force SF1 (kip)	Bending Moment SM (kip-inch)	ΔSF1/(SF1 at Estimated Construction Load)	ΔSM/(SM at Estimated Construction Load)
0.960	0	0	-2,106	449	---	---
0.976	1.000	0	-2,148	475	2%	3%
1.000	1.000	1.000	-2,410	943	11%	50%

3.2.5 Load Displacement Curve in the Regular Static Analysis

Figure 3.33 a) shows the load displacement curve where all seven steps were regular static steps. The horizontal axis of the graph represents the normalized total load, the ratio between the applied total load and the estimated total load of 24,482 kip. The vertical axis represents the out-of-plane displacement at the top corner on the west face of the diagonal truss member U10_L9W. The analysis predicted that the out-of-plane displacement increased with increasing load. When deck concrete was milled down, the slope of the load displacement curve was negative and the displacement decreased, as shown in Figure 3.33 b). The displacement increased from 0.114 inches to 0.128 inches when the traffic load and the approach span force increment increased from 0 percent to 100 percent of their estimated values. The displacement doubled, increasing from 0.128 inches to 0.257 inches when the construction load increased from 0 percent to 100 percent of its estimated value. Although the construction load was only 2.4 percent of the estimated total load, it contributed to half of the total out-of-plane displacement.

3.2.6 Load and Stress at Predicted Maximum Load

Riks methods and regular static analyses were performed to predict the maximum load at the onset of instability by proportionally increasing the construction load while other loads were maintained at their estimated values. Two Riks analyses were performed. The first Riks analysis had a larger maximum arc length increment, 0.06, and the second Riks analysis had a smaller maximum arc length increment, 0.03.

A displacement-controlled static analysis with adaptive static stabilization was also performed to compare the difference in predicted maximum load between the Riks method and a displacement-controlled analysis. In the displacement-controlled analysis, the displacement increments calculated from the application of the construction loads were used to define displacement boundary conditions that were applied in place of extra construction loads. In this analysis, regular static steps were carried out up to the 100 percent of the estimated construction load. In the subsequent step, extra construction loads were applied as a fixed displacement rate. The magnitude of the displacement rate at each construction load node was set from the last loading increment in the load step with the 100 percent of the construction load. See section 4.4 for more complete results from another analysis using this approach.

The first Riks analysis, the load-controlled and the displacement-controlled regular static analyses encountered divergence issues, but all four analyses show similar behavior for the deflection of the U10_L9W diagonal truss member at similar load levels, as shown in Figure 3.34. Figure 3.34 compares the load displacement curve in construction loading step for the four analyses. The first Riks analysis diverged before the load was reduced, but the load/displacement curve for this analysis and the results from the other analyses indicated that divergence occurred at approximately the peak load just before the load would be reduced to maintain equilibrium in the Riks analysis. The second Riks analysis and the displacement-controlled static analysis predicted a load reduction before the analyses completed or diverged. Table 3.7 compares the predicted maximum loads and out-of-plane displacement at the top corner on the west face of the diagonal truss member U10_L9W for the four analyses. The predicted maximum loads were close to each other for the four analyses.

Table 3.7
Maximum Loads and Displacements Predicted by Riks Methods, Load-Controlled and
Displacement-Controlled Regular Static Analyses with Load Condition A1 in the Mixed Model

Analysis Types	Predicted Maximum Total Load (kip)	Predicted Maximum Construction Load (kip)	Out-of-Plane Displacement at Top Corner on West Face of U10_L9W (inch)
Riks with Larger Max Arc Length Increment*	24,812	908	0.518
Riks with Smaller Max Arc Length Increment	24,818	914	0.529
Load-Controlled Regular Static Analysis*	24,809	905	0.551
Displacement-Controlled Regular Static Analysis	24,822	918	0.598

*: Reported loads and displacements were the values predicted at divergence point.

The first Riks analysis diverged at a construction load of 908 kip, which was 1.57 times the estimated construction loads provided by the NTSB. The divergence was caused by severe contact overclosures [11]. The nodes with the severe contact overclosures during unconverged iterations were located outside of the regions that were contacting in a converged state. The reported overclosure values for these nodes were significantly greater than the overclosures for nodes within the contacting regions. This would be an indication of physical or numerical instabilities in the model. The total load along the vertical direction at the divergence point was predicted to be 24,812 kip, or 1.013 times the estimated total load, as shown in Figure 3.34. The out-of-plane displacement at the top corner of the diagonal truss member U10_L9W was predicted to be 0.518 inches, almost double the displacement under the estimated construction load.

The second Riks analysis predicted a maximum construction load of 914 kip, or 1.58 times the estimated construction load provided by the NTSB. The maximum total load along the vertical direction was predicted to be 24,818 kip, or 1.014 times the estimated total load, as shown in Figure 3.34. The out-of-plane displacement at the top corner of the diagonal truss member U10_L9W was predicted to be 0.529 inches under the maximum total load. After the maximum total load was reached, the out-of-plane displacement continued to increase with reduced construction load, indicating that the maximum in the load was related to a geometric instability.

The load-controlled regular static analysis diverged at a total load of 24,809 kip. The corresponding load displacement curve is shown in Figure 3.34. The out-of-plane displacement at the top corner of the diagonal truss member U10_L9W was predicted to be 0.551 inches under the maximum total load.

The displacement-controlled static analysis predicted a local maximum construction load of 918 kip and a local maximum total load of 24,822 kip, as shown in Figure 3.34. The out-of-plane displacement at the top corner of the diagonal truss member U10_L9W was predicted to be 0.598 inches under the local maximum total load.

Although the construction load in the first Riks analysis did not decrease when the analysis diverged, the trend of the load displacement curve at the divergence point in both the first Riks analysis and the regular static analysis appears to predict that the maximum load at instability would be close to the value at the divergence point, as confirmed by the second Riks analysis. Section A8 of this report will discuss one example that shows the negative slope in the Riks analysis corresponded to the divergence point in the same static analysis.

File BridgeU10W_meshP2_Riks_MisesStress_Animation.gif animates the deformation and von Mises stress distribution of U10W joint under increasing and then decreasing construction load in Riks step with load condition A1. Nonuniform deformation scale factors are used in the animation. The deformation scale factor is 1 for X- and Y-directions and is 30 for Z-direction. The animation shows that the diagonal truss member U10_L9W moved outwards with increasing and then decreasing construction load. Figure 3.35 displays the enlarged deformed shape of the U10W joint under the maximum load predicted by the Riks analysis. The enlarged deformed shape of the gusset plates under the maximum load is shown in Figure 3.36. In these two figures, a uniform deformation scale factor of 15 is used.

Significant plastic deformation occurred in the two gusset plates under the maximum load predicted by the first Riks analysis, as shown in Figure 3.37. The maximum von Mises stress was predicted to be 81 ksi in the vicinity of the upper corner rivet in the east gusset plate, as shown in Figure 3.38 and Figure 3.39. The maximum equivalent plastic strain was predicted to be 5.7 percent, as shown in Figure 3.40. The maximum stress in the east gusset plate changed from 66 ksi to 81 ksi, a 23 percent increase, when the additional 57 percent of the estimated construction load was applied.

After the maximum total load was reached, the second Riks analysis predicted that the von Mises stress and equivalent plastic strain continued increasing with reduced construction load. When the total load was reduced to 24,796 kip, the maximum von Mises stress was predicted to be 85.5 ksi on the east face of the east gusset plate, as shown in Figure 3.41. Figure 3.41 shows that the maximum equivalent plastic strain was predicted to be 8.2 percent.

Table 3.8 summarizes the axial force and bending moment at the lower end of diagonal truss member U10_L9W, the out-of-plane displacement at the top corner of that truss member, the maximum von Mises stress, and the maximum equivalent plastic strain in the east gusset plate with increasing construction load. The axial force and bending moment were predicted to be -2,550 kip and 1,612 kip-inch under the maximum load at instability predicted by the second Riks analysis. The axial force increased by 6 percent, and the bending moment increased by 71 percent. This corresponds to the extra 58 percent increase in the construction load or 1.4 percent increase in the total load. The increase in the displacement and maximum plastic strain doubled when the extra 58 percent of the construction load was added.

Table 3.8

Summary of Force, Displacement, Stress, and Strain with Increasing Construction Load in Load Condition A1

Normalized Total Load	Normalized Construction Load	Axial Force at Lower End of U10_L9W (kip)	Bending Moment at Lower End of U10_L9W (kip-inch)	Out-of-Plane Displacement at Top Corner of U10_L9W (inch)	Max von Mises Stress in East Gusset (ksi)	Max Equivalent Plastic Strain in East Gusset
0.976	0	-2,148	475	0.128	56	1.0%
1.000	1.000	-2,410	943	0.257	66	2.2%
1.014	1.580	-2,550	1,612	0.529	81	5.7%

3.3 Analysis Results When Embedding U10W 3D Local Model with Load Condition A2 (5 Percent Increase in Bridge Deadweight and Traffic Load)

3.3.1 Bowed Gusset Plates Prior to Applying Construction Load

The initial gusset bowing geometry was the same as that used for condition A1. With the 5 percent increase in the deadweight of the bridge and the traffic load in the load condition A2, the predicted bowing geometry was similar to that with the load condition A1. Before the construction load was applied, the deformed maximum out-of-plane deflection was predicted to be 0.746 inches in the east gusset plate, and 0.758 inches in the west gusset plate. These maximum out-of-plane deflections were larger than those with the load condition A1, 0.676 inches in the east gusset plate and 0.684 inches in the west gusset plate.

3.3.2 Stress and Strain Distribution Under the Estimated Construction Load

Similar to load condition A1, no apparent plastic deformation occurred in any bridge truss members under the estimated construction load with load condition A2. Plastic deformation occurred mainly in the two gusset plates at the U10W joint, as shown in Figure 3.42 and Figure 3.43. The deformation scale factor in Figure 3.42 is 5. The maximum von Mises stress predicted, 74 ksi, occurred on the east face of the east gusset plate, which corresponded to an equivalent plastic strain of 3.8 percent. Figure 3.43 shows the distribution of the von Mises stress on the east face of the east gusset at the end of three loading steps: bridge design weight, traffic load, and construction load. Similar to load condition A1, the maximum stress in the east gusset always occurred on the edge of the upper fastener connecting the east gusset and the diagonal truss member U10_L9W. The maximum stresses in the east gusset plate at the end of each loading step were predicted to be 54 ksi, 59 ksi, and 74 ksi. The difference in the stress distribution in the east gusset plate between the load conditions A1 and A2 was small under the bridge design weight, as shown in Figure 3.29 and Figure 3.43. As the traffic load and the construction load were applied, the pattern of the stress distribution in the east gusset remained similar between the two load conditions. However, load condition A2 predicted a larger maximum stress in the east

gusset plate, 74 ksi for load condition A2 and 66 ksi for load condition A1 under the construction load.

3.3.3 Force and Moment in the Diagonal Truss Member U10_L9W in the Regular Static Analysis

Table 3.9 summarizes the axial force and bending moment at the lower end of the diagonal truss member U10_L9W when the approach span force increment, traffic load, and construction load were increased in the regular static analysis. The total load, traffic load, and construction load are normalized with respect to their values at the end of the construction loading step. The trend of the axial force and bending moment with increasing external force was similar to that with load condition A1. The percentage increase in the axial force and bending moment due to the traffic load and the approach span force increment was comparable to the percentage increase in the total load: 2 percent for both the axial force and bending moment versus 1.6 percent for the total load. The percentage increase in the axial force due to the construction load was larger than the percentage increase in the total load: 10 percent for the axial force versus 2.3 percent for the total load. The most significant increase due to the construction load is the increase in the bending moment, 56 percent for the bending moment versus 2.3 percent for the total load.

Table 3.9
Force and Moment at the Lower End of the Diagonal Truss Member U10_L9W with Load Condition A2

Normalized Total Load	Normalized Traffic Load and Approach Span Force Increment	Normalized Construction Load	Axial Force SF1 (kip)	Bending Moment SM (kip-inch)	ΔSF1/(SF1 at Estimated Construction Load)	ΔSM/(SM at Estimated Construction Load)
0.961	0	0	-2,209	518	---	---
0.977	1.000	0	-2,252	546	2%	2%
1.000	1.000	1.000	-2,507	1,245	10%	56%

With the 5 percent increase in the bridge deadweight and the traffic load, the axial force in the diagonal truss member U10_L9W increased by 5 percent, and the bending moment increased by 15 percent at the end of the traffic loading step. The axial force increased by 4 percent, and the bending moment increased by 32 percent at the end of the construction loading step, compared to the results in load condition A1.

3.3.4 Load Displacement Curve in the Regular Static Analysis

Figure 3.44 shows the load displacement curve where all seven steps were regular static steps. The horizontal axis of the graph represents the normalized total load, the ratio between the applied total load and the estimated total load of 25,600 kip. The vertical axis represents the out-of-plane displacement at the top corner on the west face of the diagonal truss member U10_L9W.

The variation of the displacement with the applied load was similar to that with load condition A1. The displacement increased from 0.147 inches to 0.163 inches when the traffic load and the approach span force increment increased from 0 percent to 100 percent of their estimated values. The out-of-plane displacement doubled, increasing from 0.163 inches at the end of the traffic load step to 0.396 inches at the end of the construction load step, when the construction load increased from 0 percent to 100 percent of its estimated value. Although the construction load was only 2.3 percent of the estimated total load, it contributed to more than half of the total out-of-plane displacement.

With the five percent increase in the bridge deadweight and the traffic load in load condition A2, the out-of-plane displacement increased from 0.128 inches to 0.163 inches after the traffic load was applied. This corresponded to a 27 percent increase from load condition A1 to load condition A2. After the construction load was applied, the out-of-plane displacement changed from 0.257 inches to 0.396 inches, which corresponded to a 54 percent increase from load condition A1 to load condition A2.

3.3.5 Load and Stress at Predicted Maximum Load, Riks Method

As with load condition A1, two Riks analyses were performed to predict the maximum load at the onset of instability by proportionally increasing the construction load while other loads were maintained at their estimated values. The only difference between the two Riks analyses was the maximum arc length specified. The maximum arc length parameter was 0.1 for the first Riks analysis, and was 0.03 for the second Riks analysis. As with the first Riks analysis with load condition A1, the two Riks analyses for load condition A2 failed to converge before the loads began to decrease, but the point of divergence appears consistent with the peak load just before the load would be reduced to maintain equilibrium in the Riks analysis.

For load condition A2, the two Riks analyses predicted similar peak load and out-of-plane displacement at their respective divergence points. The first Riks analysis diverged at a construction load of 672 kip, which was 1.16 times the estimated value of the construction loads provided by the NTSB. The total load along the vertical direction was predicted to be 25,694 kip, or 1.004 times the estimated total load (which for load condition A2 includes a 5 percent increase in loads other than the construction loads and approach span reaction forces), as shown in Figure 3.45. The out-of-plane displacement at the top corner of the diagonal truss member U10_L9W was predicted to be 0.529 inches. The second Riks analysis diverged at a construction load of 680 kip, which was 1.18 times the estimated value of the construction loads provided by the NTSB. The total load along the vertical direction was predicted to be 25,702 kip, or 1.004 times the estimated total load (which for load condition A2 includes a 5 percent increase in loads other than the construction loads and approach span reaction forces), as shown in Figure 3.45. The out-of-plane displacement at the top corner of the diagonal truss member U10_L9W was predicted to be 0.530 inches. Load condition A2 showed that when the bridge deadweight and the traffic load were increased by five percent, the construction load needed to achieve the predicted maximum load decreased by 35 percent.

Although the construction load in the two Riks analyses for load condition A2 did not decrease when the analyses diverged, the slope of the displacement-load curve was approaching vertical In addition, the axial force in U10_L9W and the out-of-plane displacement at the top corner of that member at the divergence point in the Riks analyses were similar to values found at the

point where the load did decrease for load condition A1. These results indicate that the maximum load at instability would be close to the value at the divergence point, as discussed in Section 3.2.6 and later in Section A8 of this report. The results presented in Section 3.2.6 for load condition A1 show that the similar divergence for a Riks analysis with a maximum arc length parameter of 0.06 and for a regular static analysis gave consistent predictions of instability when compared with analyses using a smaller Riks maximum arc length parameter or using an applied displacement rate. The displacement-controlled analysis was not performed for load condition A2.

Significant plastic deformation occurred in the two gusset plates under the maximum load predicted by the second Riks analysis, as shown in Figure 3.46. The deformation scale factor in this figure is 5. The maximum von Mises stress was predicted to be 82 ksi in the vicinity of the upper corner rivet in the east gusset plate, as shown in Figure 3.47. The maximum equivalent plastic strain was predicted to be 6.1 percent. The maximum stress at the predicted maximum load at instability with load condition A2 was almost the same as that with load condition A1. More material in the gusset plates had higher stress than that with load condition A1. For example, load condition A2 had 331 elements with von Mises stress higher than 70 ksi, and load condition A1 had 281 elements with von Mises stress higher than 70 ksi.

Table 3.10 summarizes the axial force and bending moment at the lower end of truss member U10_L9W, the out-of-plane displacement at the top corner of that truss member, the maximum von Mises stress and the maximum equivalent plastic strain in the east gusset plate with increasing construction load. The axial force and bending moment were predicted to be -2,547 kip and 1,547 kip-inch under the maximum load at instability predicted by the second Riks analysis. The axial force increased by 2 percent, and the bending moment increased by 24 percent. This corresponds to the extra 18 percent increase in the construction load or 0.4 percent increase in the total load. The out-of-plane displacement increased by 34 percent, and the maximum equivalent plastic strain increased by 61 percent when the extra 18 percent of the construction load was added. Under their maximum load at instability predicted by the Riks analysis in the two load conditions A1 and A2, the axial force was identical, and the difference in the bending moment was 4 percent, with the load condition A1 having higher values. The similar values in the axial force and bending moment between the two load conditions resulted in a similar out-of-plane displacement, a similar maximum stress, and a similar maximum strain.

Table 3.10
Summary of Force, Displacement, Stress, and Strain with Increasing Construction Load in Load Condition A2

Normalized Total Load	Normalized Construction Load	Axial Force at Lower End of Truss Member U10_L9W (kip)	Bending Moment at Lower End of Truss Member U10_L9W (kip-inch)	Out-of-Plane Displacement at Top Corner of Truss Member U10_L9W (inch)	Max von Mises Stress in East Gusset (ksi)	Max Equivalent Plastic Strain in East Gusset
0.977	0	-2,252	546	0.163	59	1.4%
1.000	1.00	-2,507	1,245	0.396	74	3.8%
1.004	1.18	-2,547	1,547	0.530	82	6.1%

Table 3.11 summarizes the axial force, bending moment, out-of-plane displacement, von Mises stress, and equivalent plastic strain under their estimated construction loads for the two load conditions A1 and A2. Table 3.12 summarizes these variables under their maximum load at instability predicted by the Riks analysis for the two load conditions.

Table 3.11
Comparison of Force, Displacement, Stress and Strain Under Their Estimated Construction Loads between the Two Load Conditions A1 and A2

Load Condition	Estimated Total Load (kip)	Estimated Construction Load (kip)	Axial Force at Lower End of Truss Member U10_L9W (kip)	Bending Moment at Lower End of Truss Member U10_L9W (kip-inch)	Out-of-Plane Displacement at Top Corner of Truss Member U10_L9W (inch)	Maximum Mises Stress in East Gusset (ksi)	Maximum Equivalent Plastic Strain in East Gusset
A1	24,482	579	-2,410	943	0.257	66	2.2%
A2	25,600	579	-2,507	1,245	0.396	74	3.8%

Table 3.12

Comparison of Force, Displacement, Stress and Strain Under their Predicted Maximum Loads
between the Two Load Conditions A1 and A2

Load Condition	Predicted Maximum Total Load at Instability (kip)	Construction Load at Instability (kip)	Axial Force at Lower End Node of Truss Member U10_L9W (kip)	Bending Moment at Lower End Node of Truss Member U10_L9W (kip-inch)	Out-of-Plane Displacement at Top Corner of Truss Member U10_L9W (inch)	Max von Mises Stress in East Gusset (ksi)	Max Equivalent Plastic Strain in East Gusset
A1	24,818	914	-2,550	1,612	0.529	81	5.7%
A2	25,702	680	-2,547	1,547	0.530	82	6.1%

3.4 Summary: U10W 3D Local Model Embedded into the FHWA Structural Element Bridge Model

Nonlinear finite element analyses have been performed to predict the stress distribution in the gusset plates at the U10W joint of the Minneapolis I-35W bridge under the loadings of original bridge design weight, additional concrete weight from increased deck thickness and barrier modifications, reduced concrete weight from the repaving operation underway on the day of the collapse, traffic load, and construction load. The U10W joint was represented by a 3D local model, which was embedded into the sixth structural element bridge model provided by FHWA in April 2008. Bowed gusset plates were assumed, and 0.5 inches was the maximum out-of-plane deflection defined before any loads were applied. Typical mesh size in the highly stressed region of the gusset plates was 0.2 inches. Riks analysis methods were utilized to predict the maximum load at instability of the bridge by proportionally increasing the construction load while keeping the other loads constant. Two load conditions, A1 and A2, were specified. Load condition A2 had five percent increase in the dead weight of the bridge and the traffic load, compared to that of load condition A1. Load condition A1 had an estimated total load of 24,482 kip, and load condition A2 had an estimated total load of 25,600 kip.

The analyses predicted initial plastic deformation in the gusset plates when the bridge was subjected to the weight of the original bridge design. The plastic deformation in the gusset plates became more severe with the application of additional concrete weight, traffic load, and construction load. Under the estimated total load, load condition A1 predicted a maximum von Mises stress of 66 ksi on the edge of the upper fastener connecting the east gusset plate and the diagonal truss member U10_L9W, which corresponded to an equivalent plastic strain of 2.2 percent. Load condition A2 predicted a maximum von Mises stress of 74 ksi in the same location, which corresponded to an equivalent plastic strain of 3.7 percent.

The bending moment at the lower end of the diagonal truss member U10_L9W was raised significantly when the construction load was applied, which forced the transversely outward movement of the diagonal truss member. The bending moment doubled as the estimated construction load was applied for both load conditions A1 and A2, increasing from 475 kip-inch

to 943 kip-inch for load condition A1 and increasing from 546 kip-inch to 1,245 kip-inch for load condition A2. Accordingly, the out-of-displacement at the top corner on the west face of the diagonal truss member doubled under the estimated construction load, increasing from 0.128 inches to 0.257 inches for load condition A1 and increasing from 0.163 inches to 0.396 inches for load condition A2.

The Riks method predicted that local structural instability occurred at the U10W joint under a total load of 24,818 kip or a construction load of 914 kip for load condition A1. The method also predicted that the instability occurred at a total load close to 25,702 kip or a construction load close to 680 kip for load condition A2. The instability was demonstrated by the significant increase in the out-of-displacement at the top corner of the diagonal truss member U10_L9W as extra construction load was applied. At the load close to the maximum load at instability, the maximum von Mises stress was predicted to be 81 ksi for load condition A1, which corresponded to an equivalent plastic strain of 5.7 percent. The maximum von Mises stress was predicted to be 82 ksi for load condition A2, which corresponded to an equivalent plastic strain of 6.1 percent.
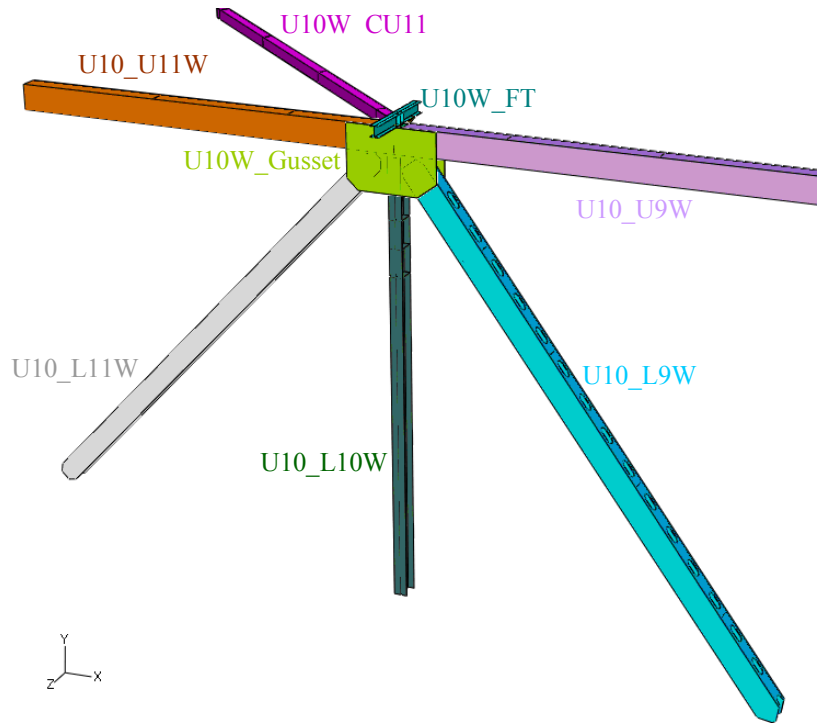
Figure 3.1: CAD model of the U10W joint; provided by NTSB
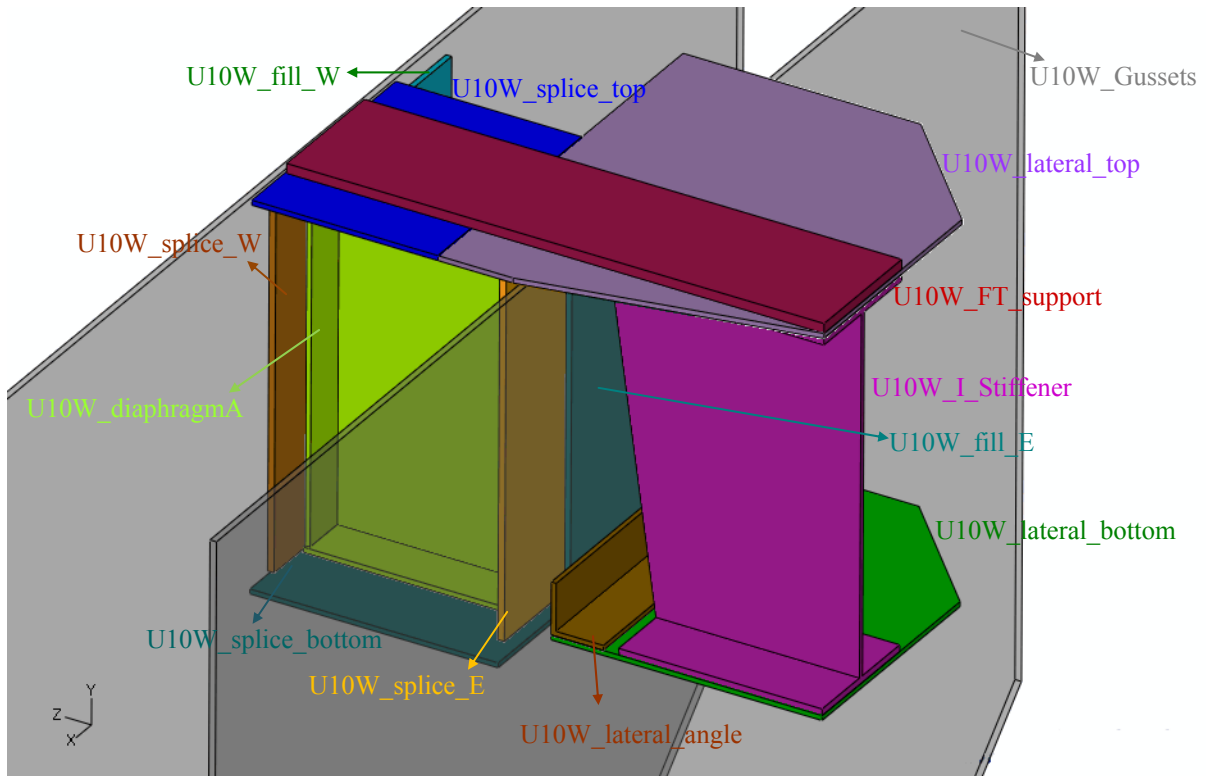
Figure 3.2: CAD model of connecting plates at the U10W joint; provided by NTSB
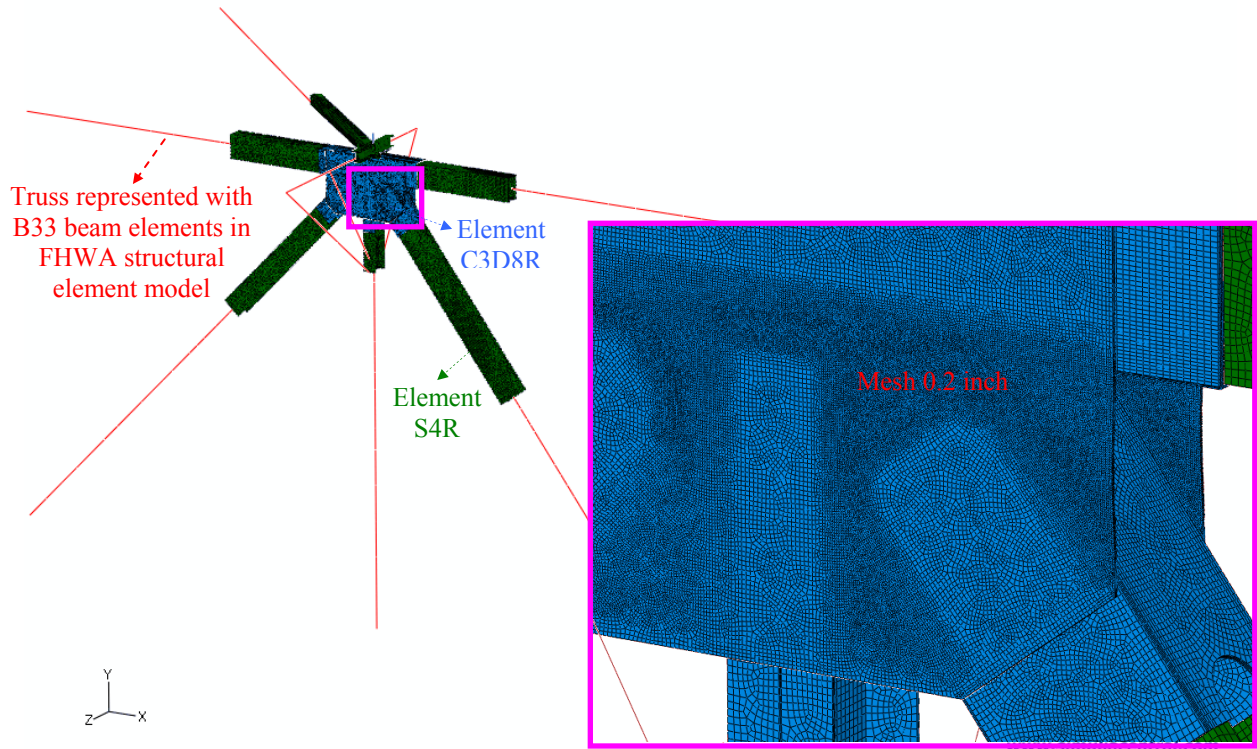
Figure 3.3: CAE model of the U10W joint; 0.2-inch mesh in highly stressed gusset region
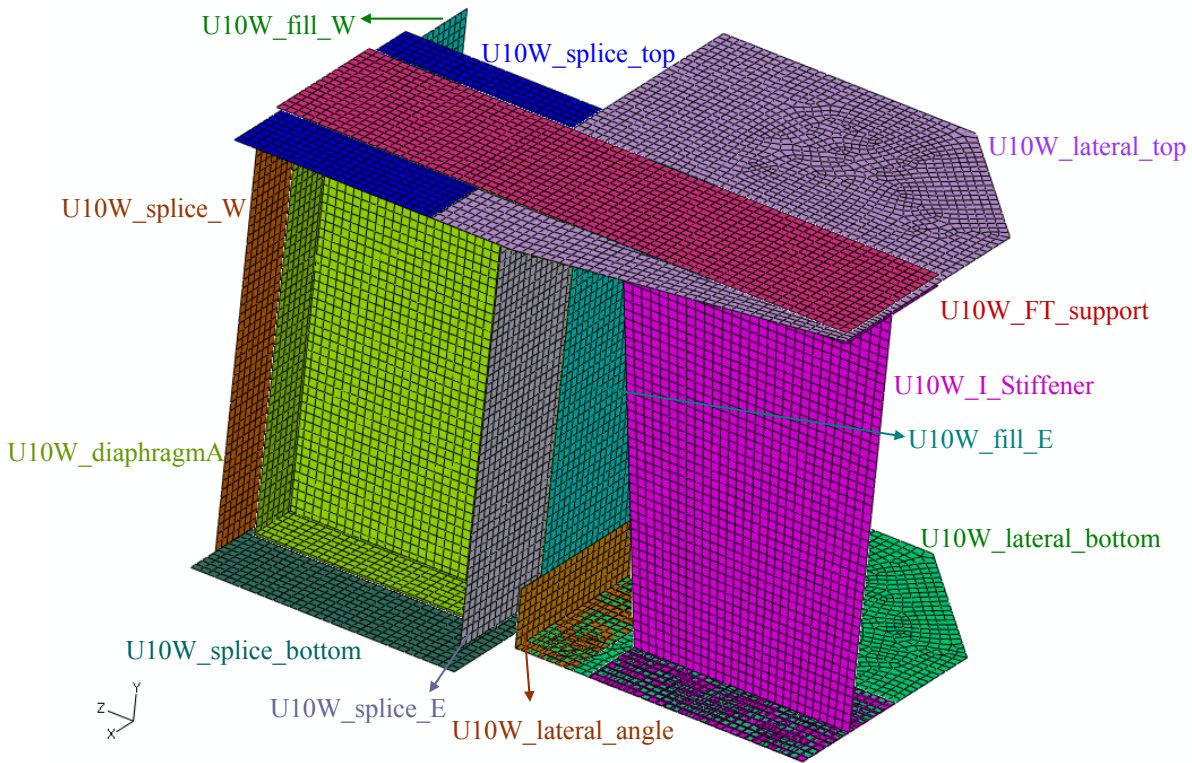
Figure 3.4: CAE model of connecting plates at the U10W joint; 0.6 inch mesh

Figure 3.5: Bowed gusset plates observed at the U10W joint
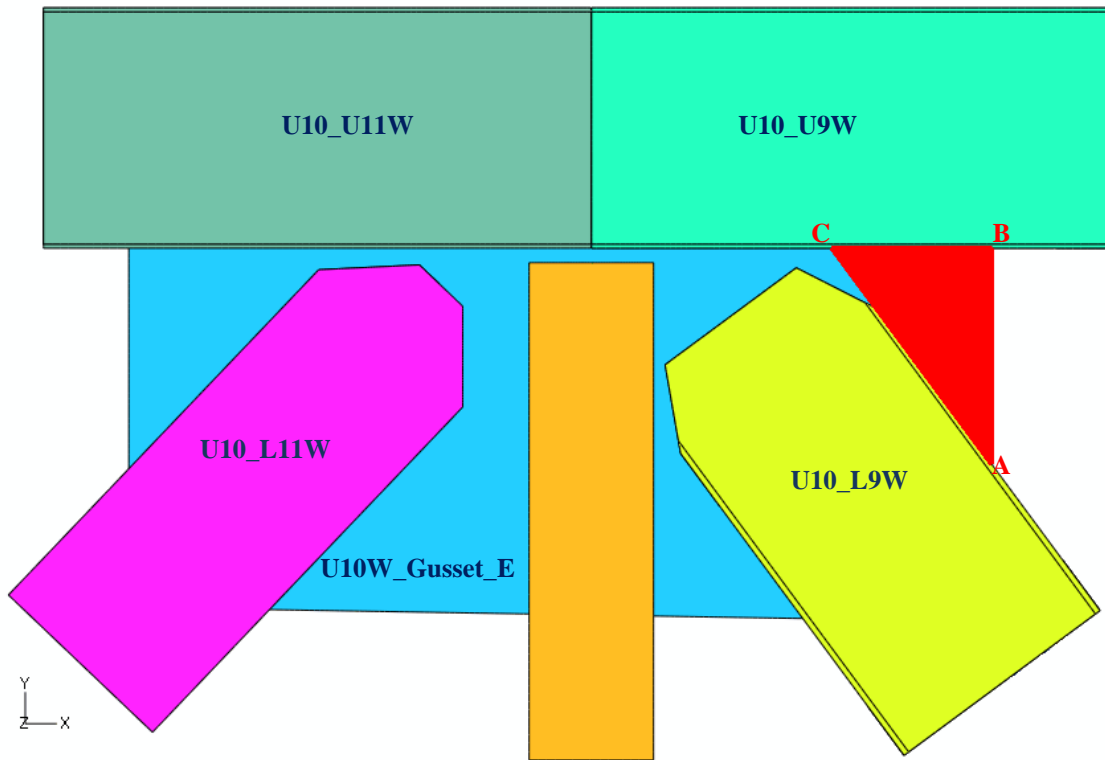
Figure 3.6: Initial bowing region of gusset plates at the U10W joint in the 3D local model
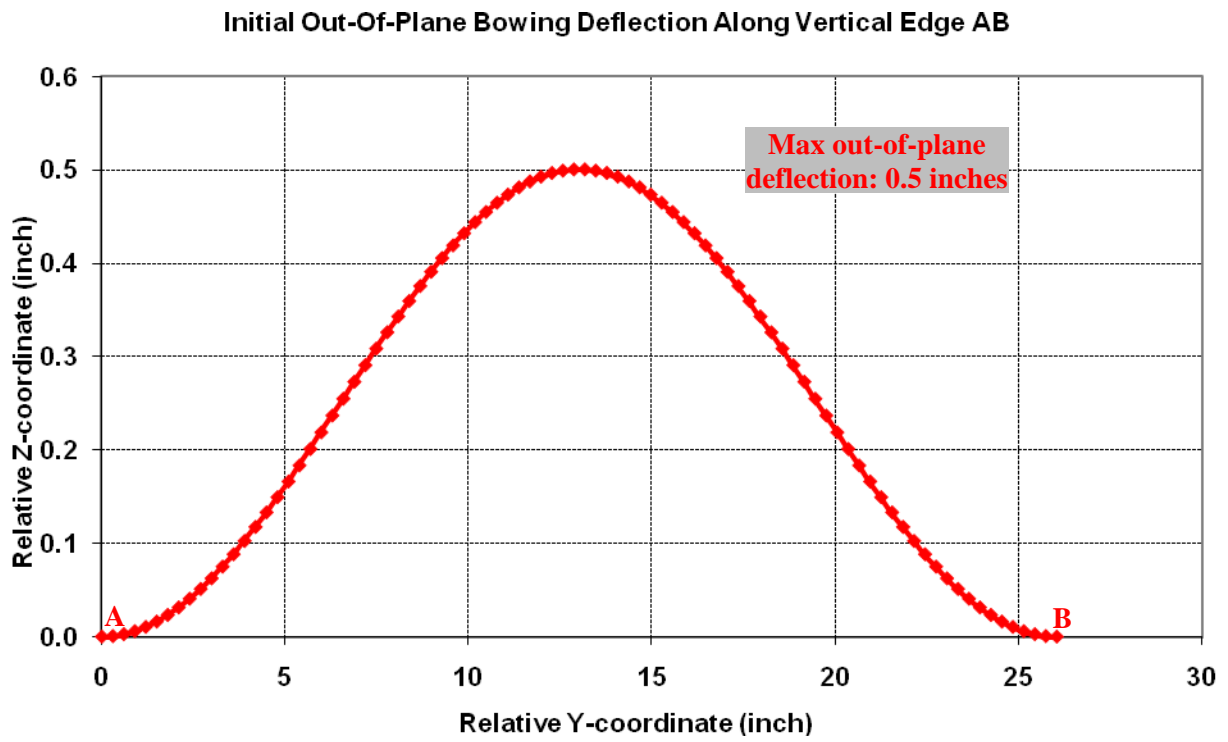
Figure 3.7: Initial out-of-plane bowing deflection along vertical edge AB at the U10W joint
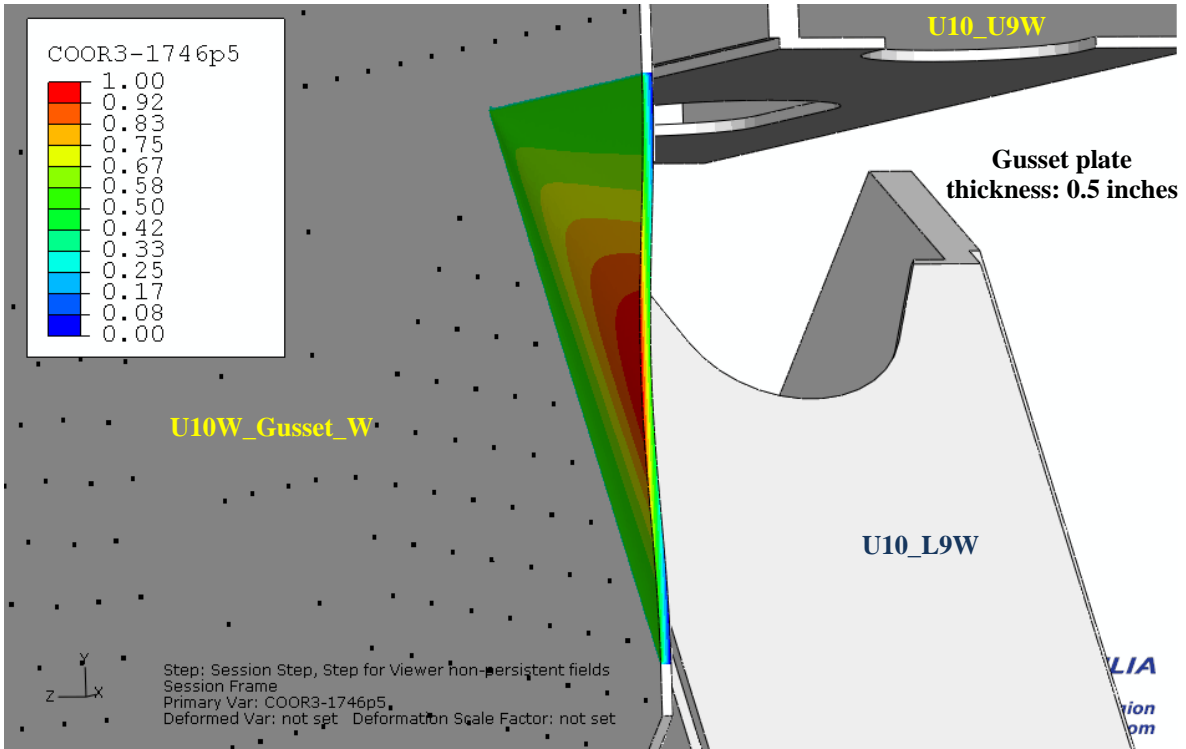
Figure 3.8: Initial relative Z-coordinates of bowed region at west gusset plate of the U10W joint
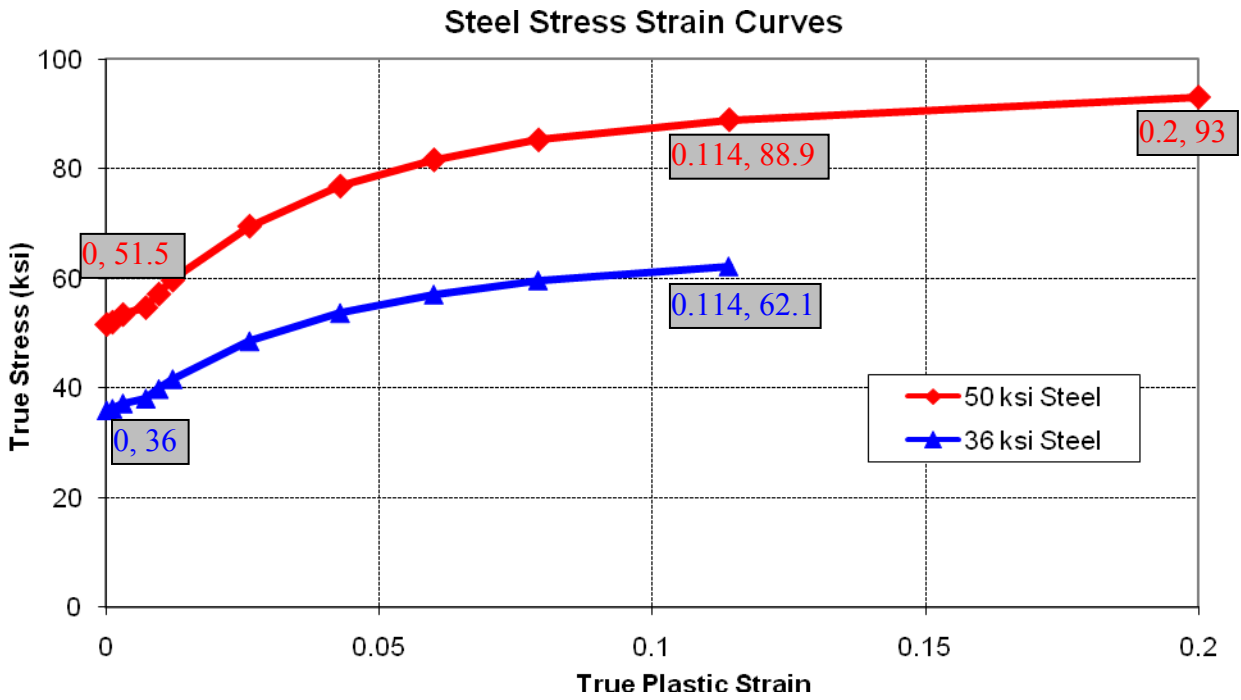
Figure 3.9: True stress-plastic strain curves of the steel used in the local model
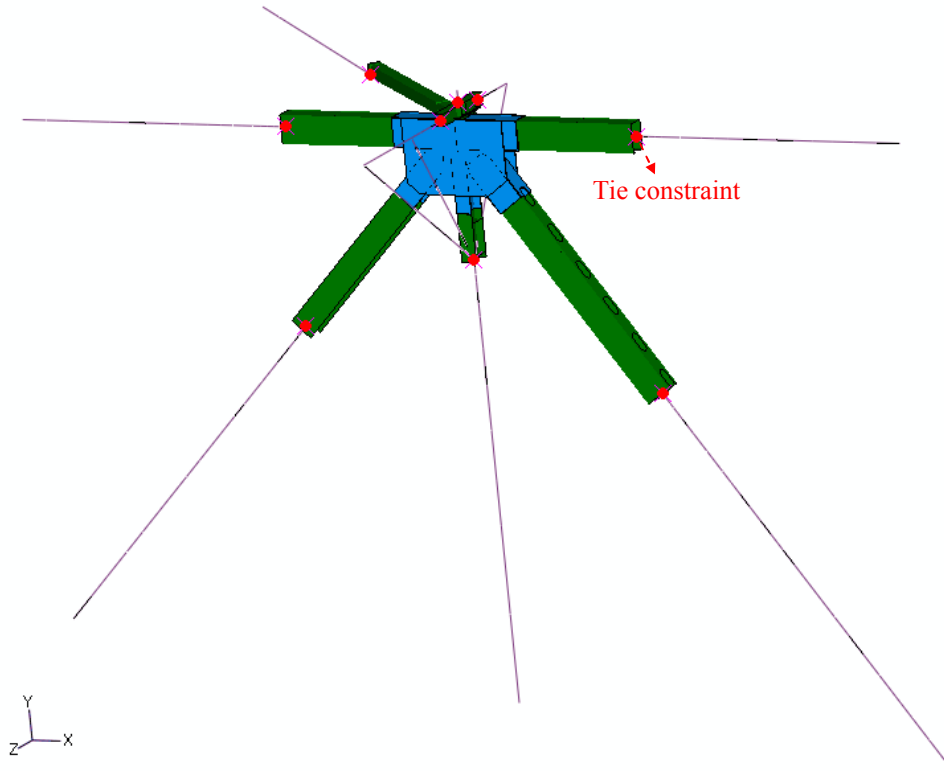
Figure 3.10: Nine tie constraints between reference points and beam nodes at the U10W joint
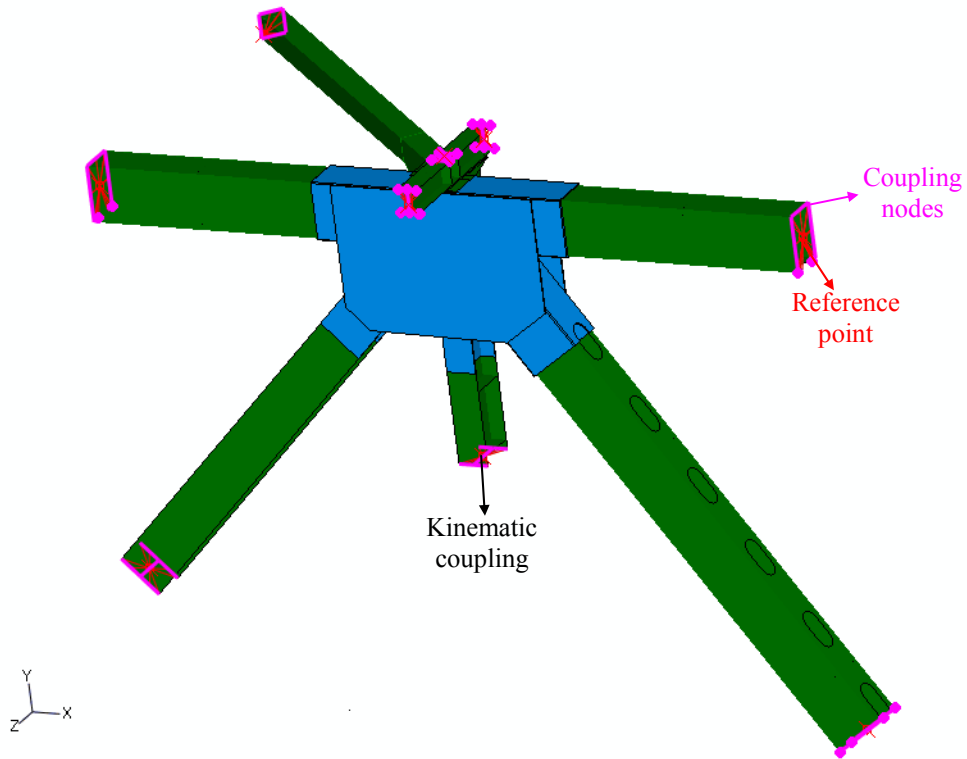
Figure 3.11: Nine couplings between the reference points and shell cut planes at the U10W joint
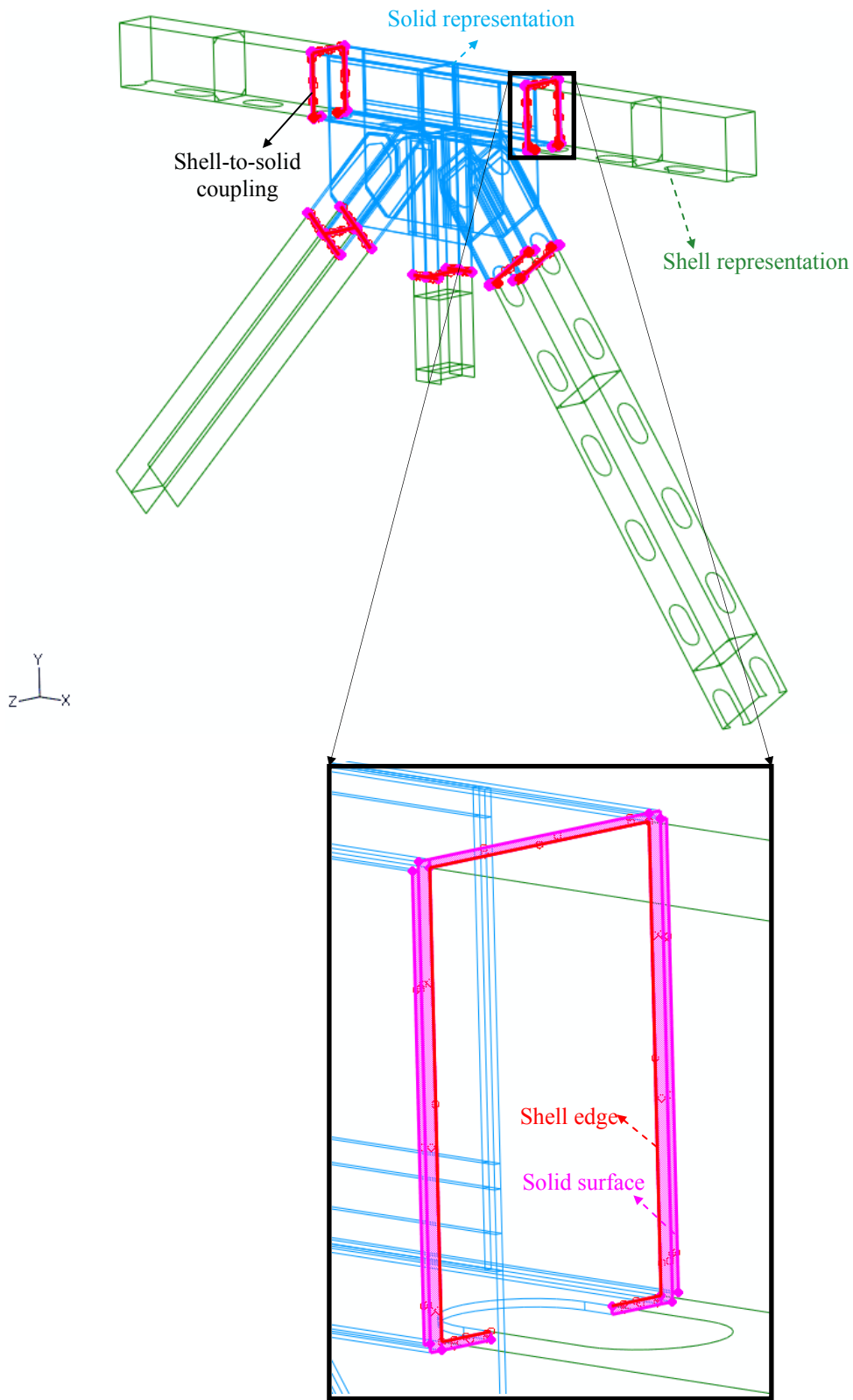
Figure 3.12: Five shell-to-solid couplings at the U10W joint
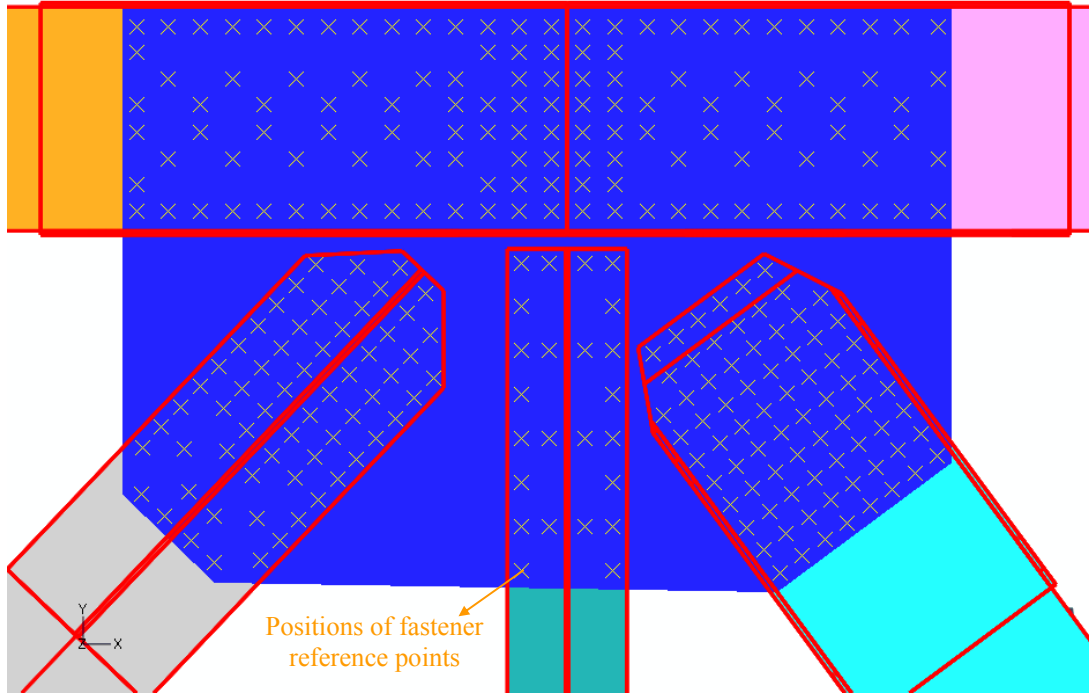
Figure 3.13: Reference points of fasteners related to vertical faces at the U10W joint
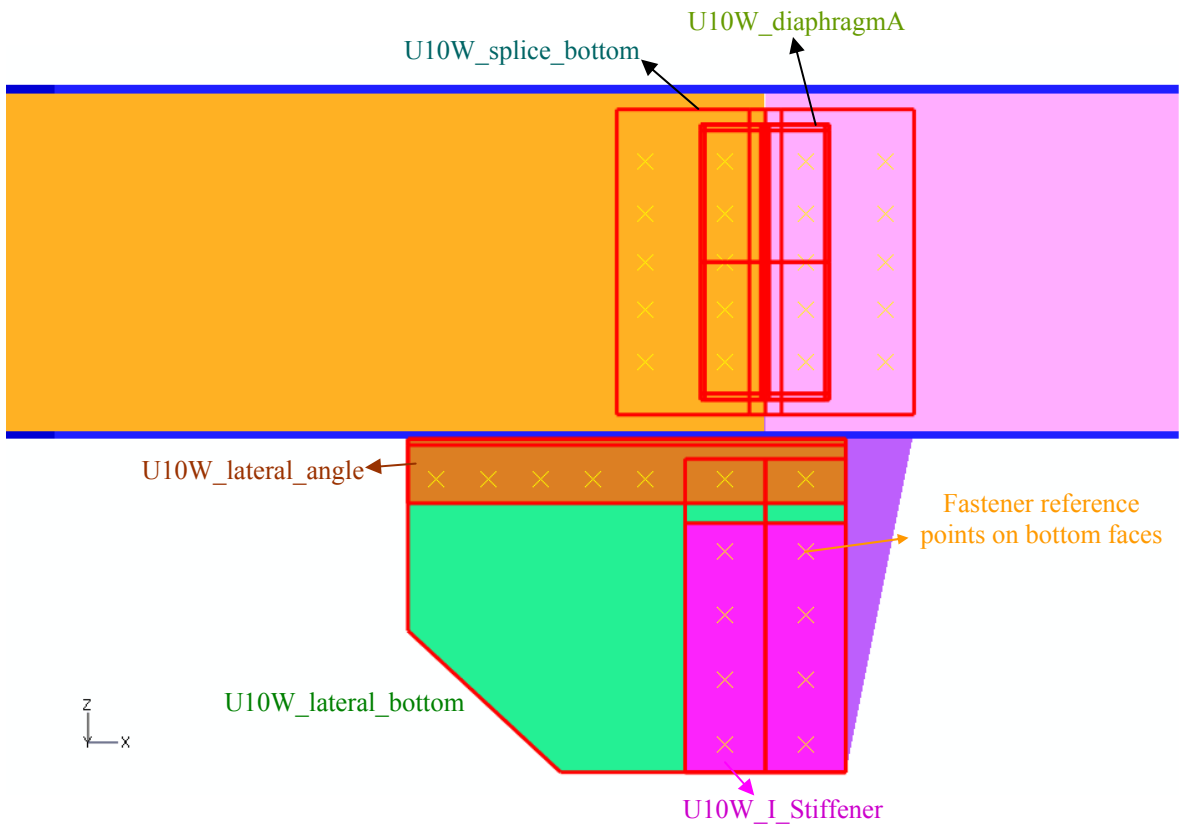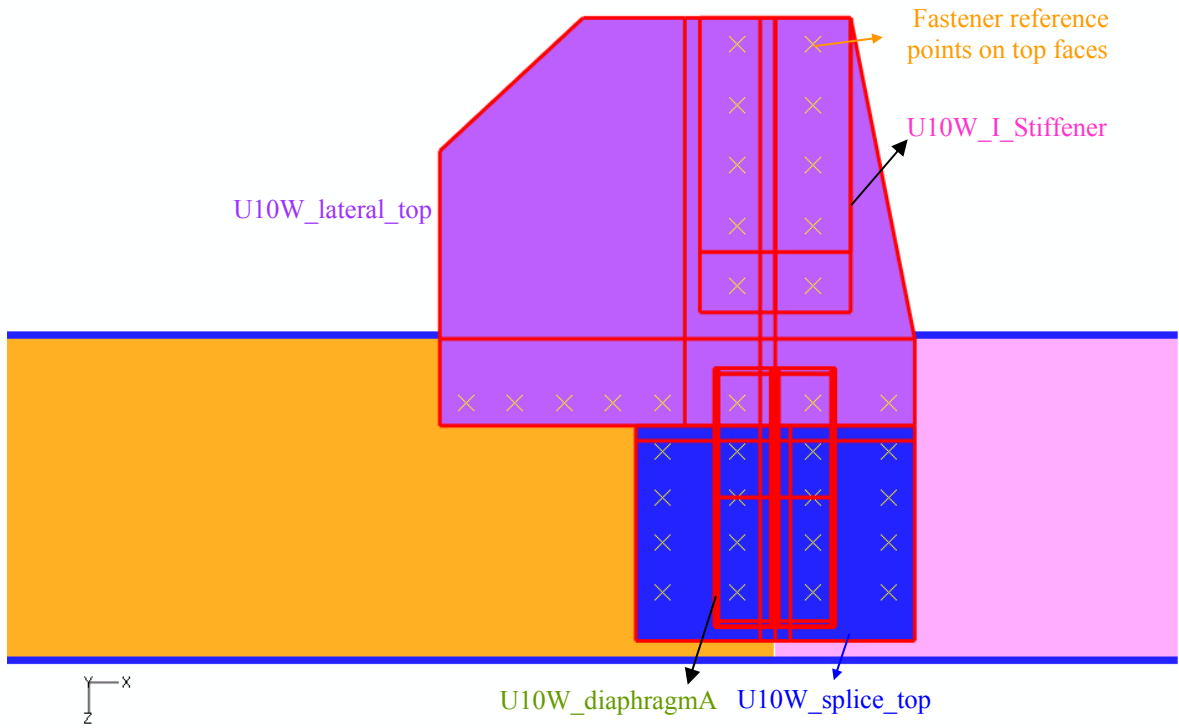
Figure 3.14: Reference points of fasteners related to horizontal faces at the U10W joint
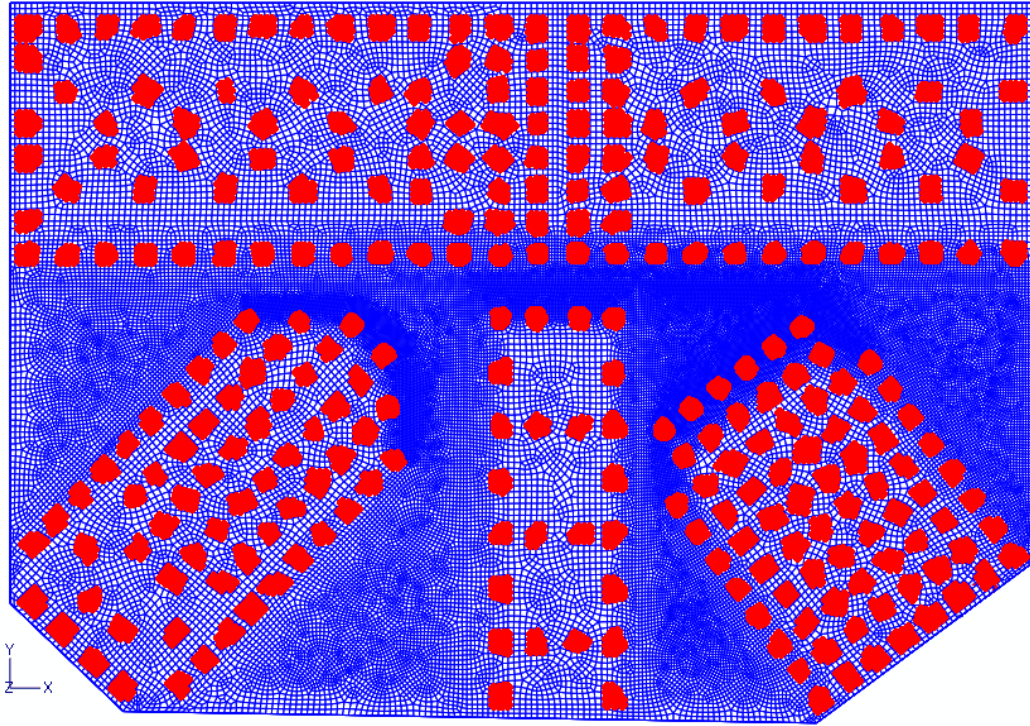
Figure 3.15: Fastened nodes of the west gusset plate at the U10W joint; 0.2 inch mesh
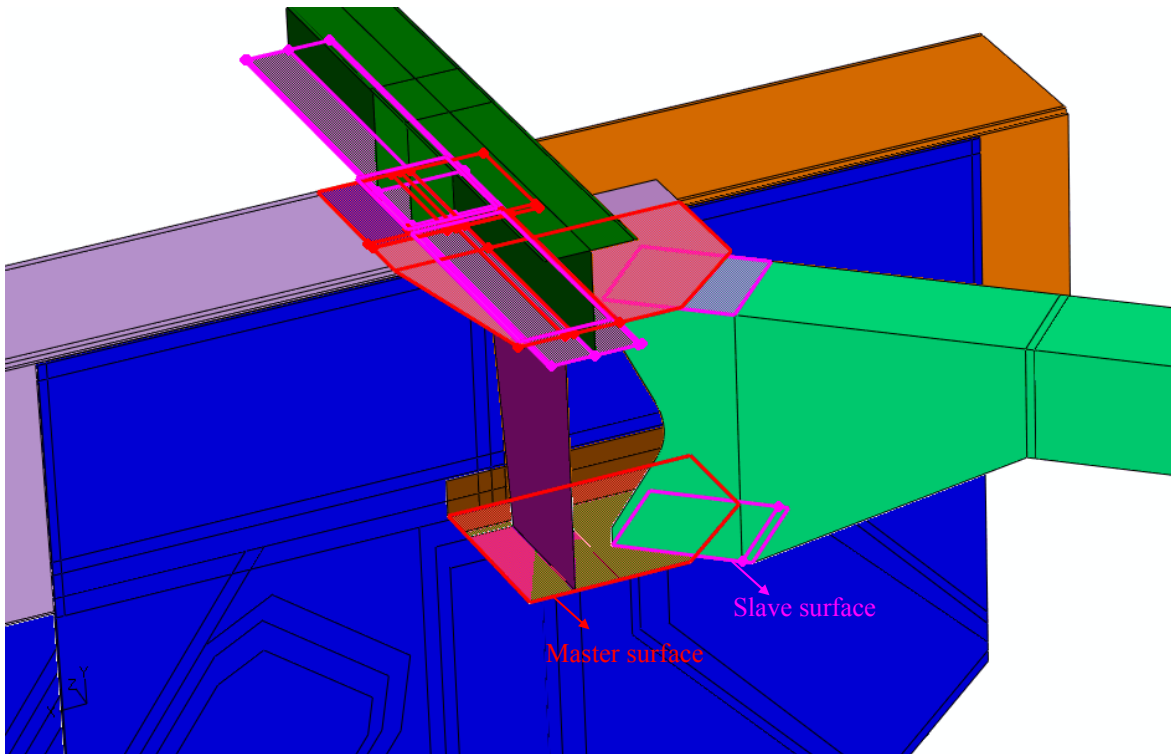
Figure 3.16: Surface-based tie constraints at the U10W joint

Slave surface

Master surface
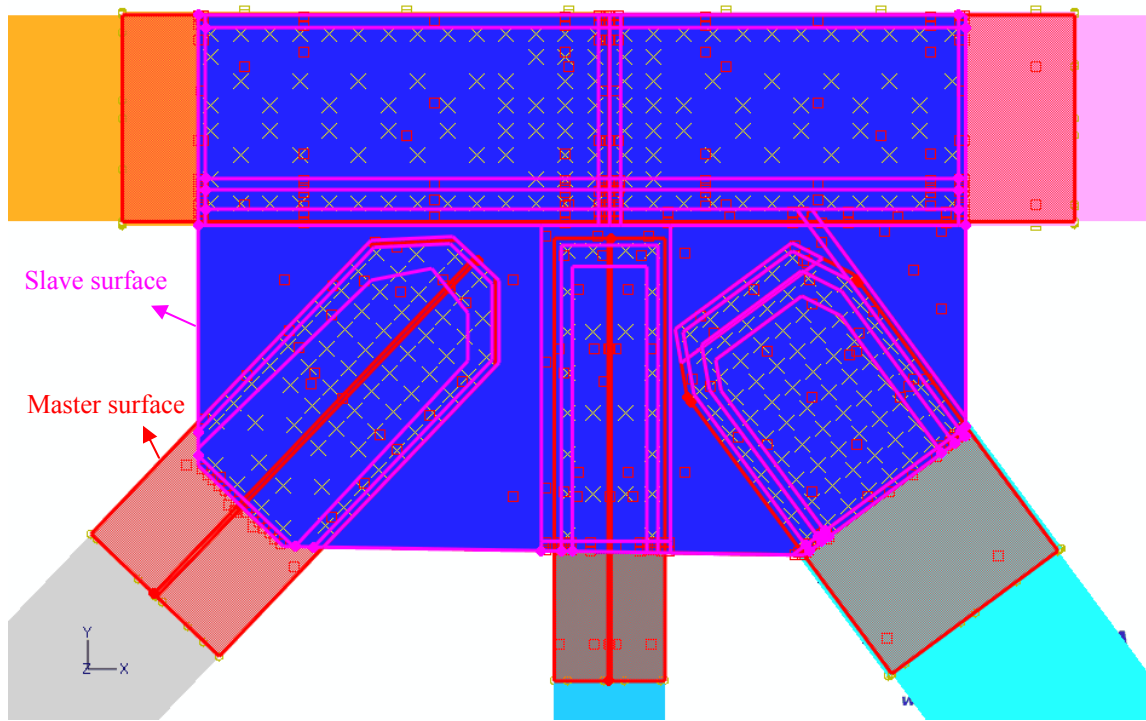
Figure 3.17: Contact pairs defined between gusset plates and five truss members at the U10W joint
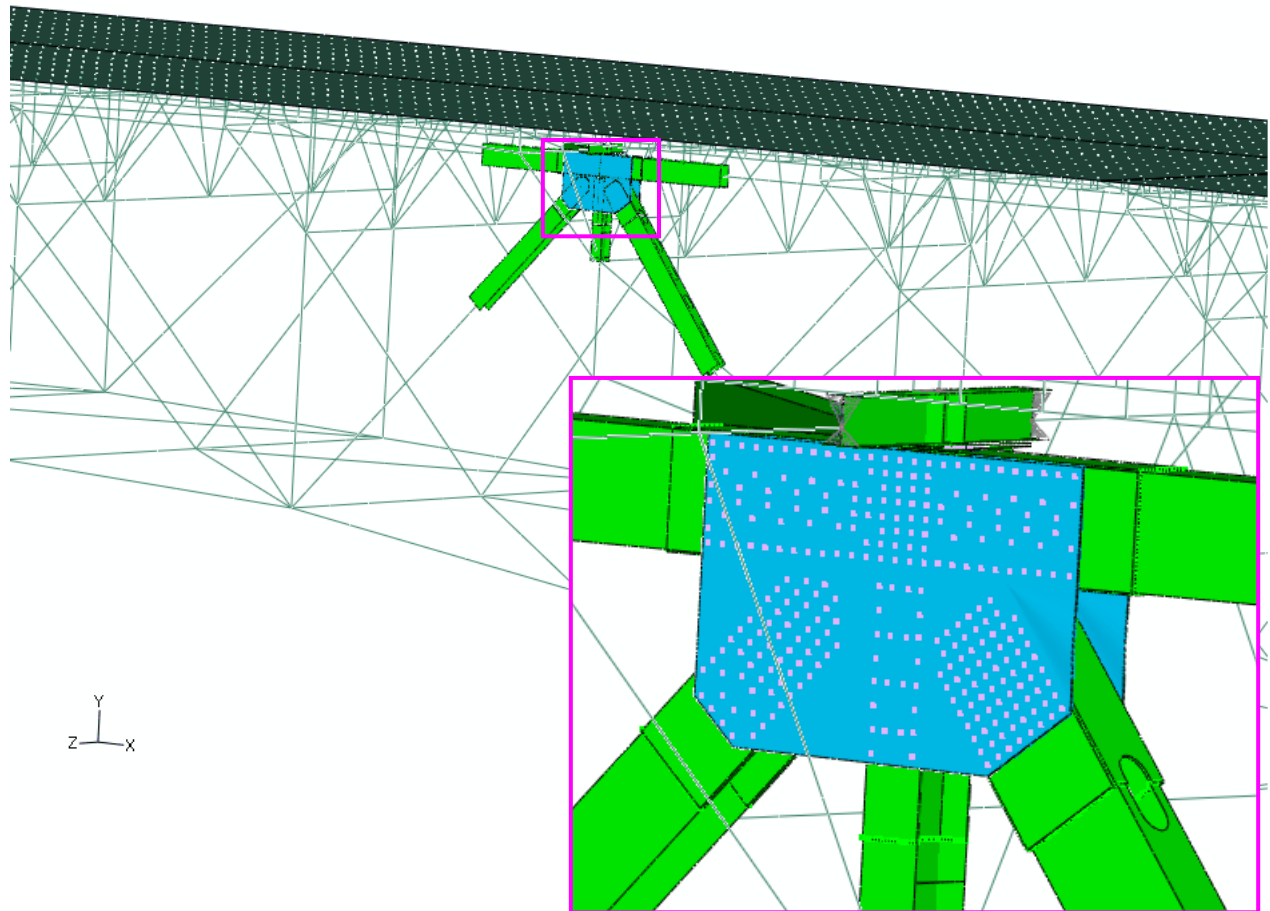
Figure 3.18: The U10W joint embedded in the FHWA structural element bridge model
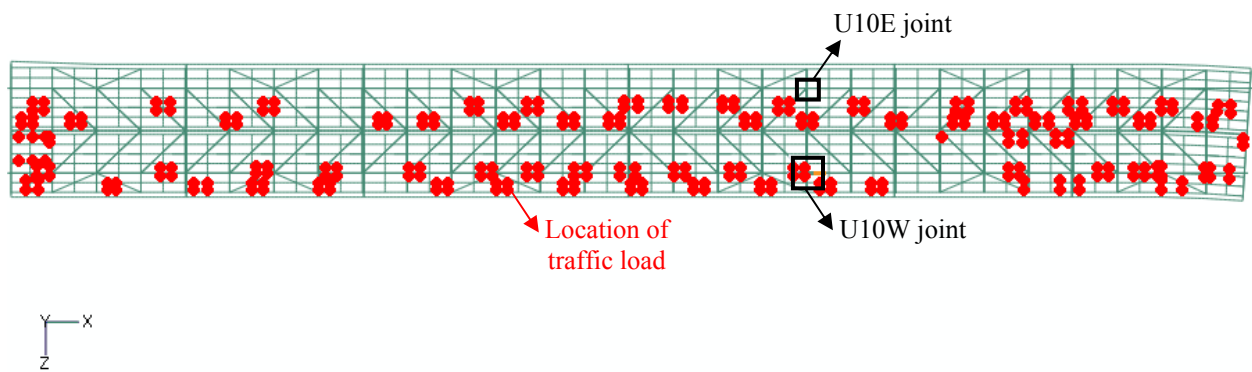
Figure 3.19: Location of traffic load at the time of collapse
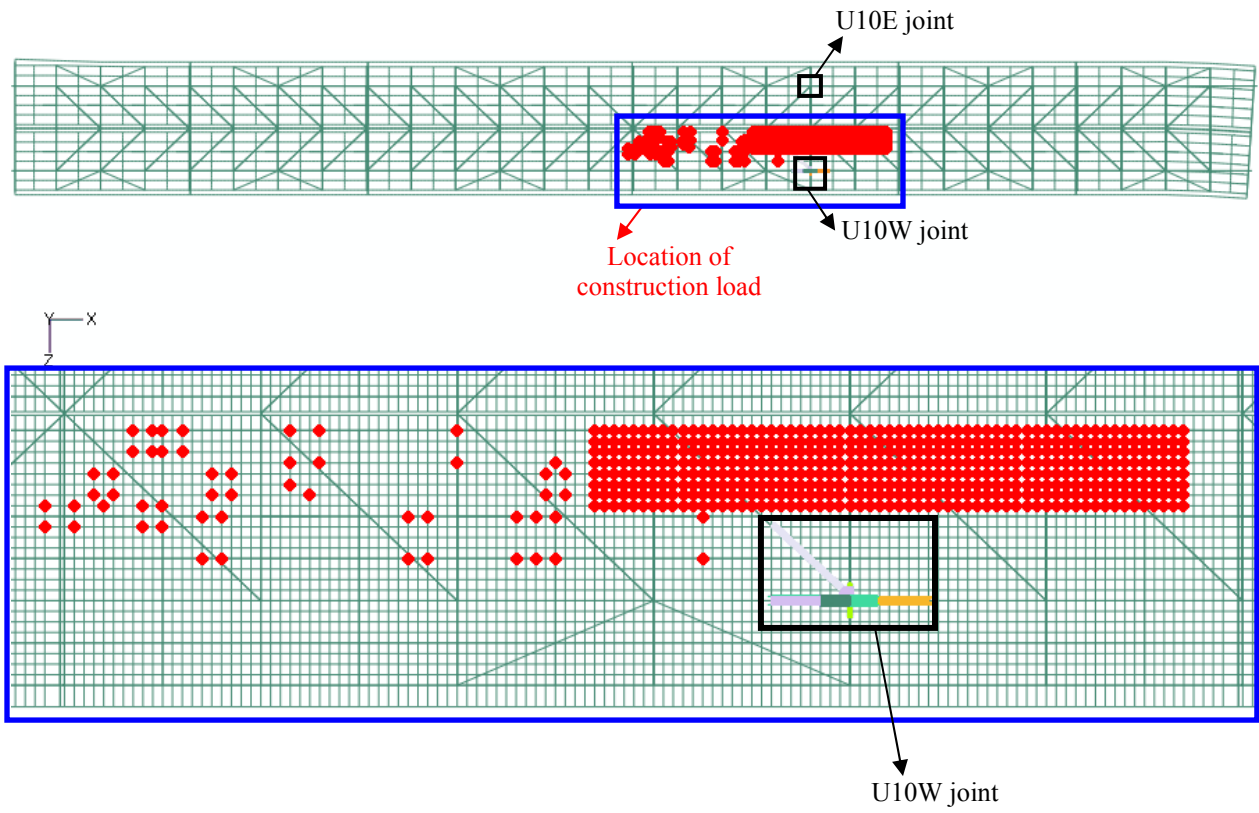
Figure 3.20: Location of construction materials and vehicles at the time of collapse

Report No. Gusset
bowing

Figure 3.
U10 WEST

URS 1st
June 2003
Disk 5
DSK5-03S.JPG

JUN 10 2003

ImageNo:0801A00472, Project No:2008010010

**Predicted: Prior to
construction load**

B

Westward bow: bowing
away from bridge

A

Step: TrafficLoad, Add the known traffic loads at the time of collapse
Increment   7: Step Time =   1.000

Deformed Var: U   Deformation Scale Factor: +1.0000e+00
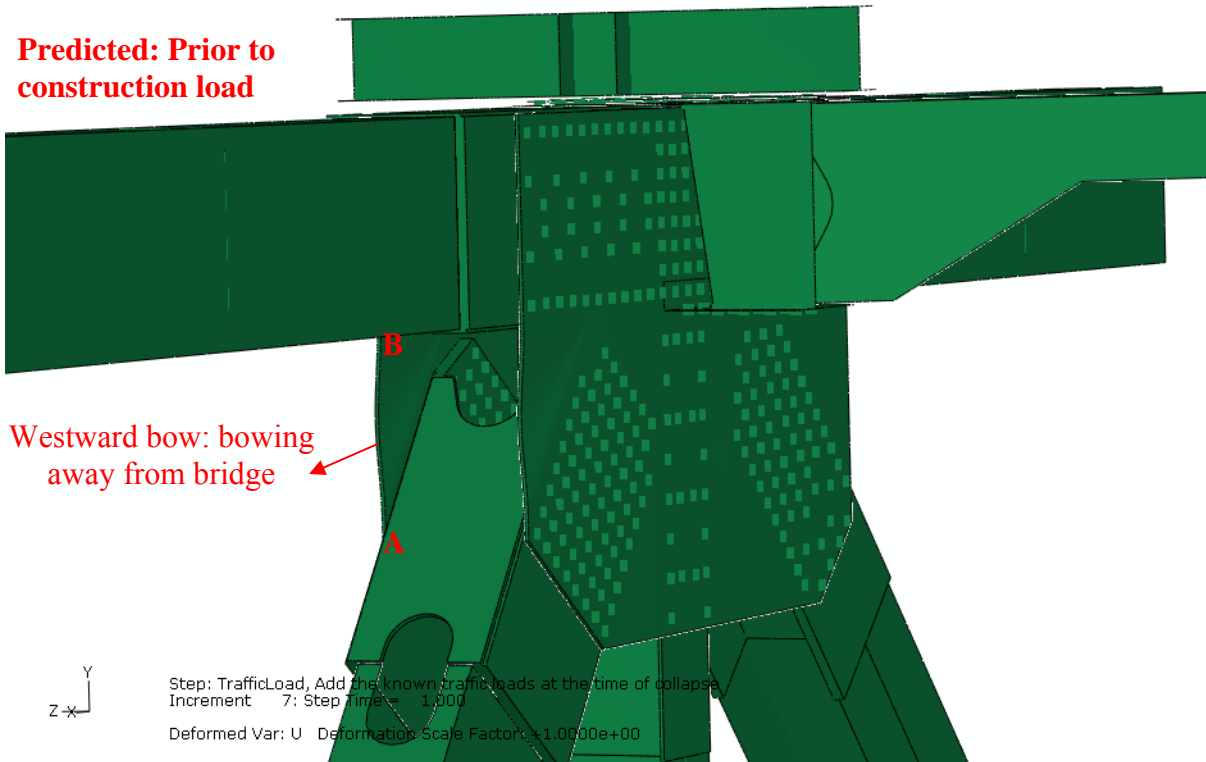
Figure 3.21: Visual comparison of bowed gusset plates observed at the U10W joint and predicted
gusset plates prior to construction load with load condition A1
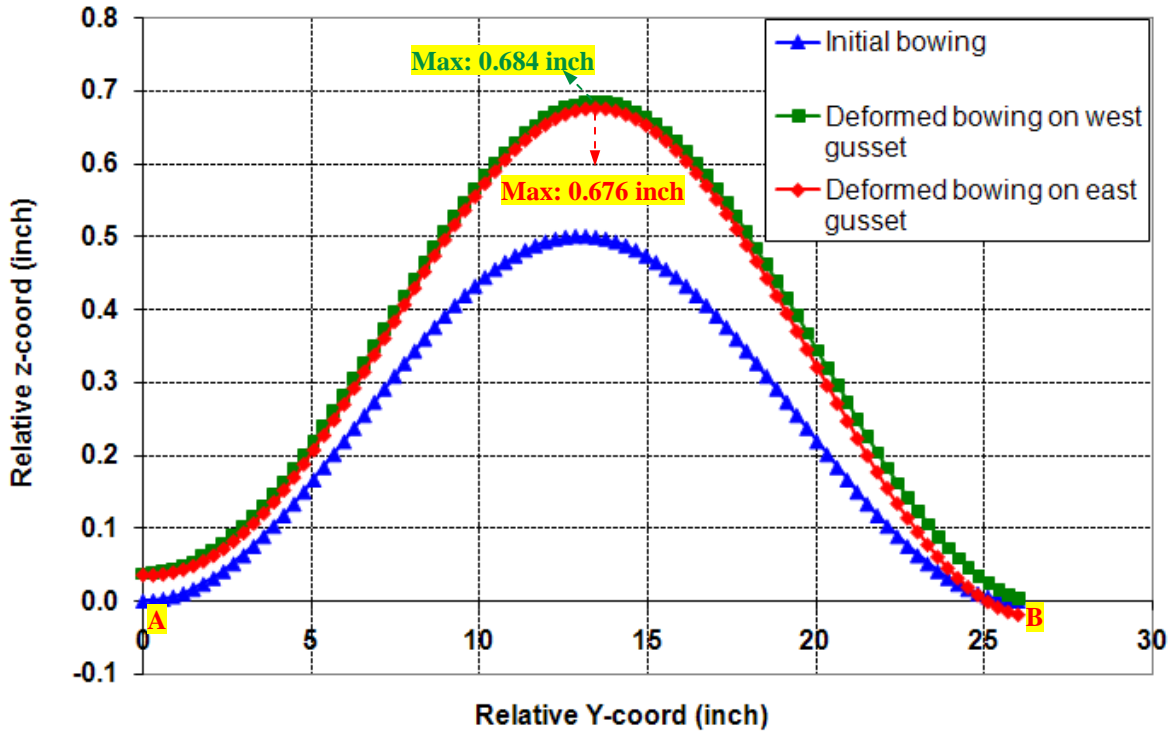
Figure 3.22: Deformed bowing edges prior to applying construction load at the U10W joint with load condition A1
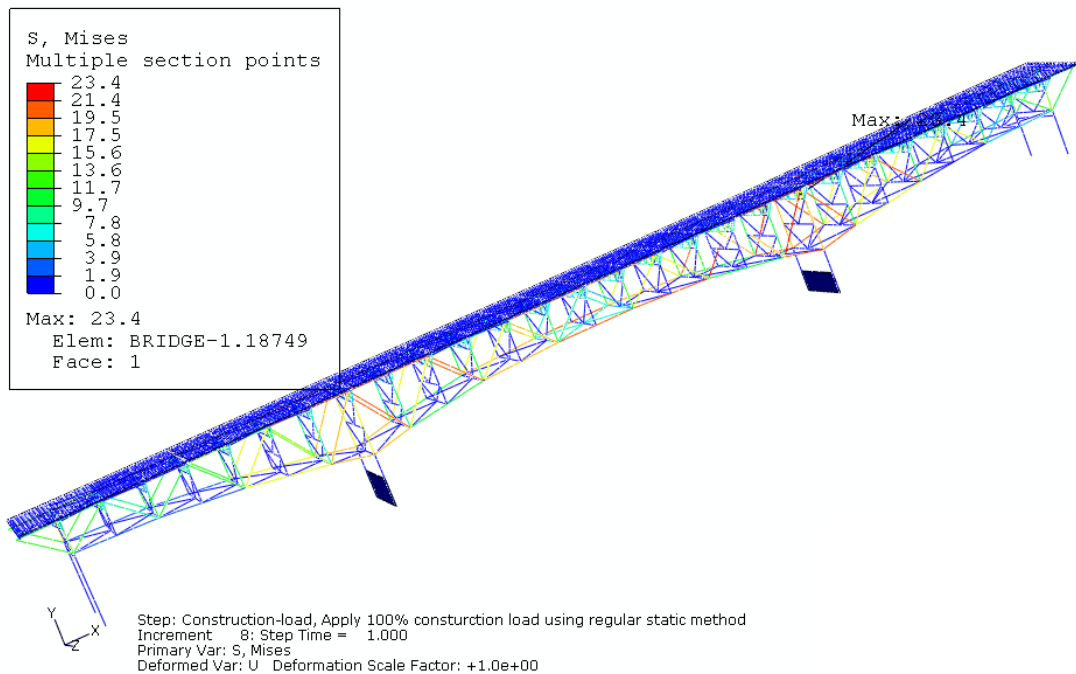
Figure 3.23: Von Mises stress distribution under estimated construction load in mixed model when embedding U10W local model with load condition A1; The U10W local model is not included in this figure.
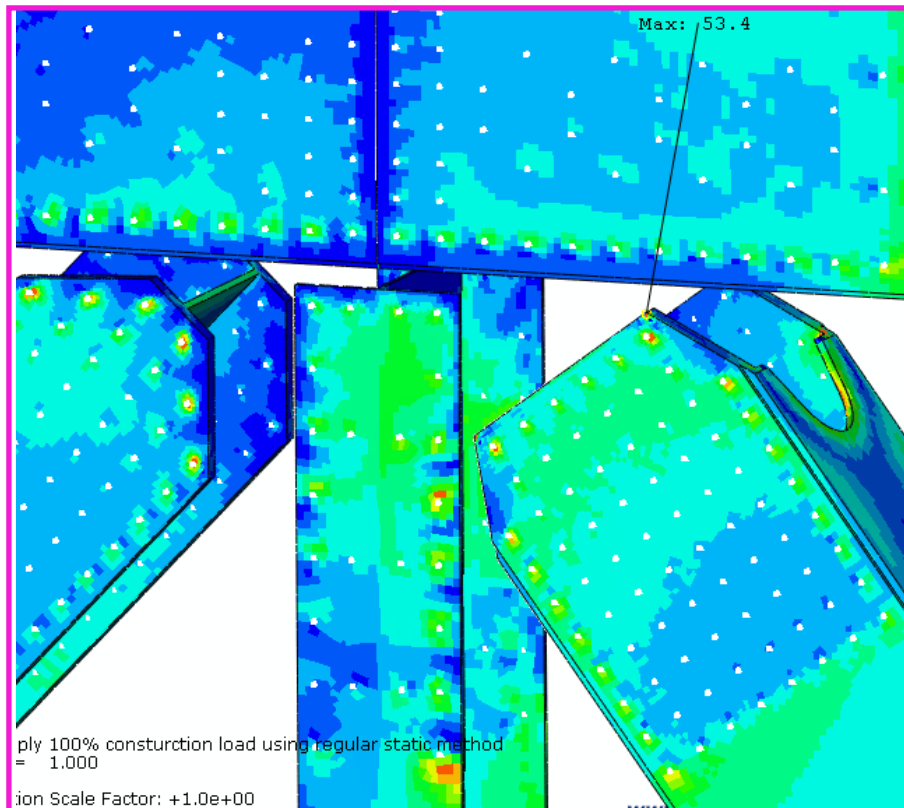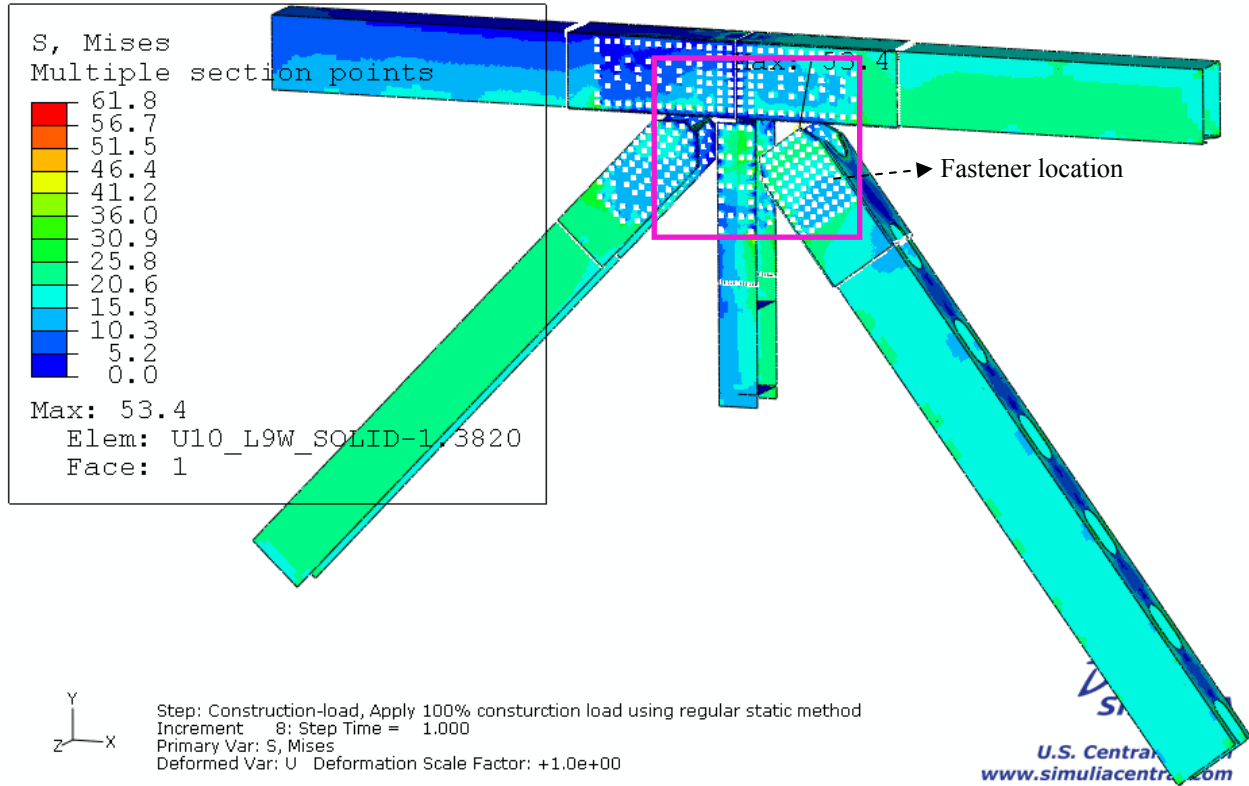
Figure 3.24: Von Mises stress distribution under estimated construction load in the five main truss members at the U10W joint with load condition A1
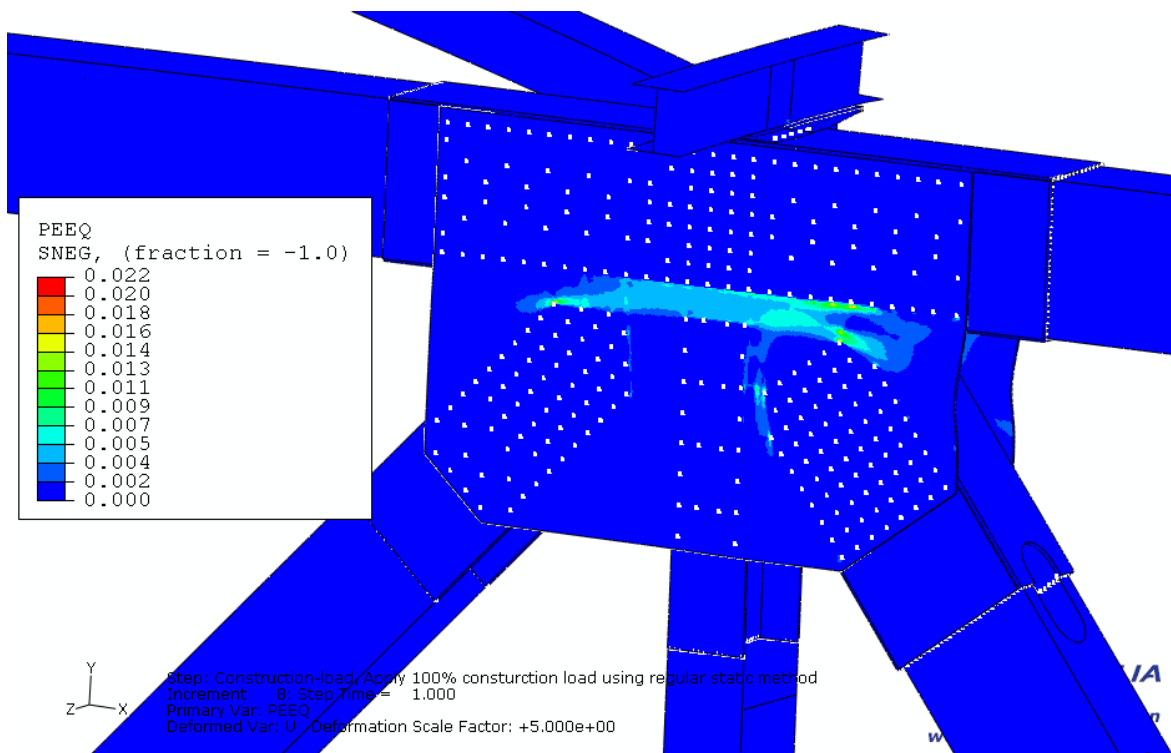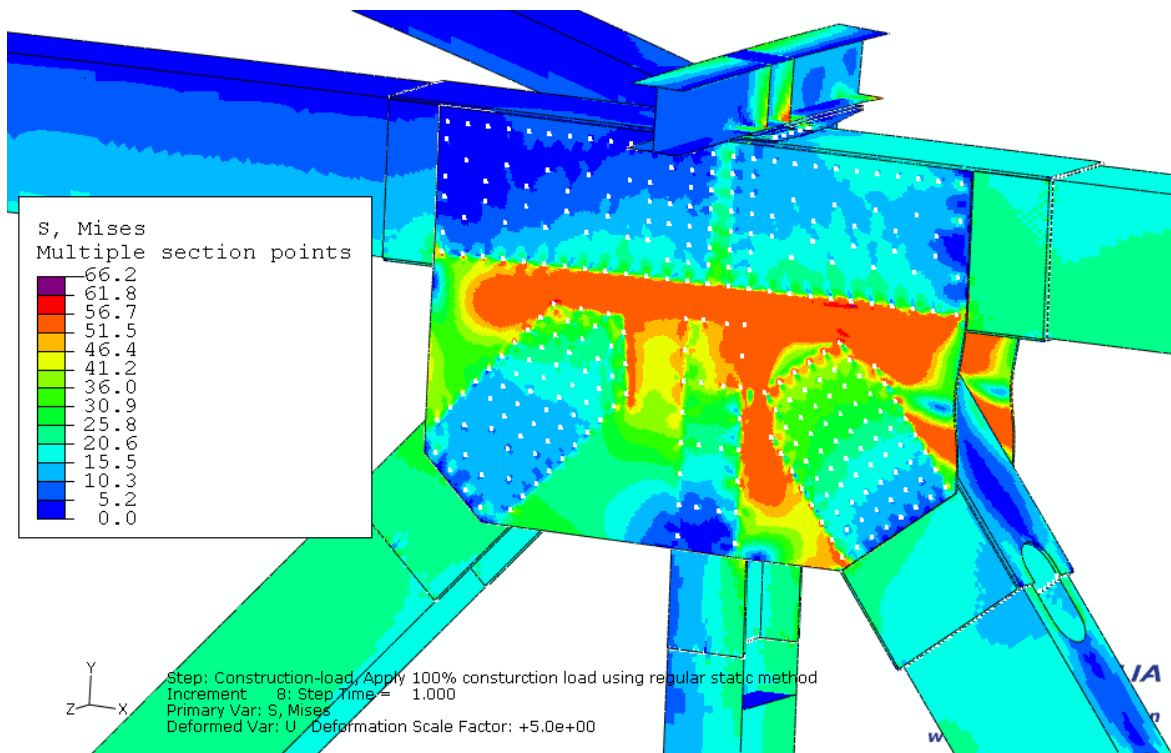
Figure 3.25: Von Mises stress and equivalent plastic strain (PEEQ) distribution under estimated construction load at the U10W joint with load condition A1 (deformation magnified 5x)
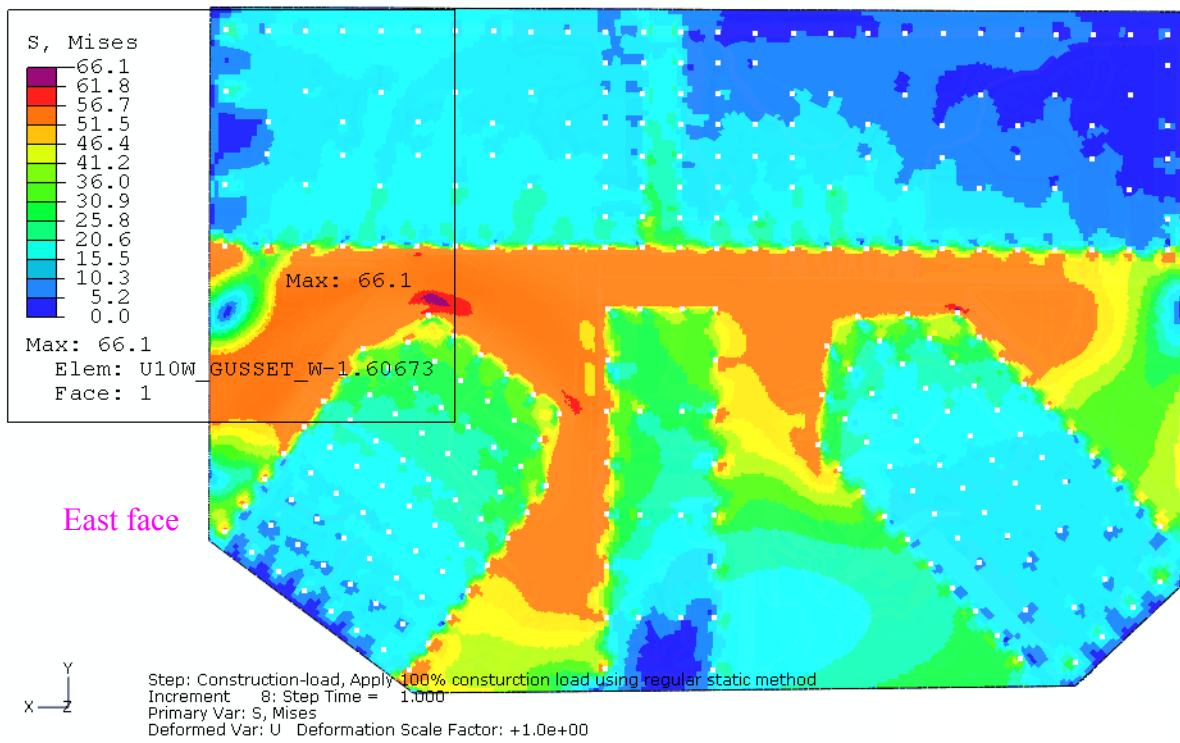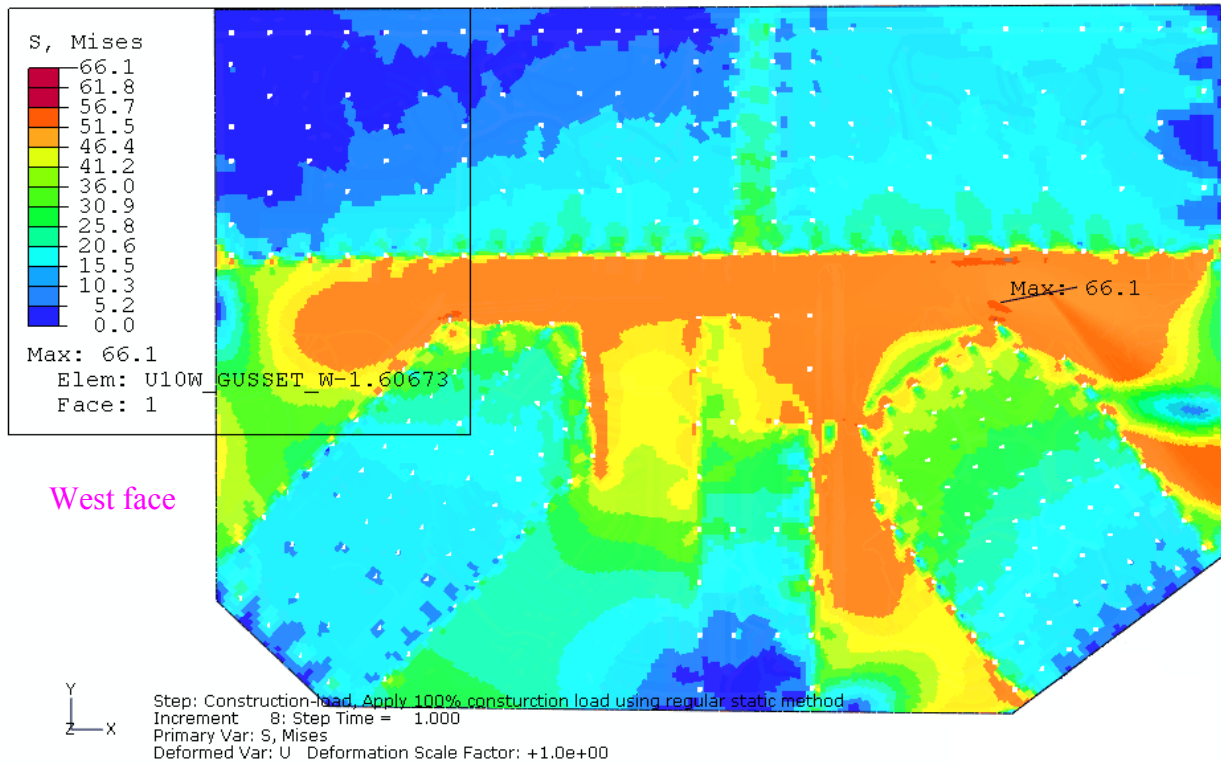
Figure 3.26: Von Mises stress distribution under estimated construction load in the west gusset at the U10W joint with load condition A1
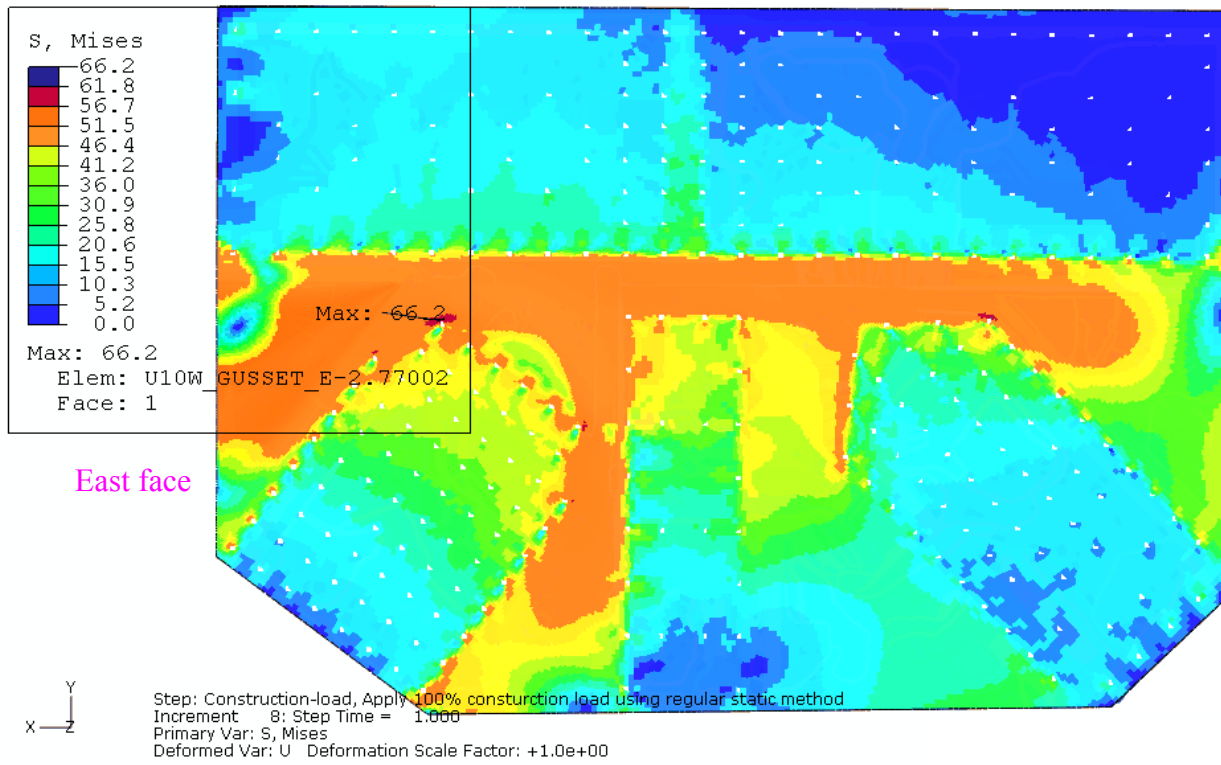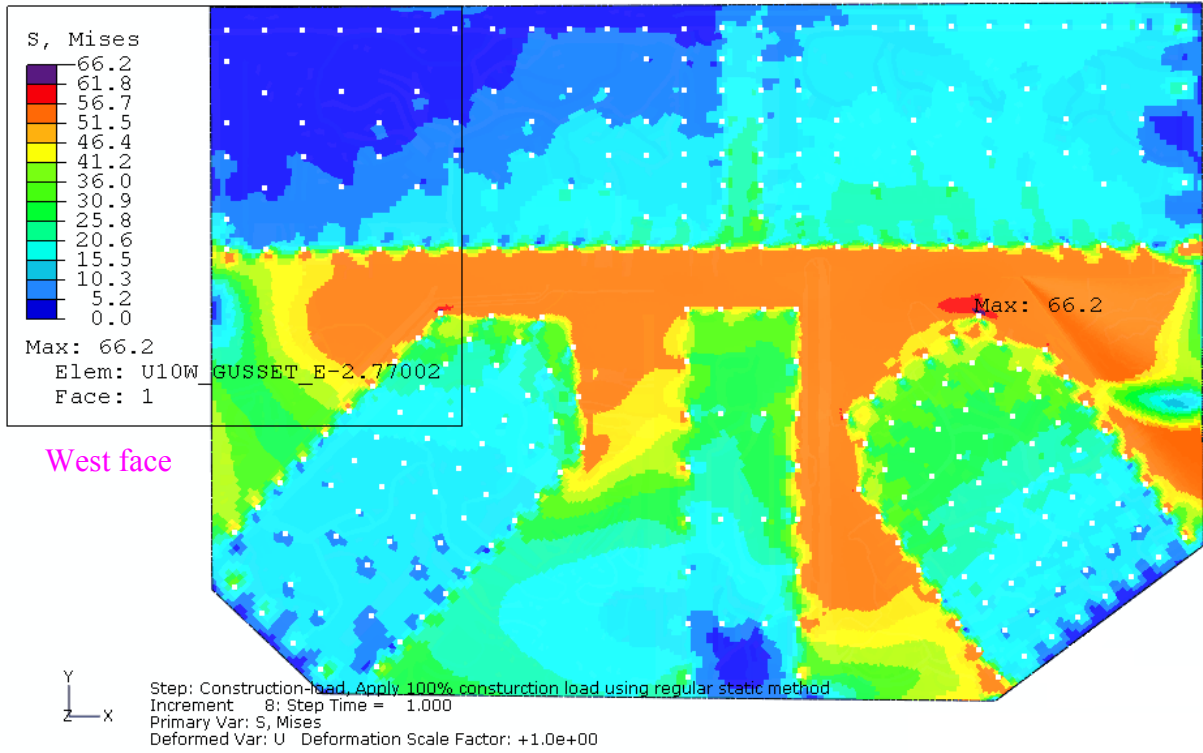
Figure 3.27: Von Mises stress distribution under estimated construction load in the east gusset at the U10W joint with load condition A1
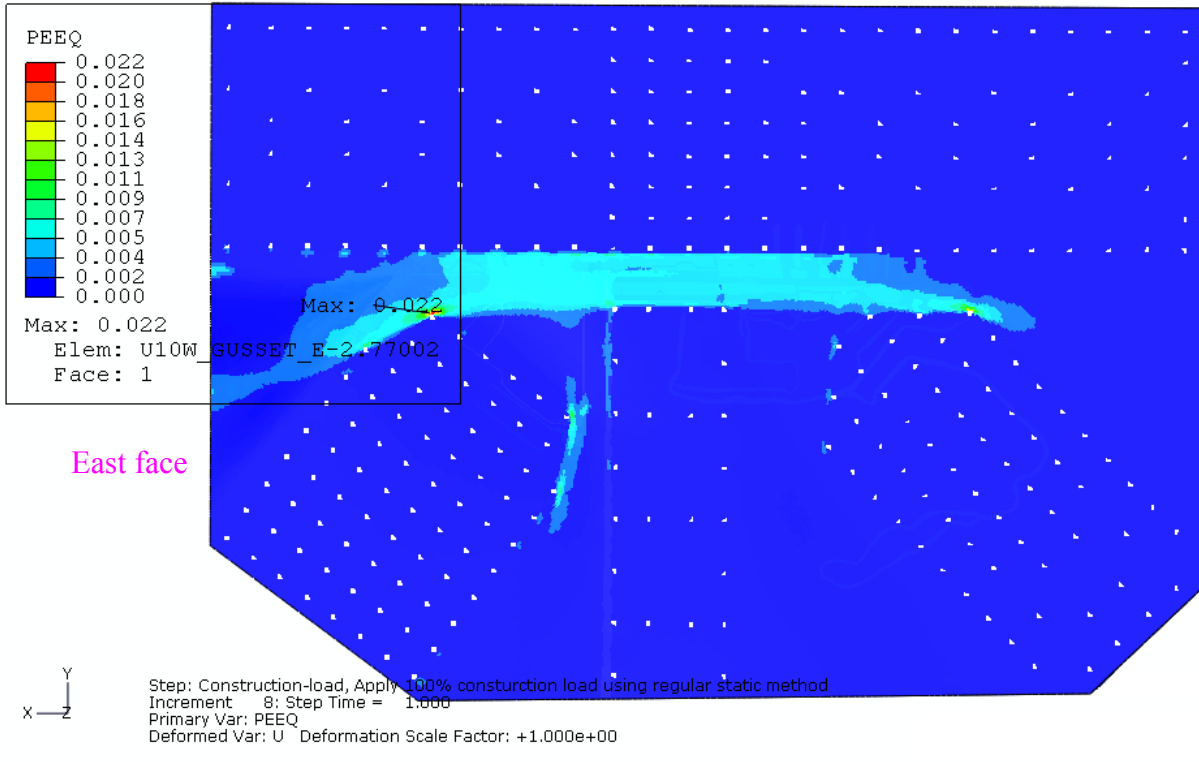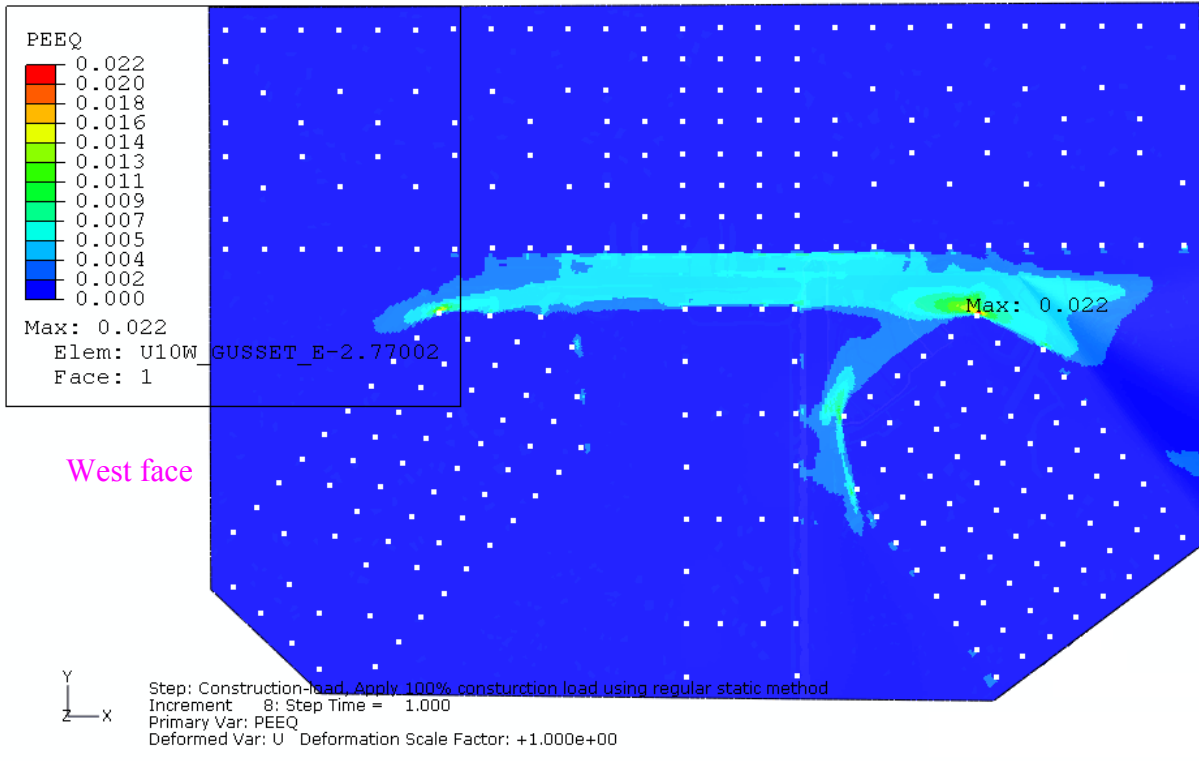
Figure 3.28: Equivalent plastic strain (PEEQ) distribution under estimated construction load in the east gusset at the U10W joint with load condition A1
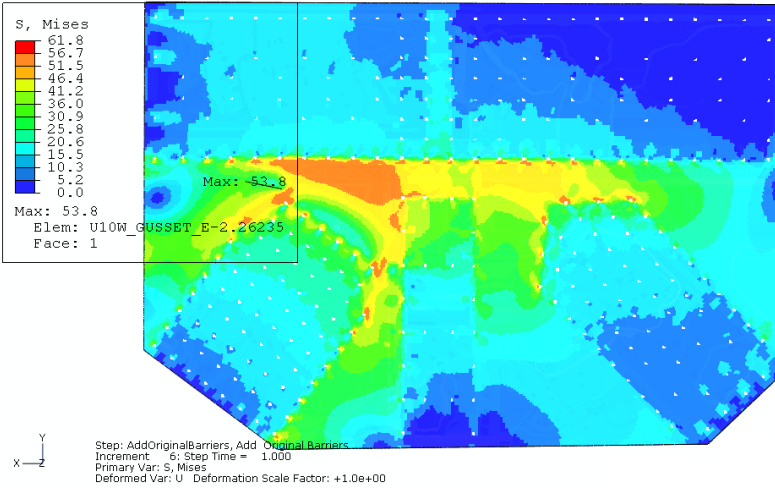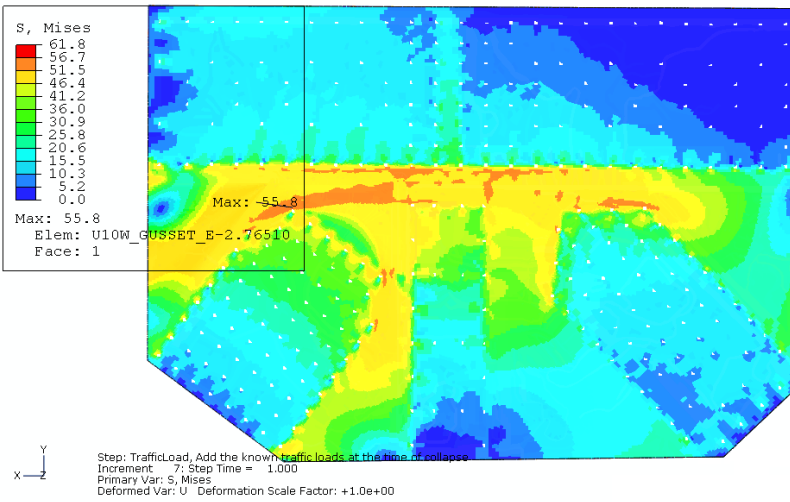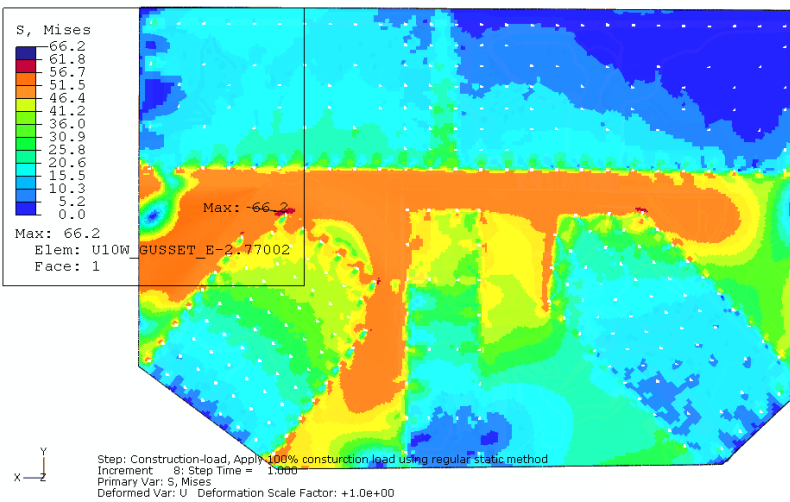
Figure 3.29: Von Mises stress evolution on the east face of the east gusset at the U10W joint
with load condition A1

S, Mises

61.8
56.7
51.5
46.4
41.2
36.0
30.9
25.8
20.6
15.5
10.3
5.2
0.0

Max: 57.6
Max: 57.6
Elem: U10W_GUSSET_E-2.76510
Face: 1

Step: NewBarriersAndConcreteThickness, New Barriers And Concrete Thickness
Increment   6: Step Time =   1.000
Primary Var: S, Mises
Deformed Var: U   Deformation Scale Factor: +1.0e+00

S, Mises

61.8
56.7
51.5
46.4
41.2
36.0
30.9
25.8
20.6
15.5
10.3
5.2
0.0

Cut through the plane
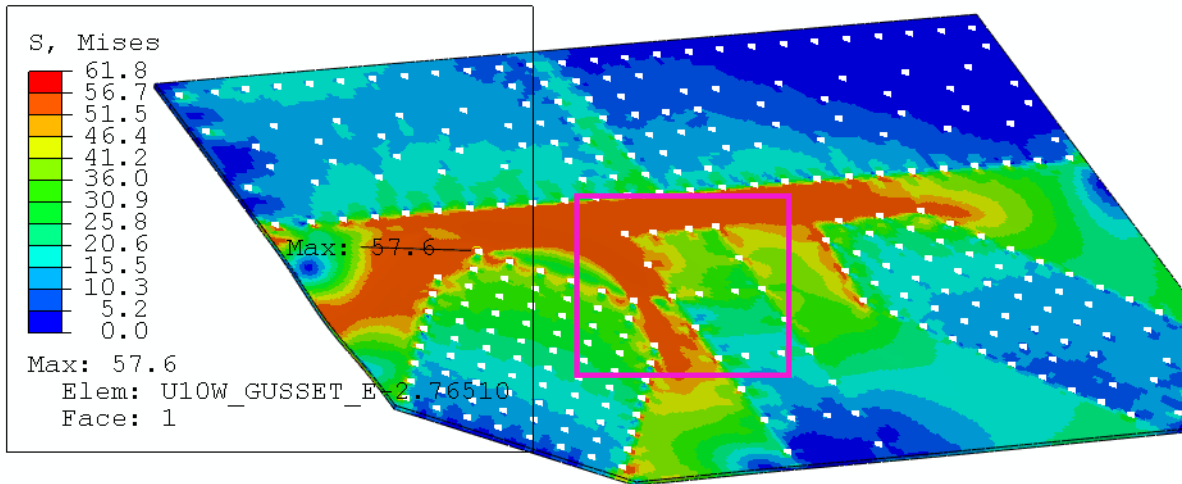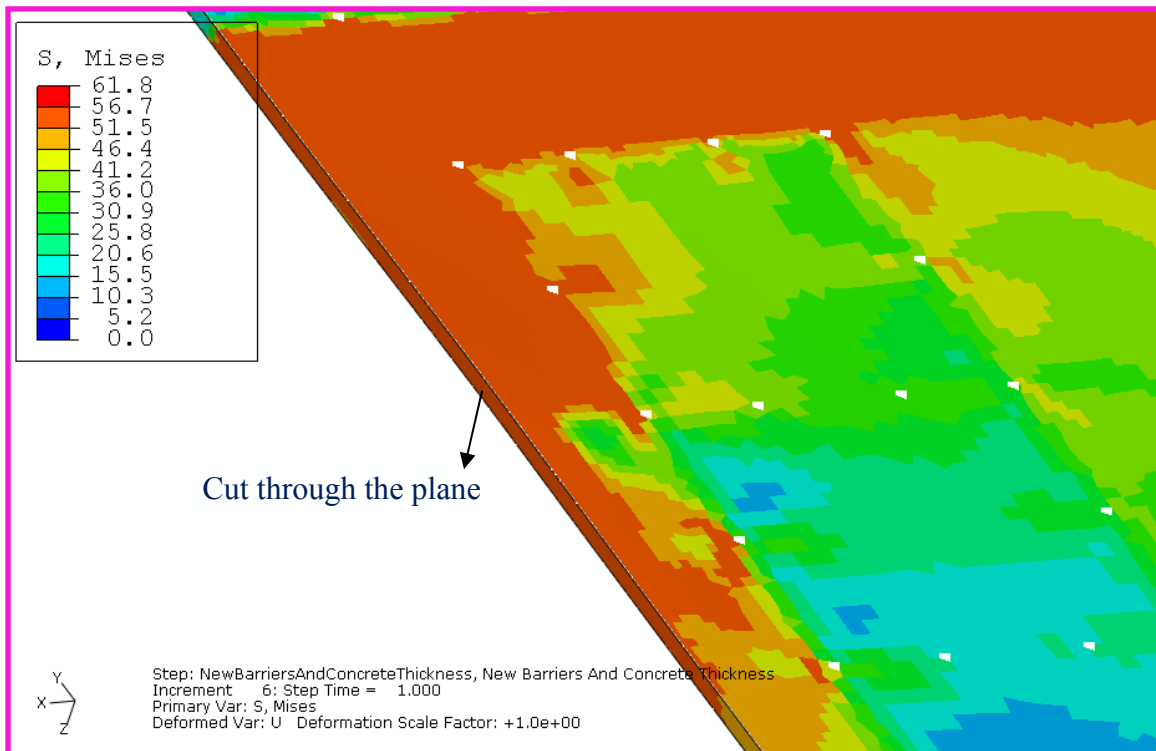
Step: NewBarriersAndConcreteThickness, New Barriers And Concrete Thickness
Increment   6: Step Time =   1.000
Primary Var: S, Mises
Deformed Var: U   Deformation Scale Factor: +1.0e+00

Figure 3.30: Von Mises stress distribution through thickness in the east gusset at the U10W joint under additional concrete weight from added deck and barriers with load condition A1

- 67 -
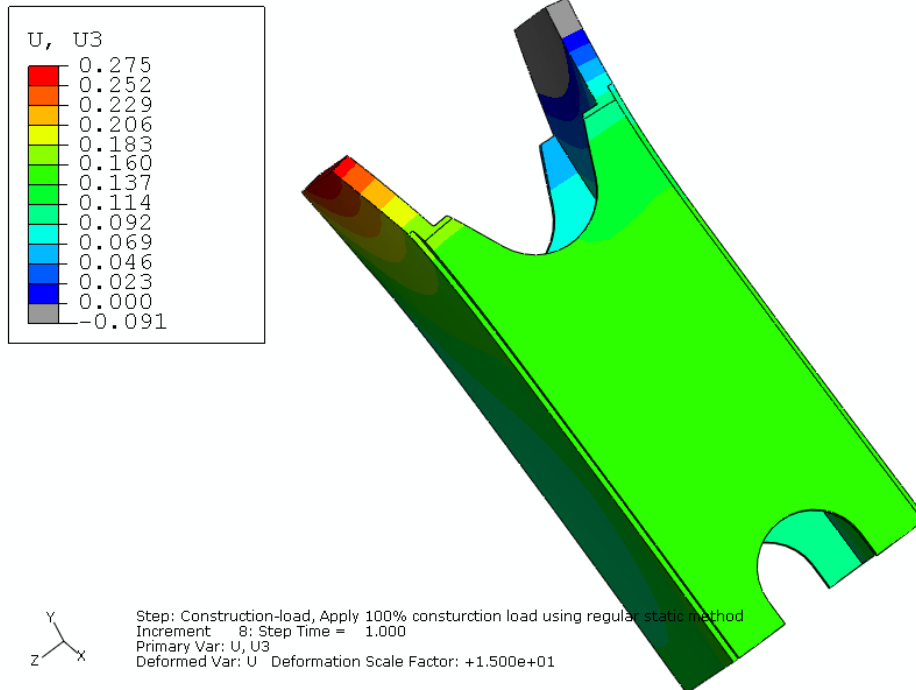
Figure 3.31: Out-of-plane displacement of diagonal truss member U10_L9W at the U10W joint under estimated construction load with load condition A1 (deformation magnified 15x)
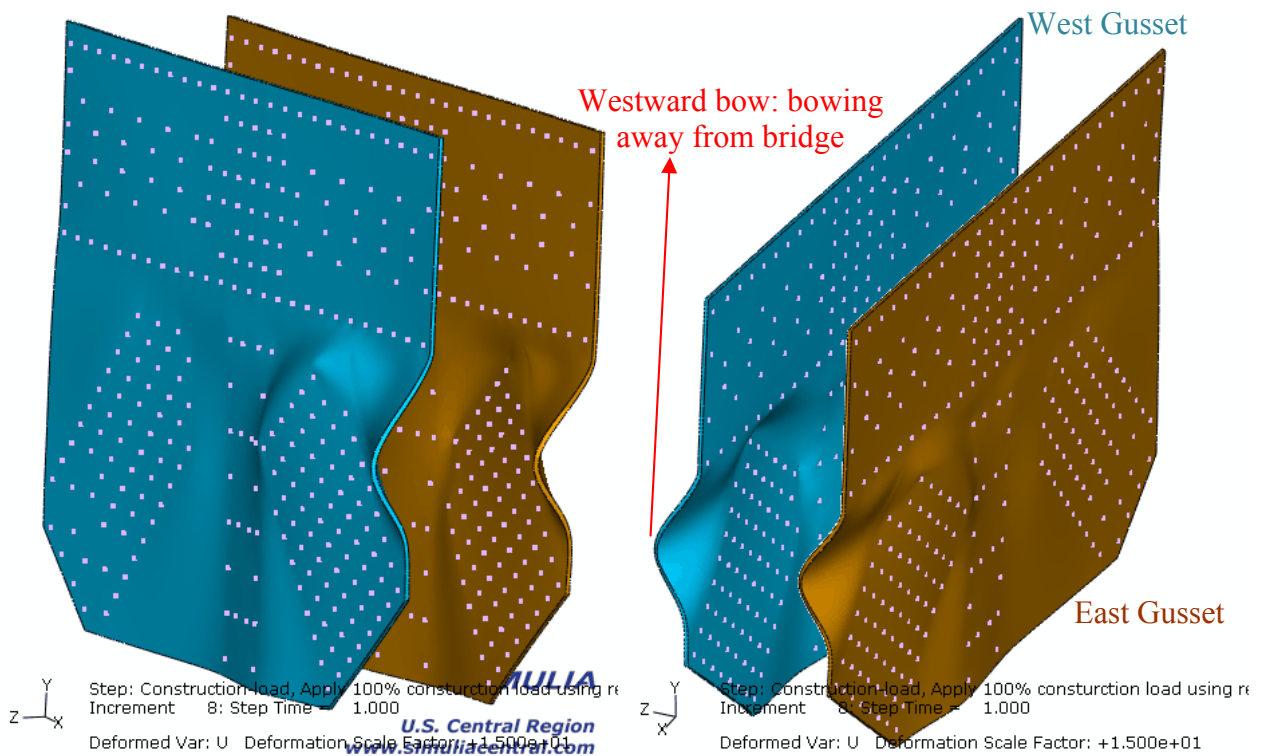
Figure 3.32: Deformed shape of the gusset plates at the U10W joint under estimated construction load with load condition A1 (deformation magnified 15x)
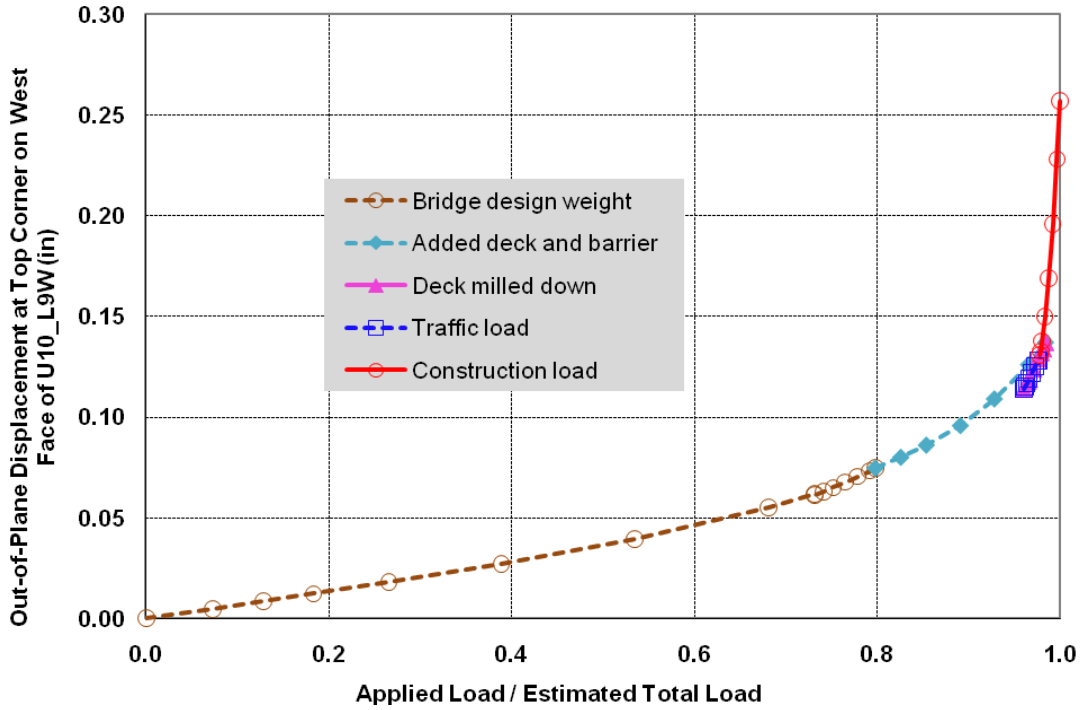
a)
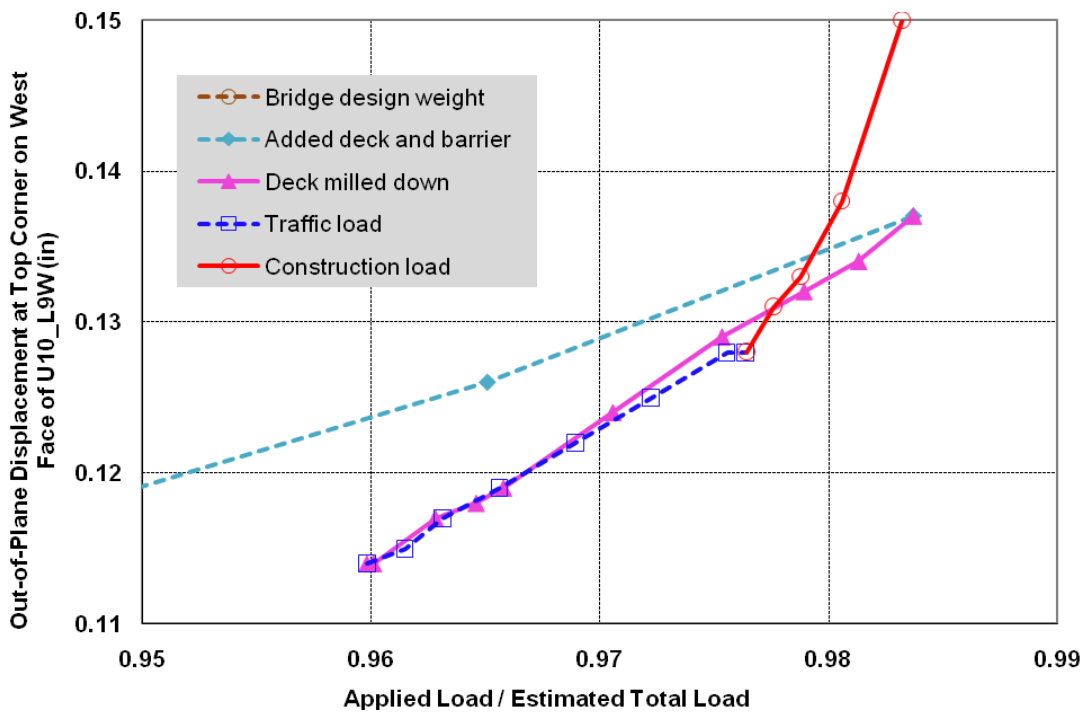
b)

Figure 3.33: Normalized total load versus displacement; all steps were regular static steps with load condition A1 (bottom figure is a magnified view of part of the top figure)
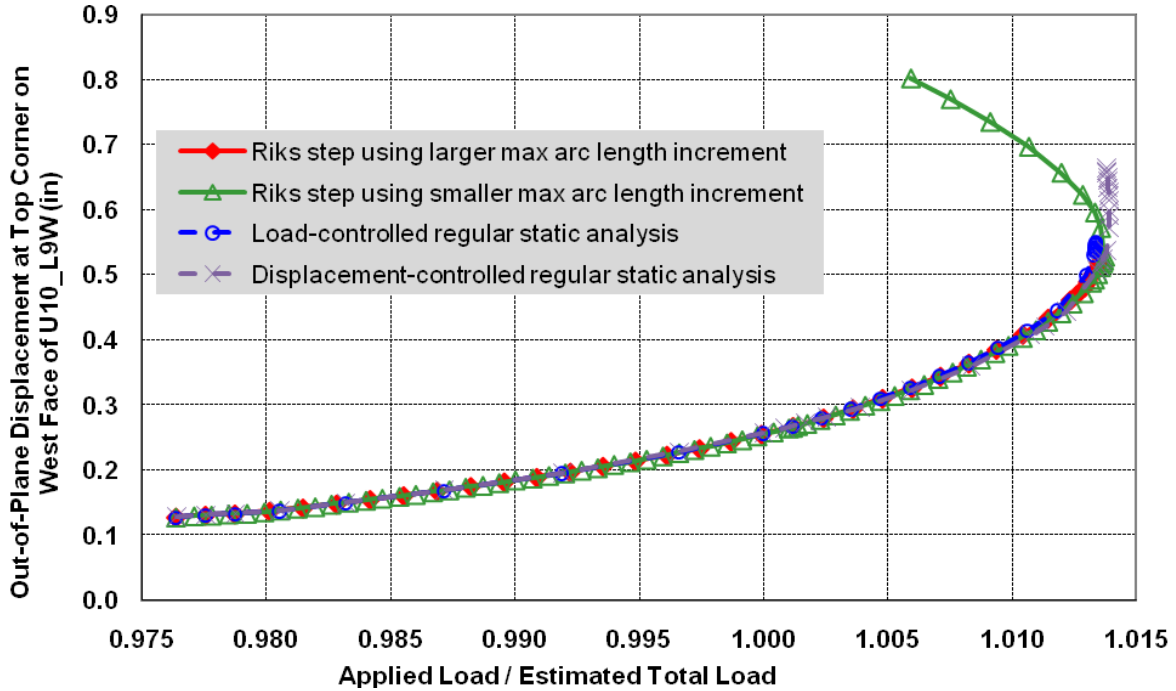
Figure 3.34: Normalized total load versus displacement in construction loading step in Riks analyses and in load-controlled and displacement-controlled regular static analyses with load condition A1
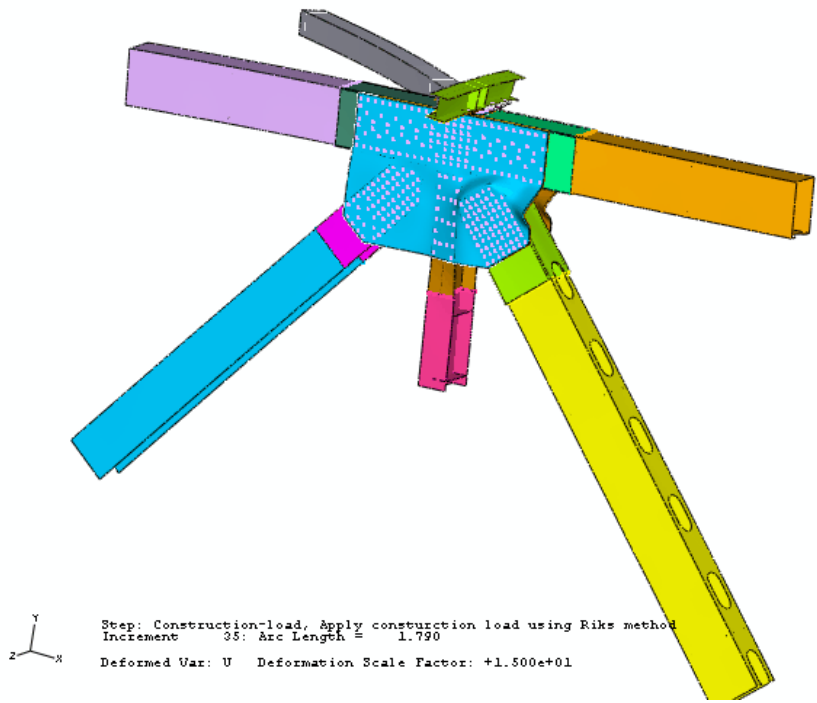
Figure 3.35: Deformed shape of the U10W joint under the predicted maximum load at instability with load condition A1 (deformation magnified 15x)
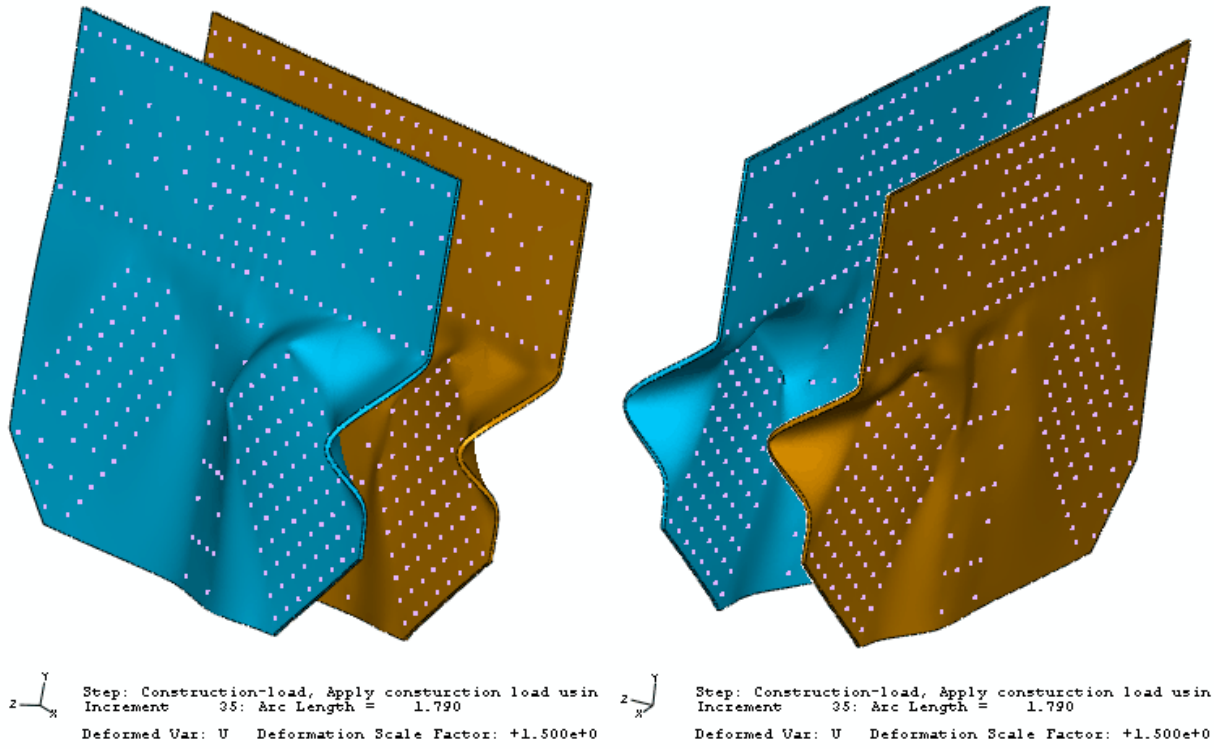
Figure 3.36: Deformed shape of the gusset plates at the U10W joint under the predicted maximum load at instability with load condition A1 (deformation magnified 15x)
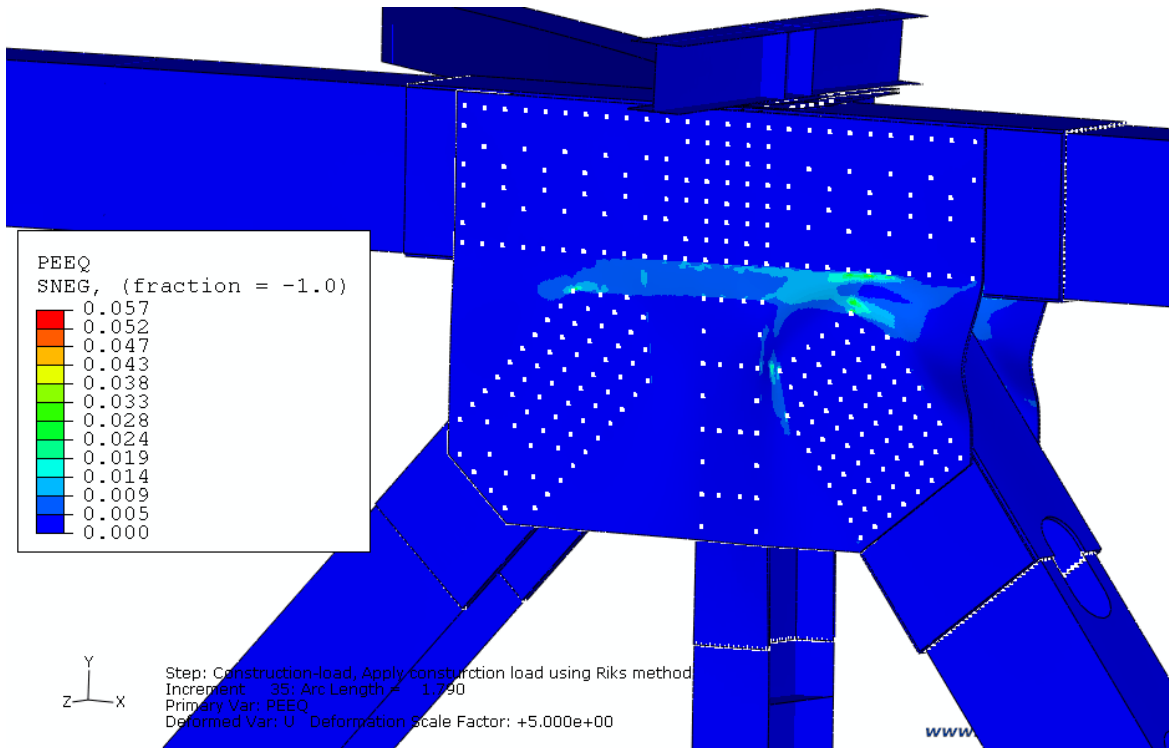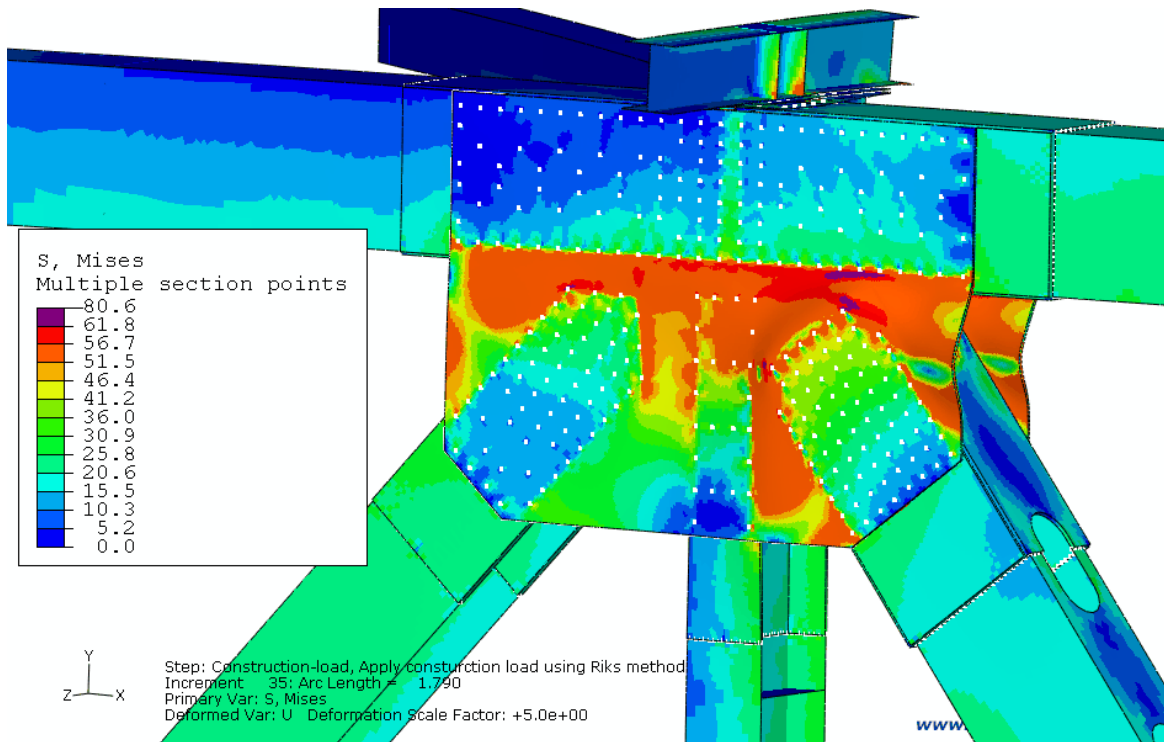
Riks step: Total load 24,812 kips

Figure 3.37: Von Mises stress and equivalent plastic strain (PEEQ) distribution under the predicted maximum load at instability at the U10W joint with load condition A1 (deformation magnified 5x)

West face

Step: Construction-load, Apply consturction load using Riks method
Increment   35: Arc Length =   1.790
Primary Var: S, Mises
Deformed Var: U   Deformation Scale Factor: +1.0e+00

East face

Step: Construction-load, Apply consturction load using Riks method
Increment   35: Arc Length =   1.790
Primary Var: S, Mises
Deformed Var: U   Deformation Scale Factor: +1.0e+00
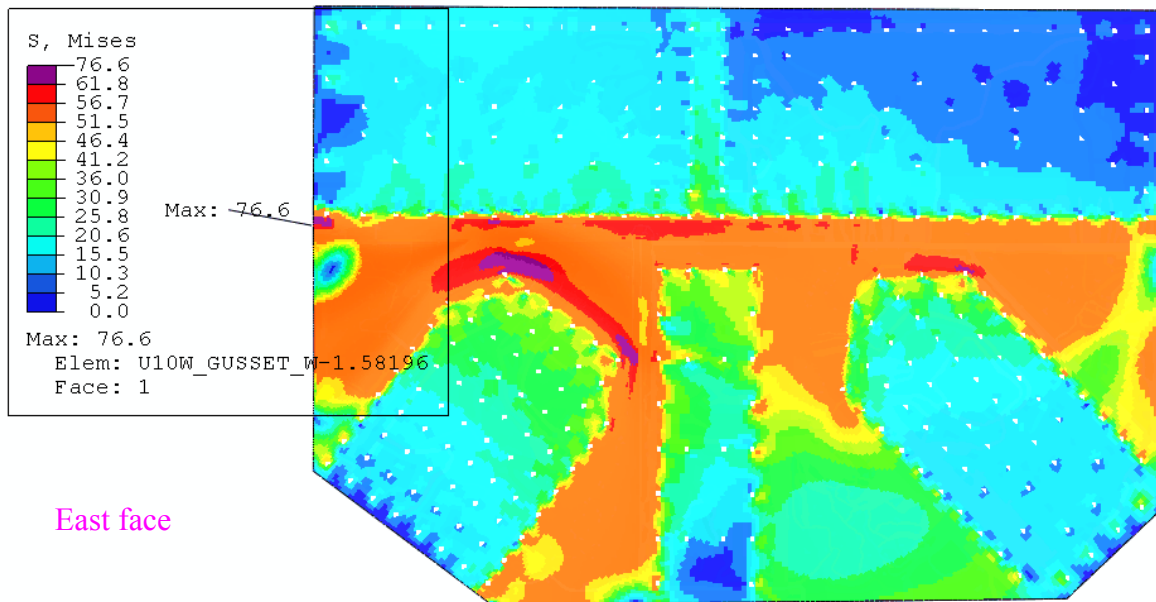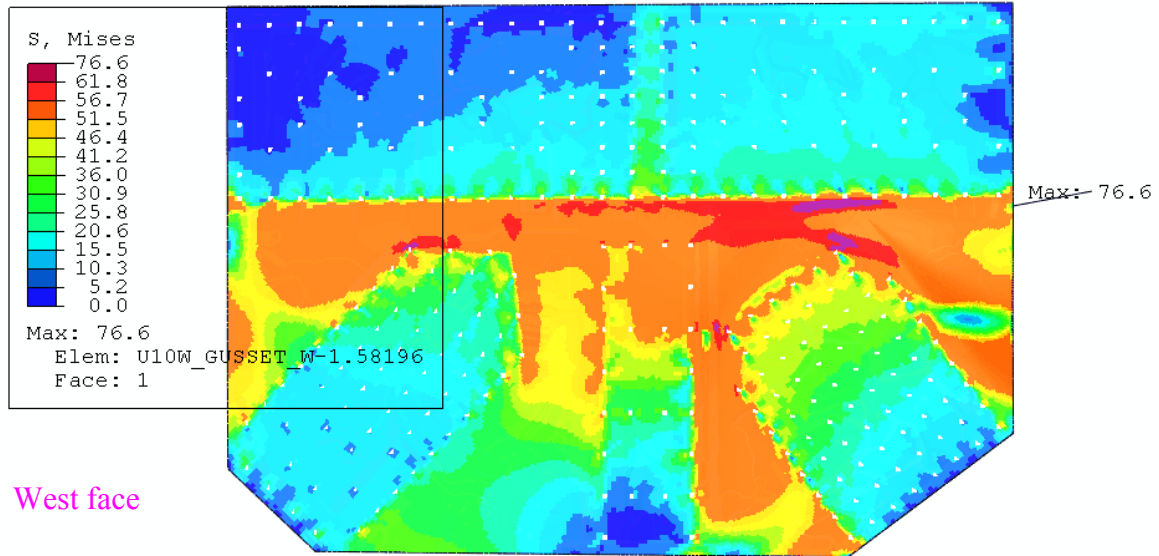
Riks step: Total load of 24,812 kips

Figure 3.38: Von Mises stress distribution under the predicted maximum load at instability in the west gusset at the U10W joint with load condition A1
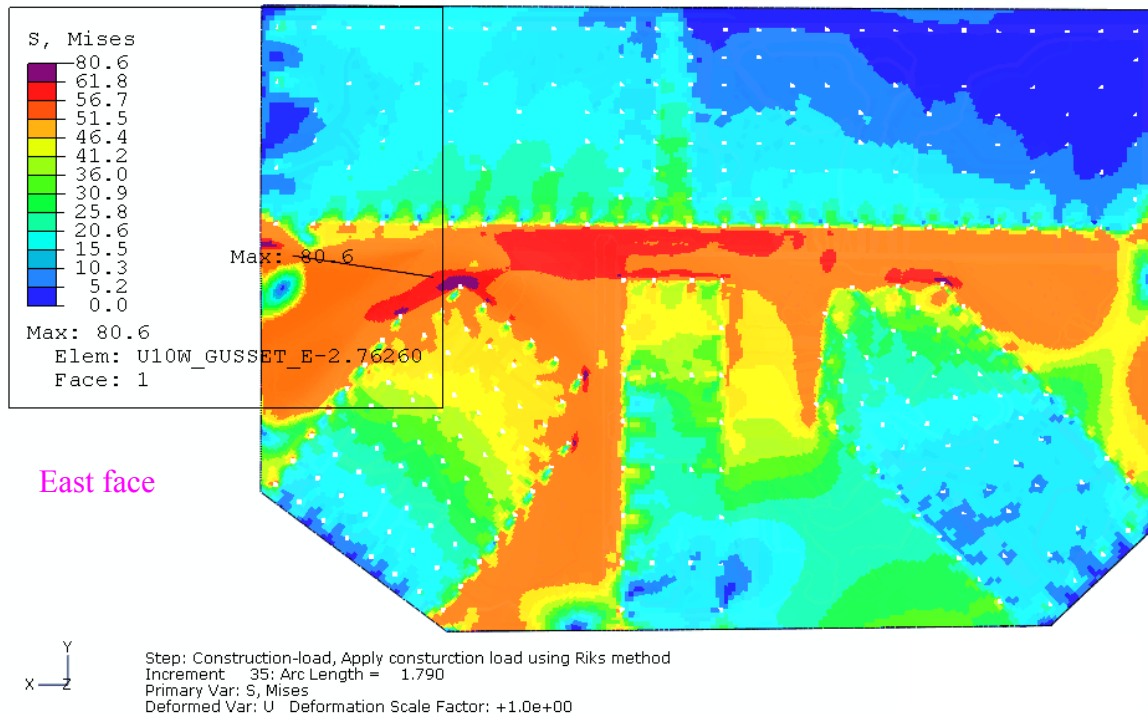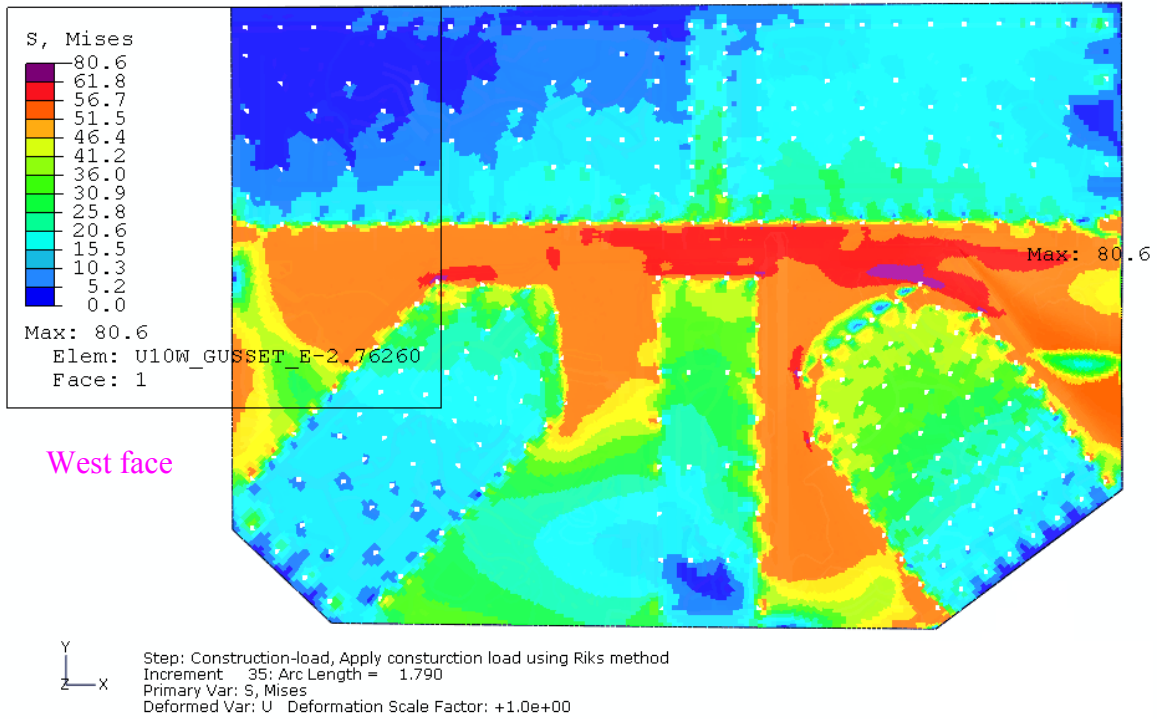
Riks step: Total load of 24,812 kips

Figure 3.39: Von Mises stress distribution under the predicted maximum load at instability in the east gusset at the U10W joint with load condition A1
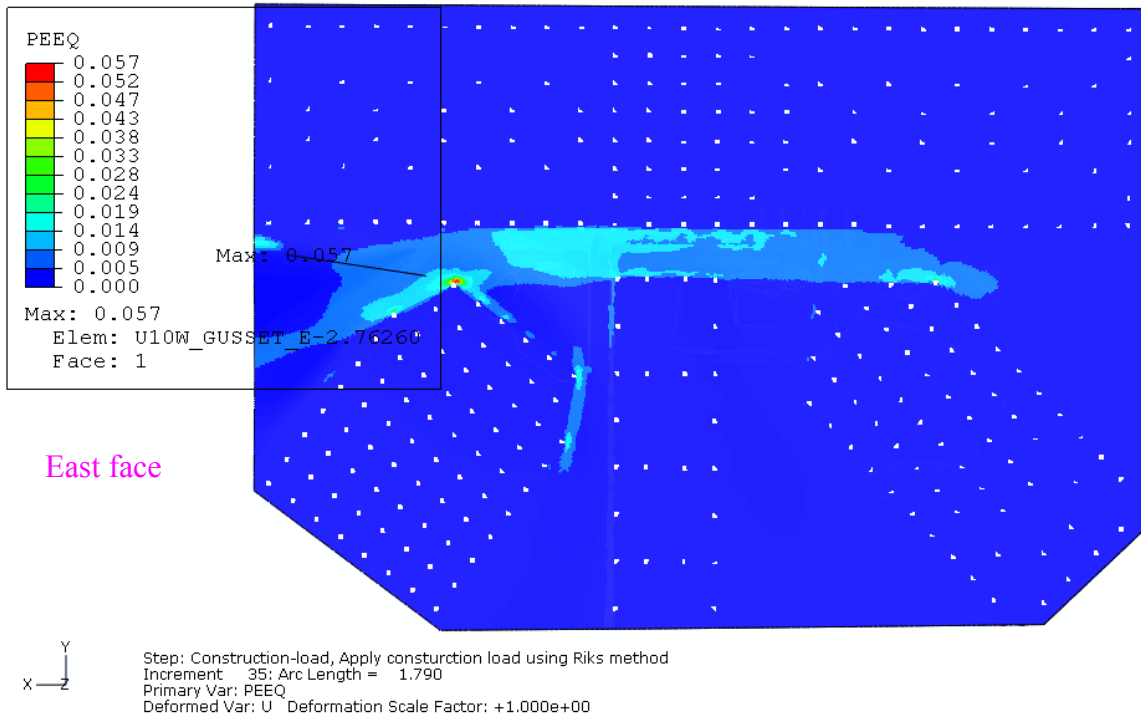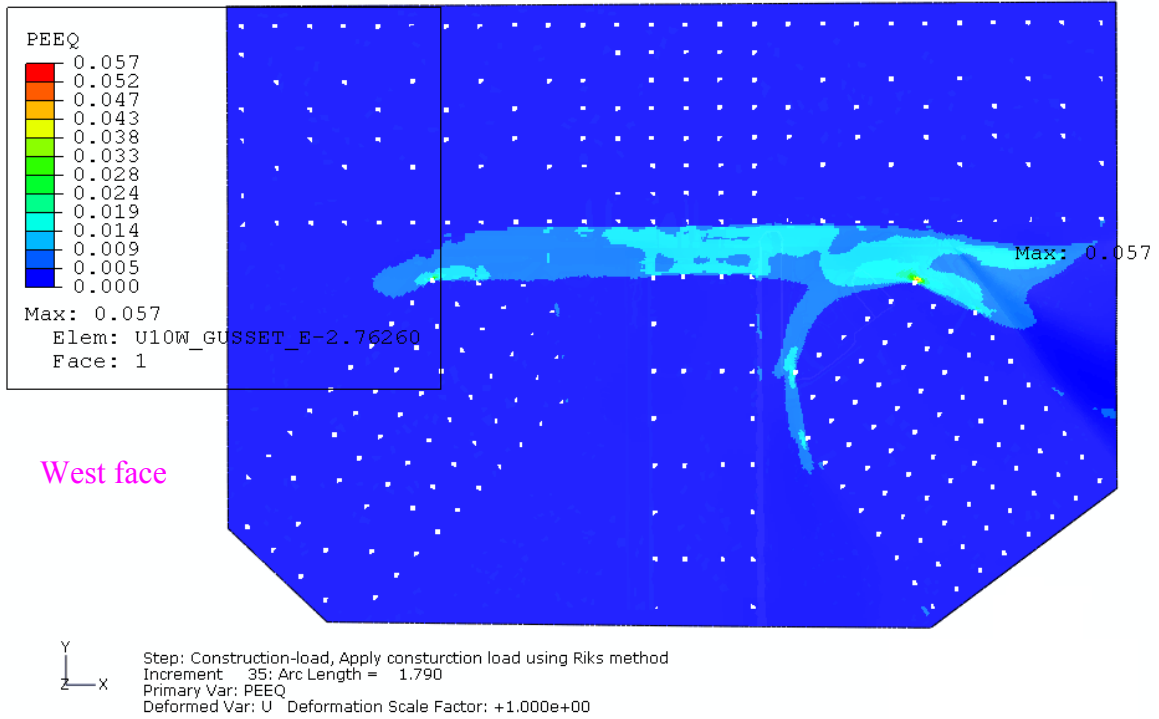
Riks step: total load of 24,812 kips

Figure 3.40: Equivalent plastic strain (PEEQ) distribution under the predicted maximum load at instability in the east gusset at the U10W joint with load condition A1
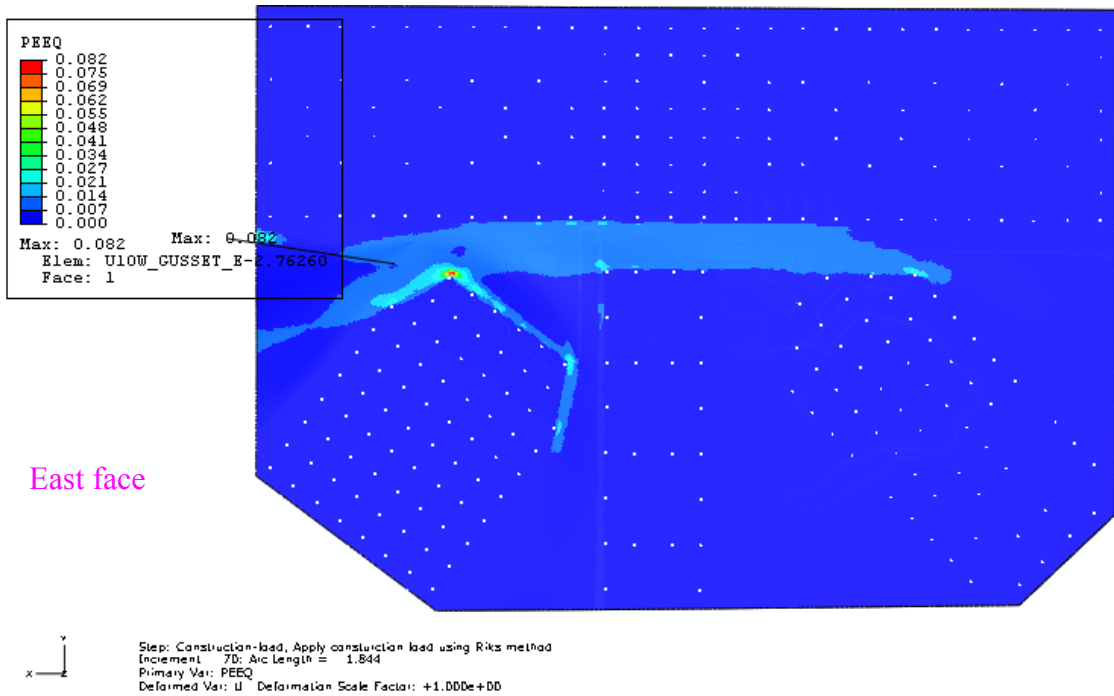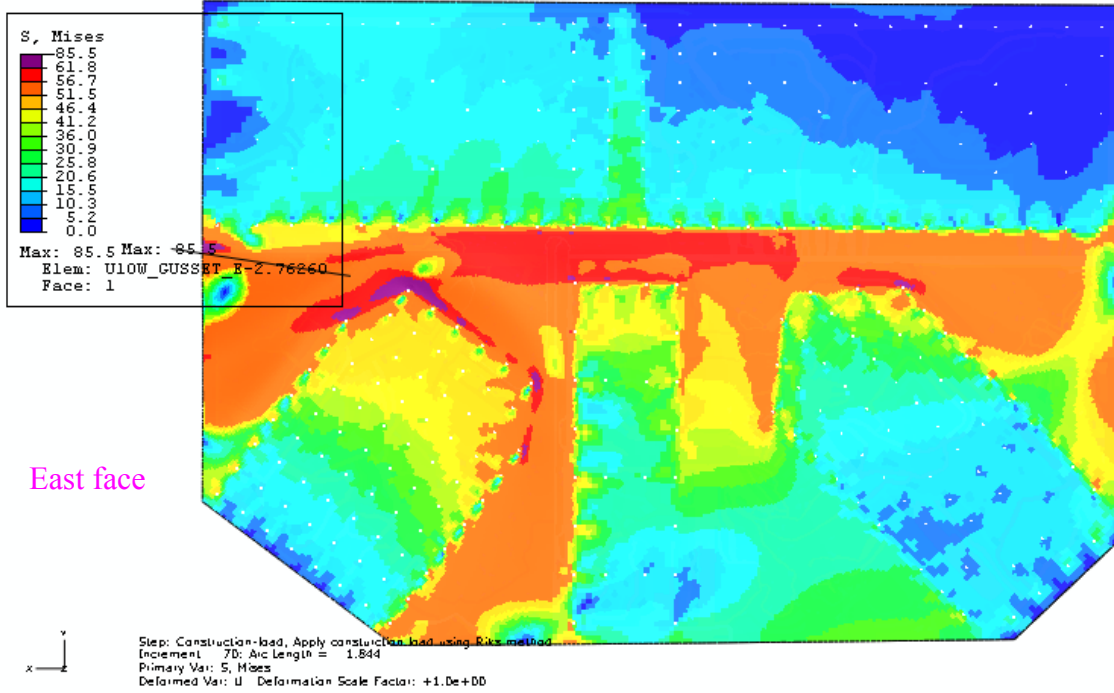
Riks step: total load of 24,796 kips

Figure 3.41: von Mises stress and equivalent plastic strain (PEEQ) distribution after the predicted maximum load at instability in the east gusset at the U10W joint with load condition A1
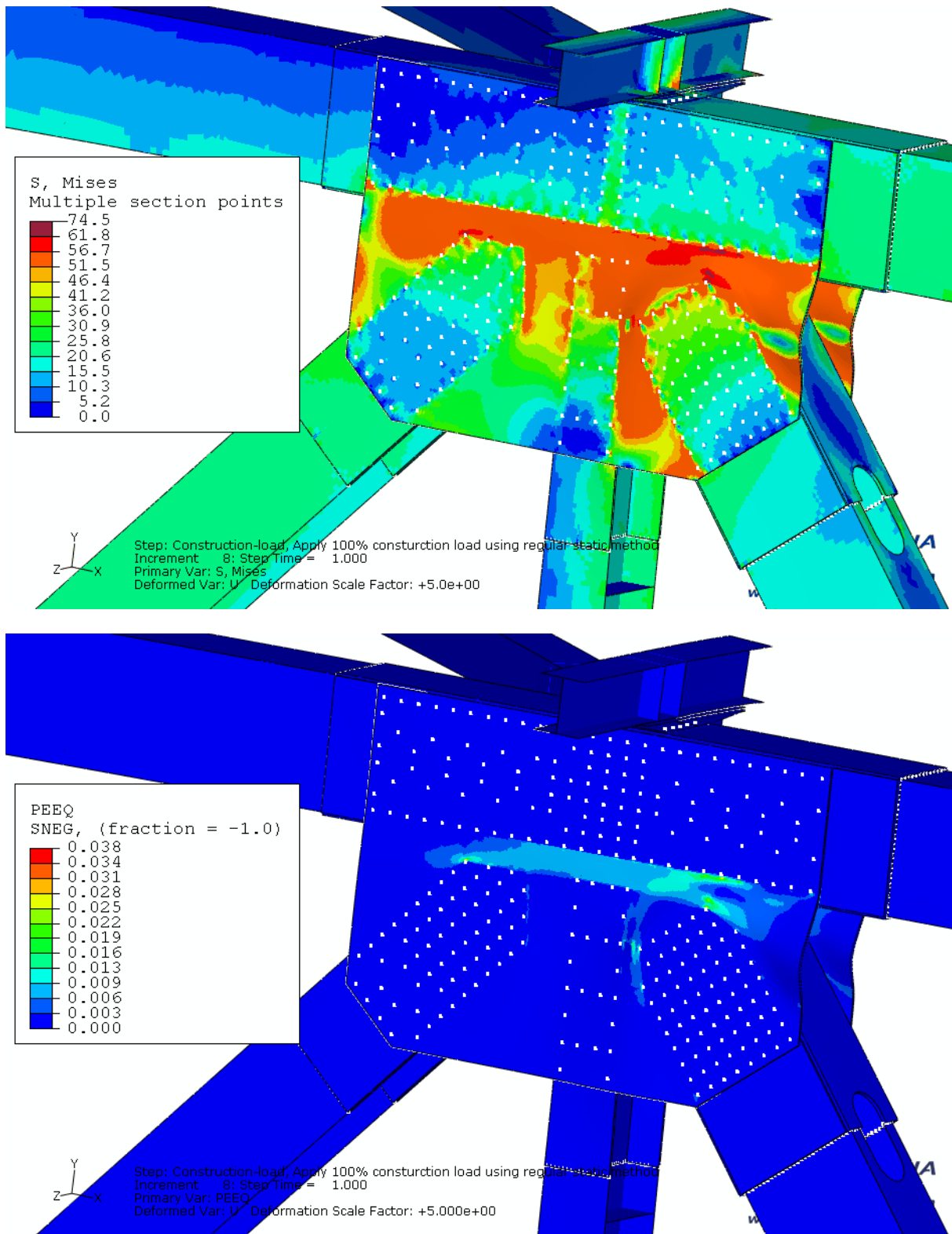
Figure 3.42: Von Mises stress and equivalent plastic strain (PEEQ) distribution under estimated construction load at the U10W joint with load condition A2 (deformation magnified 5x)
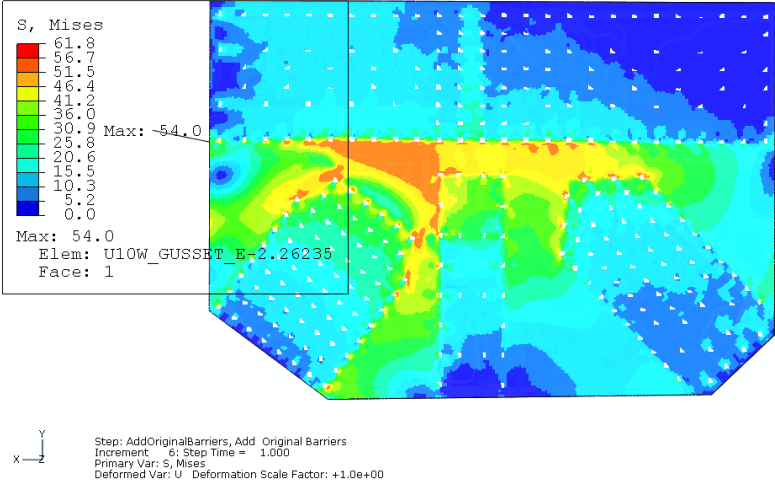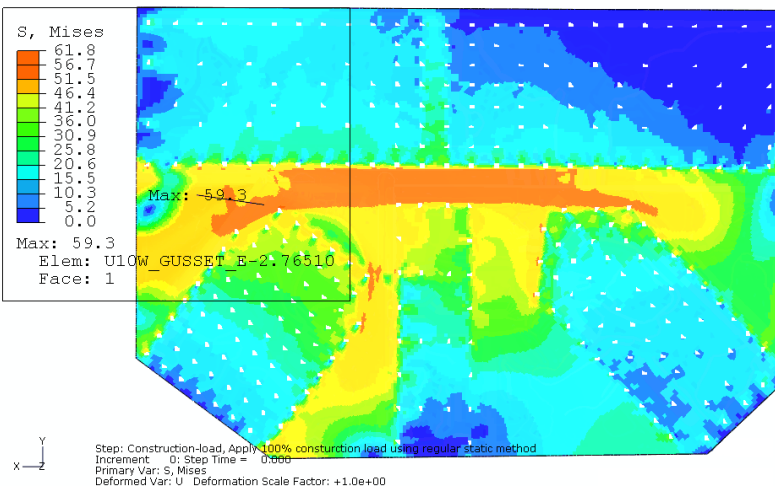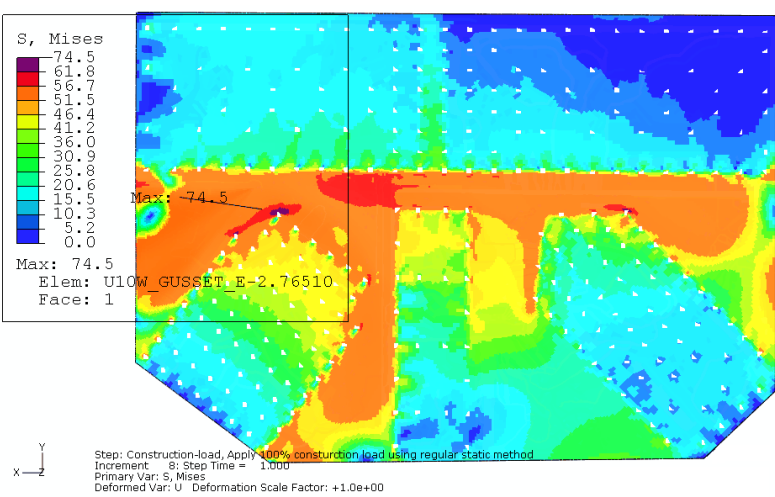
Figure 3.43: Von Mises stress evolution on the east face of the east gusset at the U10W joint with load condition A2
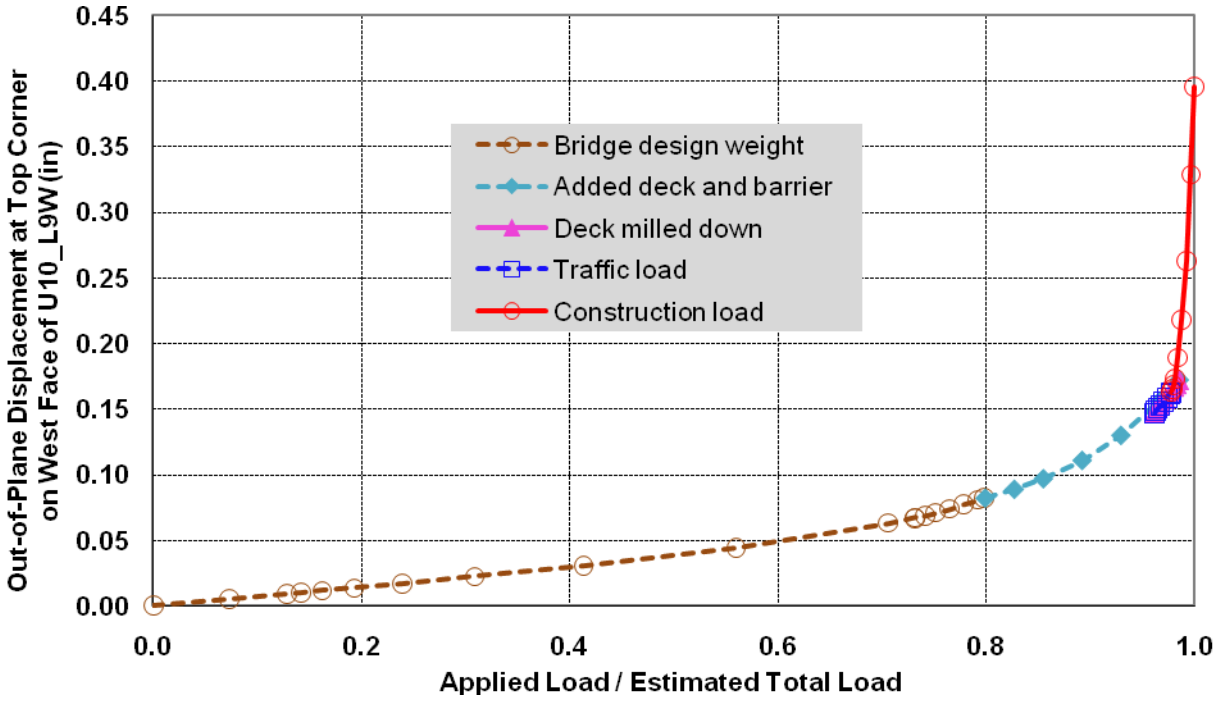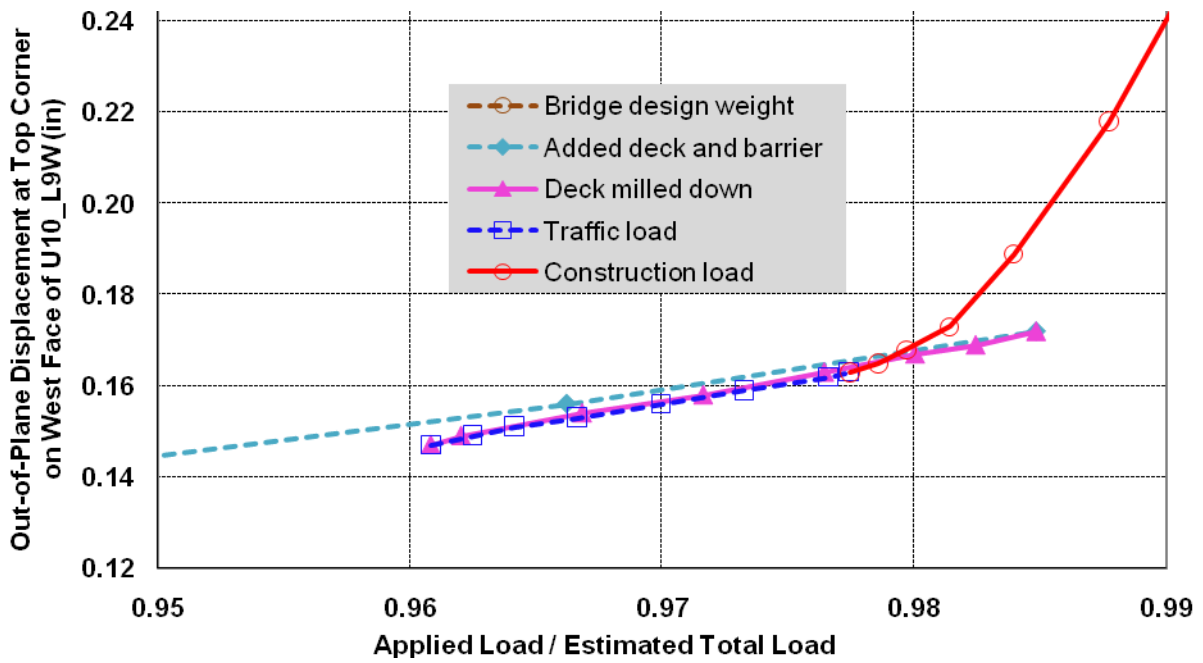
Figure 3.44: Normalized total load versus displacement with load condition A2; all steps were regular static steps (bottom figure is a magnified view of part of the top figure)
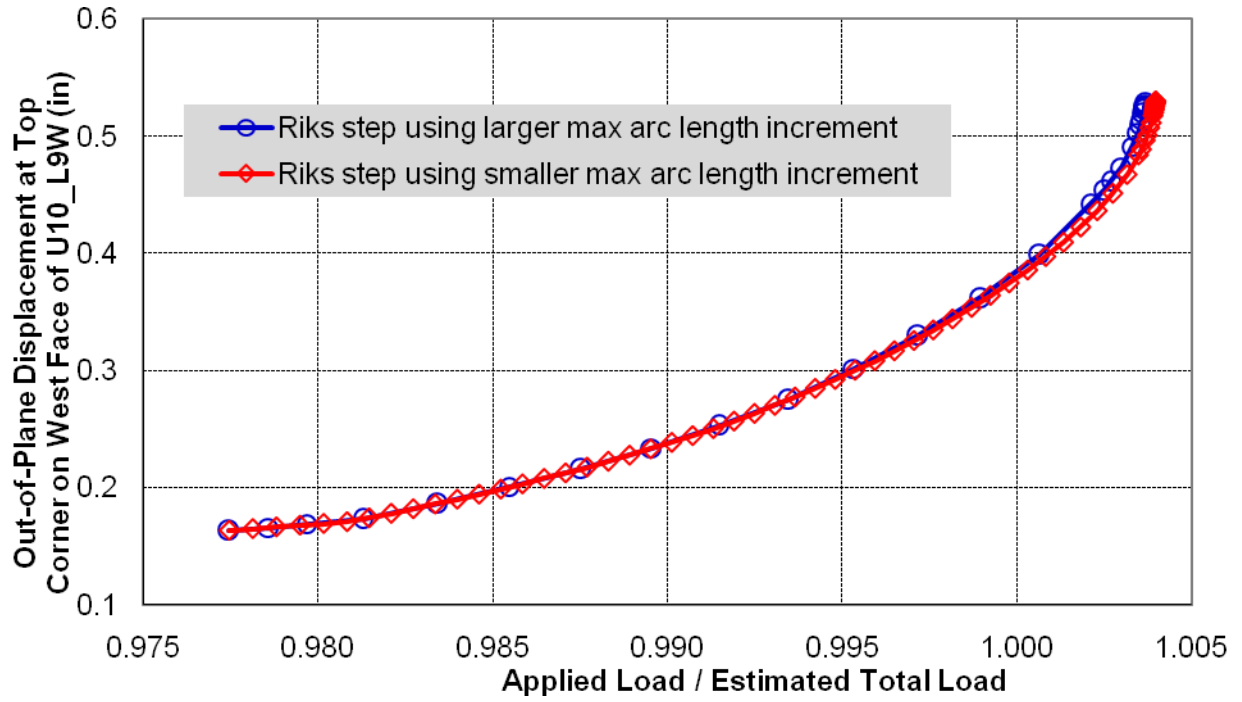
Figure 3.45: Normalized total load versus displacement in Riks construction loading step with load condition A2
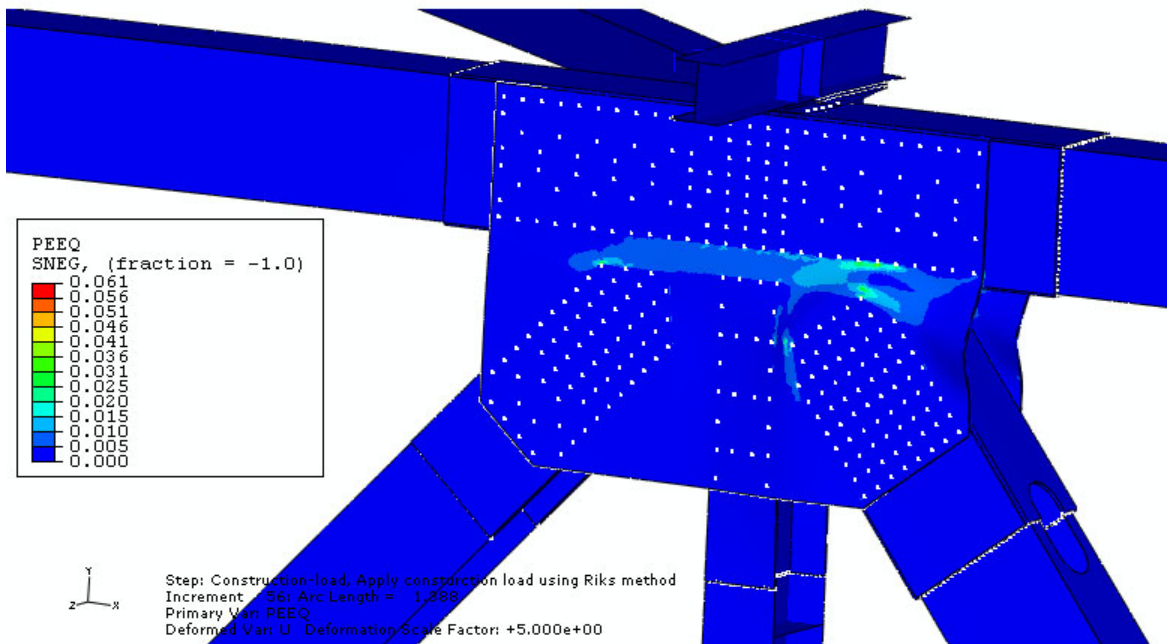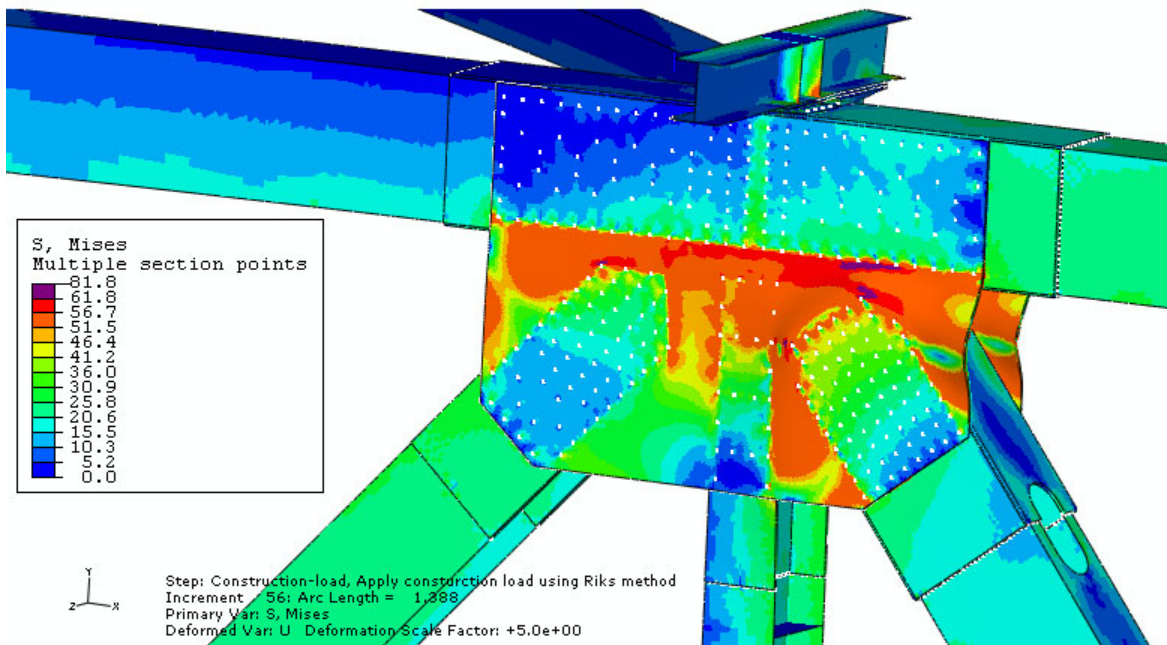
Riks step: Total load of 25,701 kips

Figure 3.46: Von Mises stress and equivalent plastic strain (PEEQ) distribution under the predicted maximum load at instability at the U10W joint with load condition A2 (deformation magnified 5x)
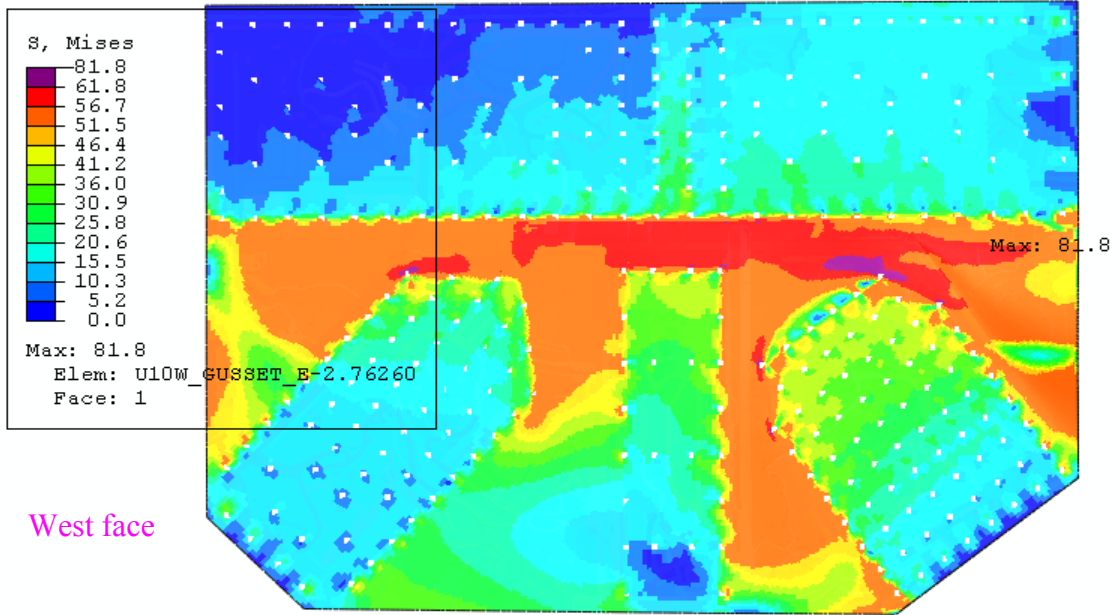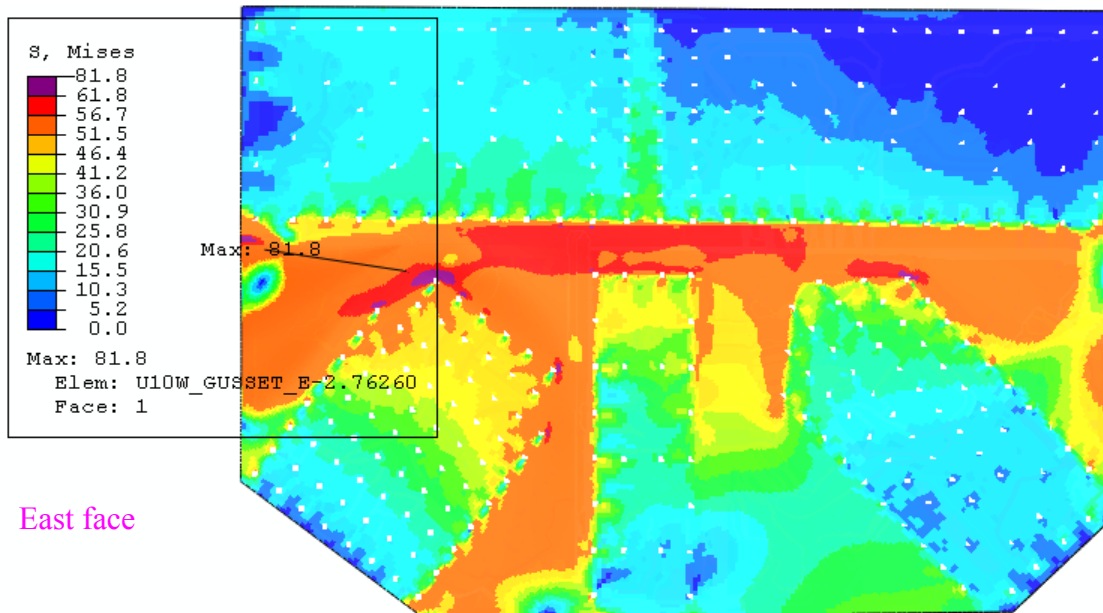
Riks step: Total load of 25,701 kips

Figure 3.47: Von Mises stress distribution under the predicted maximum load at instability in the east gusset at the U10W joint with load condition A2

4   Investigation of the Gusset Mesh Density at the U10W Joint

4.1   Model Differences, Report Sections 3 and 4

In addition to the models and analyses previously described in Section 3 of this report, two additional analyses were conducted to study the effect of mesh density on the maximum predicted bridge load at instability. Table 4.1 lists the new analyses conducted for this study. As shown, the only difference between the analyses presented in Section 4 and the analyses described in Section 3 of this report is that the analyses in Section 4 had larger in-plane mesh size for the two gusset plates and the five main truss members. The Section 4 analyses used an in-plane element size varying from 0.5 – 1.0 inch, with the 0.5 inch elements being typical in the highly stressed gusset regions, as shown in Figure 4.1. Six elements were used through the thickness of the gusset plates. Investigation of gusset plate through-thickness mesh density will be discussed in Section A7 of this report. Each gusset plate included 90,978 brick elements. The in-plane mesh size of the solid representation of the truss members ranged from 0.5 inches to 1.5 inches. The mesh size of the truss shell representation ranged from 1.5 inch to 3.0 inches.

In contrast, the Section 3 analyses used a typical mesh size of 0.2 inches in the highly stressed region of the gusset plates. Note that the larger in-plane element size used in Section 4 analyses allowed for less in-plane space between nodes constrained by the Abaqus fastener definitions. This can be seen by comparing Figure 4.2 and Figure 3.15, which present fastener-constrained nodes in the west gusset plate. The highly stressed region shown in Figure 4.2 had in-plane mesh size of 0.5 inches while the highly stressed region shown in Figure 3.15 had in-plane mesh size of 0.2 inches.

Table 4.1
Section 4 Analyses Used to Investigate Gusset Mesh Density Effects

Local Model Embedded	Typical Mesh Size (inch)	Loading Condition	FHWA Structural Element Bridge Model
U10W joint with bowed gusset plates	0.5	A1	6
U10W joint with bowed gusset plates	0.5	A2	6

4.2   Analysis Results When Embedding U10W 3D Local Model with Load Condition A1: 100 Percent of the Bridge Deadweight and the Traffic Load

4.2.1   Deformed Shape of Bowed Gusset Plates Prior to Applying the Construction Load

With the 0.5 inch in-plane mesh in the gusset plates, the predicted bowing geometry was similar to that with the 0.2 inch in-plane mesh. Before the construction load was applied, the deformed maximum out-of-plane deflection was 0.667 inches in the east gusset plate, and 0.671 inches in the west gusset plate. These maximum out-of-plane deflections were slightly smaller than those with the 0.2 inch in-plane mesh, 0.676 inches in the east gusset plate and 0.684 inches in the west gusset plate.

4.2.2 Load and Stress at Predicted Maximum Load, Riks Method

As in Section 3, the Riks method was used to predict the maximum load at the onset of instability by proportionally increasing the construction load while other loads were maintained at their estimated values. The Riks analysis predicted a maximum construction load of 1,069 kip, or 1.85 times the estimated construction load provided by the NTSB. The maximum total load along the vertical direction was predicted to be 24,973 kip, or 1.020 times the estimated total load, as shown in Figure 4.3. The out-of-plane displacement at the top corner on the west face of the diagonal truss member U10_L9W was predicted to be 0.572 inches under the maximum total load. After the maximum total load was reached, the out-of-plane displacement continued to increase with reduced construction load, indicating that the maximum in the load was related to a geometric instability. File BridgeU10W_meshP5_Riks_MisesStress_Animation.gif shows the animated deformation of the U10W joint as the construction load is applied during the Riks analysis. The animation has a deformation scale factor of 30. It shows that the diagonal truss member U10_L9W continued to move away from the bridge even after the construction load started to decrease during the Riks analysis. Figure 4.4 displays the enlarged deformed shape of the U10W joint under the maximum load predicted by the Riks analysis. The deformation scale factor is 15 in this figure.

The axial force and bending moment at the lower end of the diagonal truss member U10_L9W were predicted to be -2,618 kip and 1,738 kip-inch at the predicted maximum load. Large plastic deformation occurred in the two gusset plates under this load, as shown in Figure 4.5. The maximum von Mises stress was predicted to be 77 ksi in the vicinity of the upper corner rivet in the east gusset plate, as shown in Figure 4.6. The maximum equivalent plastic strain was predicted to be 4.5%.

Table 4.2 summarizes the effect of mesh size of the gusset plate and the main truss members on the predicted maximum load and corresponding axial force, bending moment, out-of-plane displacement, stress, and strain. As shown in Table 4.2, the maximum construction load predicted using the 0.5 inch mesh was 155 kip higher than the maximum construction load predicted using the 0.2 inch mesh in the highly stressed region of the gusset plates. This increase in the construction load raised the axial force and bending moment at the lower end of truss member U10_L9W. It also raised the out-of-plane displacement at the top corner of that truss member. However, the model with the 0.5 inch mesh predicted a lower maximum stress in the gusset plates despite its higher predicted maximum load at instability. This is not unexpected since mesh refinement often results in higher predicted stress values until mesh convergence is reached.

Table 4.2
Effect of Gusset Mesh Density Using Load Condition A1

Typical Mesh Size in Highly Stressed Gusset Region (inch)	Maximum Predicted Total Load (kip)	Construction Load at Predicted Maximum Load (kip)	Axial Force at Lower End Node of Truss Member U10_L9W (kip)	Bending Moment at Lower End Node of Truss Member U10_L9W (kip-inch)	Out-of-Plane Displacement at Top Corner of Truss Member U10_L9W (inch)	Maximum von Mises Stress in East Gusset (ksi)	Maximum Equivalent Plastic Strain in East Gusset
0.2	24,818	914	-2,550	1,612	0.529	81	5.7%
0.5	24,973	1,069	-2,618	1,738	0.572	77	4.5%

Analyses were also conducted using nearly the same construction load on models with different mesh densities. Table 4.3 shows the applied loads for the different mesh density models and summarizes the effect of the mesh differences on results of interest. The difference in the construction load between the two models was small: 3 kip, or 0.5 percent of the estimated construction load. The axial force results at the lower end of truss member U10_L9W were similar. However, the model with the coarser 0.5 inch mesh predicted a smaller bending moment than that with the 0.2 inch mesh model. This smaller bending moment caused a smaller out-of-plane displacement at the top corner of that truss member. The model with the 0.5 inch mesh also predicted a lower maximum von Mises stress in the east gusset plate, as shown in Figure 4.7 and Figure 4.8. Figure 4.7 shows the von Mises stress distribution in the east gusset plate with the 0.5 inch mesh when the construction load was 896 kip. Figure 4.8 shows the von Mises stress distribution in the east gusset plate with the 0.2 inch mesh when the construction load was 893 kip. The maximum von Mises stress predicted by the 0.2 inch mesh model was 78 ksi, and the maximum von Mises stress predicted by the 0.5 inch mesh model was 68 ksi.

Table 4.3
Effect of Gusset Mesh Density Under a Similar Total Load, Load Condition A1

Typical Mesh Size in Highly Stressed Gusset Region (inch)	Total Load (kip)	Construction Load (kip)	Axial Force at Lower End Node of Truss Member U10_L9W (kip)	Bending Moment at Lower End Node of Truss Member U10_L9W (kip-inch)	Out-of-Plane Displacement at Top Corner of Truss Member U10_L9W (inch)	Maximum von Mises Stress in East Gusset (ksi)	Maximum Equivalent Plastic Strain in East Gusset
0.2	24,797	893	-2,543	1,497	0.473	78	4.8%
0.5	24,800	896	-2,549	1,316	0.371	68	2.4%

4.3 Analysis Results When Embedding U10W 3D Local Model with Load Condition A2: 105 Percent of the Bridge Deadweight and the Traffic Load

4.3.1 Deformed Shape of Bowed Gusset Plates Prior to Applying the Construction Load

With the 0.5 inch in-plane mesh in the gusset plates, the predicted bowing geometry was similar to that with the 0.2 inch in-plane mesh. Before the construction load was applied, the deformed maximum out-of-plane deflection was 0.732 inches in the east gusset plate, and 0.737 inches in the west gusset plate. These maximum out-of-plane deflections were smaller than those with the 0.2 inch in-plane mesh, 0.746 inches in the east gusset plate, and 0.758 inches in the west gusset plate.

4.3.2 Load and Stress at Predicted Maximum Load, Riks Method

Using load condition A2, the Riks analysis predicted a maximum construction load of 832 kip at the onset of instability, or 1.44 times the estimated construction load provided by the NTSB. The maximum total load along the vertical direction was predicted to be 25,854 kip, or 1.010 times the estimated total load, as shown in Figure 4.9. The out-of-plane displacement at the top corner of the diagonal truss member U10_L9W was predicted to be 0.549 inches under the maximum total load. Similar to load condition A1, after the maximum total load was attained, the out-of-plane displacement continued to increase with reduced construction load, indicating that the maximum in the load was related to a geometric instability.

The axial force and bending moment at the lower end of the diagonal truss member U10_L9W were predicted to be -2,615 kip and 1,637 kip-inch at the predicted maximum load. Significant plastic deformation occurred in the two gusset plates under this load, as shown in Figure 4.10. The maximum von Mises stress was predicted to be 77 ksi in the vicinity of the upper corner rivet in the east gusset plate, as shown in Figure 4.11. The maximum equivalent plastic strain was predicted to be 4.3%.

Table 4.4 summarizes the effect of mesh size of the gusset plate and the main truss members when analyzed with load condition A2. The maximum construction load predicted using the 0.5 inch mesh was 152 kip higher than the maximum construction load predicted using the 0.2 inch mesh in the highly stressed region of the gusset plates. These results for load condition A2 were nearly identical to the difference in construction load results using load condition A1. Similar to load condition A1 results, the increase in the construction load from the A2 analyses raised the axial force and bending moment at the lower end of truss member U10_L9W. It also raised the out-of-plane displacement at the top corner of that truss member. Again, the model with the 0.5 inch mesh predicted a lower maximum stress in the gusset plates despite its higher predicted maximum load at instability.

Table 4.4
Effect of Gusset Mesh Density Using Load Condition A2

Typical Mesh Size in Highly Stressed Gusset Region (inch)	Maximum Predicted Total Load (kip)	Construction Load at Predicted Maximum Load (kip)	Axial Force at Lower End Node of Truss Member U10_L9W (kip)	Bending Moment at Lower End Node of Truss Member U10_L9W (kip-inch)	Out-of-Plane Displacement at Top Corner of Truss Member U10_L9W (inch)	Maximum Mises Stress in East Gusset (ksi)	Maximum Equivalent Plastic Strain in East Gusset
0.2	25,702	680	-2,547	1,547	0.530	82	6.1%
0.5	25,854	832	-2,615	1,637	0.549	77	4.3%

Table 4.5 compares the maximum predicted load, axial force, bending moment, displacement, stress, and strain between the two load conditions A1 and A2. These results were obtained using the 0.5 inch gusset mesh density models.

With the five percent increase in the deadweight of the bridge and the traffic load in load condition A2, the construction load corresponding to the maximum predicted load at instability was reduced by 237 kip. This decrease in the construction load in load condition A2 caused a smaller bending moment at the lower end of truss member U10_L9W. It also caused a smaller out-of-plane displacement at the top corner of that truss member. However, the axial force at the lower end of the truss member, the maximum von Mises stress, and the maximum equivalent plastic strain in the east gusset plate were very close to each other for the two load conditions.

Table 4.5
Results Comparison Under Load Conditions A1 and A2 Using Gusset Mesh Density of 0.5 Inch

Load Condition	Predicted Maximum Total Load (kip)	Construction Load at Predicted Maximum Load (kip)	Axial Force at Lower End Node of Truss Member U10_L9W (kip)	Bending Moment at Lower End Node of Truss Member U10_L9W (kip-inch)	Out-of-Plane Displacement at Top Corner of Truss Member U10_L9W (inch)	Maximum Mises Stress in East Gusset (ksi)	Maximum Equivalent Plastic Strain in East Gusset
A1	24,973	1,069	-2,618	1,738	0.572	77	4.5%
A2	25,854	832	-2,615	1,637	0.549	77	4.3%

4.4 Analysis with Prescribing Displacements as Construction Loads: Load Condition A1

4.4.1 Procedure

In order to estimate structural behavior past the critical load, the loading corresponding to the construction materials on the deck (at 535 nodes) is simulated by a displacement-controlled boundary condition. Here regular static steps are carried out up to the traffic load and then in the subsequent step, the construction loads are prescribed as a fixed displacement rate (with velocity option in static). The magnitude of the displacement rate at each node is set from the last displacement increment in the final step of a separate analysis with the traffic and construction loads.

4.4.2 Instability from Total Load Change

As the displacement is increased, the total load measured at the pier supports increases until a critical load is reached as shown in Figure 4.12. In this total load and displacement plot, three critical increments (T1, T2, T3) can be identified as: T1 is the local peak load, T2 is the local minimum and T3 is where the load level recovers to T1. Here T1 to T2 represents unstable and T2 to T3 represents stable overall behavior. It is noted that even though the total load does not drop on the actual bridge, once the critical load is reached, the deformation state (of the gusset plates and U10_L9W member) must still pass nearly along the path of the results shown here. [In this procedure, "stabilize" is used to achieve convergence. Artificial stabilization energy is about 3% of total strain energy and 10% of total plastic dissipation.]

4.4.3 Deformation Behavior Near the Bowed Region.

To monitor the deformation changes, displacements at three nodal points (A, B, C) along the gusset plate are recorded. An additional node where the leading edge of U10_L9W member drives outward (D) is also chosen and out-of-plane and vertical displacements are shown in Figure 4.13.

Although not shown here, similar displacement behaviors are obtained from the "east" gusset plate of U10W joint. To clarify the local deformation evolution, the relative shortening and bulging along the edge of gusset plate are computed and shown in Figure 4.14.

The deformation behavior of gusset plate is a clear representation of a buckling-type structural instability near the critical load. Note the plate is initially bowed 0.5 inch which is not included in the bulging in the Figure 4.14.

The deformed shapes as well as the von Mises stress distribution of the U10W joint at the end of unstable deformation (T2) is shown in Figure 4.15. The large stresses near the end of the U10_L9W member is caused by the shifting of its location after the instability of the gusset plates. The side view of the joint also confirms the misalignment of U10_L9W member (compared with U10_L11W member behind) and its tilting out-of-plane behavior. Rapid changes in the stress and deformation fields during the post critical load period (from T1 to T3) can be observed in the Figures 4.16-4.18. In all fields, the changes from T1 to T2 states are drastic. The maximum von Mises stress exceeds 88 ksi at T2 as shown in Figure 4.16. A rapid out-of-plane deformation change during this period is also visible in Figure 4.17 where significant bulging of

the edges of the two gusset plates can be observed. Perhaps the greatest change occurs in the maximum equivalent plastic strain. As indicated in Figure 4.18, it is only 5.6% at the critical load (T1), but it increases to 30% at the end of instability (T2).

Once the same load level as the critical load is recovered (T3) during the stable re-load process, the plastic strain reaches almost 41%. Note that maximum stress and plastic strain are sensitive to sizes of elements in the model, and in a mesh with smaller elements (e.g., 0.2-inch size), these parameters are expected to be even greater. The sub-modeling analysis in Section 5 shows the maximum plastic strain to be 3 times higher when the rivet holes are modeled with smaller elements (e.g.,Figure 5.9).

4.4.4   Initiation of Material Failure

The comparison of the two gusset plates (east and west) indicates slightly higher stress states to exist in the east plate. To examine the region of high plastic strains further, the contours of equivalent plastic strain at T2 are shown on the both surfaces of east plate in Figure 4.19. The bands of intense strains (shown in gray) emanating from the contact with the tip of U10_L9W member imply potential locations of material failure following the structural instability of U10W joint.

Possible failure paths can be also estimated from the inspection of maximum principal stress. Contour plots on two sides of east gusset plate are shown in Figure 4.20. The results show that the maximum tensile state reaches 126 ksi at T2 state (well above the maximum von Mises stress input to the model, indicating significant stress triaxiality, and likely above the failure stress of the steel). The contours also indicate different bands of large tensile stress on two sides of the plate. The band along the horizontal direction (along the bottom U10_U9W member) suggests to failure to be initiated from the outer surface of east plate (view A). On the other hand, the failure around the tip of U10_L9W member is likely initiated from the inner surface (view B).

4.5   Summary: U10W 3D Local Models with 0.5-inch Gusset Mesh Density Embedded into the FHWA Structural Element Bridge Model

Two models with a typical in-plane mesh size of 0.5 inches in the highly stressed region of the gusset plates were analyzed to investigate the effect of mesh size on the maximum predicted load at instability. A larger in-plane mesh size generally introduced smaller space between the two sets of fastened nodes of two adjacent Abaqus fasteners. The analyses predicted that the maximum load at instability increased when using the 0.5-inch mesh instead of the 0.2-inch mesh. The increase in the maximum predicted load at instability was 155 kip for load condition A1 and 152 kip for load condition A2.

The model with a finer mesh in the gusset plates predicted a larger von Mises stress than that with a coarser mesh when a similar construction load was applied. The model with the 0.2-inch mesh predicted a maximum von Mises stress of 78 ksi under a construction load of 893 kip. The model with the 0.5-inch mesh predicted a maximum stress of 68 ksi under a construction load of 896 kip. Both models used load condition A1. The model with the 0.2-inch mesh also predicted a significantly larger bending moment at the lower end of the diagonal truss member U10_L9W. The difference in the bending moment was predicted to be 181 kip-inch. The larger bending moment was related to a larger out-of-plane displacement at the top corner of the diagonal truss member and an earlier occurrence of instability.

The local peak in total load in the analysis with displacement control was predicted to be 24,980 kip. The maximum total load predicted by the Riks analysis was 24,973 kip. The difference between this local peak value in the analysis with the displacement control and the maximum total load predicted by the Riks analysis was 7 kip.

Mesh 0.5 inch
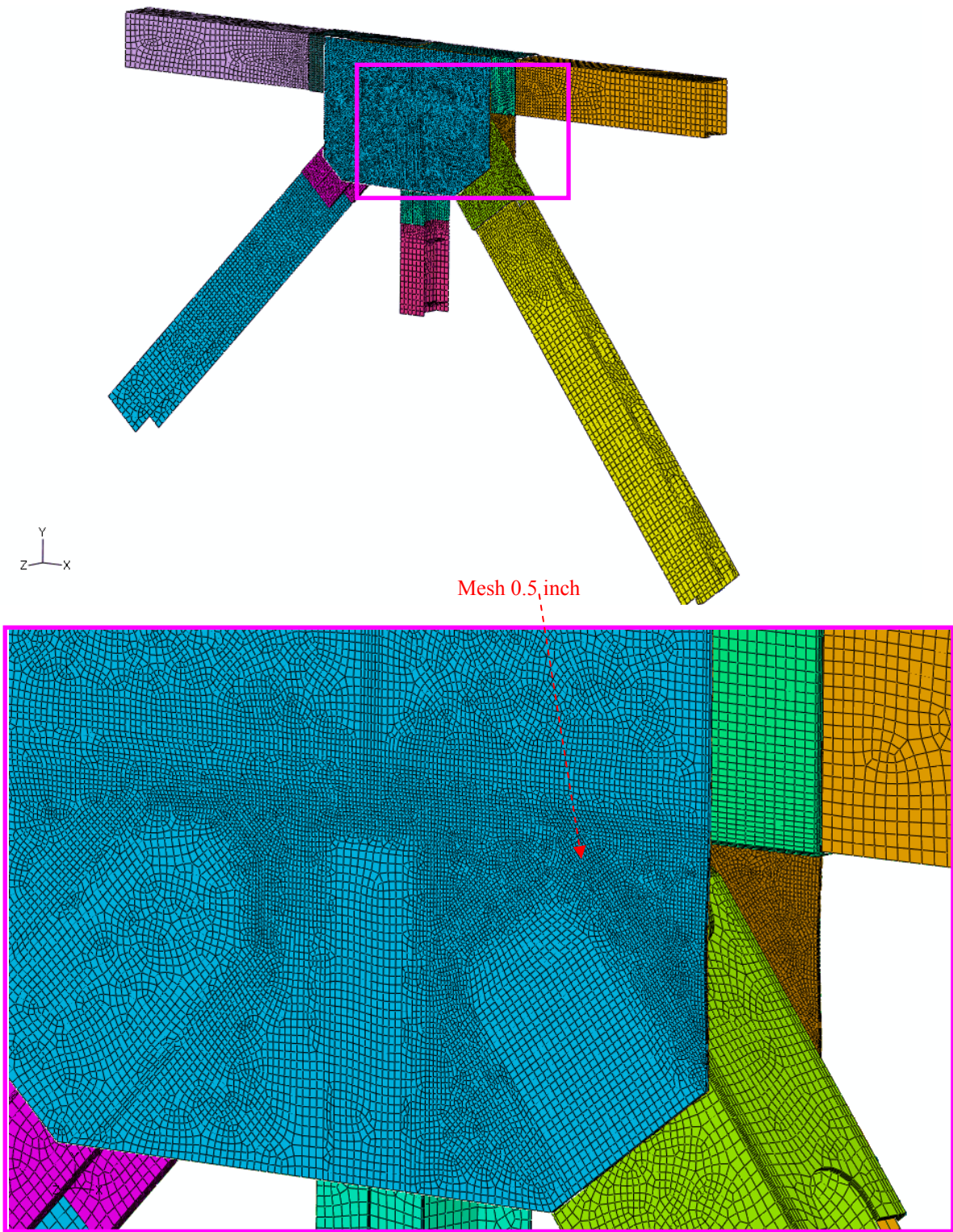
Figure 4.1: CAE model of the U10W joint; 0.5 inch mesh in highly stressed gusset region
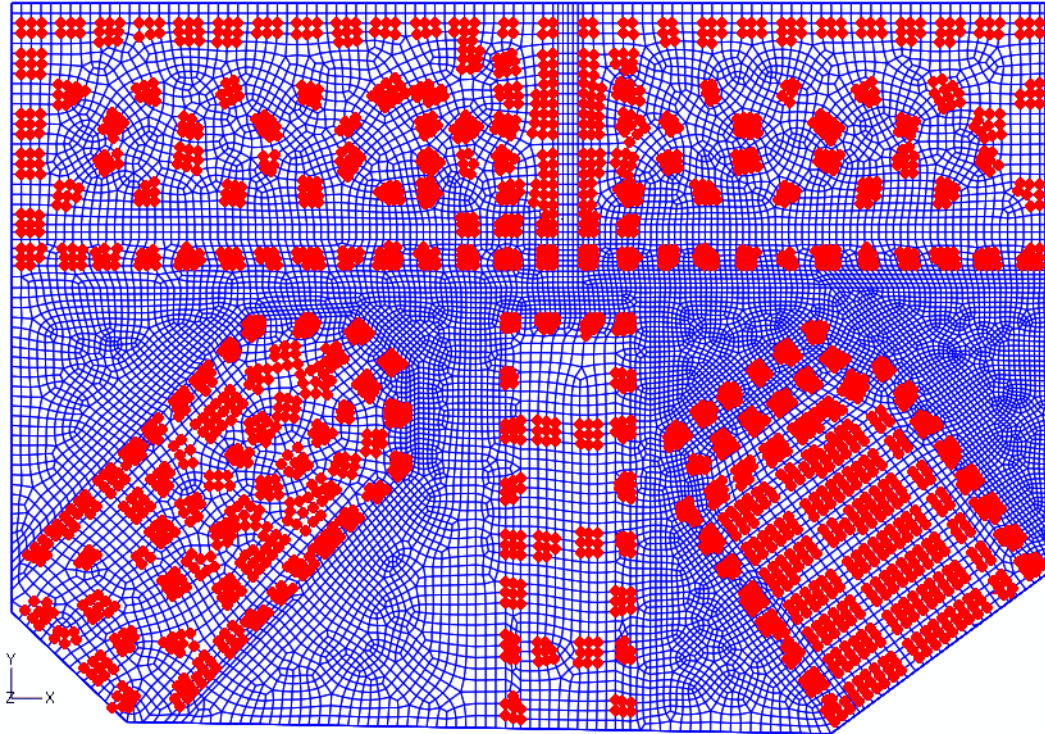
Figure 4.2: Fastened nodes of the west gusset plate at the U10W joint; 0.5 inch mesh
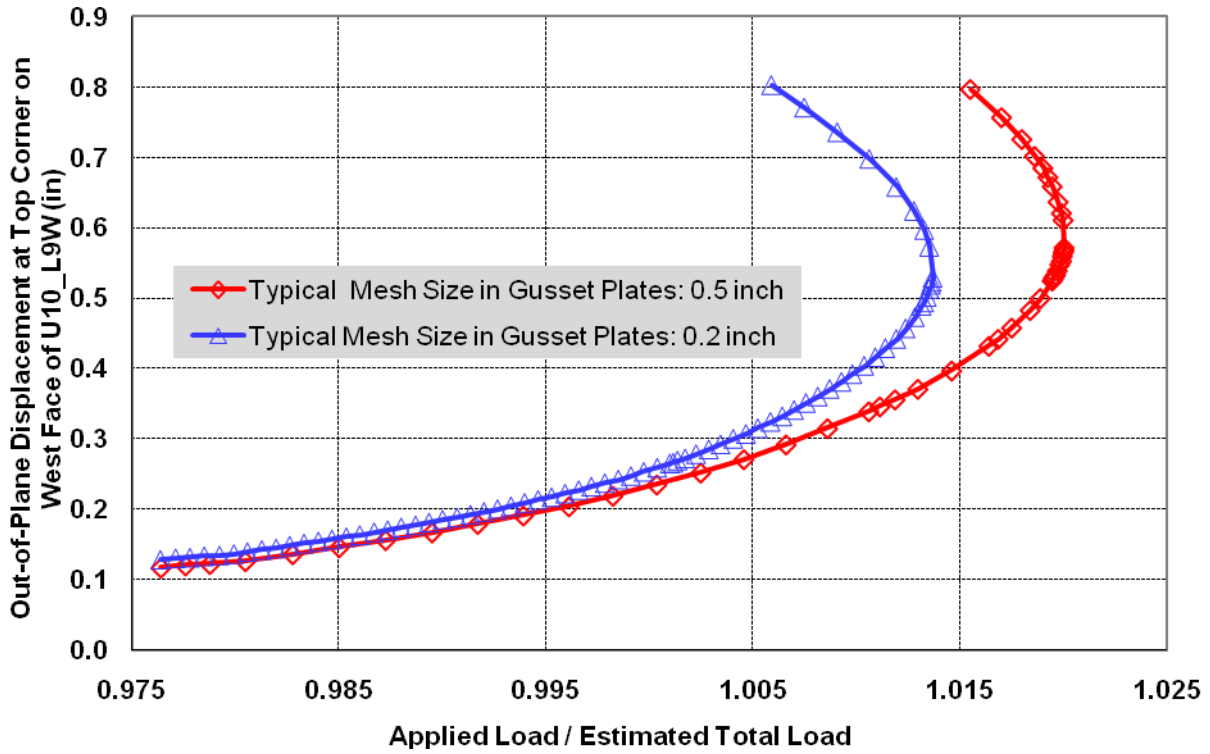
Figure 4.3: Comparison of normalized total load versus displacement in Riks construction loading step with load condition A1 between gusset mesh size of 0.5 inch and 0.2 inch

Step: Riks, Apply consturction load using Riks method
Increment   35: Arc Length =   2.106

Deformed Var: U   Deformation Scale Factor: +1.500e+01
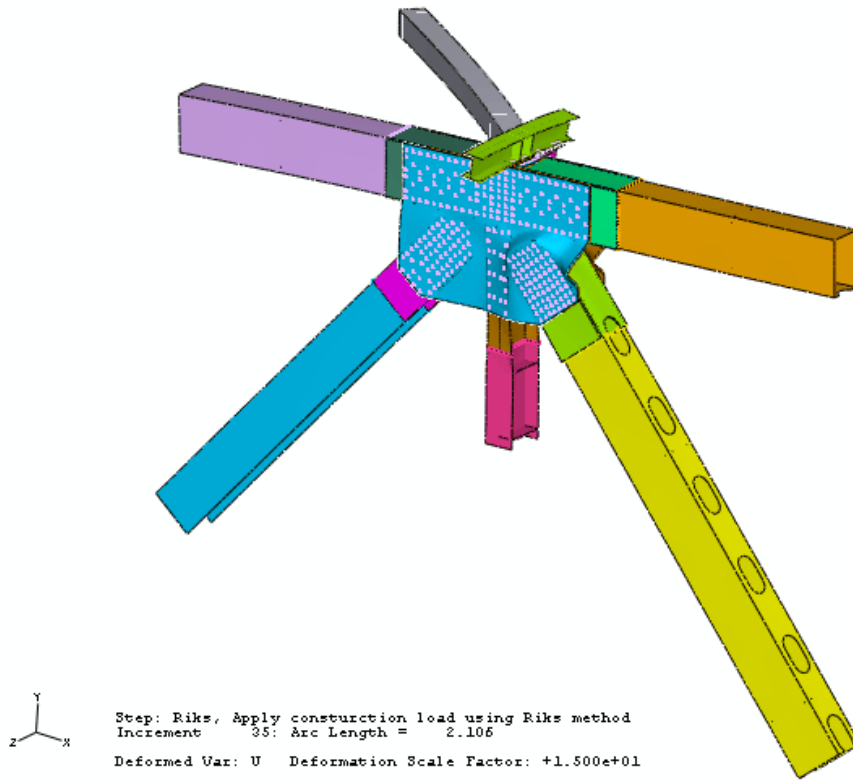
Figure 4.4: Deformed shape of the U10W joint under the predicted maximum load at instability with load condition A1 (deformation magnified 15x)
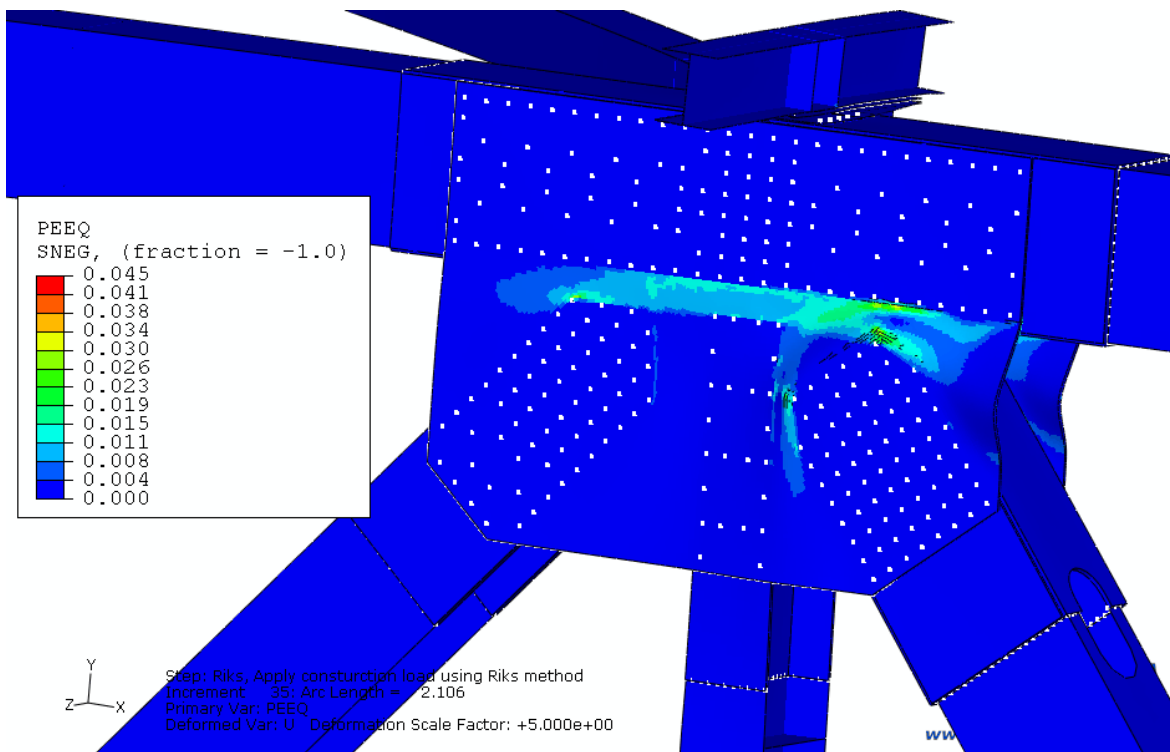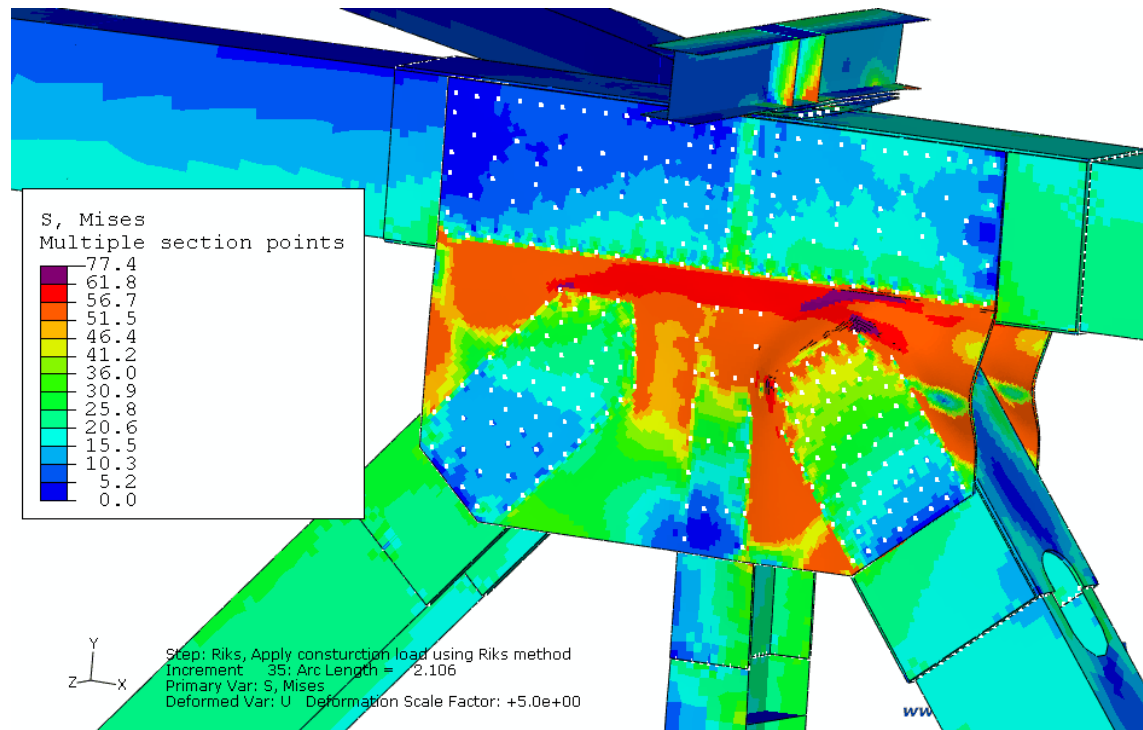
Riks step: Total load of 24,972 kips

Figure 4.5: Von Mises stress and equivalent plastic strain (PEEQ) distribution under the load close to the predicted maximum load at instability at the U10W joint with load condition A1 (deformation magnified 5x)

West face

Step: Riks, Apply consturction load using Riks method
Increment 35: Arc Length = 2.106
Primary Var: S, Mises
Deformed Var: U   Deformation Scale Factor: +1.0e+00

East face

Step: Riks, Apply consturction load using Riks method
Increment 35: Arc Length = 2.106
Primary Var: S, Mises
Deformed Var: U   Deformation Scale Factor: +1.0e+00
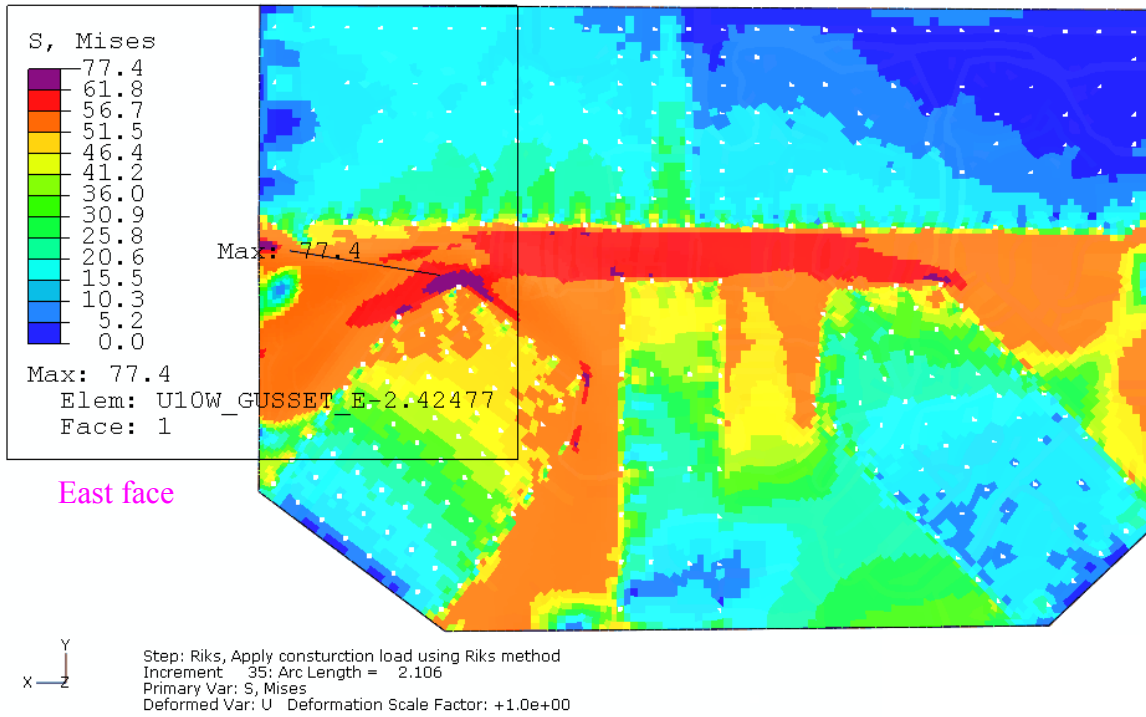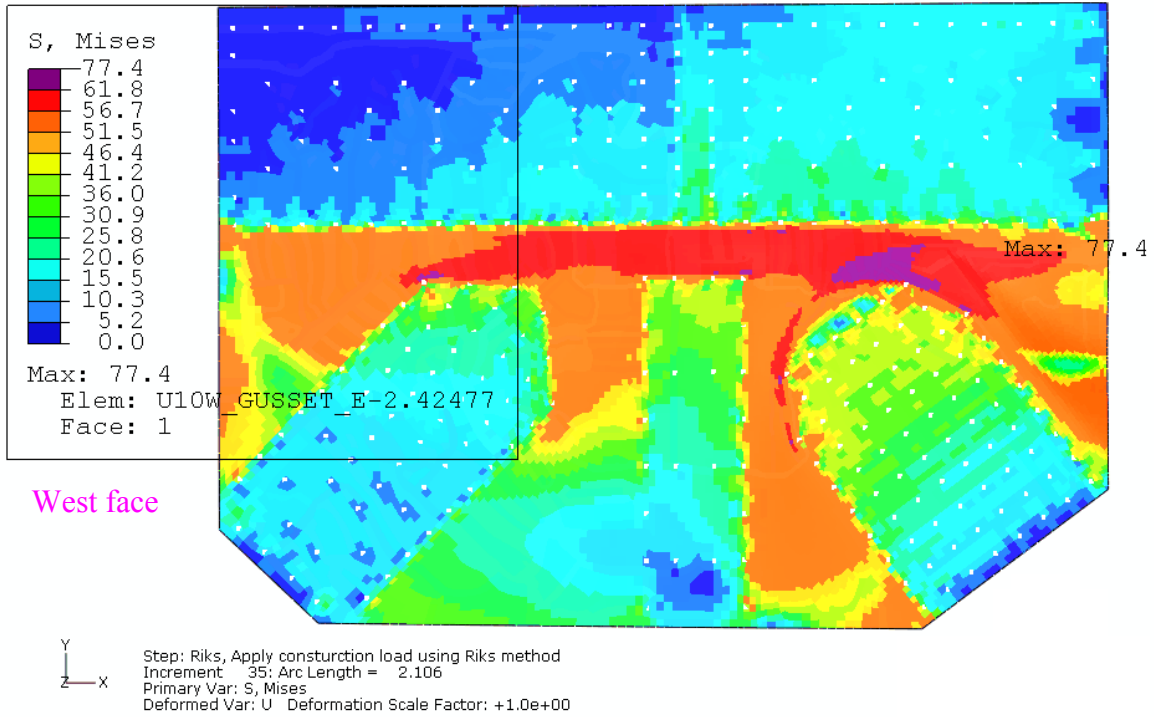
Riks step: Total load of 24,972 kips

Figure 4.6: Von Mises stress distribution under the load close to the predicted maximum load at instability in the east gusset plate at the U10W joint with load condition A1

West face

East face
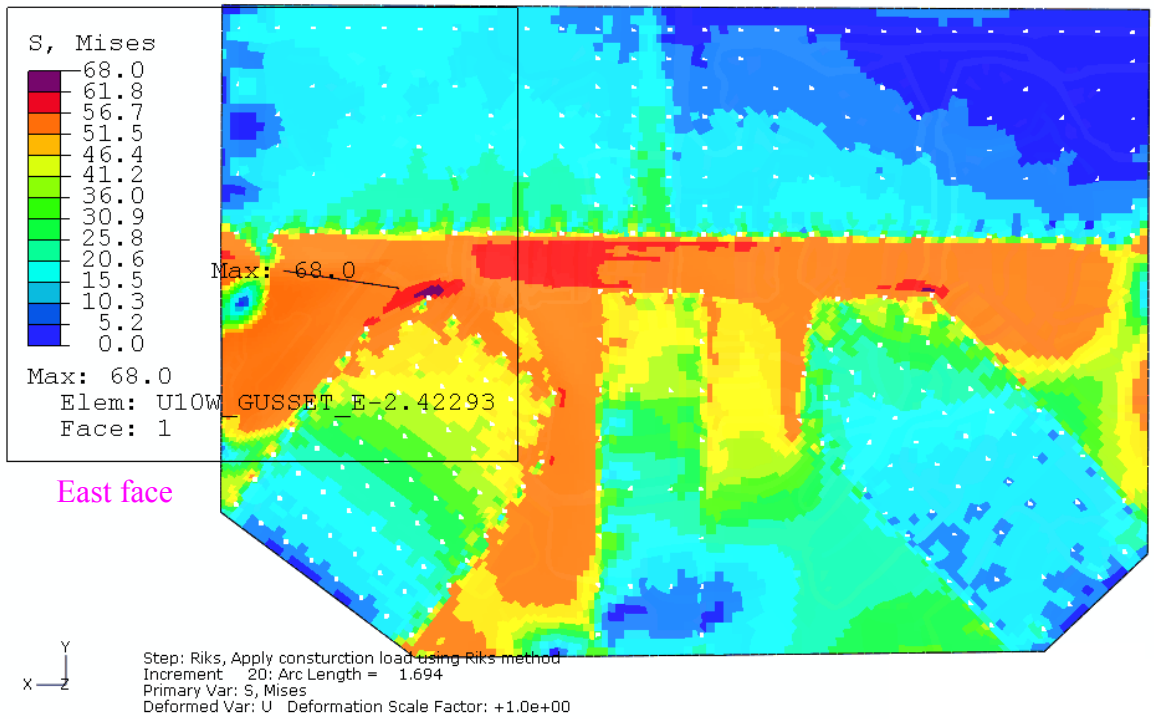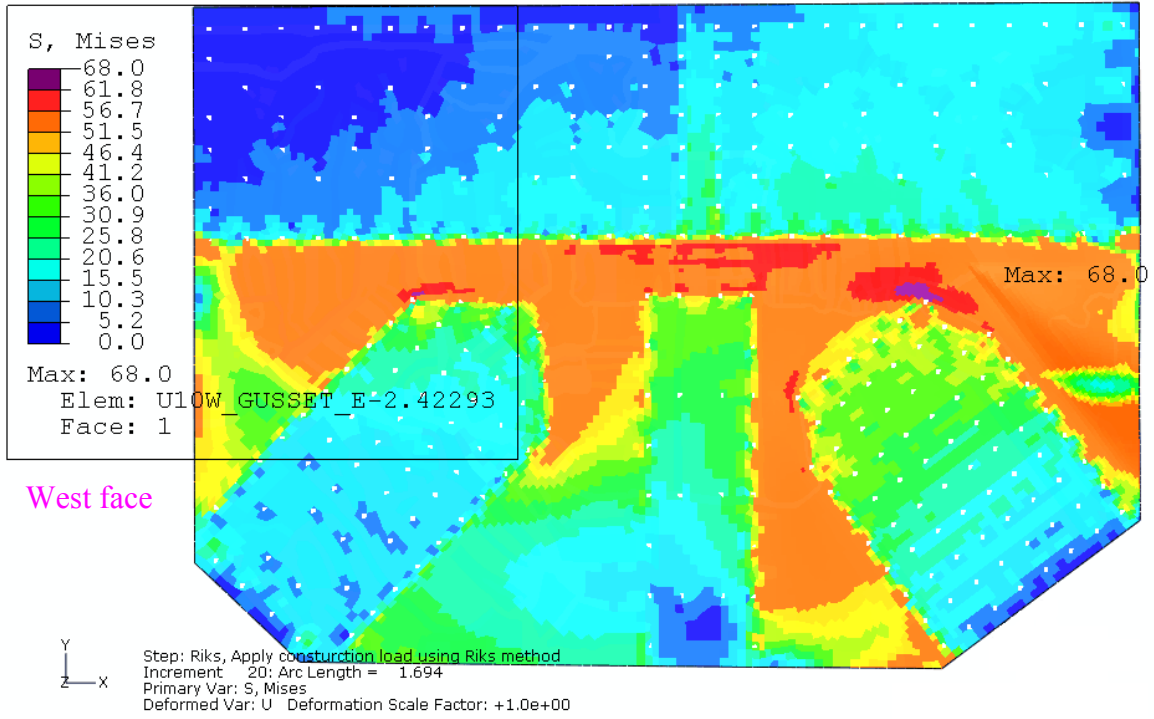
Riks step: Total load of 24,800 kips

Figure 4.7: Von Mises stress distribution under a total load of 24,800 kips in the east gusset plate at the U10W joint with load condition A1
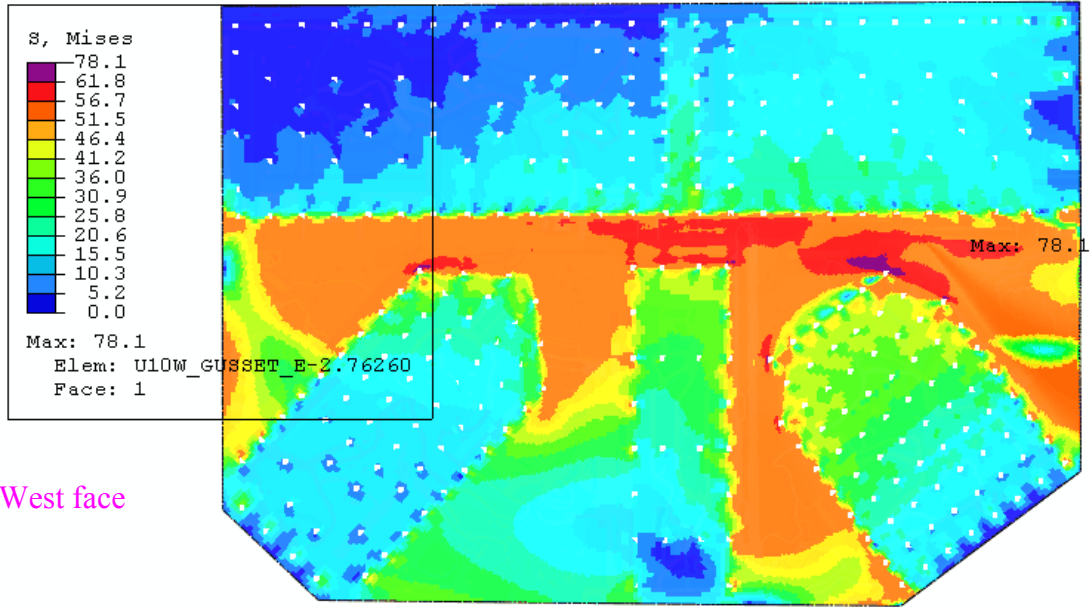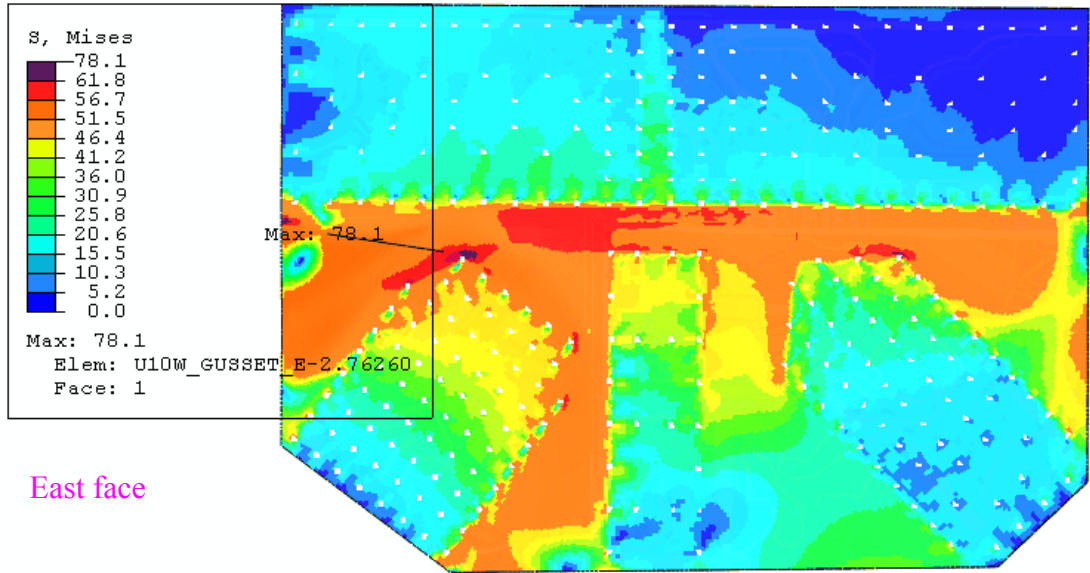
Riks step: Total load of 24,797 kips and gusset mesh size of 0.2 inches

Figure 4.8: Von Mises stress distribution under a total load of 24,797 kips in the east gusset plate at the U10W joint with load condition A1 and typical gusset mesh size of 0.2 inches
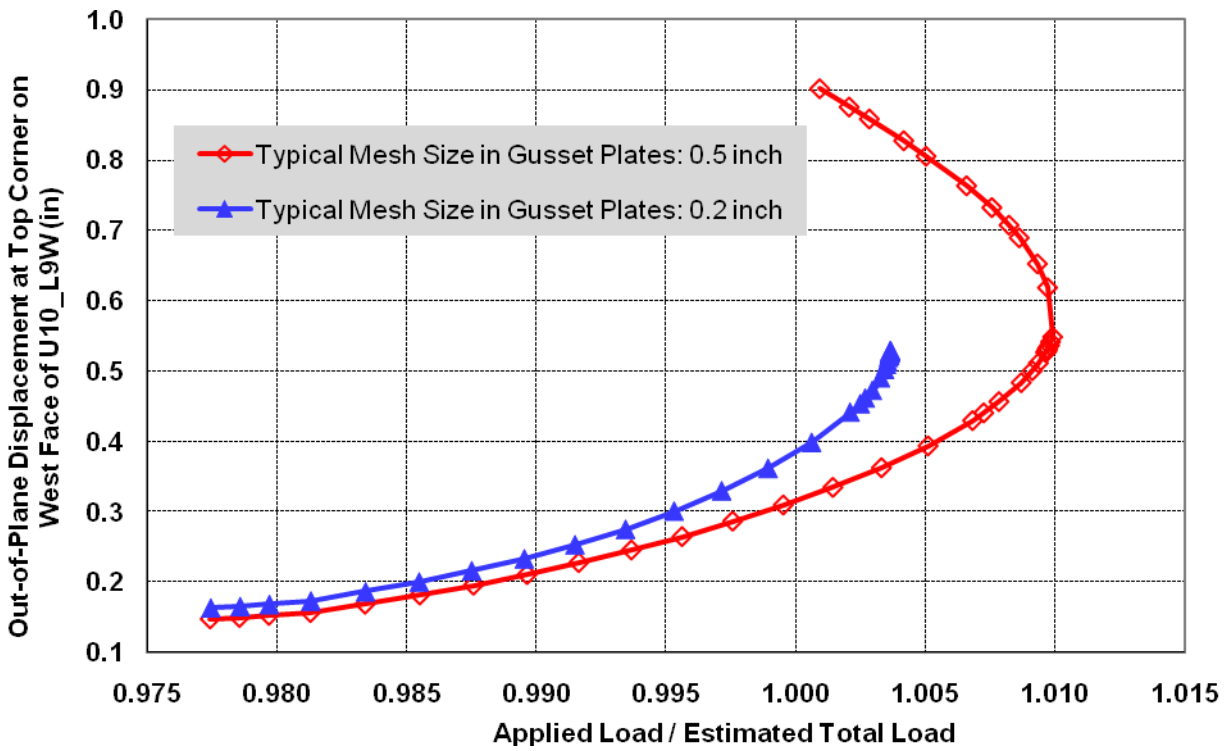
Figure 4.9: Comparison of normalized total load versus displacement in Riks construction loading step with load condition A2 between gusset mesh size of 0.5 inch and 0.2 inch
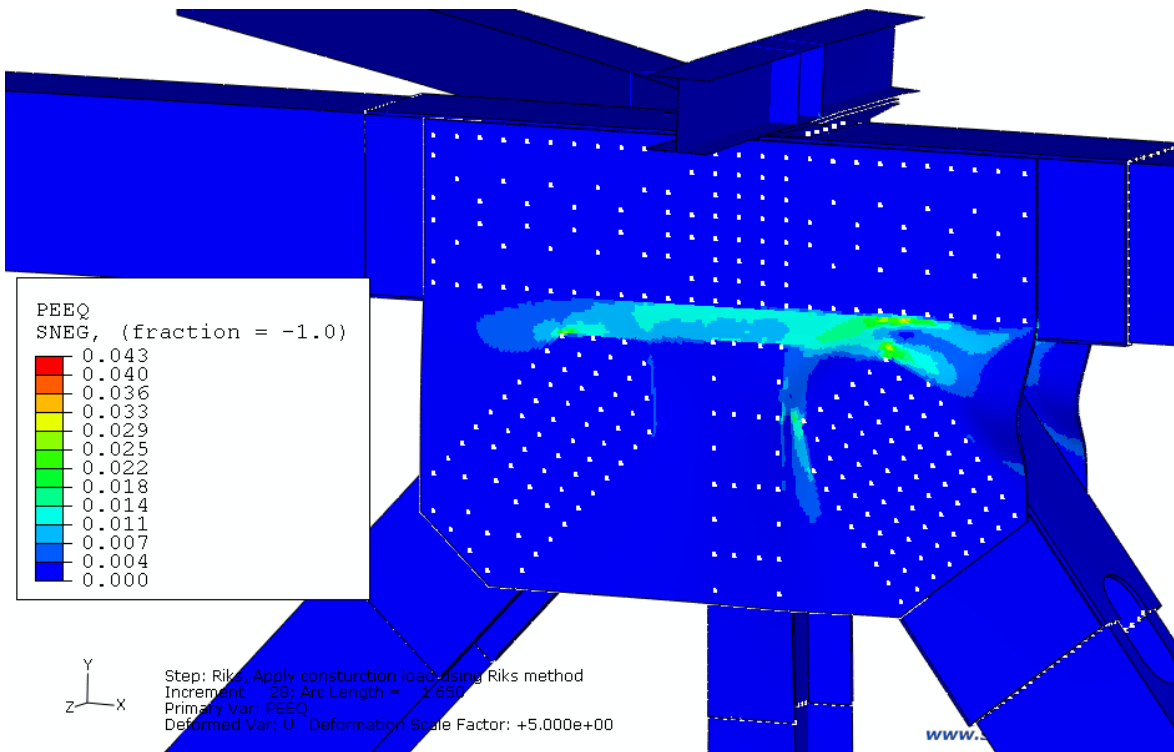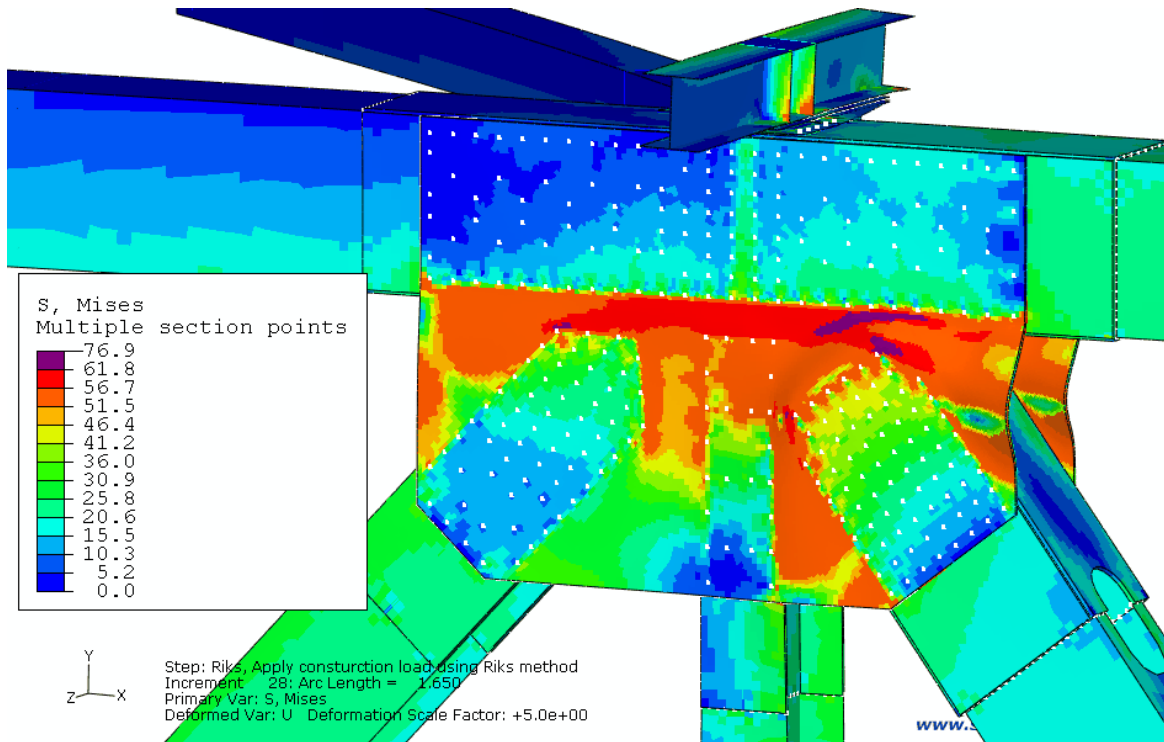
Riks step: Total load of 25,852 kips

Figure 4.10: Von Mises stress and equivalent plastic strain (PEEQ) distribution under the load
close to the predicted maximum load at instability at the U10W joint with load condition A2
(deformation magnified 5x)
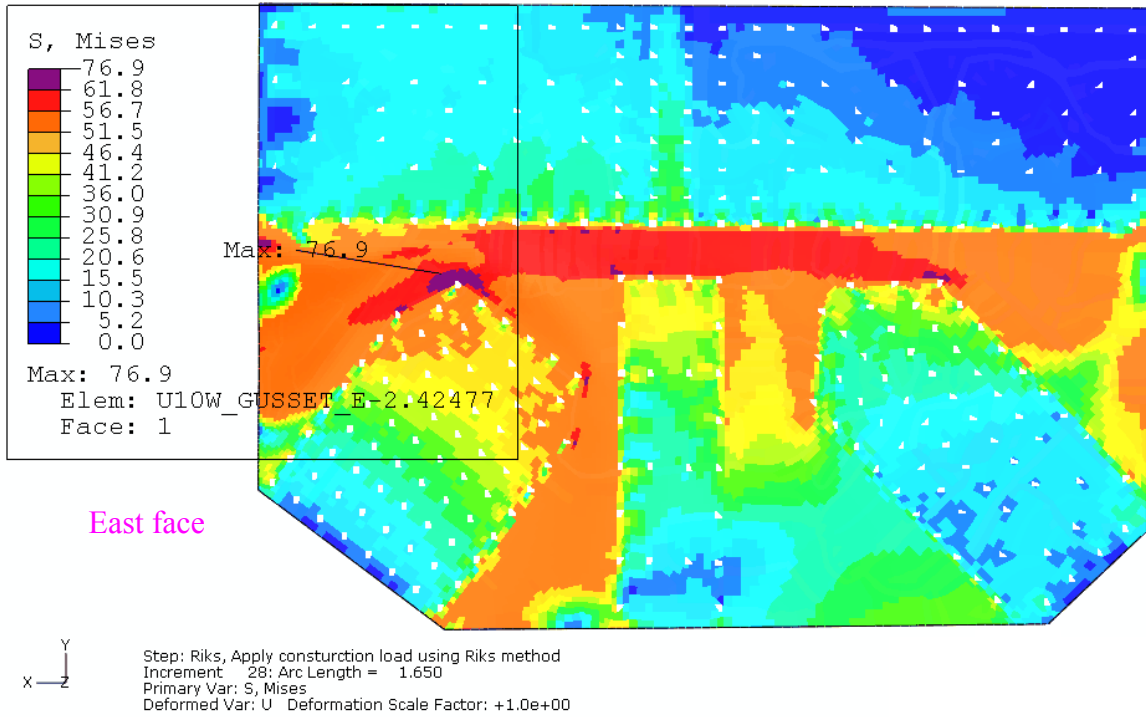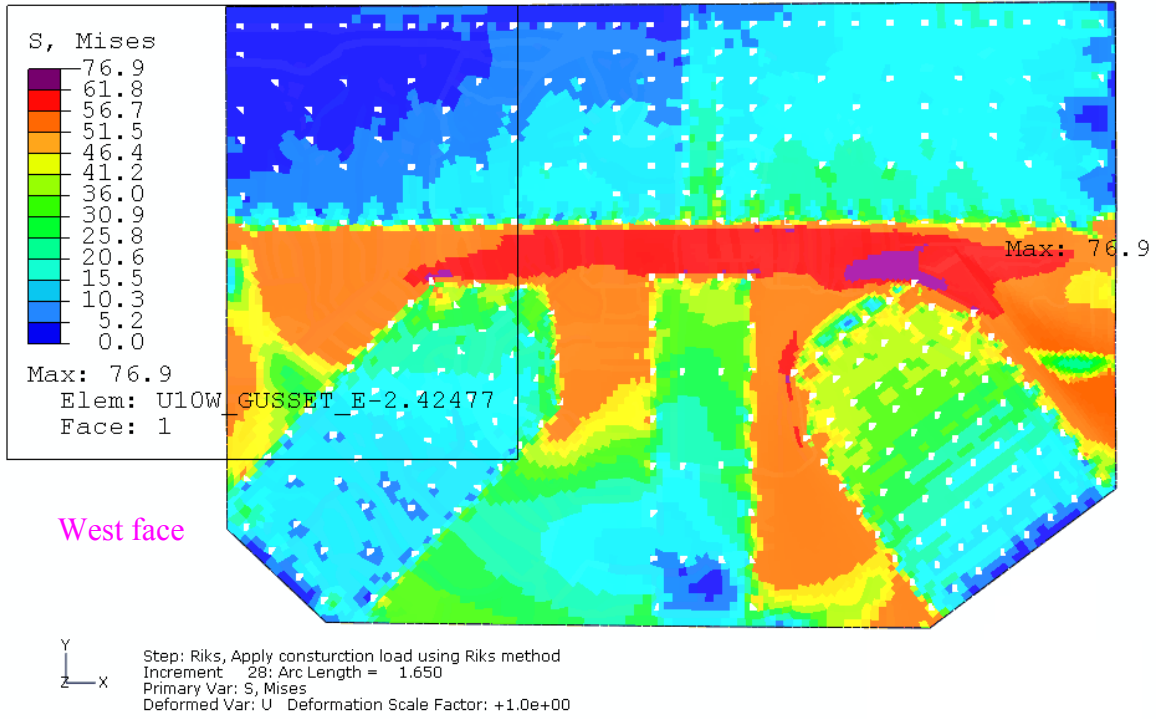
Riks step: Total load of 25,852 kips

Figure 4.11: Von Mises stress distribution under the load close to the predicted maximum load at instability in the east gusset plate at the U10W joint with load condition A2
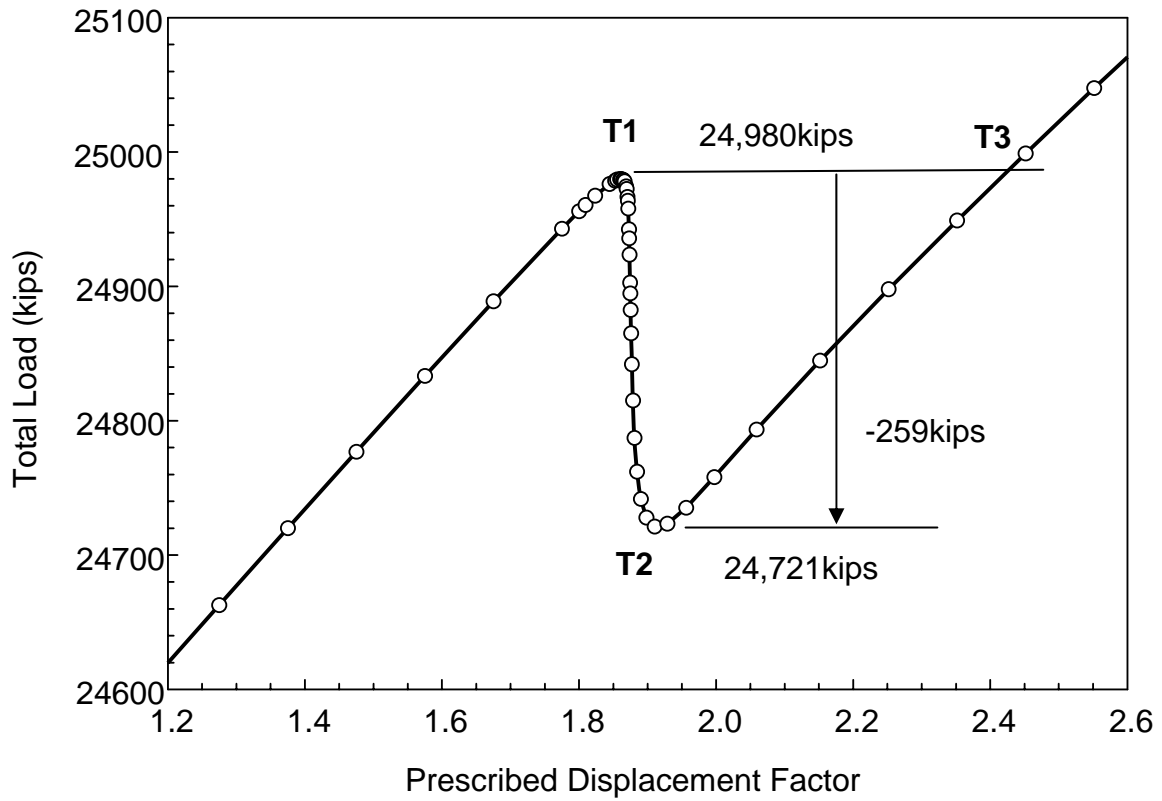
Figure 4.12 : Total load shown as a function of increasing prescribed displacements
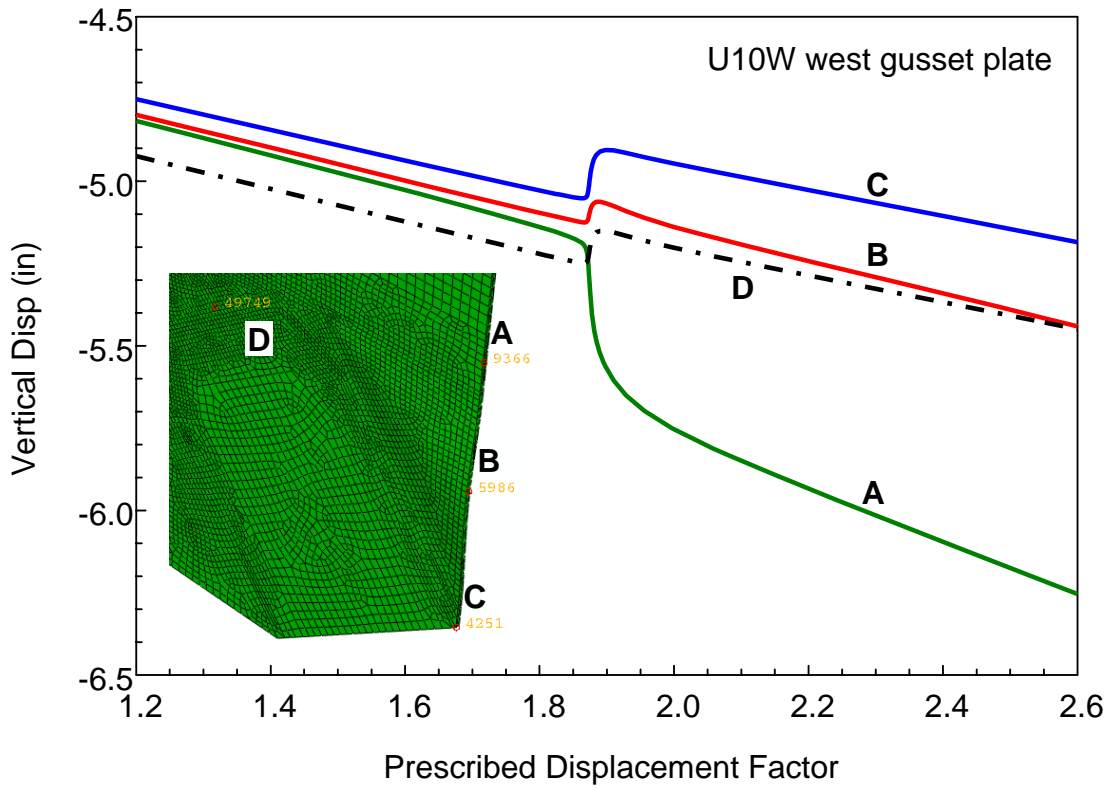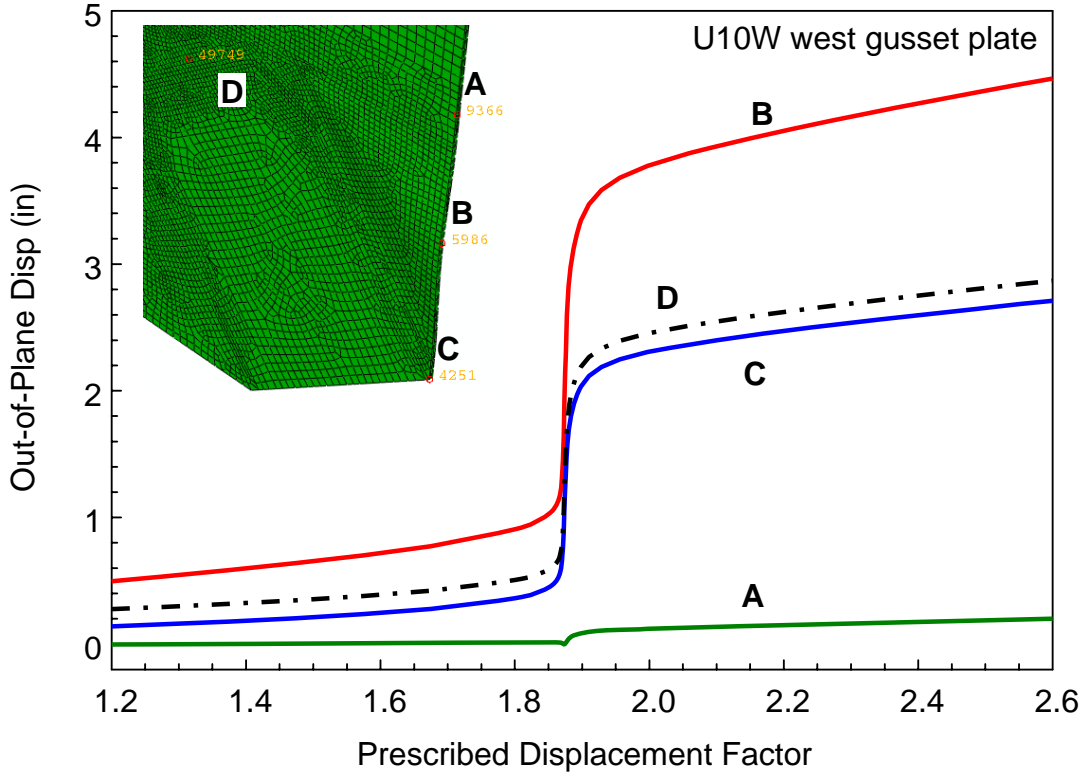
Figure 4.13: Out-of-plane and vertical displacements at four nodes near and along the edge of the bowed region
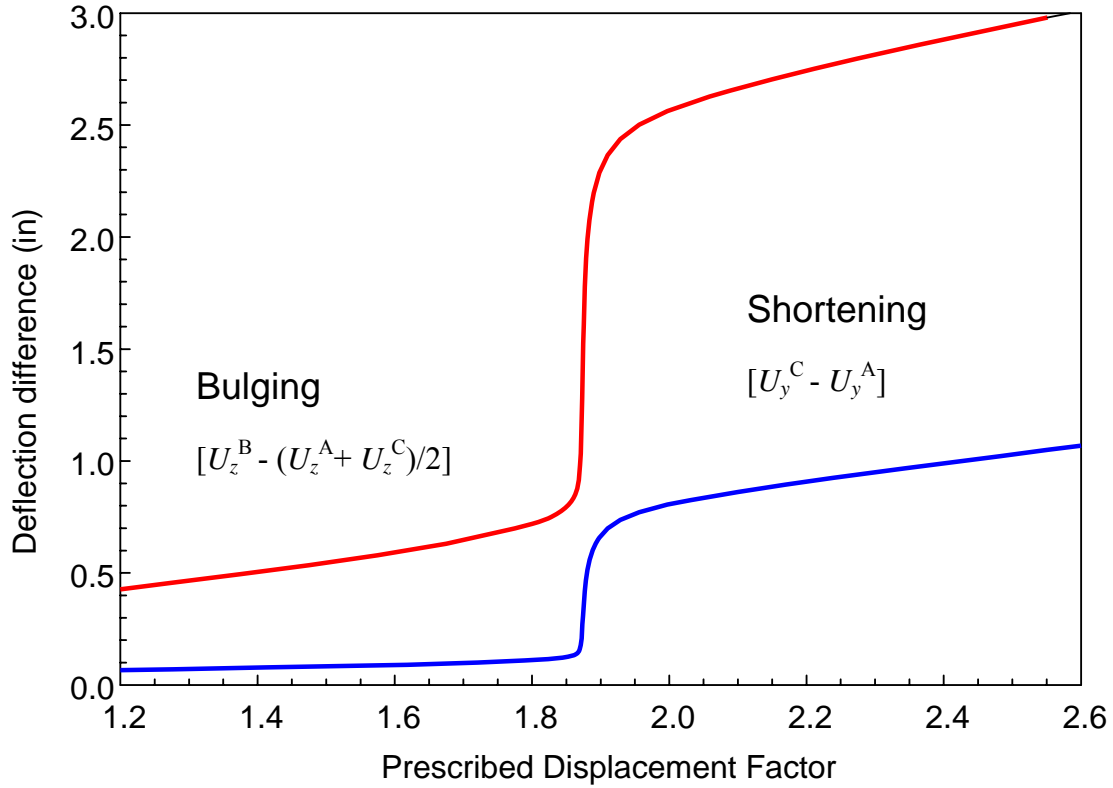
Figure 4.14: Relative displacement changes along the edge of gusset plate
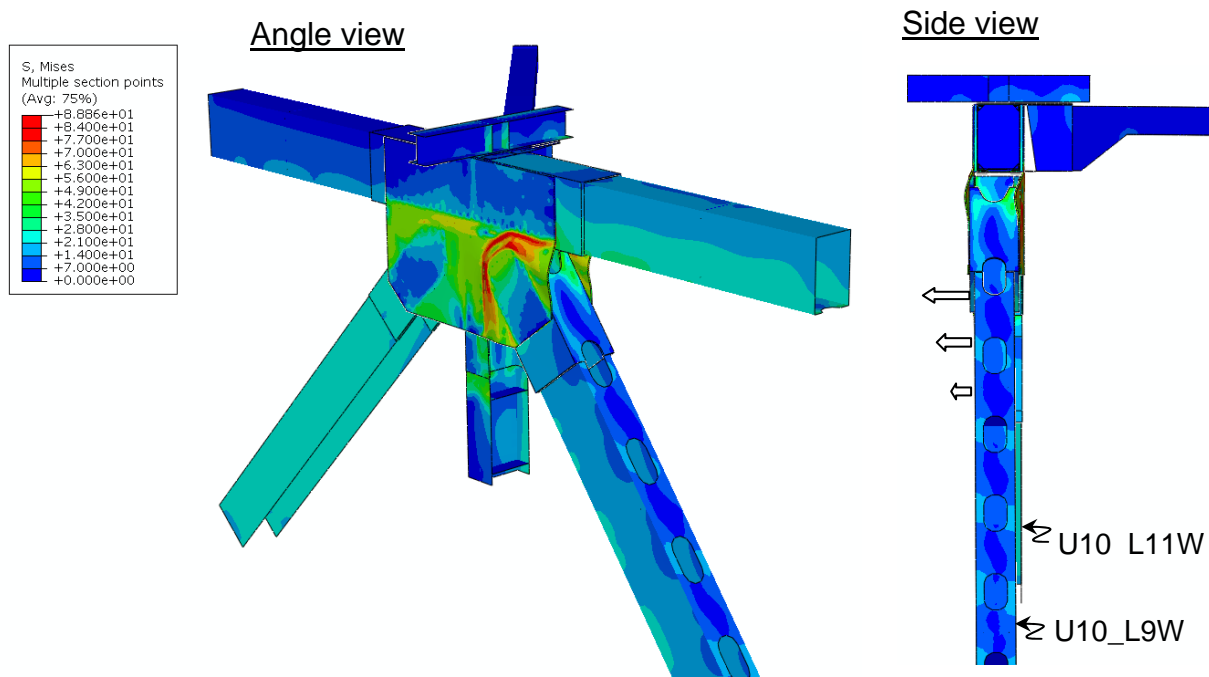
Figure 4.15: von Mises stress of U10W joint region at T2 (without deformation magnification)
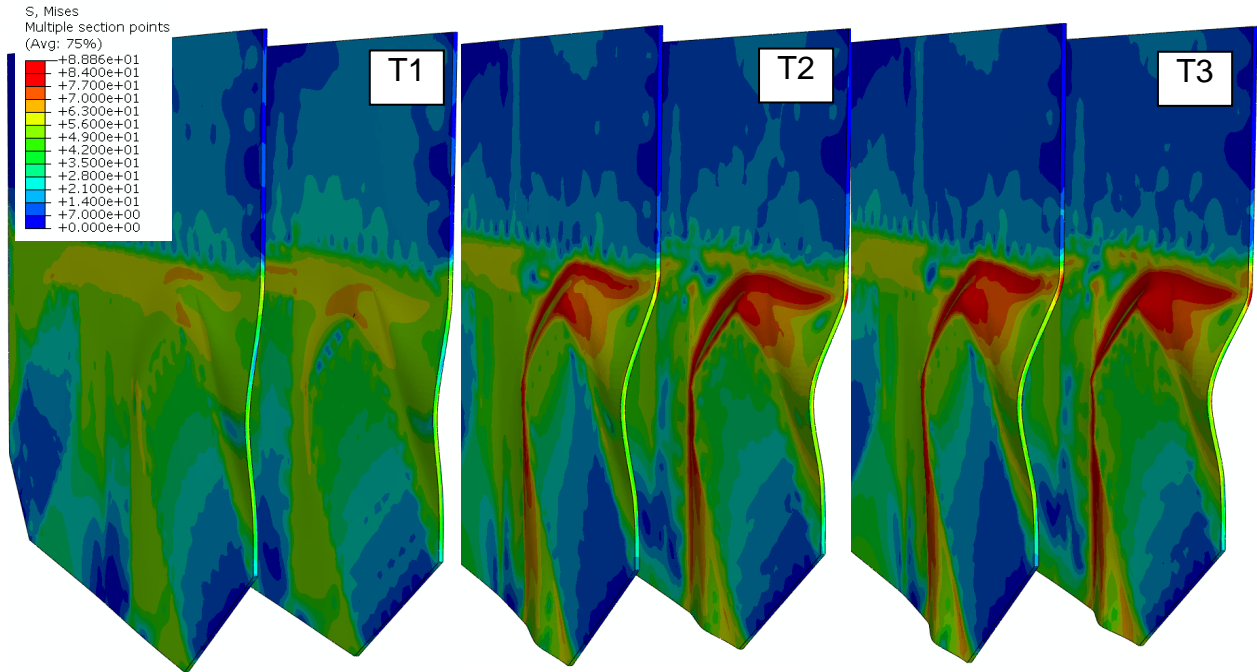
Figure 4.16: Evolution of von Mises stress of two gusset plates at U10W joint region
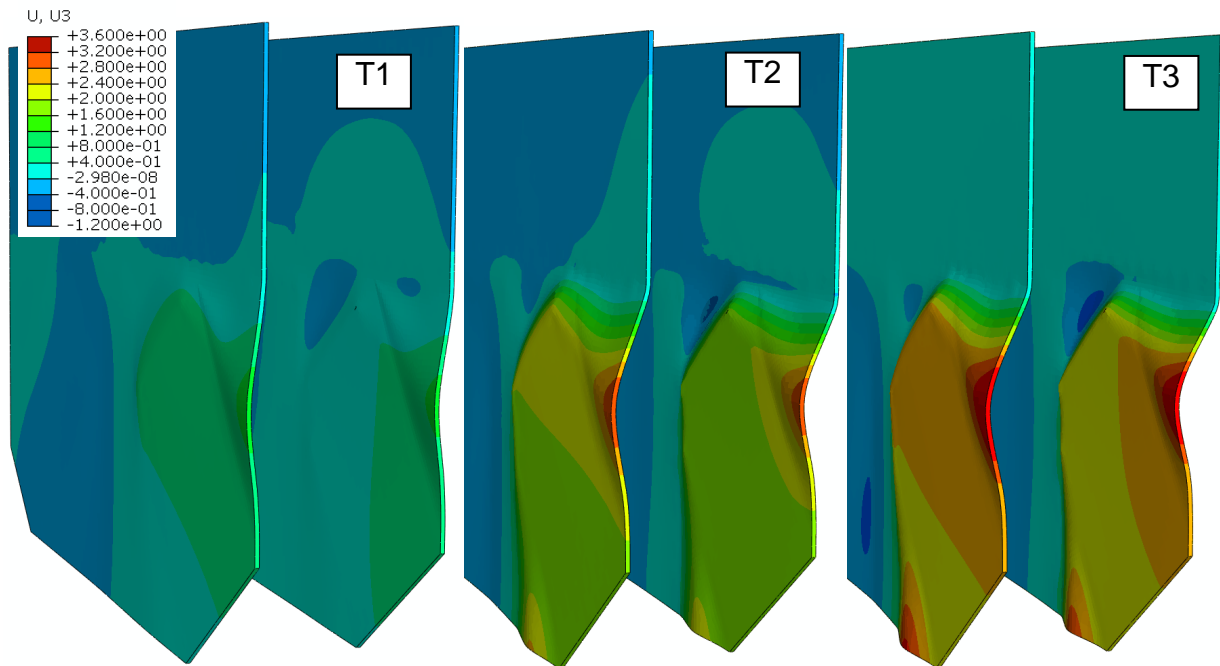
Figure 4.17 : Evolution of out-of-plane displacement of two gusset plates at U10W joint region
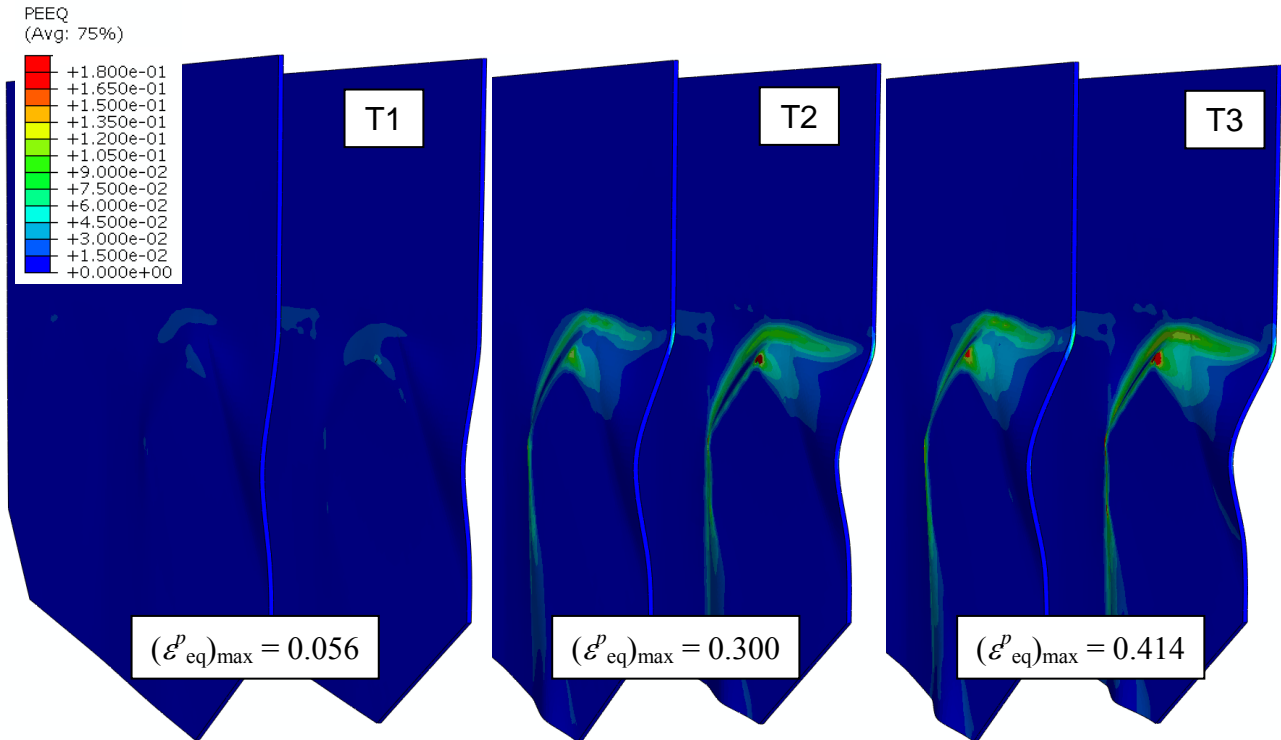
Figure 4.18: Evolution of equivalent plastic strain of two gusset plates at U10W joint
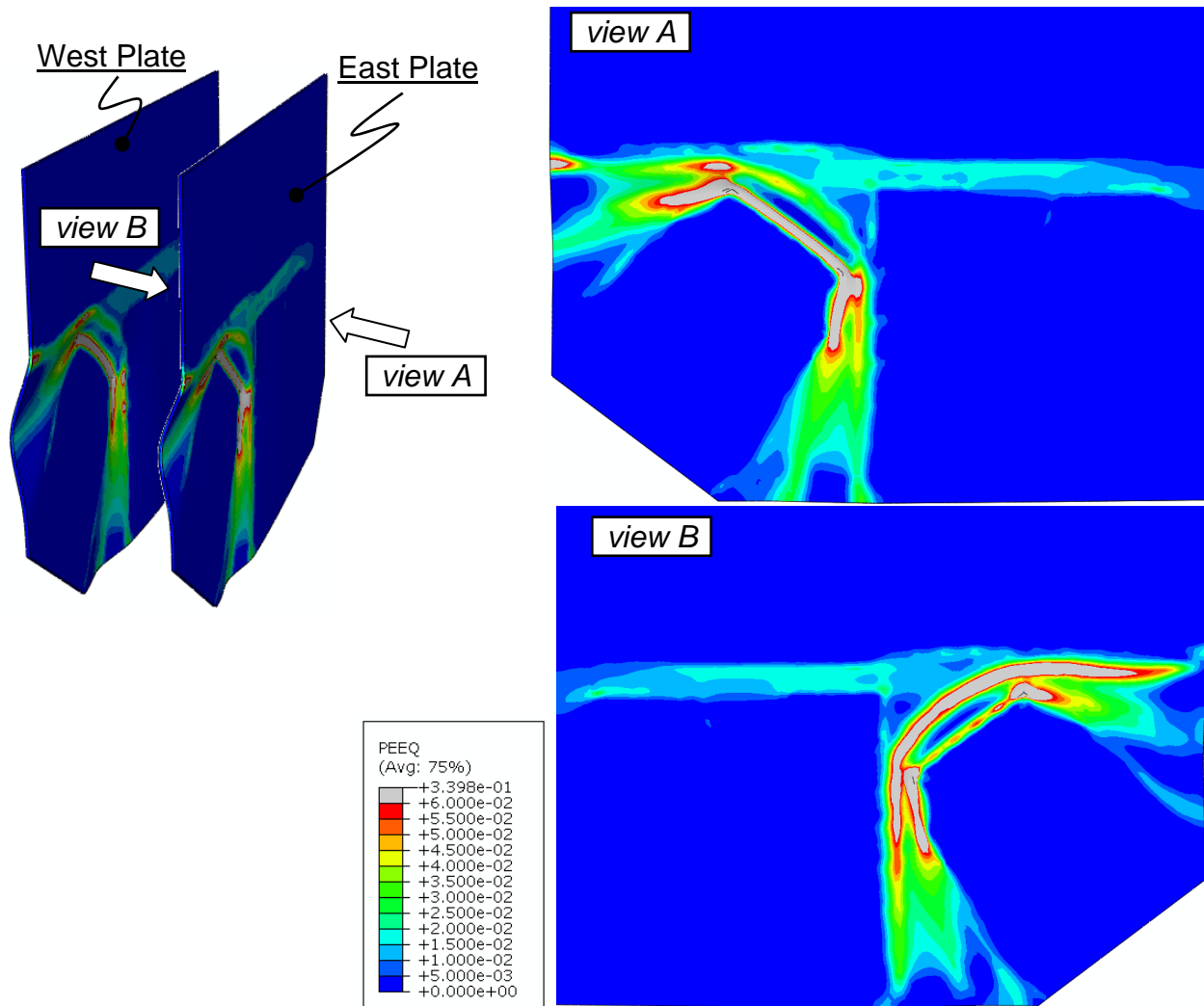
Figure 4.19: Equivalent plastic strain of east gusset plates at T2
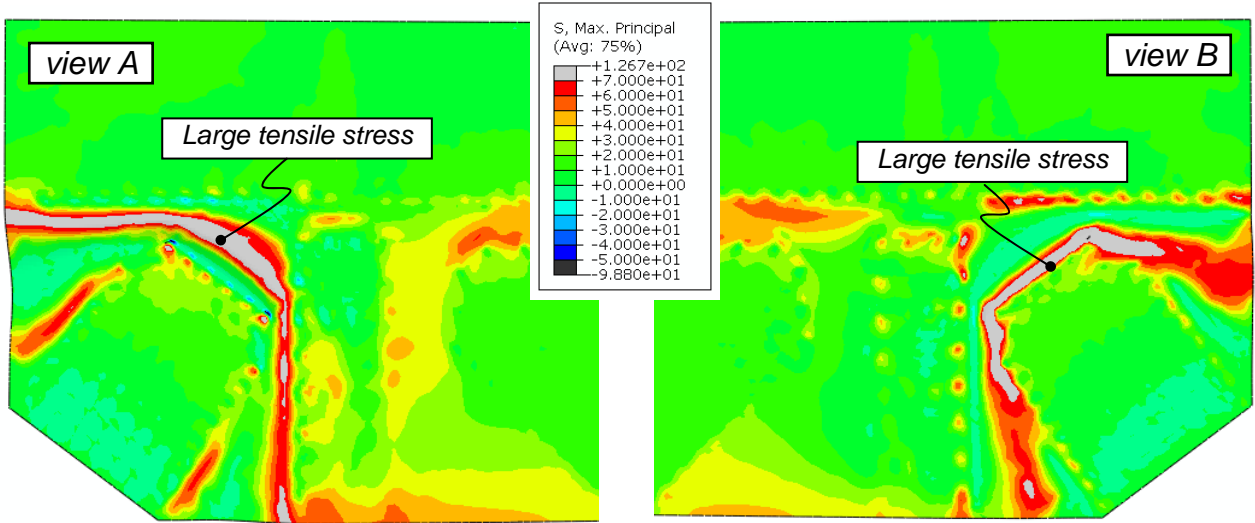
Figure 4.20: Maximum principal stress contours on surfaces of east gusset plates at T2

5   Submodeling the Highly Stressed Region of the Gusset Plate and Rivets at the U10W Joint

5.1   Submodel Description

The fasteners used to connect the truss members to the gusset plates in the models in the prior sections 3 and 4 are distributed couplings that would average out any stress concentrations associated with the actual attachment rivets and holes. In order to explore those stress concentrations, a node-based submodeling technique was used to investigate the highly stressed region of the east gusset plate and rivets at the U10W joint. A submodel was created with a refined mesh and two rivets modeled with solid elements. The submodel was driven at its boundaries by corresponding displacement results from a global model. The global model was chosen to be the mixed model with load condition A1, as described in Section 3 of this report.

5.1.1   Geometry and Meshing in the Submodel

The submodel was obtained by cutting the global mixed model to incorporate the highly stressed region of the east gusset plate. The submodel region is designated by the two red polygons in Figure 5.1. The submodel consisted of one portion of the east gusset plate, one portion of the main truss upper chord member U10_U9W, one portion of the vertical truss member U10_L10W, one portion of the diagonal truss member U10_L9W, and two rivets to replace the two Abaqus fasteners located in the highly stressed region. These components are shown in Figure 5.2.

Small portions of connecting plates, including U10W_splice_bottom, U10W_lateral_angle, U10W_lateral_bottom, and U10W_splice_E, were within the submodel region. However, these portions were not incorporated in the submodel because their effect on the stress distribution in the highly stressed region was assumed to be negligible. These small portions were located at the submodel boundaries, and were away from the region of interest.

The initial bowing in the east gusset plate was incorporated in the submodel in the same manner and shape as in the global model. The east gusset plate was represented with C3D8R elements with enhanced hourglass control [11]. An in-plane mesh size of 0.03 inches was typical in the highly stressed region of the plate. This is in contrast to a typical element size of 0.2 inch in the highly stressed region of the global model. The largest in-plane element size in the submodel was about 0.5 inches. Eight elements were used through the thickness of the gusset plate. The plate contained 221,640 brick elements. Figure 5.3 shows the meshing details of the plate submodel.

The three main truss members were represented with C3D8R elements. Four elements were used through the thickness of the main truss members. A mesh size ranging from 0.05 inches to 0.5 inches was used in the truss member region in contact with the plate.

The two rivets were represented with C3D8R elements. A mesh size of 0.03 inches was used in the circumferential direction of the rivets, and a mesh size of 0.1 inches was used in their axial direction. A cross-section of the rivet joint showing the mesh density of the joined components is shown in Figure 5.4.

5.1.2   Material Properties

The gusset plate and the truss members were represented with the 50 ksi steel, the same as in the global model. The true stress-plastic strain curve of the 50 ksi steel was extrapolated to a plastic strain of 20 percent, as shown in Figure 5.5. The extrapolation was used to avoid potential divergence issues which might occur if the von Mises stress in the submodel reached the largest value provided. The steel for the rivets was assumed to have the same elastic modulus, Poisson's ratio, and density as those of the 50 ksi steel. Figure 5.5 shows the true stress-plastic strain curve of the steel defined for the rivets, which was estimated based on the difference in hardness between the rivets and the plates [8, 9]. The yield stress of the rivet steel was estimated to be 75 ksi.

5.1.3   Boundary Conditions, Loading Conditions, Rivets, and Contacts

As stated previously, the submodel boundaries were driven by the global model displacement results. The submodel driven nodes are denoted by the red dots in Figure 5.6. The displacements of the driven nodes in the submodel were constrained to match the displacements from the global model at the same locations as the submodel boundaries. No other translational or rotational boundary conditions were defined in the submodel. Gravity load was applied to all components in the submodel, which is the same as the global model.

All rivets, except the two modeled with solid elements at the top corner of the diagonal truss member, were represented by Abaqus fasteners. Contact pairs were defined between the components wherever the fasteners were employed to connect them. A Coulomb friction model with a friction coefficient of 0.1 was used for the contact pairs, which is the same as the global model.

Contact was also defined between the modeled rivets and the gusset plate, and between the rivets and the diagonal truss member, as shown in Figure 5.7. The contact involving the cylindrical surfaces of the rivets was the same as that defined between the gusset plate and the truss members. One difference was the contact definition between the heads of the rivets and their adjacent mating surfaces. It was assumed that no separation between rivet head and adjoining surface would occur, so a "no separation" surface behavior definition was used.

5.2   Analysis Results in the Submodel at the U10W Joint

5.2.1   Stress and Strain Distribution Under the Estimated Construction Load

Analysis results indicated that when subjected to the estimated construction loads, plastic deformation occurred primarily in the east gusset plate modeled. This is shown in Figure 5.8, Figure 5.9, Figure 5.10 and Figure 5.11. Figure 5.8 and Figure 5.9 show a comparison between global model and submodel stress and equivalent plastic strain results. Note that the shading in the gusset region below the horizontal truss member in Figure 5.8 and Figure 5.9 was not a contour difference. The plots on the left side of the two figures are from the submodel and the plots on the right side are from the global model. The comparison shows that the solution at the submodel boundaries was similar to the global model results, helping to validate the submodel. Figure 5.9 shows that the global model and submodel had identical results in the gusset plate, except in the local region where holes and rivets were modeled – which was expected. Figure 5.10 and Figure 5.11 show the von Mises stress and equivalent plastic strain distribution in the submodel of the east gusset plate. The maximum von Mises stress in the east gusset plate was

predicted to be 82 ksi on the edge of the rivet hole at the top corner. This corresponded to an equivalent plastic strain (PEEQ) of 6.3%. The maximum von Mises stress predicted by the submodel was larger than that predicted by the global model, which was induced by the much smaller mesh size and the incorporation of the two rivets in the submodel. The maximum von Mises stress under the estimated construction load was predicted to be less than the maximum measured tensile stress of the material, 88.86 ksi, even with the highly refined mesh size of 0.03 inches in the highly stressed region and the incorporation of the two rivets.

5.2.2   Stress and Strain Distribution under the Predicted Maximum Load at Instability

The global model with all regular static steps diverged at a total load of 24,809 kip, or a construction load of 905 kip, which is 1.57 times the estimated construction load. Under this predicted maximum load at instability, plastic deformation in the submodel occurred primarily in the east gusset plate and the rivet at the top corner. Figure 5.12 and Figure 5.13 show the von Mises stress and equivalent plastic strain distribution in the east gusset plate under the maximum predicted load at instability. The maximum von Mises stress was predicted to be 90 ksi on the edge of the rivet hole at the top corner, which corresponded to an equivalent plastic strain of 13.5%. The maximum von Mises stress was predicted to be larger than the maximum measured tensile stress of the gusset material. However, the highest von Mises stress occurred in a small region that was constrained by contact with the rivet, and all three principal stresses of the maximum von Mises stress were predicted to be compressive stresses, -47 ksi, -71 ksi, and -146 ksi.

Figure 5.14 shows the von Mises stress and equivalent plastic strain distribution in the two rivets when subjected to the predicted maximum load at instability. The maximum von Mises stress was predicted to be 97 ksi, which corresponded to an equivalent plastic strain of 2.6%. These maximum values occurred where the rivet contacted the gusset, and where the gusset rivet hole stress was maximum, as shown in Figure 5.15.

Table 5.1 summarizes the maximum von Mises stress and the maximum equivalent plastic strain in the east gusset plate between the submodel and the global model. The second column in the table represents the results under estimated construction load, and the third column represents the results under the predicted maximum load at instability.

Table 5.1

Submodel and Global Model Comparison of Maximum Stress and Strain in the East Gusset Plate

	Results Using Construction Load	Results Using Predicted Maximum Load at Instability
Total Load (kip)	24,482	24,809
Construction Load (kip)	578	905
Maximum von Mises Stress in Submodel (ksi)	82	90
Maximum von Mises Stress in Global Model (ksi)	66	82
Maximum Equivalent Plastic Strain in Submodel	6.3%	13.5%
Maximum Equivalent Plastic Strain in Global Model	2.2%	6.4%

5.3   Summary: U10W Joint Submodel

A detailed solution in the highly stressed region of the U10W joint was obtained using a node-based submodeling technique. The global model used fasteners to represent rivets. A typical mesh size of 0.2 inches was used in the highly stressed region of the gusset plates in the global model. In the submodel two actual rivets and corresponding holes in the highly stressed region were modeled and other rivets were represented with fasteners. A typical mesh size of 0.03 inches was used in the highly stressed region of the gusset plates in the submodel. The analysis indicated that the global model and submodel had identical results in the gusset plate, except in the local region where holes and rivets were modeled – which was expected. The submodel predicted a higher stress in the hole region. These results indicated the validity of modeling the rivets with fasteners.

The higher stress in the hole region does not lead to a material failure. The maximum von Mises stress in the east gusset plate under the estimated construction load was predicted to be 82 ksi, which corresponded to an equivalent plastic strain of 6.3%. This maximum von Mises stress was less than the maximum measured tensile strength of the material. Under the predicted maximum load at instability, the maximum von Mises stress in the east gusset plate was predicted to be 90 ksi, which corresponded to an equivalent plastic strain of 13.5%. While this von Mises stress was slightly above the maximum measured tensile stress of the gusset material of 89 ksi, all three principal stresses of the maximum von Mises stress were compressive stresses.
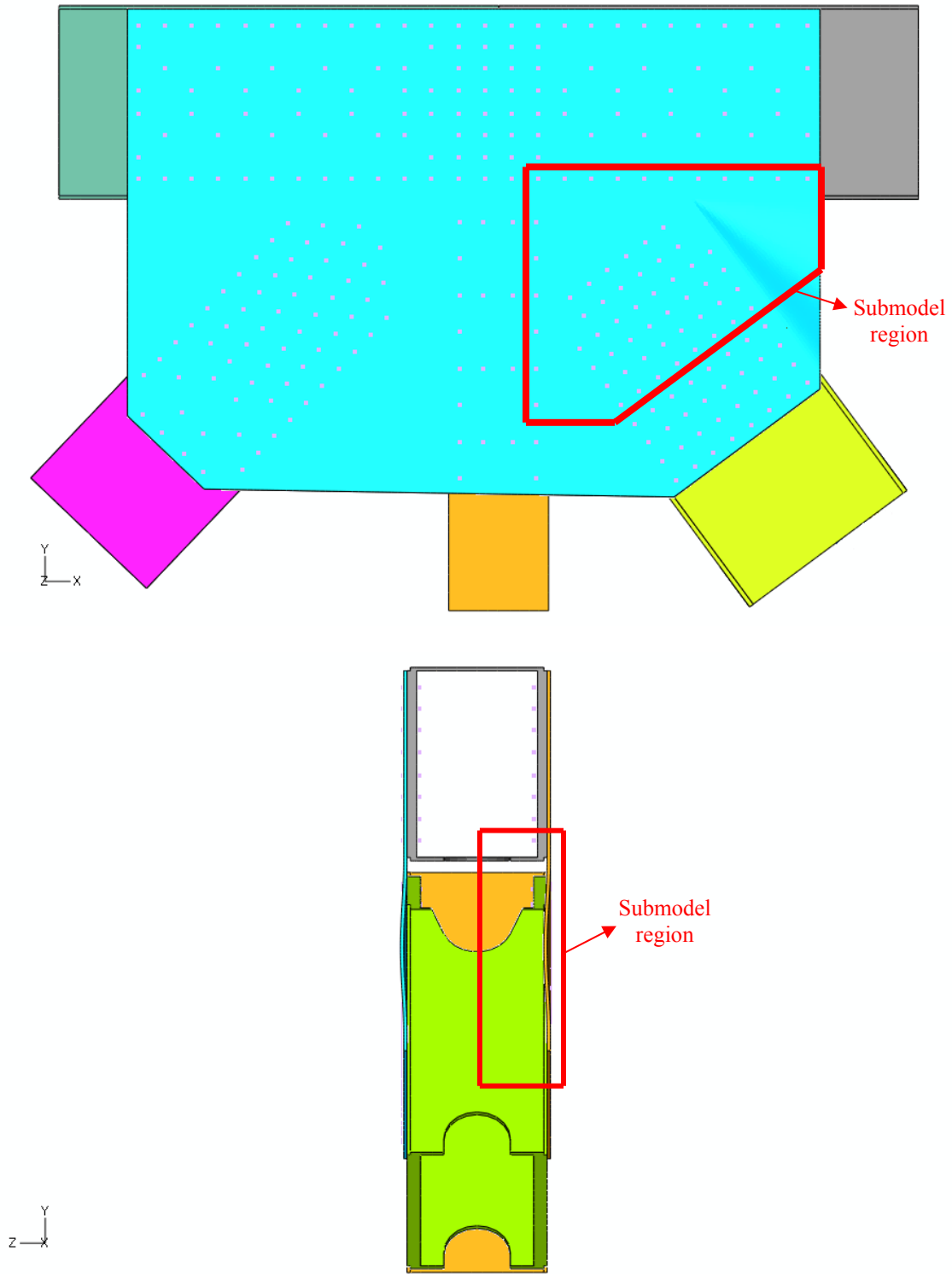
Figure 5.1: Submodel region in the global model at the U10W joint
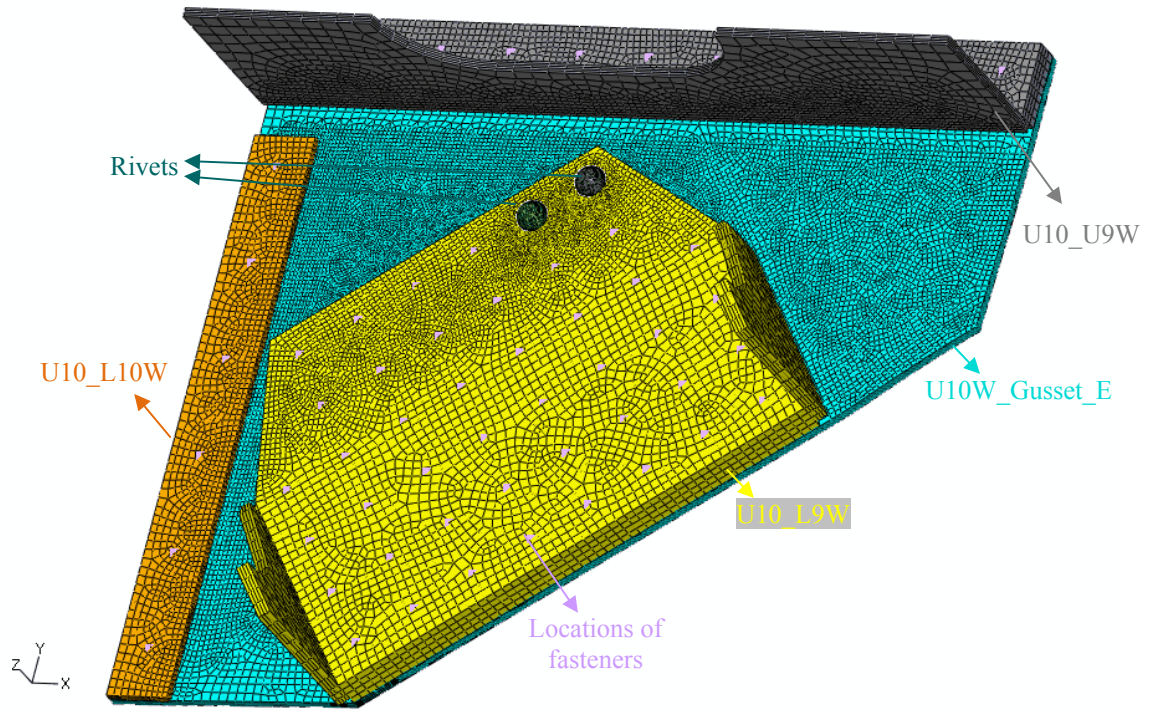
Figure 5.2: Components and meshing of the submodel at the U10W joint
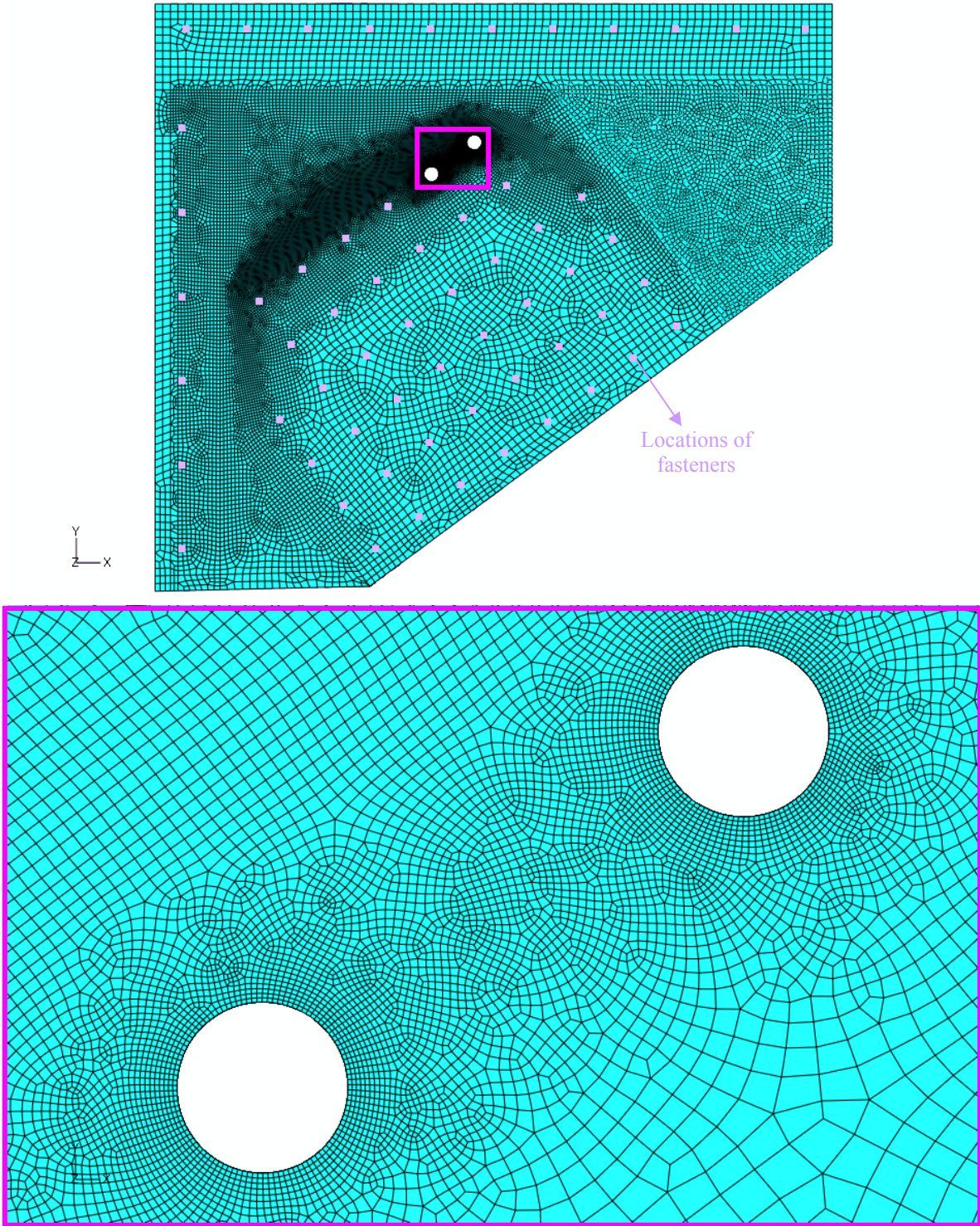
Figure 5.3: Meshing of the east gusset plate in the submodel at the U10W joint
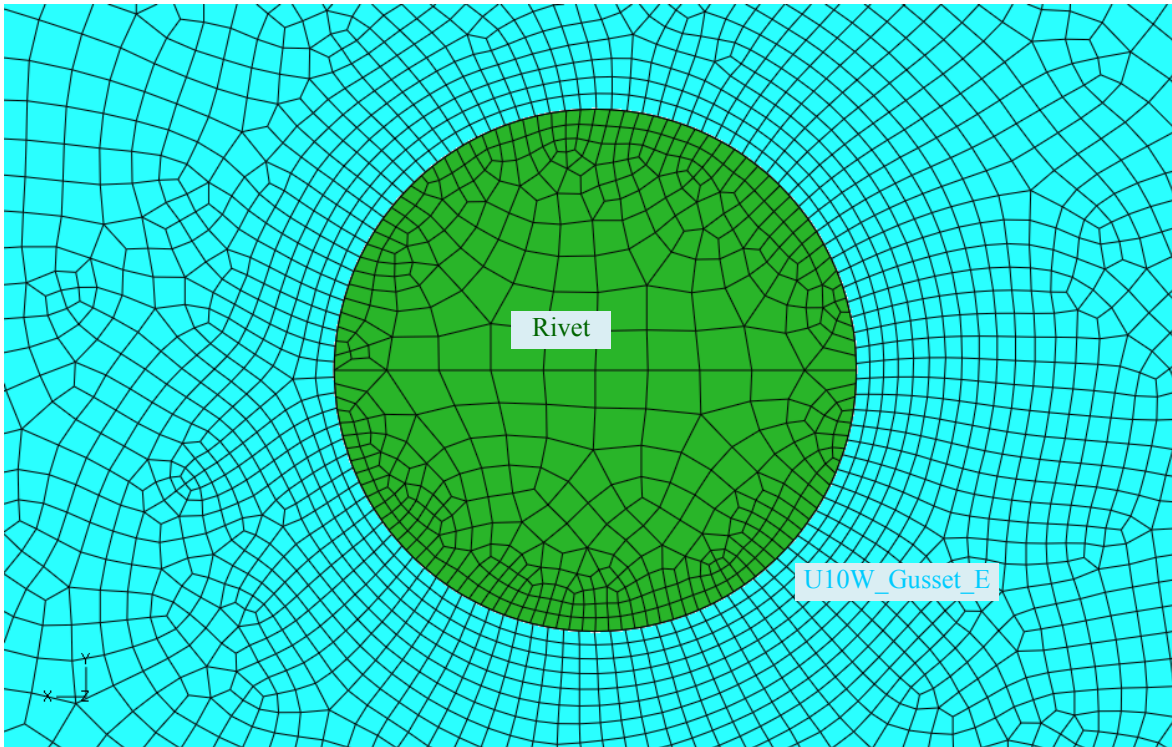
Figure 5.4: Cross-section meshing of the rivet joint in the submodel at the U10W joint
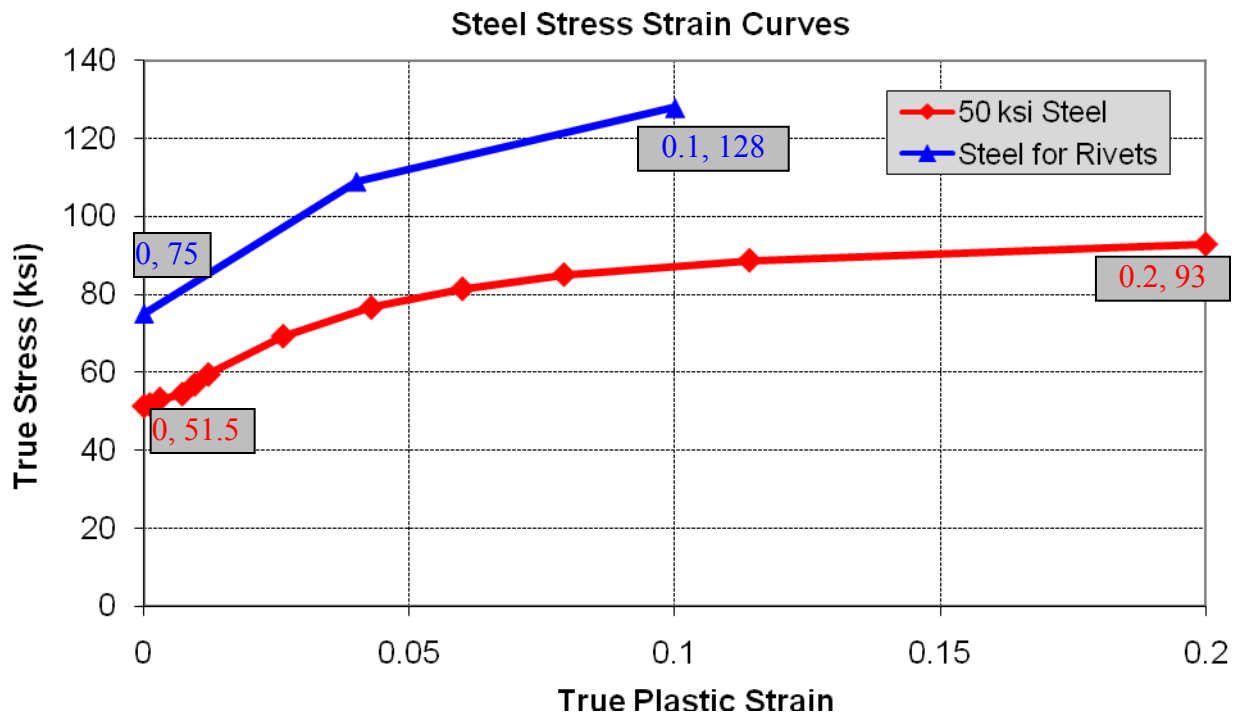
Figure 5.5: True stress-plastic strain curves of the steel used in the submodel at the U10W joint
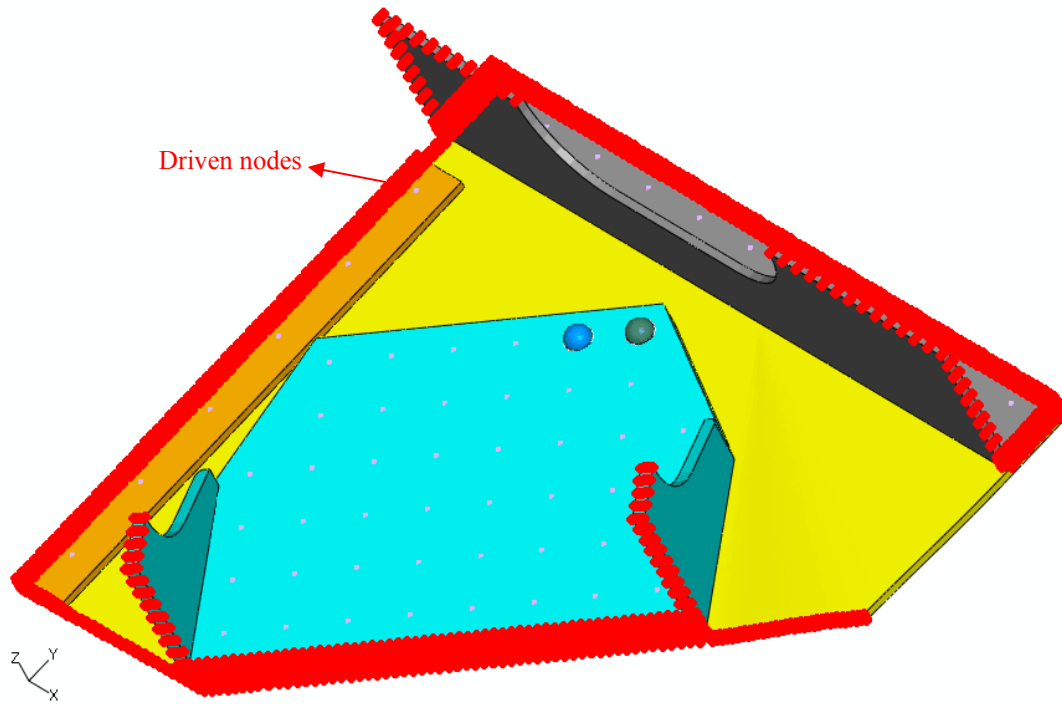
Figure 5.6: Driven nodes at the submodel boundaries at the U10W joint
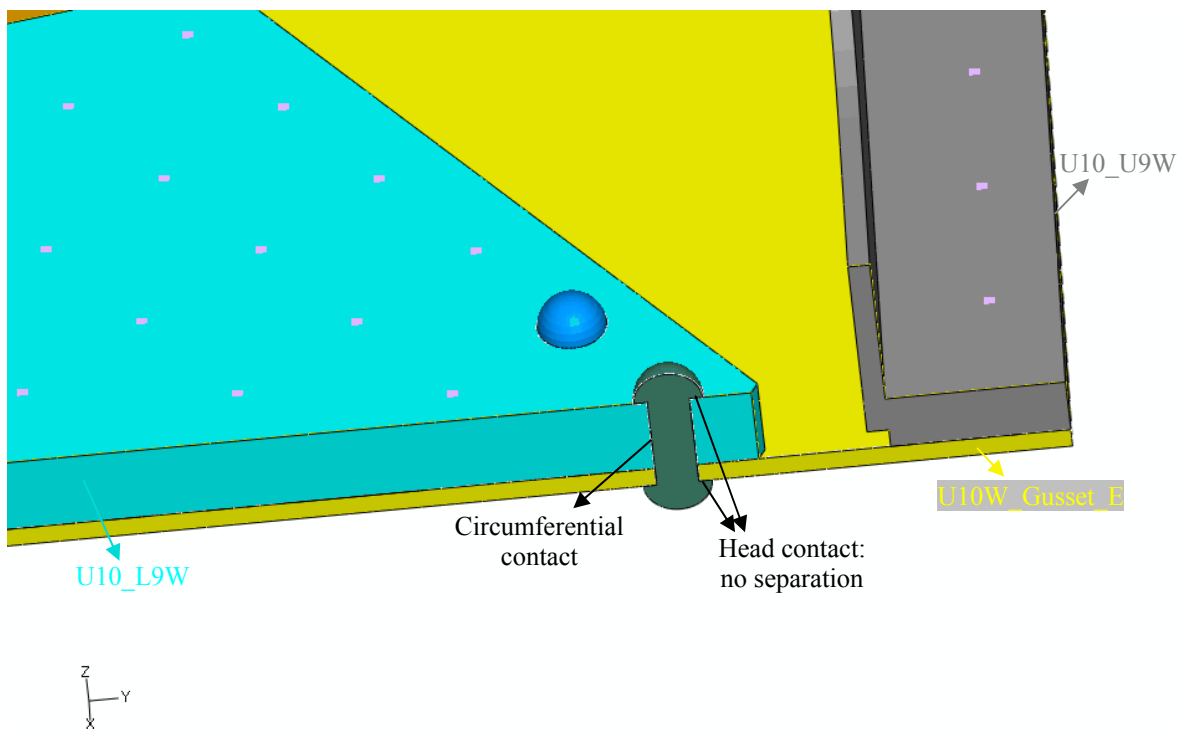
Figure 5.7: Contact definition for rivets in the submodel at the U10W joint
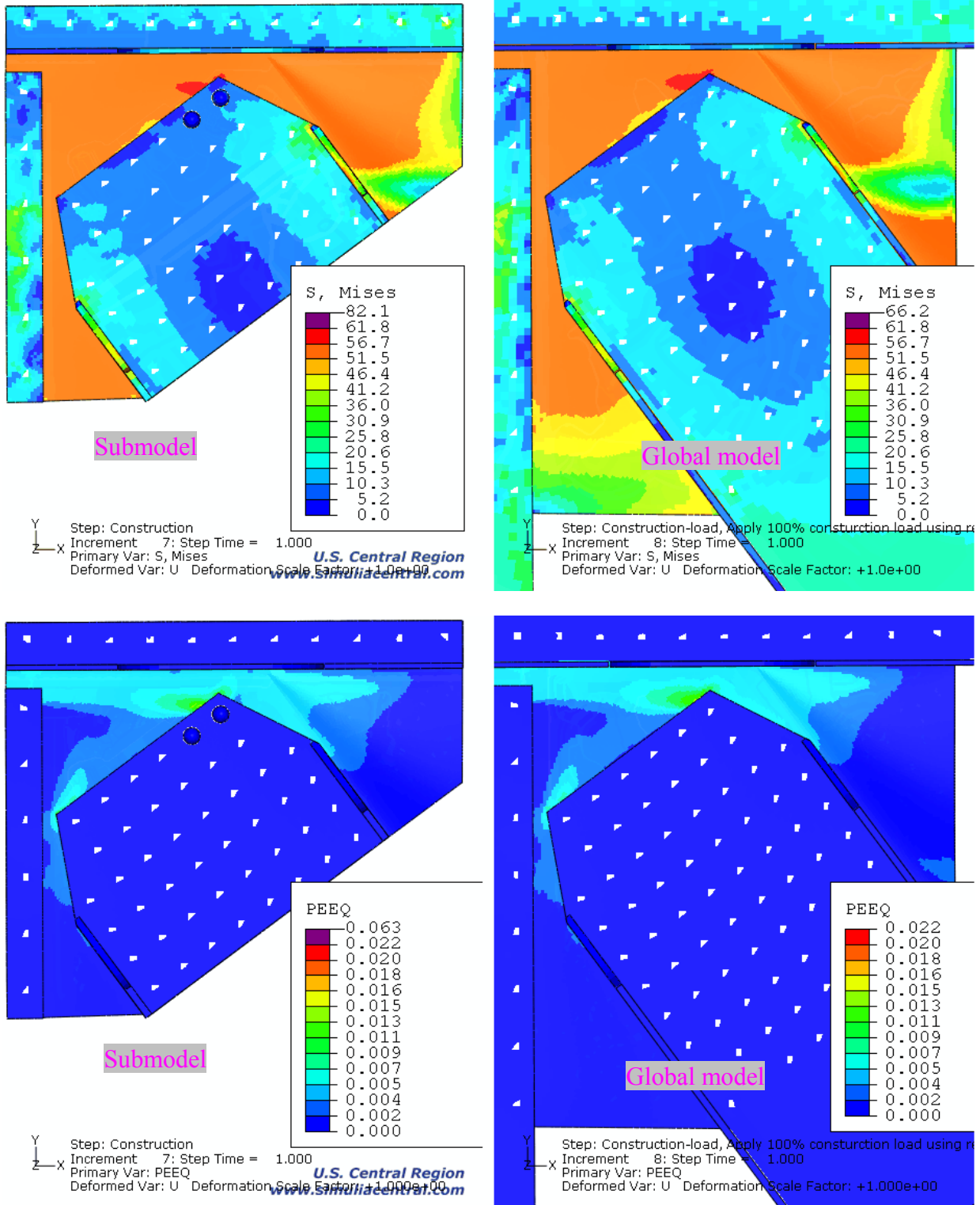
Figure 5.8: Von Mises stress and equivalent plastic strain distribution under the construction load in the submodel and global model at the U10W joint
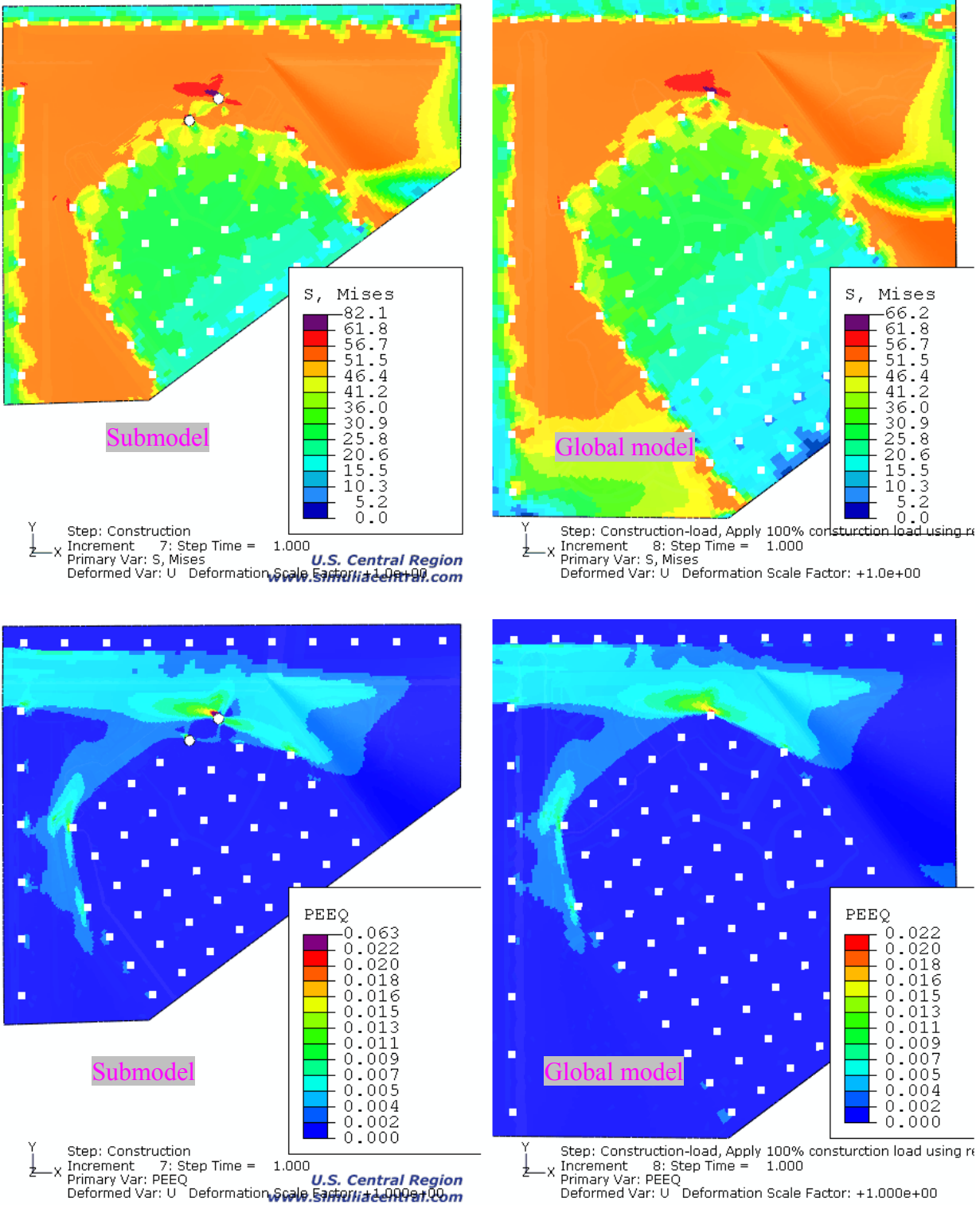
Figure 5.9: Von Mises stress and equivalent plastic strain distribution under the construction load in the east gusset plate in the submodel and global model at the U10W joint
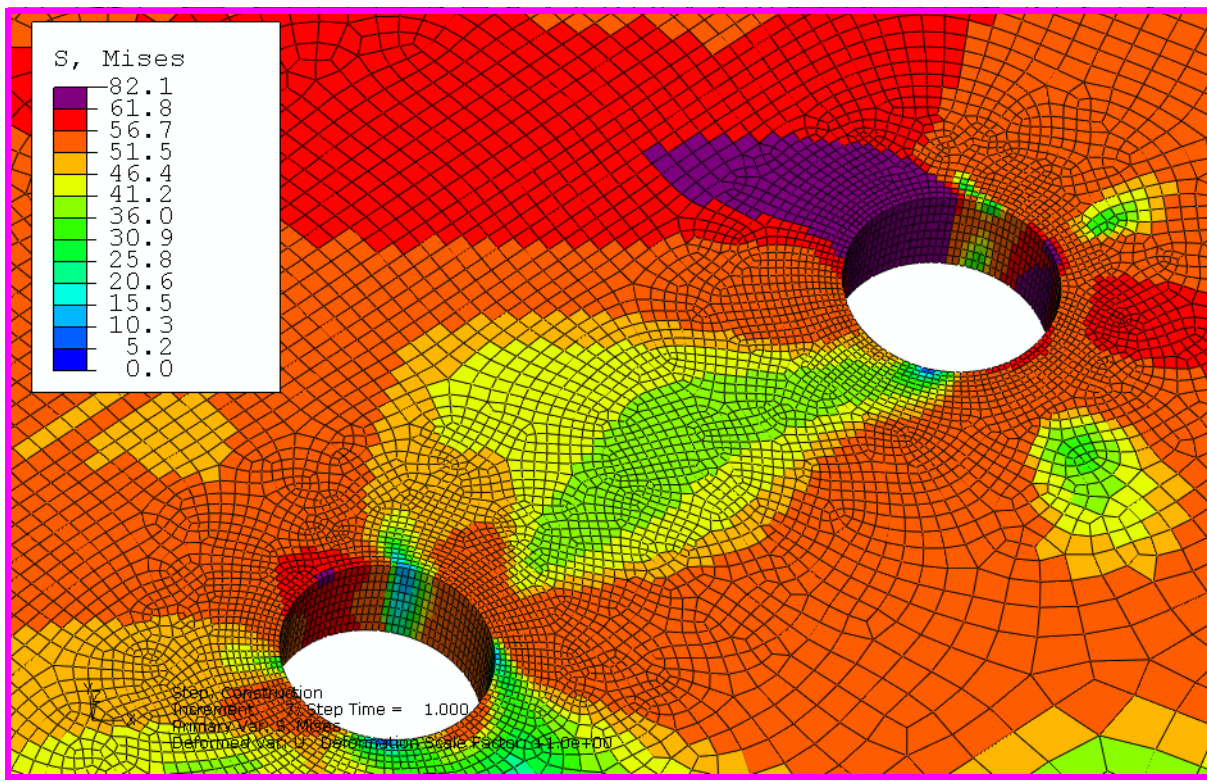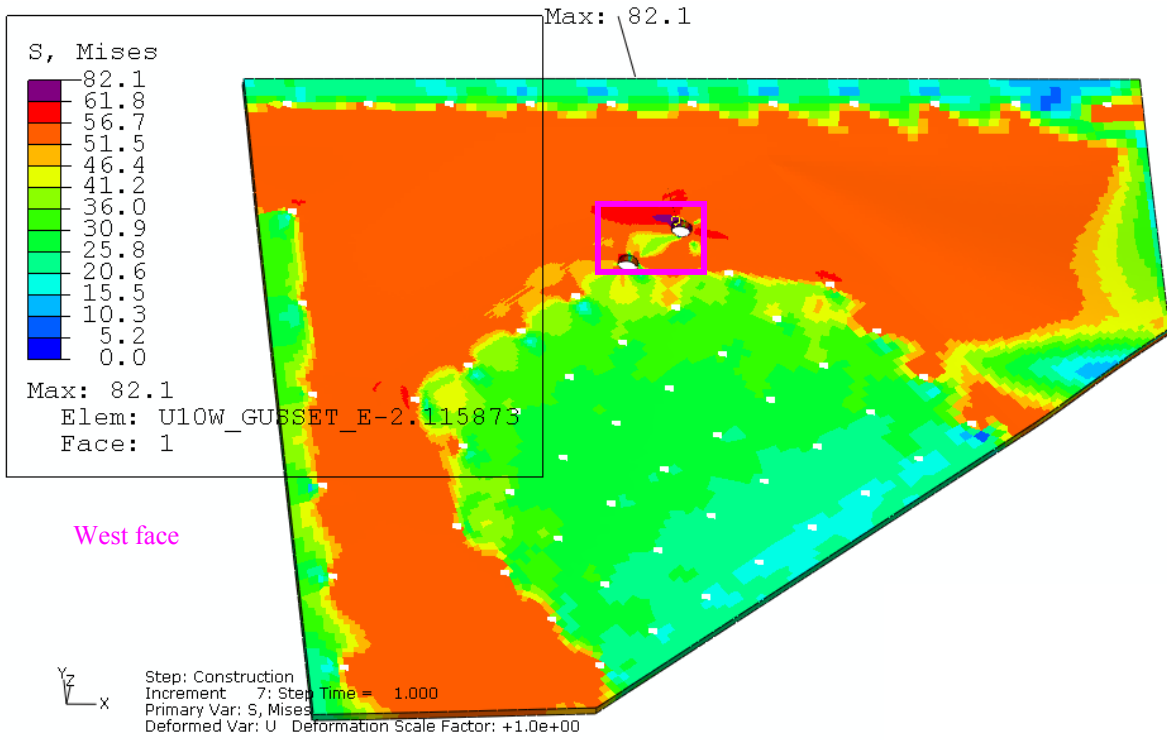
Figure 5.10: Von Mises stress distribution under the construction load in the east gusset plate in the submodel at the U10W joint

Figure 5.11: Equivalent plastic strain distribution under the construction load in the east gusset plate in the submodel at the U10W joint
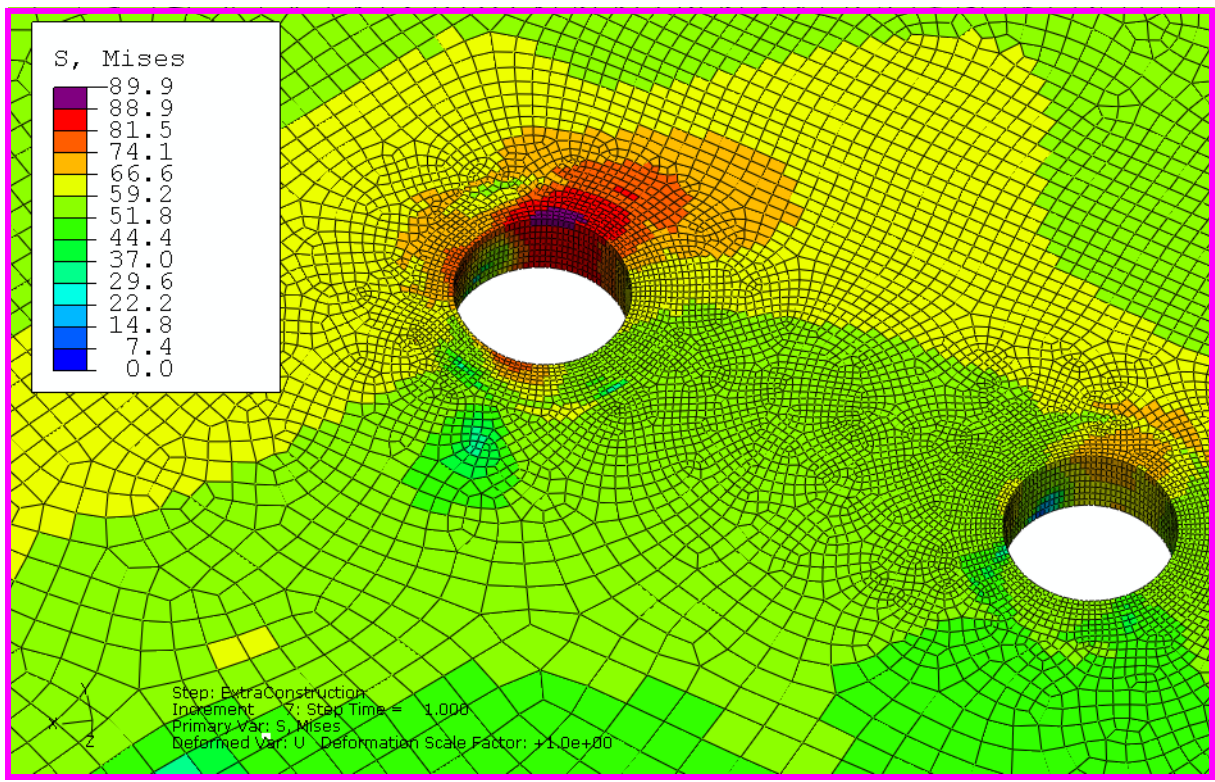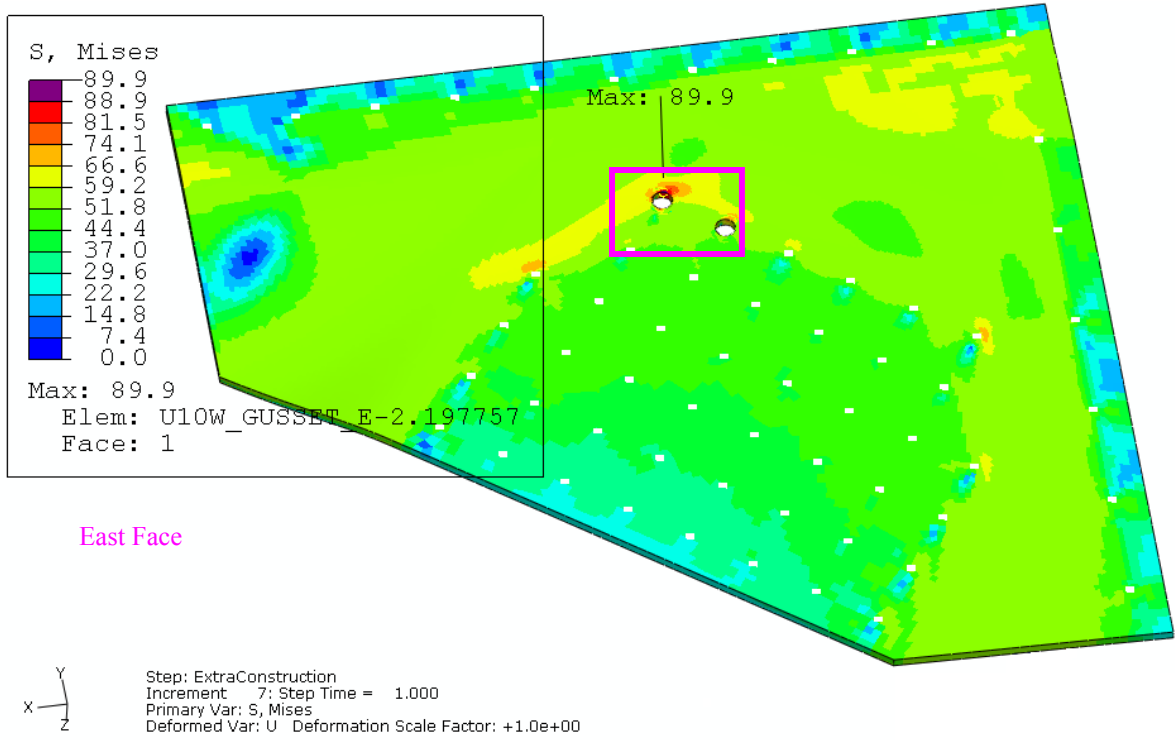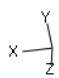
Figure 5.12: Von Mises stress distribution under the predicted maximum load at instability in the east gusset plate in the submodel at the U10W joint
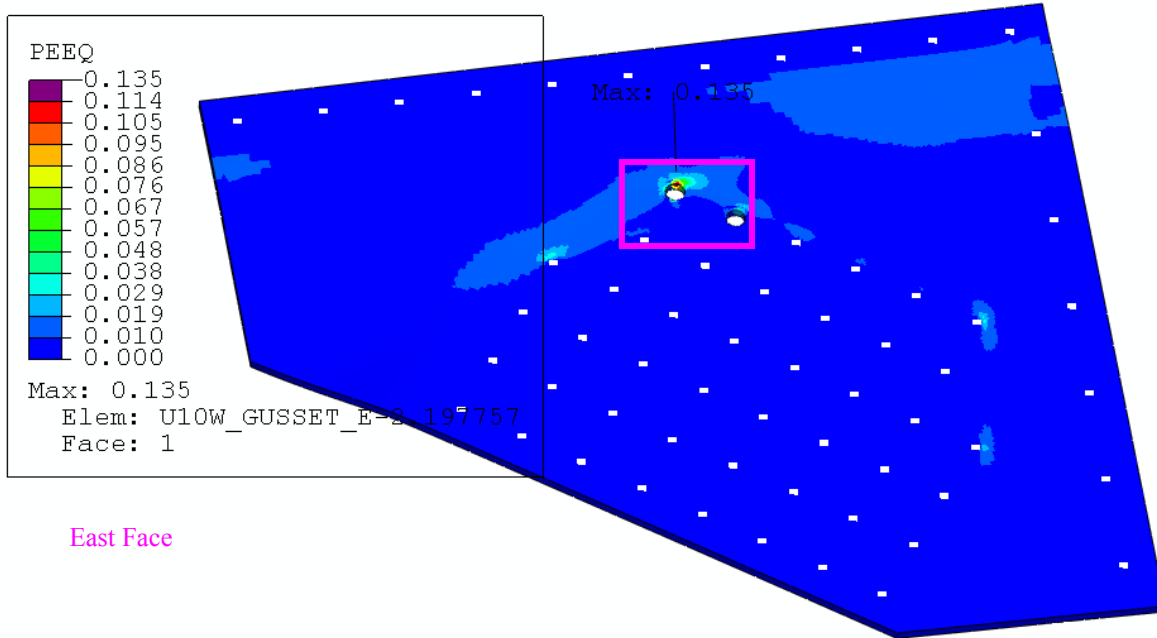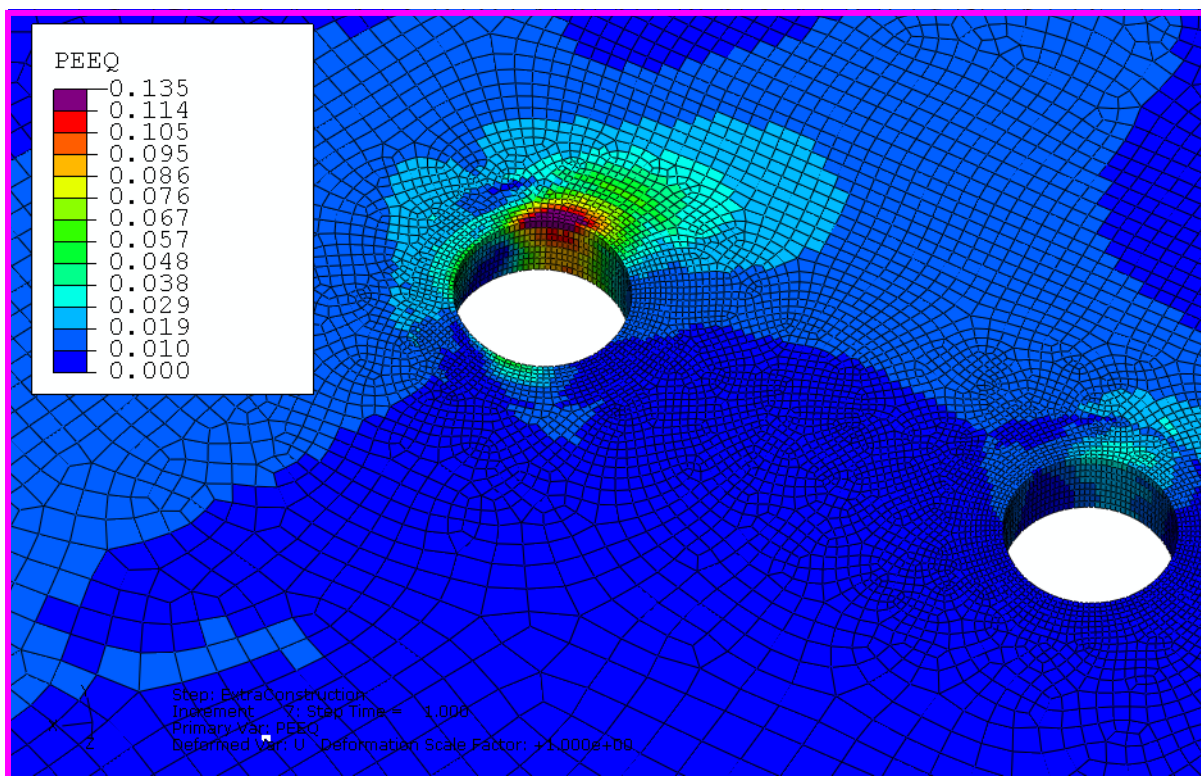
Figure 5.13: Equivalent plastic strain distribution under the predicted maximum load at instability in the east gusset plate in the submodel at the U10W joint
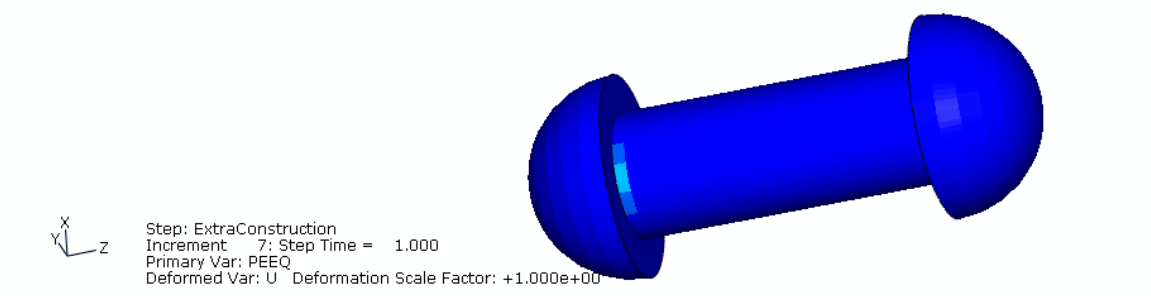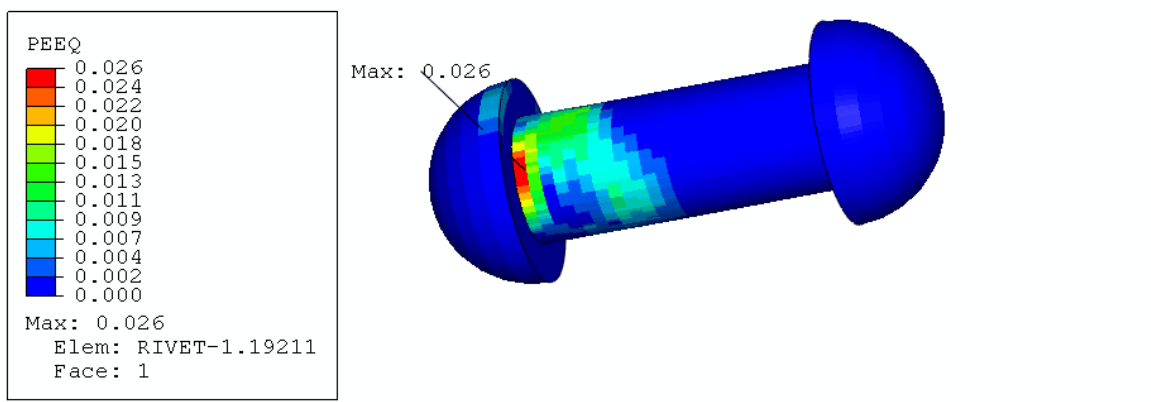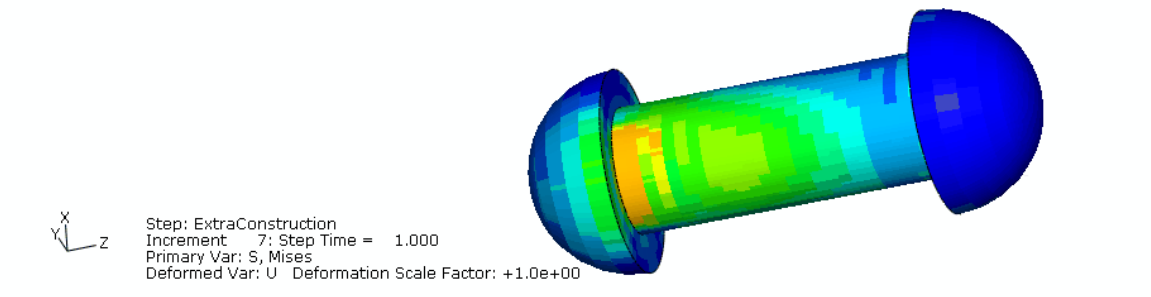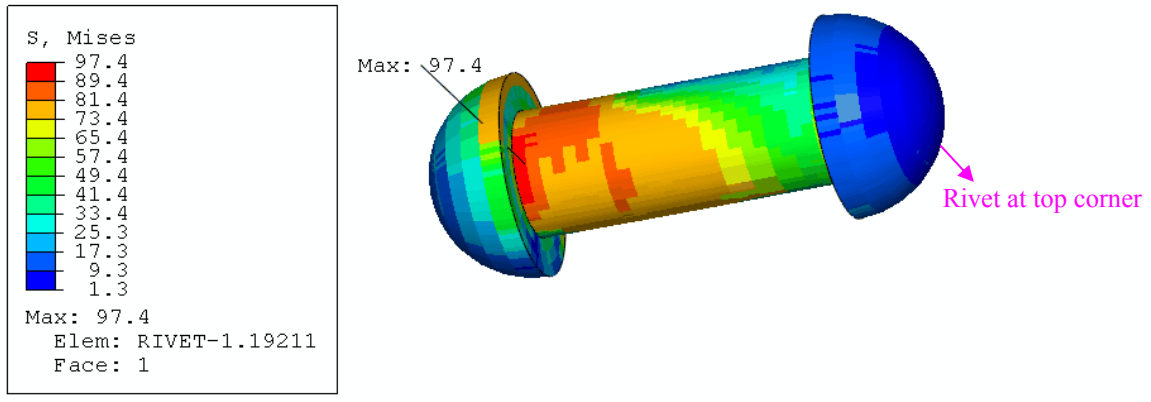
Figure 5.14: Von Mises stress and equivalent plastic strain distribution under the predicted maximum load at instability in the two rivets in the submodel at the U10W joint
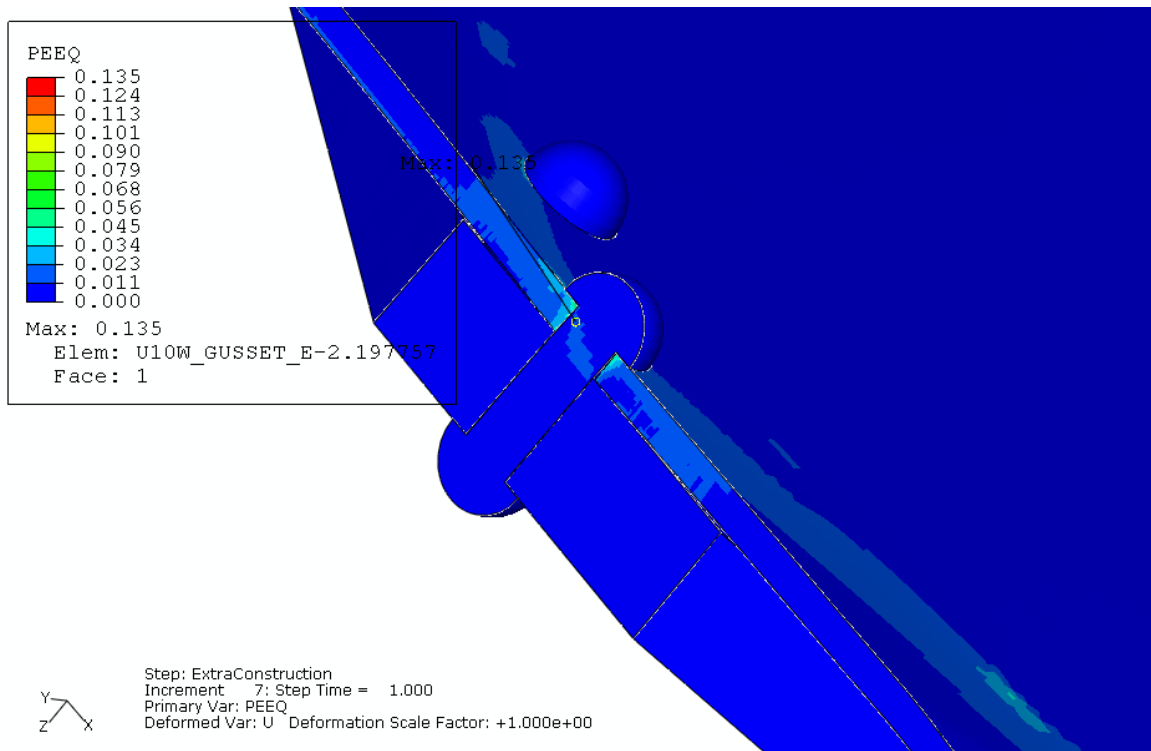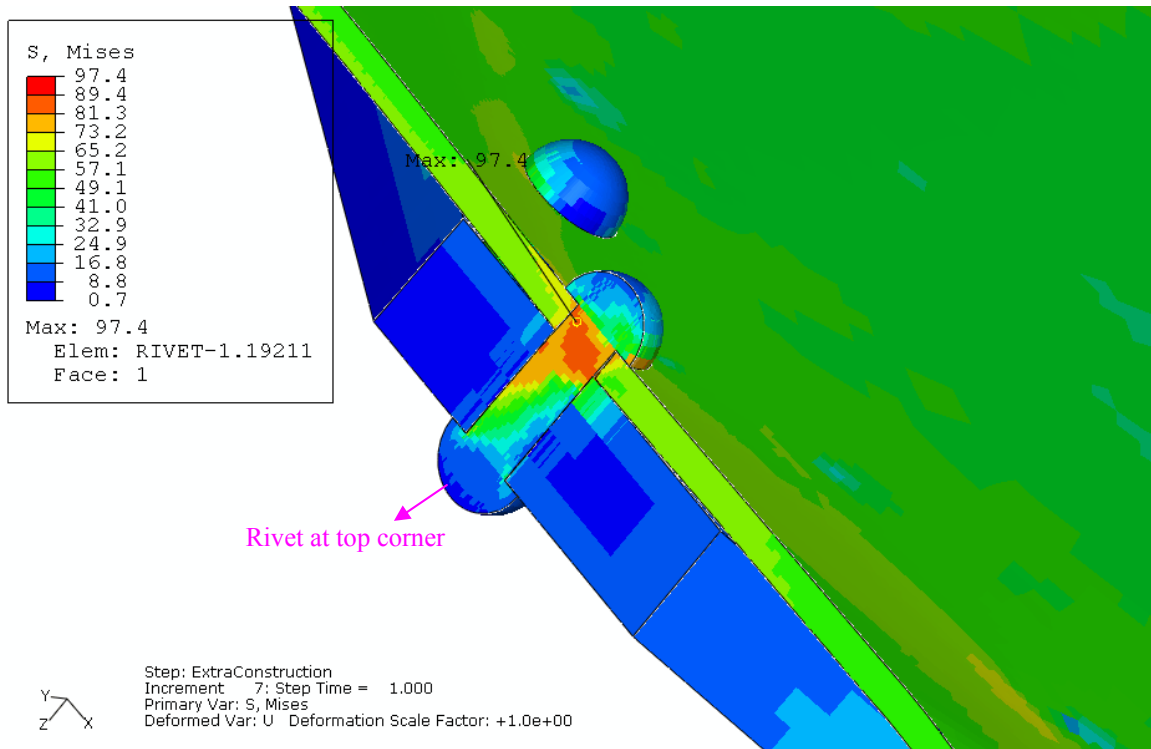
Figure 5.15: Von Mises stress and equivalent plastic strain distribution under the predicted maximum load at instability in the submodel with a view cut at the U10W joint

6   Comparison of Initially Bowed and Initially Flat Gusset Plates

6.1   Description of the U10W 3D Local Models

Analyses were conducted to investigate the difference in behavior between initially flat gusset plates and initially bowed gusset plates located at the U10W joint. Table 6.1 lists the two mixed models used for the gusset plate shape comparison. The two mixed models were exactly the same except for the initial shape of the two gusset plates at the U10W joint. The gusset plates in the first model had no initial bowing, and the gusset plates in the second model were initially bowed towards the west with an initial maximum out-of-plane deflection of 0.5 inches. Both models used load condition A1. The typical in-plane mesh size in the highly stressed region of the gusset plates was 0.5 inches. Note that the second model used in this study was previously discussed in Section 4 of this report.

Table 6.1
Mixed Models Used to Investigate Gusset Plate Bowing

Local Model Embedded	Typical Mesh Size (inch)	Loading Condition	FHWA Structural Element Bridge Model
U10W joint with initially flat gusset plates	0.5	A1	6
U10W joint with gusset plates initially bowing towards the west	0.5	A1	6

6.2   Initially Flat Gusset Plate Analysis Results

The Riks method was used to predict the maximum load at the onset of instability for both the flat gusset plate model and the bowed gusset plate model. The construction load was increased proportionally while other loads were maintained at their estimated values. The first model with the initially flat gusset plates predicted a maximum construction load at instability of 1,349 kip, which was 2.33 times the estimated value. The total load in the vertical direction was predicted to be 25,253 kip, or 1.031 times the estimated total load, as shown in Figure 6.1. The horizontal axis of the graph represents the normalized total load, the ratio between the applied total load and the estimated total load of 24,482 kip. The vertical axis represents the out-of-plane displacement at the top corner on the west and east faces of the diagonal truss member U10_L9W. Figure 6.2 shows the positions of the two corner nodes in the truss member U10_L9W. Note that negative out-of-plane displacement of a node indicated that the node moved towards the east direction, moving towards the bridge. The out-of-plane displacement at the node on the west face started with a positive value, the node moving away from the bridge, and increased with increasing load until the total load exceeded 1.022 times the estimated value. After that, the out-of-plane displacement decreased with increasing load and changed from positive to negative just after the predicted maximum load at instability. That is, the node on the west face moved towards the bridge after the predicted maximum load at instability. The out-of-plane displacement at the node on the east face was negative under all the load conditions. That is, the node on the east face moved towards the bridge under all the load conditions.

File BridgeU10W_bow0_Riks_U3_Animation.gif shows the time history animation of the out-of-plane displacement contour plot of the U10W joint in the Riks step. The animation demonstrates that the two initially flat gusset plates bowed towards the bridge in the later stage of the Riks step. This eastward bowing was opposite to the field observations of the bowed gusset plates in the actual bridge. The animation also shows that the top edge of the east side of the diagonal truss member U10_L9W moved towards the center of the bridge with increasing construction load, but the top edge of the west side first moved away from the center of the bridge then later moved towards the center of the bridge. The reverse of the movement direction of the west side appeared to be related to the formation of the eastward bowing in the two gusset plates. Figure 6.3 shows the out-of-plane displacement of the U10W joint under the predicted maximum load at instability. Figure 6.4 shows the enlarged deformed shape of the two gusset plates under the predicted maximum load at instability. These two figures show the eastward bowing of the two gusset plates, bowing towards the bridge. The deformation scale factor is 10 in this animation and in the two figures.

Figure 6.5 compares the out-of-plane displacements at the top corner on the west face of the diagonal truss member U10_L9W and at two gusset plate nodes of which the out-of-plane deflections were largest in magnitude. Figure 6.6 shows the positions of the three nodes. The two nodes in the gusset plates were located in the edge center of the bowing region. Figure 6.5 shows that the out-of-plane deflection of the node in the west gusset plate became significant, -0.149 inches, when the total load reached 1.018 times the estimated total load. This significant bowing of the gusset plates occurred earlier than the reversal in the movement direction of the west corner of the truss member. Note that the east corner of the truss member did not show the reversal in the movement direction. In Figure 6.5, it is seen that the out-of-plane displacement of the center of the unsupported edges of the gusset plate begins to deflect outward at a normalized total load value of 0.996. Its rate of growth begins to increase rapidly at a normalized load level of 1.007. Evaluation of the plastic strain for this case shows the development of a permanent bend consistent with gusset plate buckling at these load levels. Hence, initially flat gusset plates are predicted to buckle at a load level equal to that assumed to exist at the time of the accident. This is consistent with the collapse load sensitivity and mechanism predicted for the initially bowed gusset plates.

The axial force and bending moment at the lower end of the truss member U10_L9W were predicted to be -2,740 kip and 818 kip-inch under the predicted maximum load at instability. Significant plastic deformation occurred in the two gusset plates at this load. The maximum von Mises stress was predicted to be 78 ksi in the vicinity of the upper corner rivet in the west gusset plate, as shown in Figure 6.7. The maximum equivalent plastic strain was predicted to be 4.7%. Figure 6.8 shows the von Mises stress distribution in the east gusset plate under the predicted maximum load at instability, where the maximum stress was predicted to be 77 ksi and the maximum strain was 4.5%.

6.3   Comparison of Analysis Results between the Flat and Bowed Gusset Plates

Figure 6.9 compares the load displacement curves between the two models, with the initially flat gusset plates and with the initially bowed gusset plates. The vertical axis in this figure represents the out-of-plane displacement at top corner on the west face of the diagonal truss member U10_L9W. Positive out-of-plane displacement indicated that the node moved westwards and moved away from the bridge. In the beginning of the Riks step, the top corner nodes in both

models had positive out-of-plane displacement and the nodes moved away from the bridge. The model with the initially bowed gusset plates had larger out-of-plane displacement, which might be caused by the initial westward bowing of the bowed gusset plates. With the increase of the construction load, the out-of-plane displacements of the U10_L9W diagonal truss members in both models increased. The figure shows that the out-of-plane displacement in the model with the initially bowed gusset plates increased faster (more out-of-plane displacement per given applied load) than the initially flat gussets. After the predicted maximum load, the top corner node in the model with the initially bowed gusset plates continued to moving away from the bridge. However, the top corner node in the model with the initially flat gusset plates reversed its out-of-plane motion, from moving away from the bridge to moving towards the bridge. The difference in the out-of-plane motion after the predicted maximum load could be that with the increasing construction load the initially flat gusset plates bowed towards the bridge, but the initially bowed gusset plates continued to bowing away from the bridge. The bow towards the bridge of the initially flat gusset plates appeared to shift the out-of-plane movement of the west corner of the diagonal truss member from away from the bridge to towards the bridge.

Table 6.2 summarizes the comparison between initially flat gussets and initially bowed gussets. The predicted maximum construction load at instability decreased from 1,349 kip to 1,069 kip if an initial westward bowing of 0.5 inches was introduced in the gusset plates. This decrease in load at instability reduced the axial force in the diagonal truss member at instability, but did not reduce the bending moment at the lower end of the diagonal truss member. It also did not reduce the maximum stress in the east gusset. Instead, under the predicted maximum loads, the bending moment predicted with the initially bowed gusset plates was twice that of the model with the initially flat gusset plates. Table 6.2 also compares the two components of the bending moment between the two models. The analysis results showed that under the predicted maximum load at instability, the model with the initially flat gusset plates had negligible bending moment about the local 1-axis, SM1. In contrast, the model with the initially bowed gusset plates had an SM1 result of -1,366 kip-inch. For reference, Figure 6.10 shows the three local axes of the beam elements of the diagonal truss member U10_L9W. The local 2-axis of the cross section of the beam elements, n2, was aligned with the global 3-axis. The red dot in the figure represents the lower end of the diagonal truss member U10_L9W.

Table 6.2
Results Comparison from Initially Flat and Initially Bowed Gusset Plates

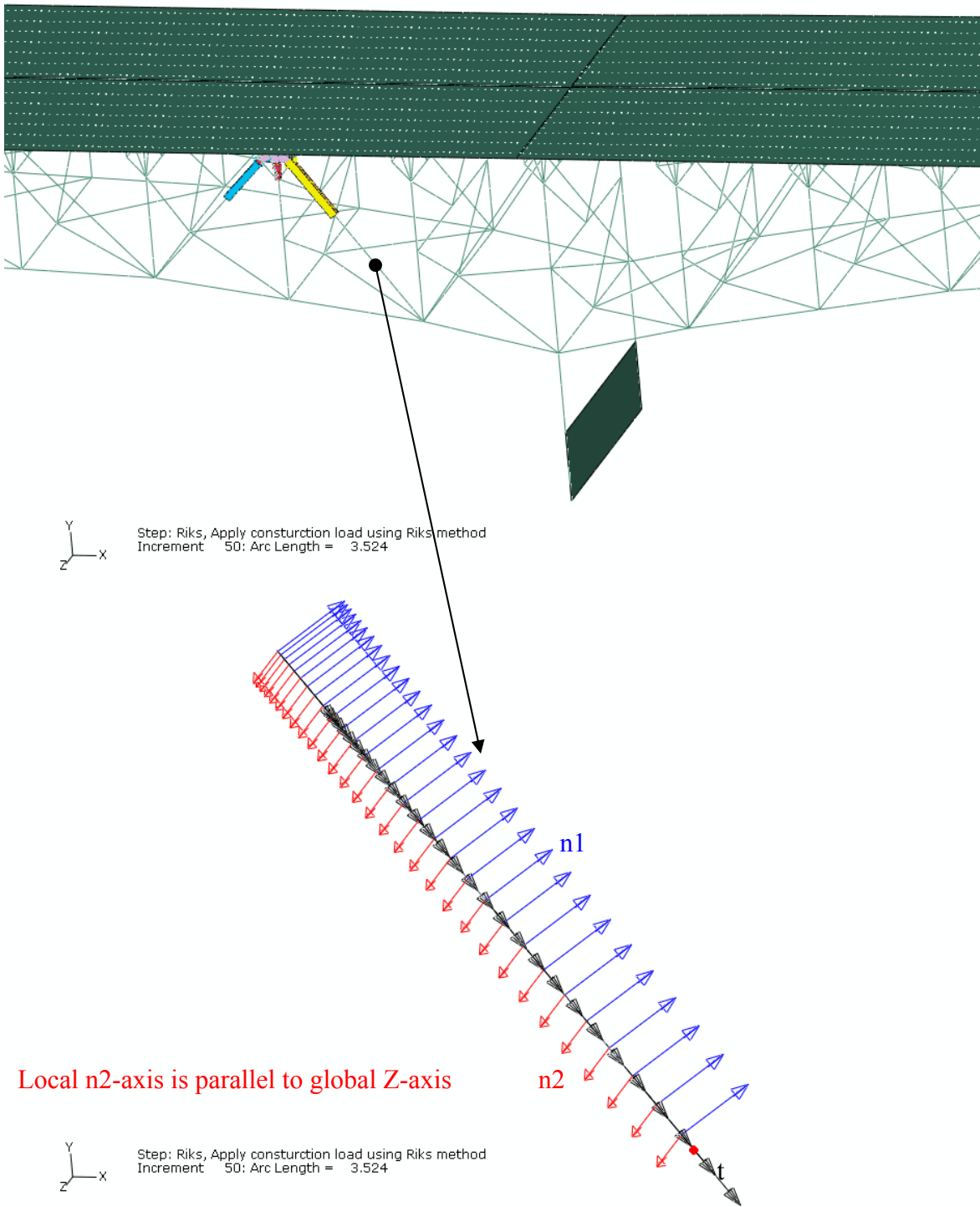|	Initially Flat Gusset Plates	Initially Bowed Gusset Plates
Initial Maximum Out-of-Plane Deflection in Gusset Plates (inch)	0.0	0.5
Predicted Maximum Total Load at Instability (kip)	25,253	24,973
Traffic Load and Approach Span Force Increment (kip)	406	406
Construction Load at Maximum Predicted Load at Instability (kip)	1,349	1,069
Axial Force at Lower End of Truss Member U10_L9W (kip)	-2,740	-2,618
Bending Moment at Lower End of Truss Member U10_L9W (kip-inch)	818	1,738
Bending Moment Component SM1 at Lower End of U10_L9W (kip-inch)	-25	-1,366
Bending Moment Component SM2 at Lower End of U10_L9W (kip-inch)	818	1,074
Out-of-Plane Displacement at Top Corner on West Face of U10_L9W (inch)	0.038	0.572
Maximum von Mises Stress in East Gusset (ksi)	77	77
Maximum Equivalent Plastic Strain in East Gusset	4.5%	4.5%

To understand the evolution of the axial force and bending moment and their effect on the stress in the east gusset, the variables listed in Table 6.2 were compared between the two models at two loads:

1. Under a total load of 23,904 kip, just after applying the traffic load but prior to applying the construction load

2. Under a total load of 24,911 kip for the first model and under a total load of 24,933 kip for the second model, which corresponded to a total load of about 1.018 times the estimated total load

Table 6.3 and Figure 6.11 compare these variables when the two models were subjected to the total load of 23,904 kip. The table shows that the axial forces in the diagonal truss member U10_L9W were almost identical between the two models, but the model with the initially bowed gusset plates predicted a larger bending moment of 471 kip-inch. The difference in the bending moment was 121 kip-inch. The ratio between the bending moments about the local 1- and 2-axes was predicted to be -1.6 in the model with the initially flat plates, and -1.5 in the model with the initially bowed plates. This ratio in the model with the initially flat plates was comparable to, but

slightly larger in magnitude than the model with the initially bowed plates. This was different from the situation when the two models were subjected to their predicted maximum loads at instability. The figure shows that the maximum von Mises stresses in the east gusset plates were almost identical between the two models, but slightly more gusset material reached yielding in the model with the initially bowed gusset plates.

Table 6.3
Results Comparison from Initially Flat and Initially Bowed Gusset Plates, Before Construction Load Application

	Initially Flat Gusset Plates	Initially Bowed Gusset Plates
Initial Maximum Out-of-Plane Deflection in Gusset Plates (inch)	0.0	0.5
Total Load (kip)	23,904	23,904
Traffic Load and Approach Span Force Increment (kip)	406	406
Construction Load (kip)	0	0
Axial Force at Lower End of Truss Member U10_L9W (kip)	-2,150	-2,149
Bending Moment at Lower End of U10_L9W (kip-inch)	350	471
Bending Moment Component SM1 at Lower End of U10_L9W (kip-inch)	-299	-390
Bending Moment Component SM2 at Lower End of U10_L9W (kip-inch)	182	265
Out-of-Plane Displacement at Top Corner on West Face of U10_L9W (inch)	0.070	0.117
Maximum von Mises Stress in East Gusset (ksi)	54	53

Table 6.4 and Figure 6.12 compare results when the two models were subjected to similar construction load, a construction load of 1,007 kip for the model with the initially flat plates and 1,029 kip for the model with the initially bowed plates. The table shows that the axial forces were almost identical between the two models. However, the model with the initially bowed gusset plates predicted a bending moment twice that of the model with the initially flat plates. This larger bending moment was related to a significantly larger out-of-plane displacement at the top corner of the diagonal truss member. The ratio between the bending moments about the local 1- and 2-axes was predicted to be -0.99 in the model with the initially flat plates, and -1.2 in the model with the initially bowed plates. This ratio in the model with the initially flat plates was still comparable to, but slightly smaller in magnitude than the model with the initially bowed plates. The figure shows that the model with the initially bowed gusset plates predicted a larger maximum von Mises stress in the east gusset plate, 67 ksi for the model with the initially flat

plates and 73 ksi for the model with the initially bowed plates. More gusset material had high von Mises stress in the model with the initially bowed gusset plates.

Table 6.4
Results Comparison from Initially Flat and Initially Bowed Gusset Plates, Similar Construction Loads

	Initially Flat Gusset Plates	Initially Bowed Gusset Plates
Initial Maximum Out-of-Plane Deflection in Gusset Plates (inch)	0.0	0.5
Total Load (kip)	24,911	24,933
Traffic Load and Approach Span Force Increment (kip)	406	406
Construction Load (kip)	1,007	1,029
Axial Force at Lower End of Truss Member U10_L9W (kip)	-2,602	-2,604
Bending Moment at Lower End of U10_L9W (kip-inch)	772	1,574
Bending Moment Component SM1 at Lower End of U10_L9W (kip-inch)	-543	-1,216
Bending Moment Component SM2 at Lower End of U10_L9W (kip-inch)	549	1,000
Out-of-Plane Displacement at Top Corner on West Face of U10_L9W (inch)	0.171	0.483
Maximum von Mises Stress in East Gusset (ksi)	67	73

6.4 Summary: Comparison of Models with Initially Bowed and Initially Flat Gusset Plates

Two mixed models were analyzed to investigate the effect of the initial bowing of the gusset plates at the U10W joint. The analyses predicted a significant increase in the maximum construction load at instability when initially flat gusset plates were incorporated, compared to the value predicted by the model with initially bowed plates. The increase in the predicted maximum load at instability was 280 kip (a 26 percent increase in the applied construction loads). The analyses also predicted that the two initially flat gusset plates bowed towards the east when the total load was more than 101 percent of the estimated total load, which was opposite to the westward bowing observed in the field. The eastward bowing changed the ratio of the two bending moment components at the lower end of the diagonal truss member U10_L9W. The change of the bending moment ratio was related to the change in the direction of the diagonal truss member U10_L9W from moving westwards to moving eastwards.

West face of diagonal truss member U10_L9W moved away from bridge first then moved towards center of bridge.

East face of diagonal truss member U10_L9W moved towards bridge under all the load conditions.

Positive out-of-plane displacement: Move towards west or away from bridge

Legend:
- Node on west face under bridge design weight
- Node on west face with added deck and barrier
- Node on west face with deck milled down
- Node on west face under traffic load
- Node on west face under construction load in Riks step
- Node on east face under bridge design weigh
- Node on east face with added deck and barrier
- Node on east face with deck milled down
- Node on east face under traffic load
- Node on east face under construction load in Riks step

Y-axis: Out-of-Plane Displacement at a Node on West Face and a Node on East Face of U10 _L9W (in)

X-axis: Applied Load / Estimated Total Load

Figure 6.1: Normalized total load versus displacement when the U10W joint had initially flat gusset plates
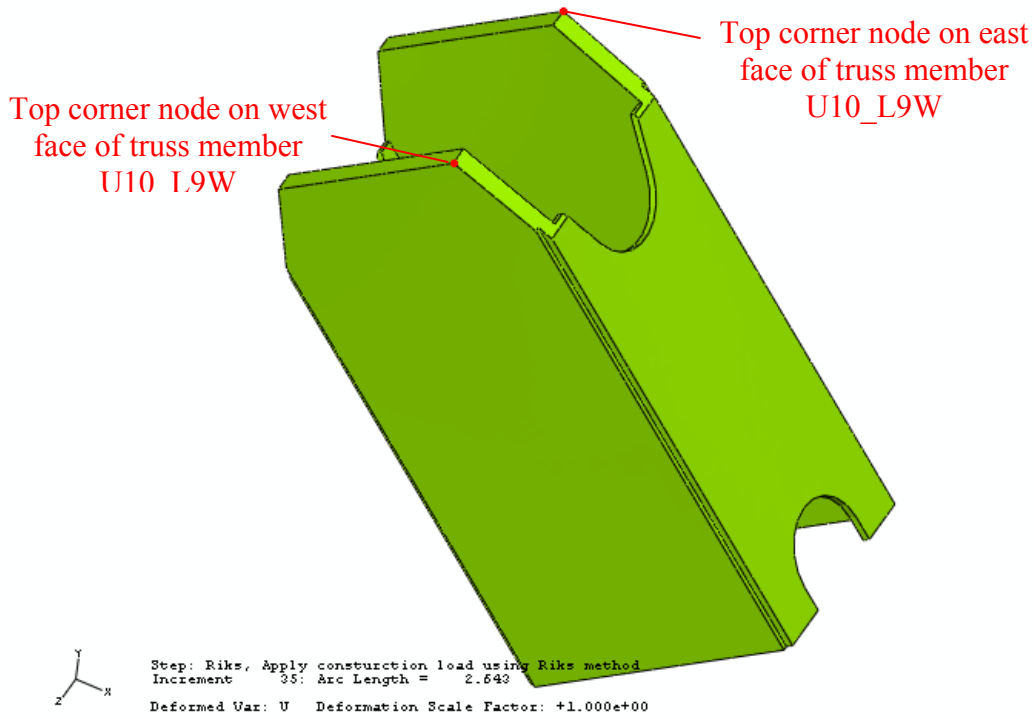
Figure 6.2: Positions of the two nodes in truss member U10_L9W in Figure 6.1
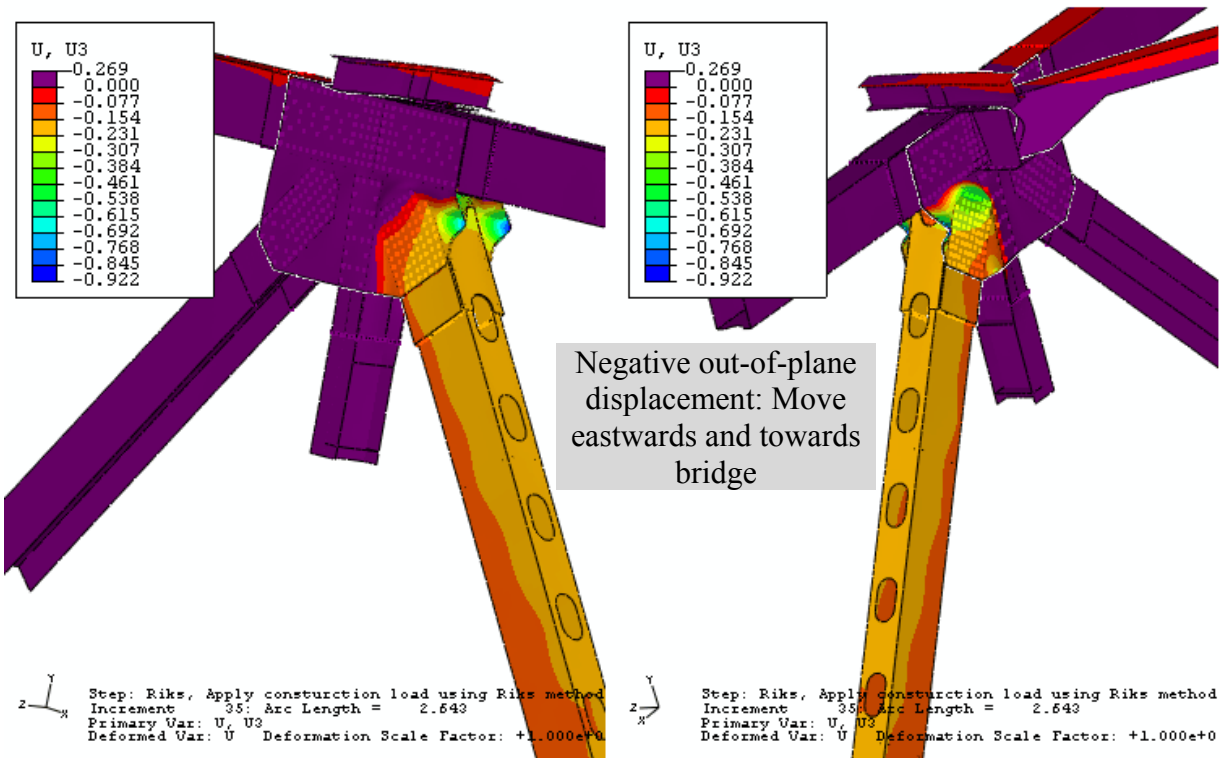
Figure 6.3: Out-of-plane displacement of the U10W joint under the predicted maximum load at instability when the initially flat gusset plates were included (deformation magnified 10x)
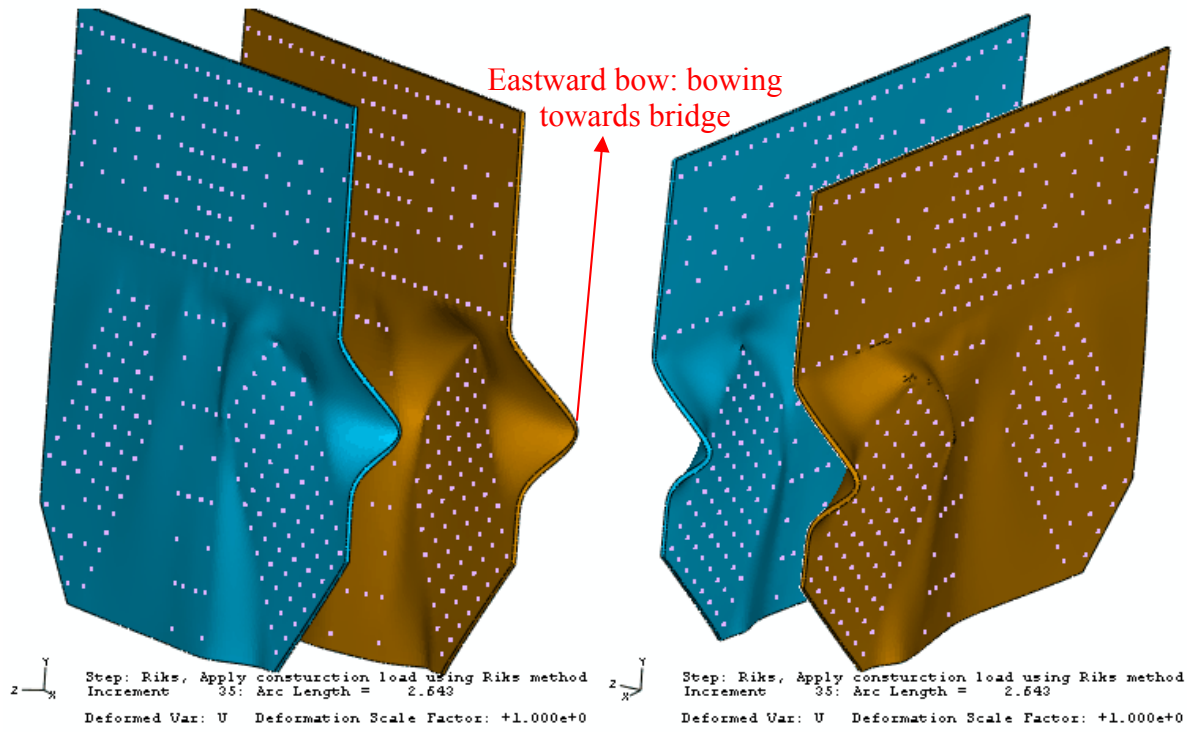
Figure 6.4: Deformed shape of the gusset plates at the U10W joint under the predicted maximum load at instability when the initially flat gusset plates were included (deformation magnified 10x)
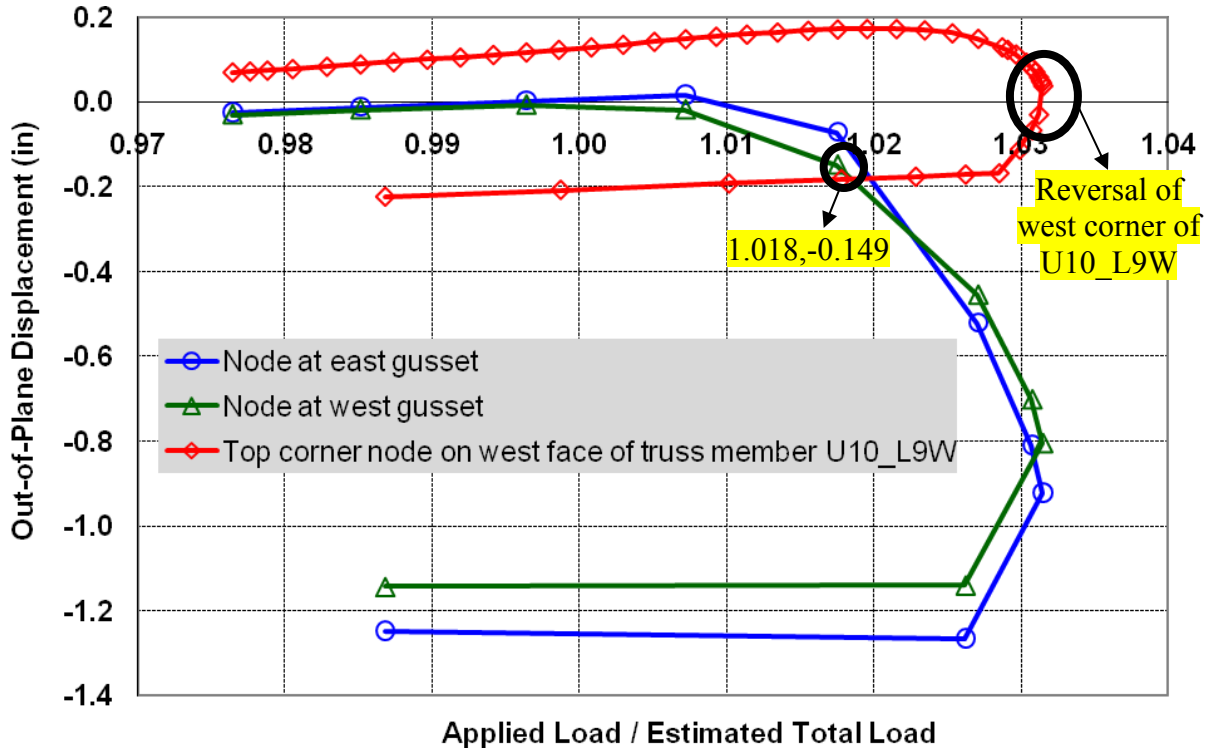
Figure 6.5: Variation of the out-of-plane displacement in Riks construction loading step when the U10W joint had the initially flat gusset plates
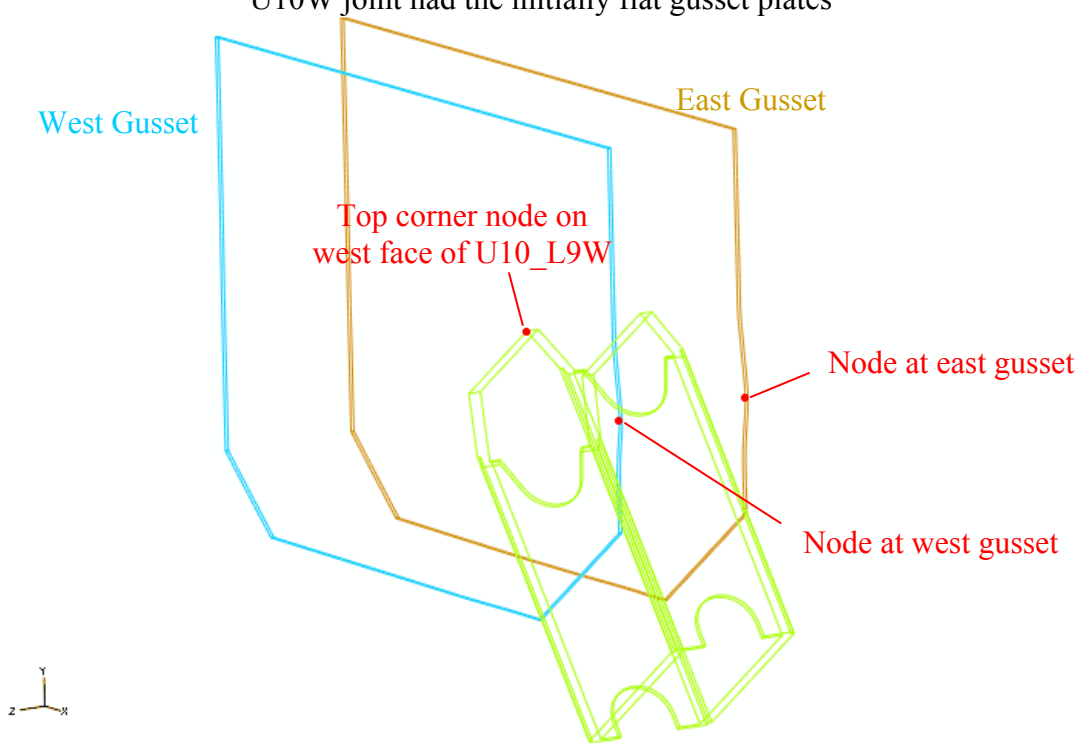
Figure 6.6: Positions of the three nodes in Figure 6.5
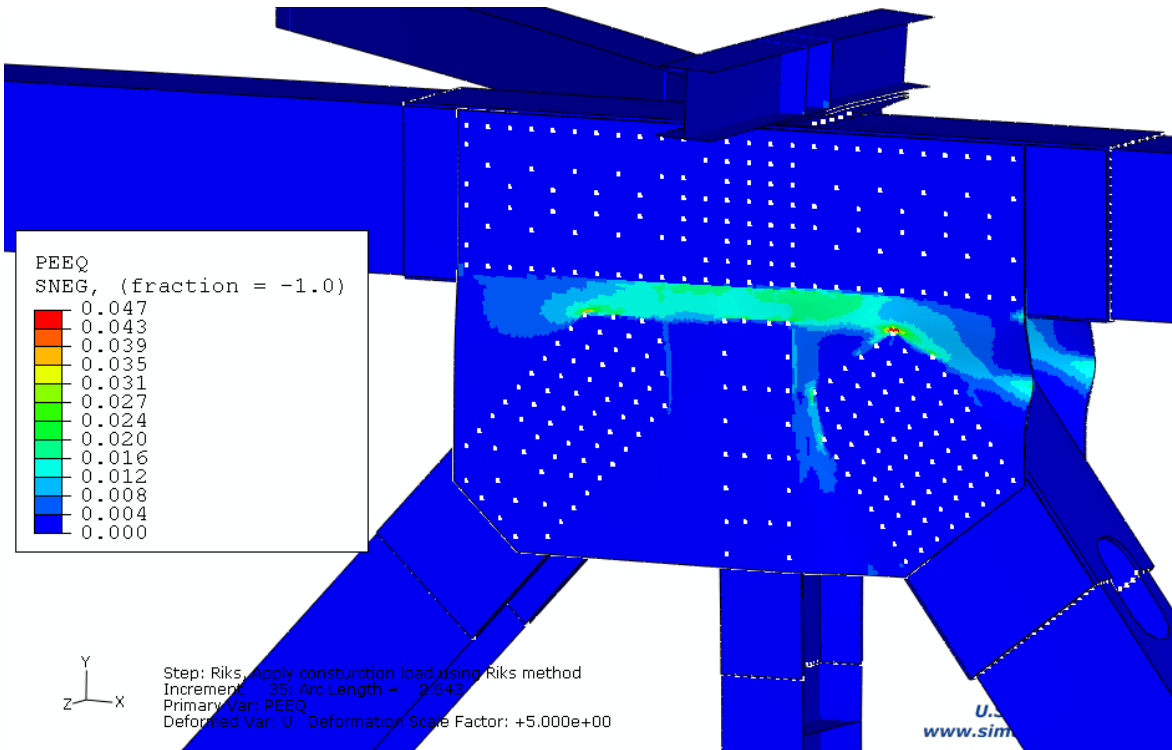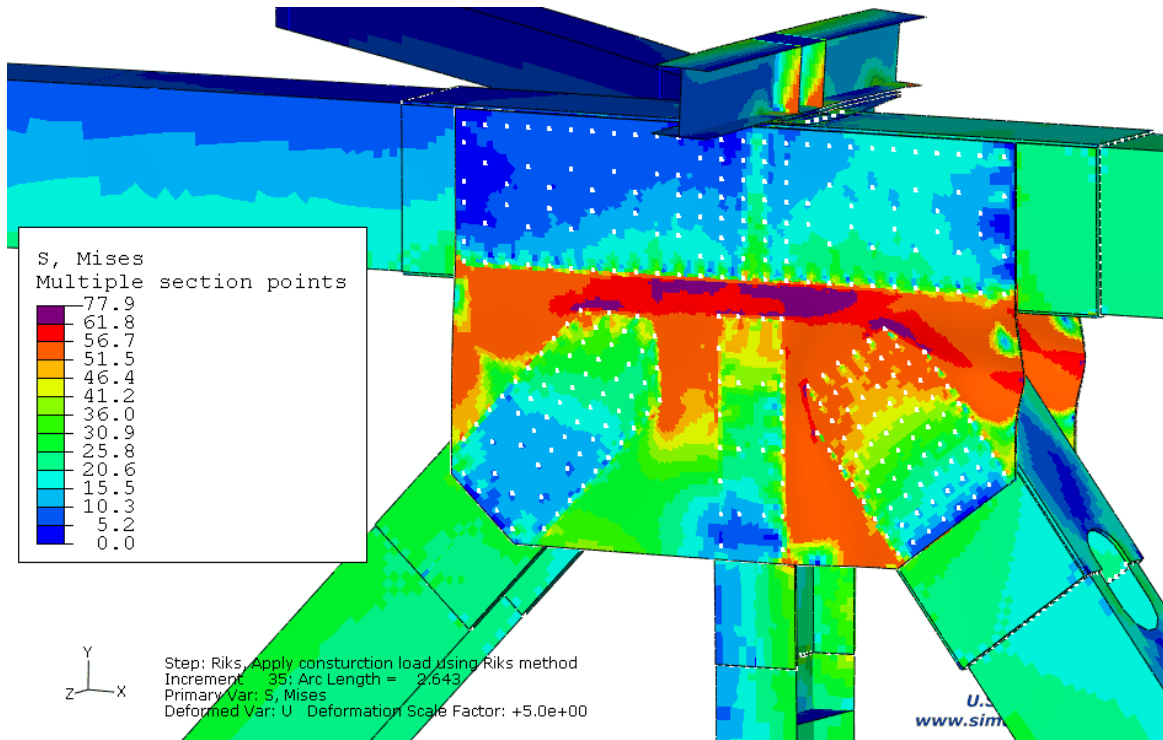
Riks step: 1.031 times the estimated total load

Figure 6.7: Von Mises stress and equivalent plastic strain (PEEQ) distribution under the predicted maximum load at instability at the U10W joint with the initially flat gusset plates (deformation magnified 5x)
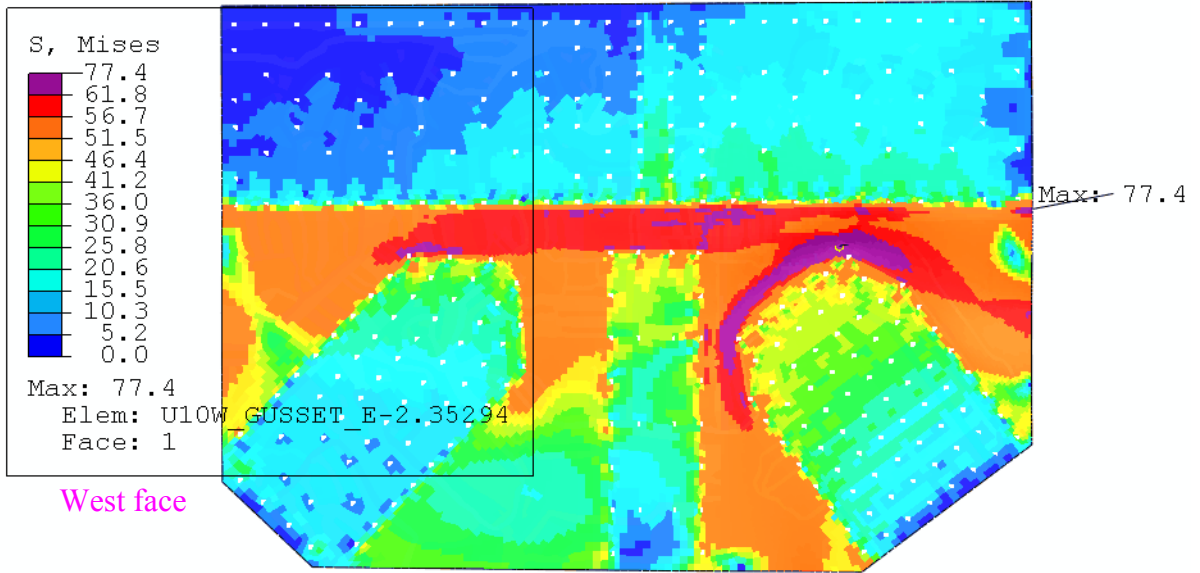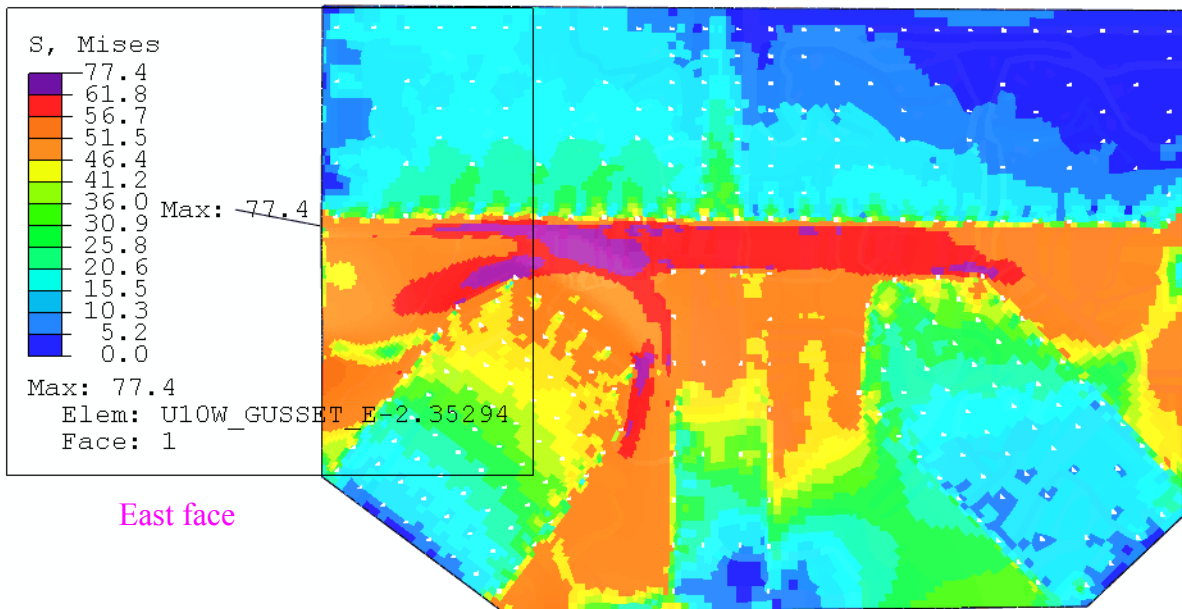
Riks step: 1.031 times the estimated total load

Figure 6.8: Von Mises stress distribution under the predicted maximum load at instability in the east gusset plate at the U10W joint with the initially flat gusset plates
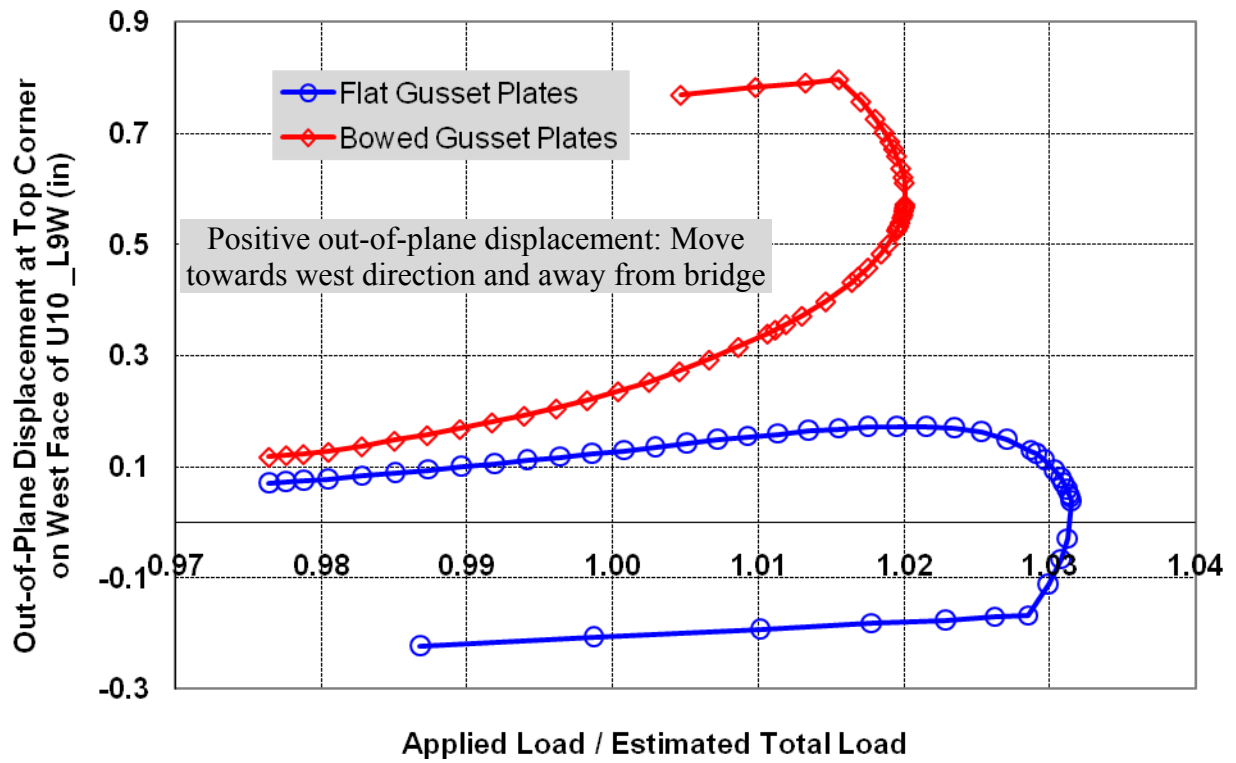
Figure 6.9: Comparison of normalized total load versus displacement in Riks construction
loading step between initially flat and bowed gusset plates

Step: Riks, Apply consturction load using Riks method
Increment   50: Arc Length =   3.524

n1

Local n2-axis is parallel to global Z-axis   n2

Step: Riks, Apply consturction load using Riks method
Increment   50: Arc Length =   3.524

t

Figure 6.10: Three local axes of the beam elements of the diagonal truss member U10_L9W at the U10W joint
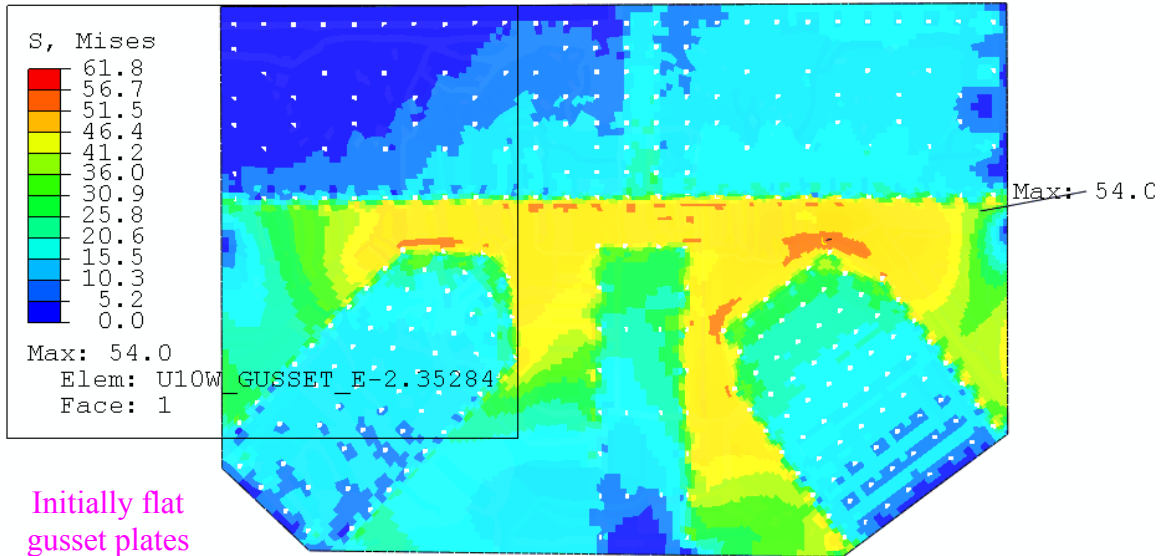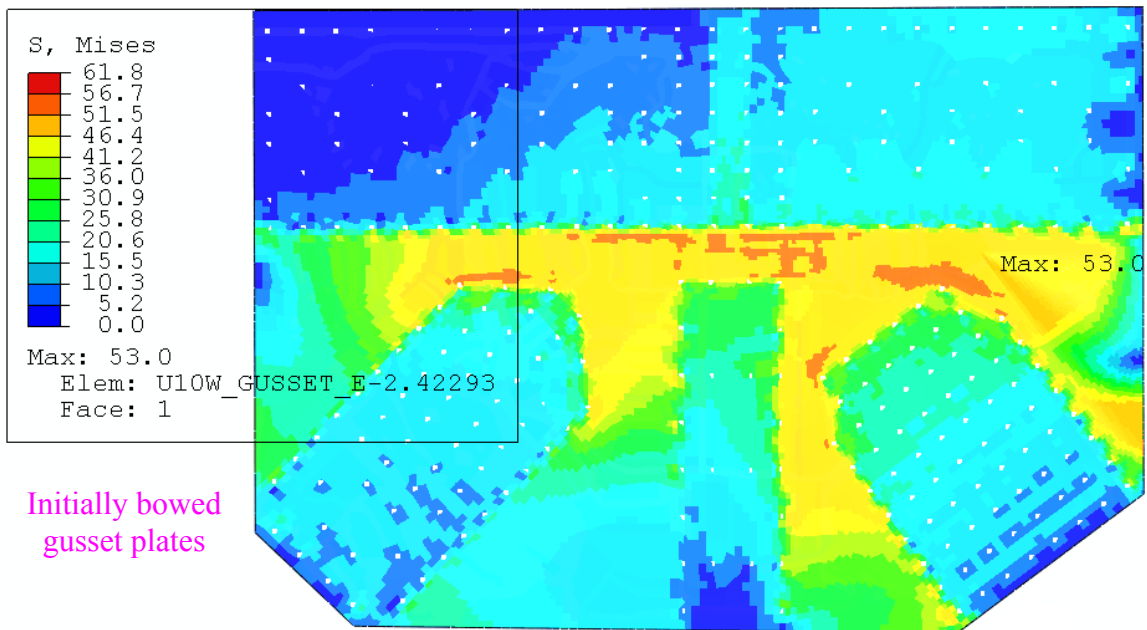
Figure 6.11: Comparison of von Mises stress in the east gusset plate before the construction load was applied between the initially flat and bowed gusset plates
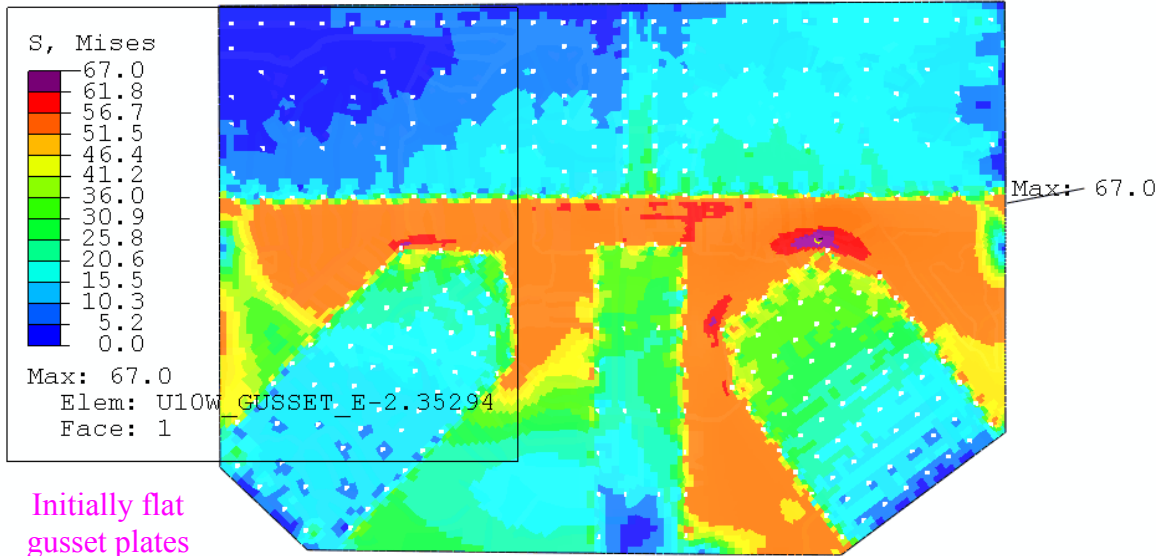
Riks step: Under a total load of 24,911 kip
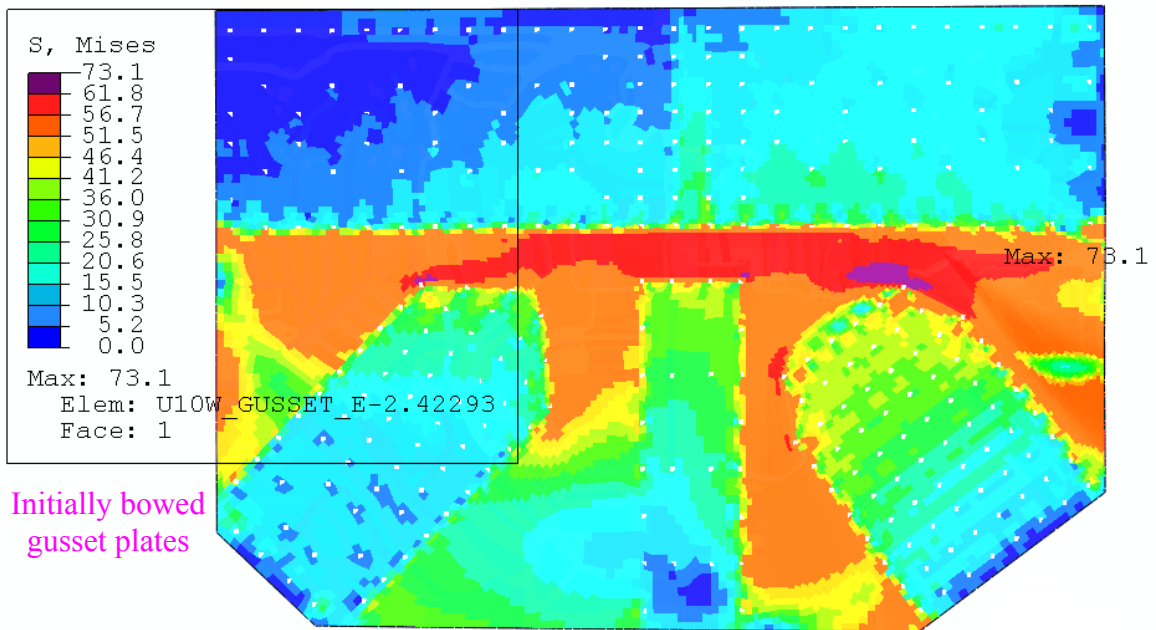
Riks step: Under a total load of 24,933 kips

Figure 6.12: Comparison of von Mises stress in the east gusset plate under similar construction load between the initially flat and bowed gusset plates

7 Embedding the U10W and U10E 3D Local Models into the FHWA Structural Element Bridge Model

Two models were used to compare results between a mixed model with an embedded U10W 3D local model and a mixed model that included both the U10W and U10E 3D local models. Table 7.1 summarizes the two models analyzed.

Table 7.1
Mixed Models Analyzed for the U10W and U10W + U10E Comparison

Local Model Embedded	Typical Mesh Size (inch)	Loading Condition	FHWA Structural Element Bridge Model
U10W joint	0.5	B	6
U10W joint and U10E joint	0.5	B	6

The U10W local models were identical in the two models analyzed. There were three major differences between the U10W only mixed model and the mixed models in Section 4. These differences are listed and described below.

1. Meshing of all components in the local model
2. Methods used to represent the rivet connections connecting secondary structures such as diaphragms, splice plates, etc. in the local model
3. Loading history

7.1 Description of the U10W 3D Local Model

7.1.1 Meshing in the U10W 3D Local Model

The gusset plates were represented with the C3D8R elements with total stiffness hourglass control [11]. An in-plane mesh size of 0.5 inches was typical in the highly stressed region of the gusset plates, as shown in Figure 7.1. The largest in-plane element size was about 1.0 inch. Each gusset plate contained 53,656 elements. Four elements were used through the thickness of the gusset plates. The in-plane mesh size of the solid representation of the five main truss members ranged from 0.5 inches to 1.5 inches. The mesh size of the truss shell representation ranged from 1.5 inch to 3.0 inches. Figure 7.2 shows the meshing of all secondary structure. The secondary structure had an average element size of 2.5 inches.

7.1.2 Rivet Connections in the U10W 3D Local Model

All rivet connections connecting the five main truss members to the two gusset plates were represented by Abaqus fasteners. Contact pairs were defined between the gusset plates and the truss members. A Coulomb friction model with a friction coefficient of 0.1 was used to define the contact pair. All other connections in the local model were represented with tie constraints.

7.2 Description of the U10E 3D Local Model

7.2.1 Geometry and Meshing in the U10E 3D Local Model

The NTSB provided one CAD model, in Abaqus/CAE format, of the U10E gusset joint. Figure 7.3 shows the parts included in the U10E 3D local model. Each part at the U10E joint had a similar geometry as that at the U10W joint, but with a mirror symmetry orientation. One asymmetry in the structure was that both gusset plates at the U10E joint were observed in the field to bow towards the west [10], as shown in Figure 7.4, in the same direction of the bowing of the gusset plates at U10W. The initial bowing geometry of the two gusset plates in the U10E local model was assumed to be the same as that in the U10W local model and was implemented using an Abaqus imperfection (previously described in Section 3.1.3). The initial maximum out-of-plane deflection was assumed to be 0.5 inches, the same as that in the U10W local model. Figure 7.5 shows a contour plot of the initial relative Z-coordinates (out-of-plane coordinates) of the bowed region of the west gusset plate at the U10E joint. Each part in the U10E local model had the same representation and meshing as that in the U10W local model.

7.2.2 Constraints and Boundary Conditions in the U10E 3D Local Model

As in the U10W local model, the cut planes of the five main truss members, lateral brace, floor truss and stringer offset in the U10E local model passed through nine member nodes in the FHWA structural element bridge model. Nine reference points coincident with these nodes were created. Nine tie constraints were applied to tie the reference points and nodes respectively. These reference points were then coupled to the cut planes of the shell truss representations. As modeled, the entire 3D local model was embedded into, and driven by, the FHWA structural element bridge model.

Also as in the U10W local model, all rivet connections connecting the five main truss members to the two gusset plates were represented by Abaqus fasteners. Contact pairs were defined between the gusset plates and the truss members. A Coulomb friction model with a friction coefficient of 0.1 was used to define the contact pair. All other connections in the local model were represented with tie constraints. No translational or rotational boundary conditions were defined in the U10E local model.

Figure 7.6 shows the mixed model that incorporates both the U10W and U10E local models. Figure 7.7 shows details of the embedded U10W and U10E joints that incorporate the bowed gusset plates, fasteners, constraints, and contact conditions described above.

7.3 Load Conditions

The two mixed models used for this study had six load steps. The first five steps were identical to those in load condition A1, described in Section 3.1.6. The sixth step of the current section applied the traffic load, the construction load, and the corresponding approach span force increment at the time of the bridge collapse, which were estimated by NTSB[5] and FHWA[1]. This new load combination in step 6 is called the "live load" hereafter. The combination of these six load steps is identified as load condition B. Table 7.2 describes and summarizes load condition B. The first five steps were regular static analysis steps. The last step used the Riks method to proportionally increase the live load while keeping the other loads constant.

Table 7.2
Loading Steps in Load Condition B

Step	Load Description	Model Change	Load Increment (kip)	Total Load (kip)	Normalized Total Load (kip)
1	Weight of steel and walkways, forces representing wet deck concrete, and approach span reaction forces	Remove decks and expansion joint springs	17,900	17,900	0.731
2	Solid deck to replace the forces representing the wet concrete	Add decks	0	17,900	0.731
3	Weight of original barriers	---	1,629	19,529	0.798
4	Weight of added deck and barriers through the life of the bridge and approach span reaction force increment	---	4,554	24,083	0.984
5	Reduce weight of deck concrete due to milling	Add expansion joint springs	-585	23,498	0.960
6	Live load including traffic load, construction load, and approach span reaction force increment	---	984 (traffic 379, construction 576, approach span force inc 29)	24,482	1.000

7.4 Results Comparison, U10W 3D Local Model and U10W + U10E 3D Local Models

7.4.1 U10W 3D Local Model Results

The Riks method was used to predict the maximum live load at instability by proportionally increasing the live load, while other loads were maintained at their estimated values. When the U10W local model was embedded into the FHWA structural element bridge model, the Riks analysis predicted a maximum live load of 1,721 kip, or 1.75 times the estimated value. The total load along the vertical direction (Y-direction) was predicted to be 25,219 kip, or 1.030 times the estimated total load, as shown by the red curve in Figure 7.8.

The out-of-plane displacement at the top corner on the west face of the diagonal truss member U10_L9W was predicted to be 0.532 inches under a total load of 25,212 kip. The diagonal truss member U10_L9W moved away from the bridge with increasing live load. The out-of-plane displacement at the top corner was predicted to be 0.625 inches at the predicted maximum live load.

At the onset of instability, the axial force and bending moment at the lower end of the diagonal truss member U10_L9W were predicted to be -2,623 kip and 1,661 kip-inch. The axial force and bending moment at the lower end of the diagonal truss member U10_L9E were predicted to be -2,457 kip and 656 kip-inch. Figure 7.9 shows the von Mises stress distribution in the east gusset plate at the U10W joint under the total load of 25,212 kip in the Riks step. The maximum von Mises stress was predicted to be 83 ksi.

7.4.2 U10W + U10E 3D Local Model Results

When both the U10W and U10E local models were embedded into the FHWA structural element bridge model, the Riks analysis predicted a maximum live load at instability of 1,732 kip, or 1.76 times the estimated value. The total load along the vertical direction was predicted to be 25,229 kip, or 1.031 times the estimated total load, as shown by the blue curve in Figure 7.8.

Instability was predicted to occur in the U10W joint when both the U10W and U10E local models were embedded. Both diagonal truss members U10_L9W and U10_L9E were predicted to move towards the west, as shown in Figure 7.10. The maximum out-of-plane displacement in the U10_L9W was approximately twice the maximum displacement in the U10_L9E. Table 7.3 compares the predicted out-of-plane displacement at the top corner on the west face of the diagonal truss members U10_L9W and U10_L9E. The out-of-plane displacement at the top corner was predicted to be significantly greater in the U10_L9W than in the U10_L9E under the two total loads listed, 25,221 kip prior to the predicted maximum load and 25,207 kip after the maximum load. Furthermore, the increment in the out-of-plane displacement at the top corner prior to and after the predicted maximum load was predicted to be much greater in the U10_L9W than in the U10_L9E, 0.149 inches in the U10_L9W versus 0.003 inches in the U10_L9E.

Table 7.3
Comparison of Out-of-Plane Displacement at Top Corner on the West Face of the Diagonal Truss Members U10_L9W and U10_L9E, Unit: inch

Position of Top Corner Node	Under a Total Load of 25,221 kip Prior to Predicted Max Load	Under Predicted Max Load	Under a Total Load of 25,207 kip after Predicted Max Load
In U10_L9W	0.540	0.619	0.649
In U10_L9E	0.420	Not Available	0.423

At the onset of instability, the axial force and bending moment at the lower end of the diagonal truss member U10_L9W were predicted to be -2,632 kip and 1,672 kip-inch. The axial force and bending moment at the lower end of the diagonal truss member U10_L9E were predicted to be -2,450 kip and 621 kip-inch.

7.4.3 Results Comparison

The bending moment at the lower end of the west diagonal U10_L9W was significantly larger than that of the east diagonal U10_L9E. The out-of-plane displacements at the two diagonals and the bending moment at their lower ends indicated that when both the U10W and U10E 3D local

models were embedded into the FHWA structural element bridge model, an instability occurred at the U10W joint. Figure 7.11 shows the von Mises stress distribution in the east gusset plates at the U10W and U10E joints under the total load of 25,221 kip in the Riks step. Figure 7.12 shows the von Mises stress distribution in the west gusset plates at the U10W and U10E joints under this load. The maximum von Mises stress was predicted to be 83 ksi in the east gusset at the U10W joint.

Table 7.4 compares the results of interest in the two mixed models. The table shows that for the results of interest, the effect of embedding the U10E local model into the FHWA structural element bridge model with the U10W local model was negligible.

Table 7.4
Effect of Embedding the U10E Local Model with the U10W Local Model

	U10W Only	U10W + U10E
Embedded U10E Local Model	No	Yes
Predicted Maximum Total Load at Instability (kip)	25,219	25,229
Traffic/Construction/Approach Span Force Increment (Live Load) at Instability (kip)	1,721	1,732
Axial Force at Lower End of Truss Member U10_L9W (kip) *	-2,623	-2,632
Axial Force at Lower End of Truss Member U10_L9E (kip) *	-2457	-2,450
Bending Moment at Lower End of U10_L9W (kip-inch) *	1,661	1,672
Bending Moment at Lower End of U10_L9E (kip-inch) *	656	621
Out-of-Plane Displacement at Top Corner of U10_L9W (inch) *	0.532	0.540
Maximum von Mises Stress in East Gusset at U10W (ksi) *	83	83

* Values under a load of 25,212 kip when only the U10W local model was embedded or under a load of 25,221 kip when both the U10W and U10E local models were embedded

7.5   Summary: Embedding the U10E 3D Local Model into the FHWA Structural Element Bridge Model with the U10W 3D Local Model

Two mixed models were analyzed to investigate the effect of embedding the U10E 3D local model into the FHWA structural element bridge model with the U10W 3D local model. Load condition B was used, where the traffic load, construction load, and approach span force increment were proportionally increased in the Riks step. The first model incorporated only the U10W local model while the second model incorporated both the U10W and U10E 3D local models. Analysis results indicated that the incorporation of the U10E 3D local model had negligible effect on the predicted maximum load at instability and corresponding results of interest. The first model predicted a maximum total load at instability of 25,219 kip, and the second model predicted a maximum total load at instability of 25,229 kip. The instability

observed during the Riks analysis occurred at the U10W joint in both mixed models.
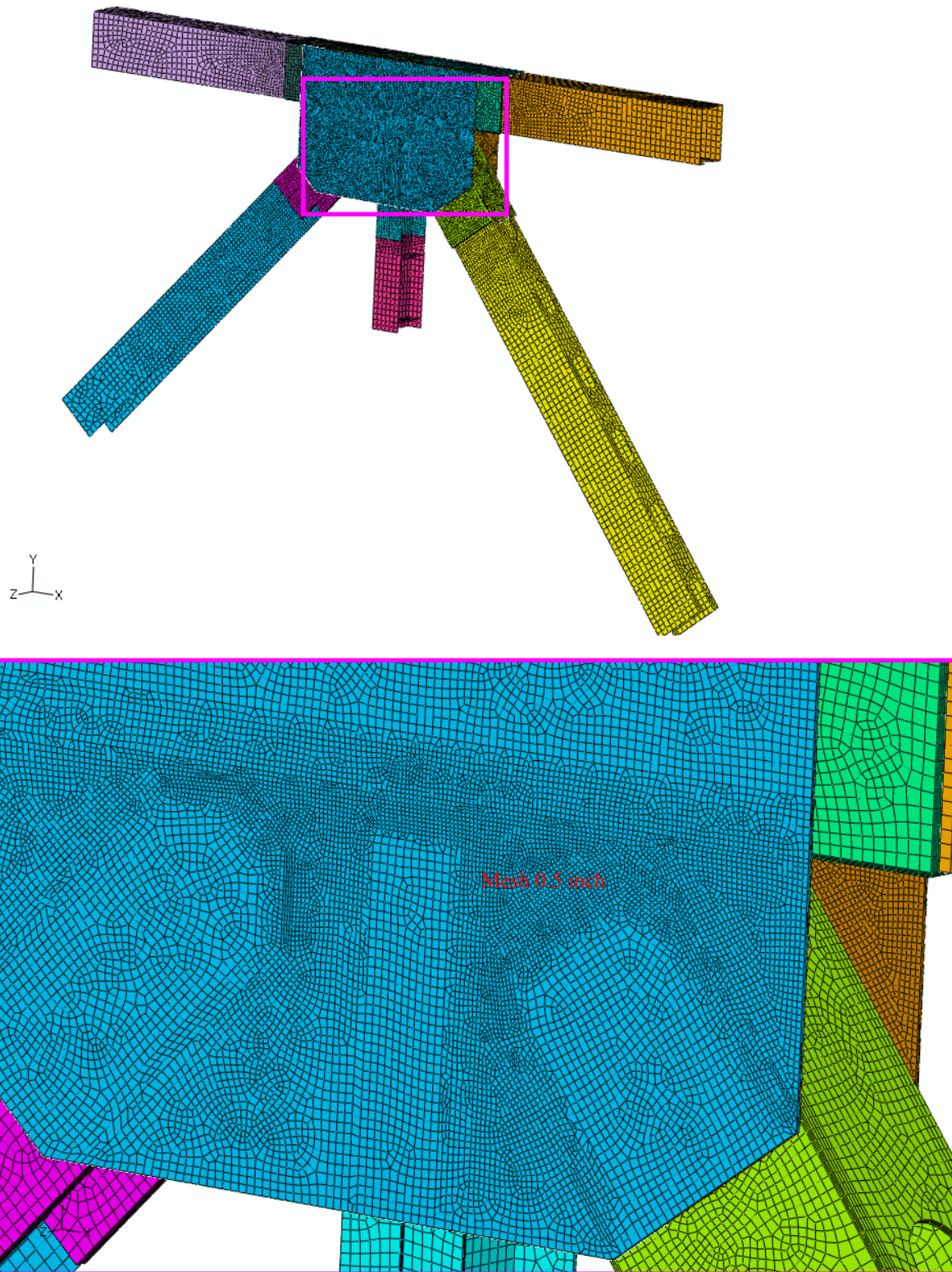
Figure 7.1: CAE model of the U10W joint; 0.5-inch mesh in highly stressed gusset region
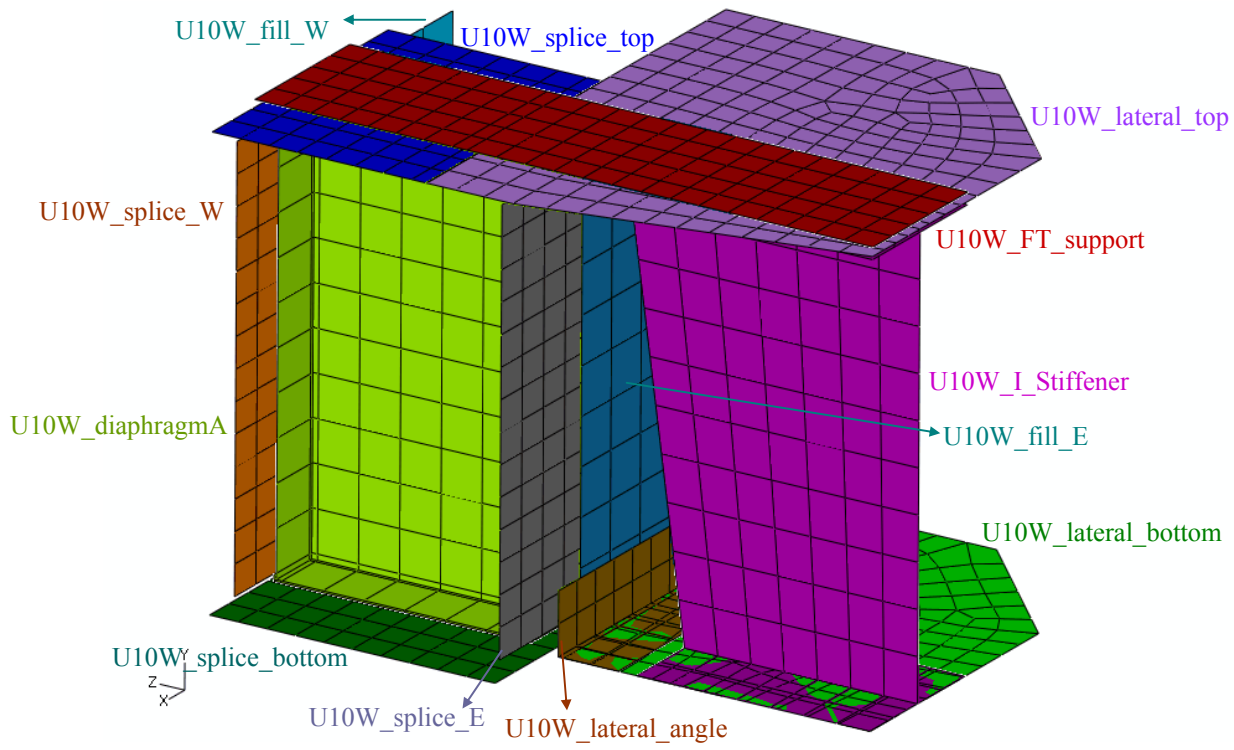
Figure 7.2: CAE model of connecting plates at the U10W joint; 2.5-inch mesh
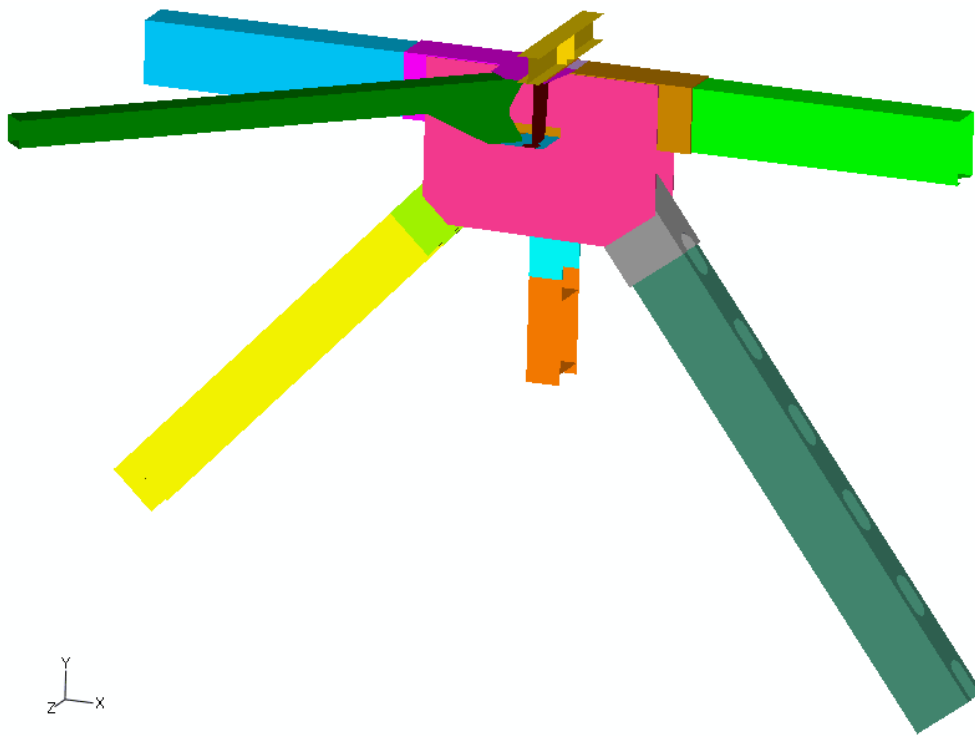
Figure 7.3: Parts included in the U10E 3D local model
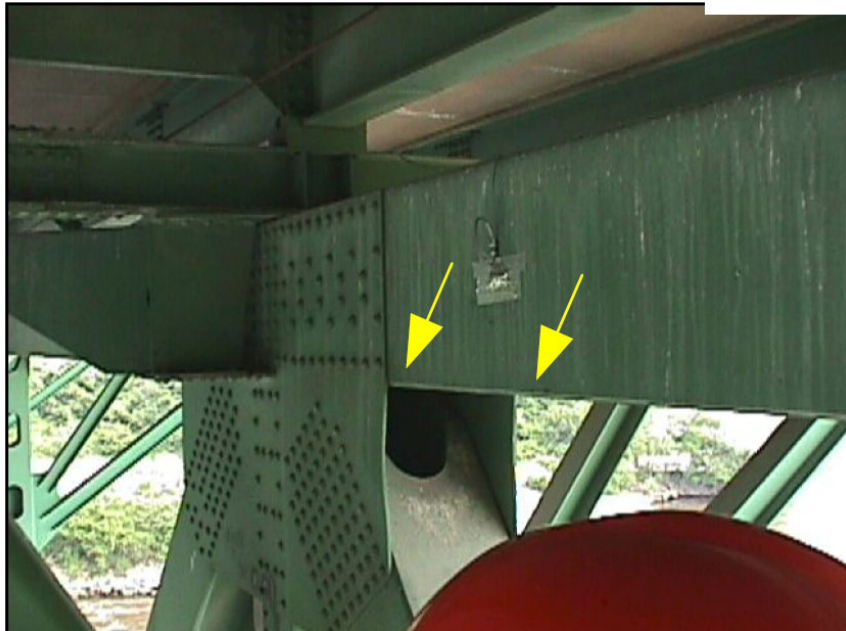
Figure 7.4: Westward bowing observed in the gusset plates at the U10E joint
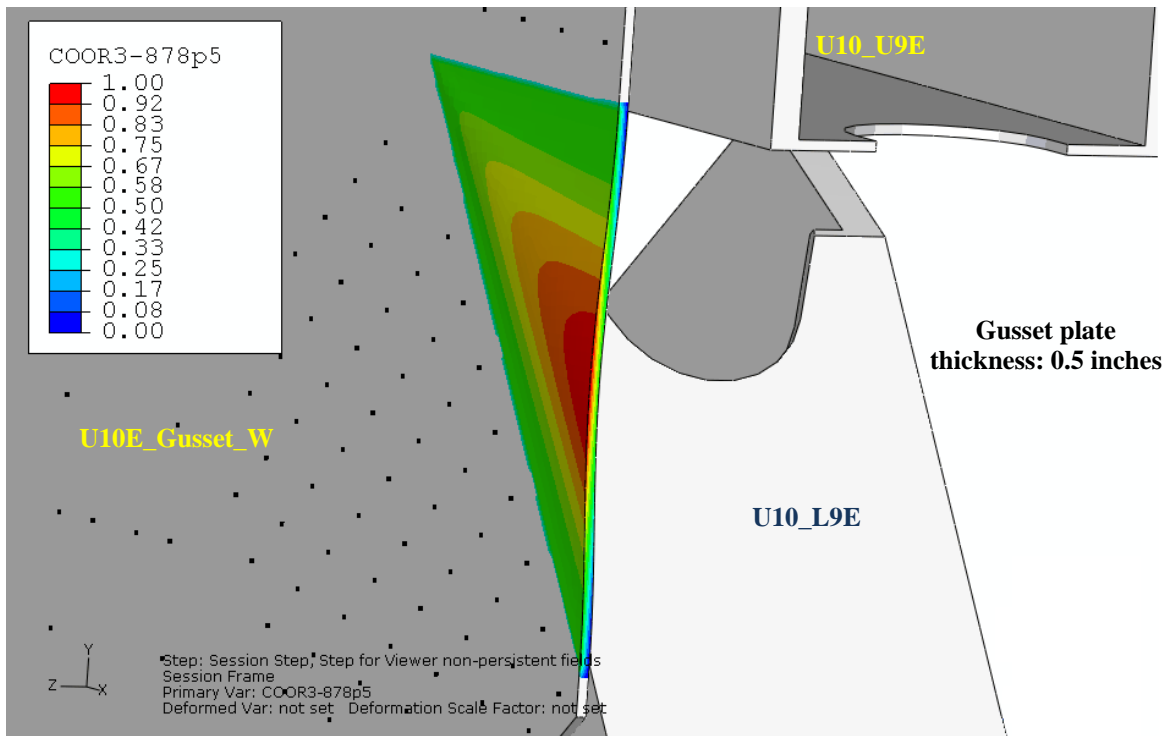
Figure 7.5: Initial relative Z-coordinates of bowed region in the west gusset plate at the U10E joint
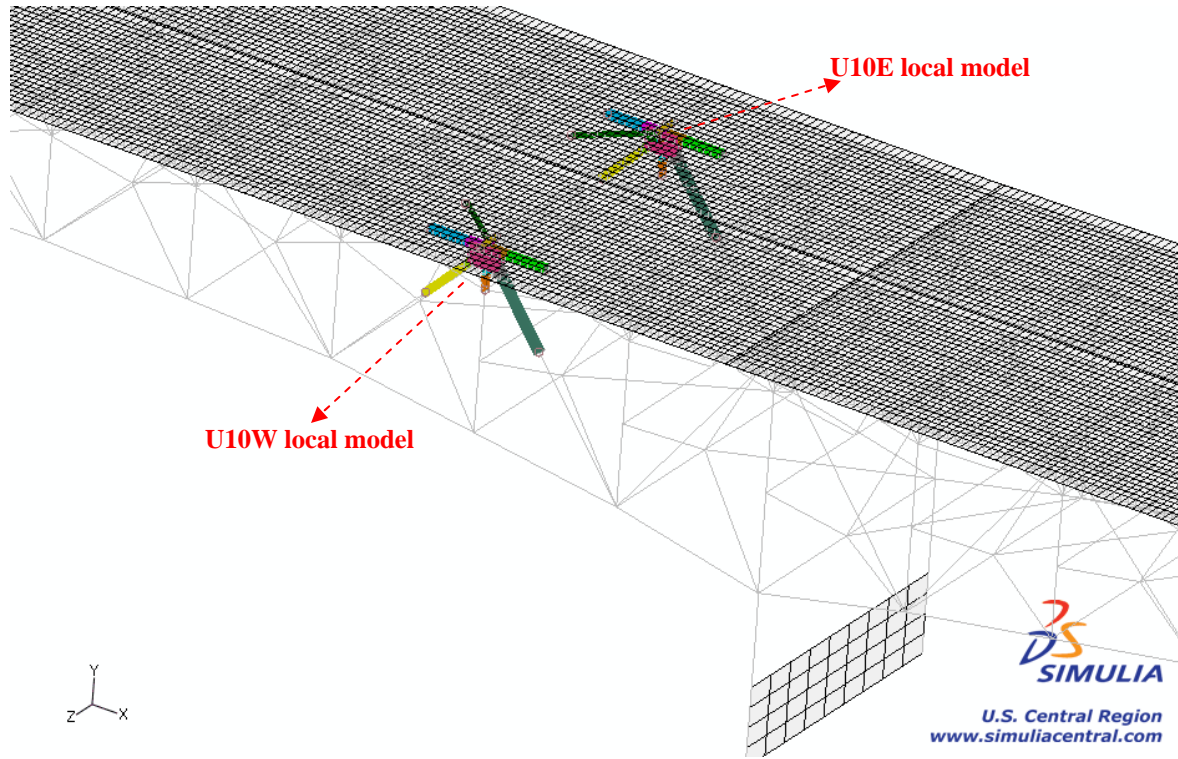
Figure 7.6: Mixed model incorporating both U10W and U10E 3D local models
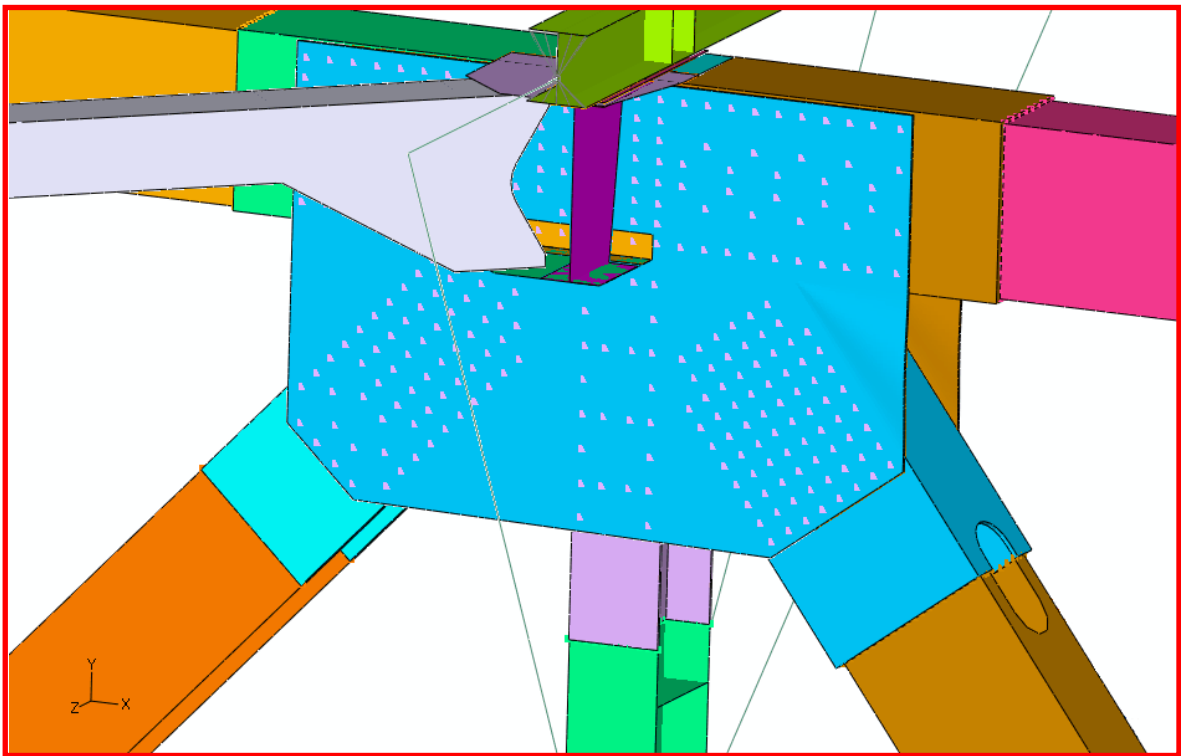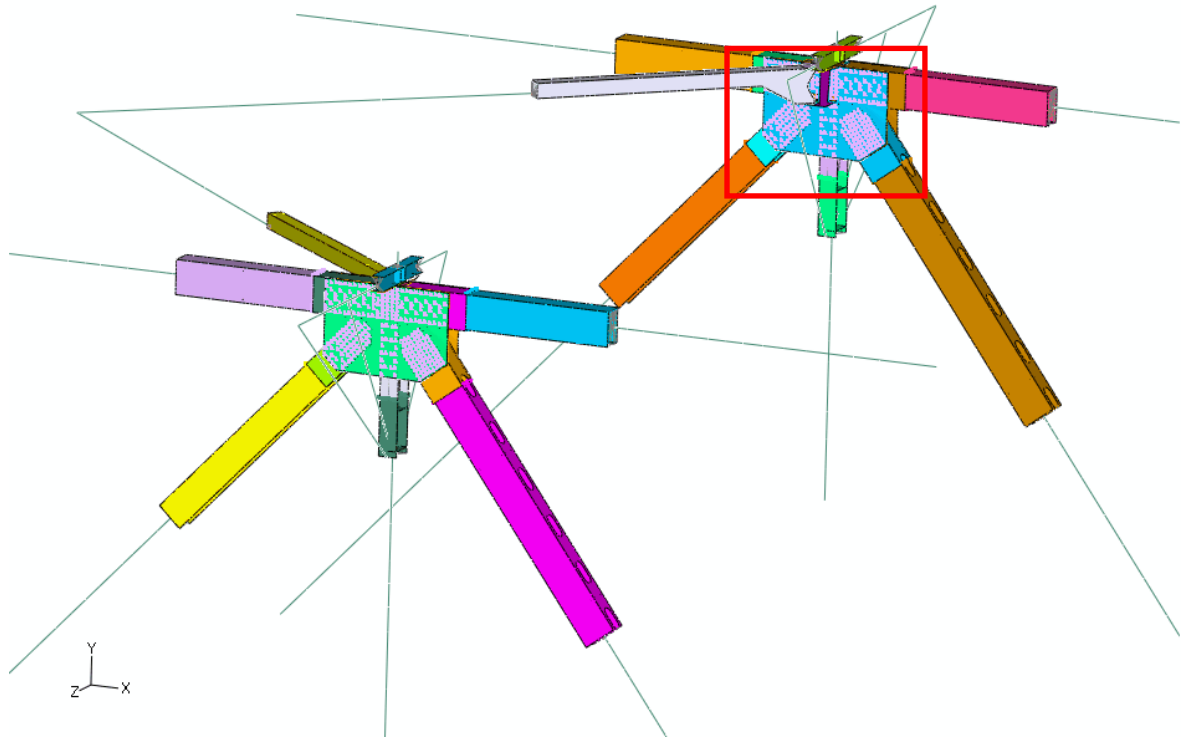
Figure 7.7: CAE model of the U10W and U10E joints
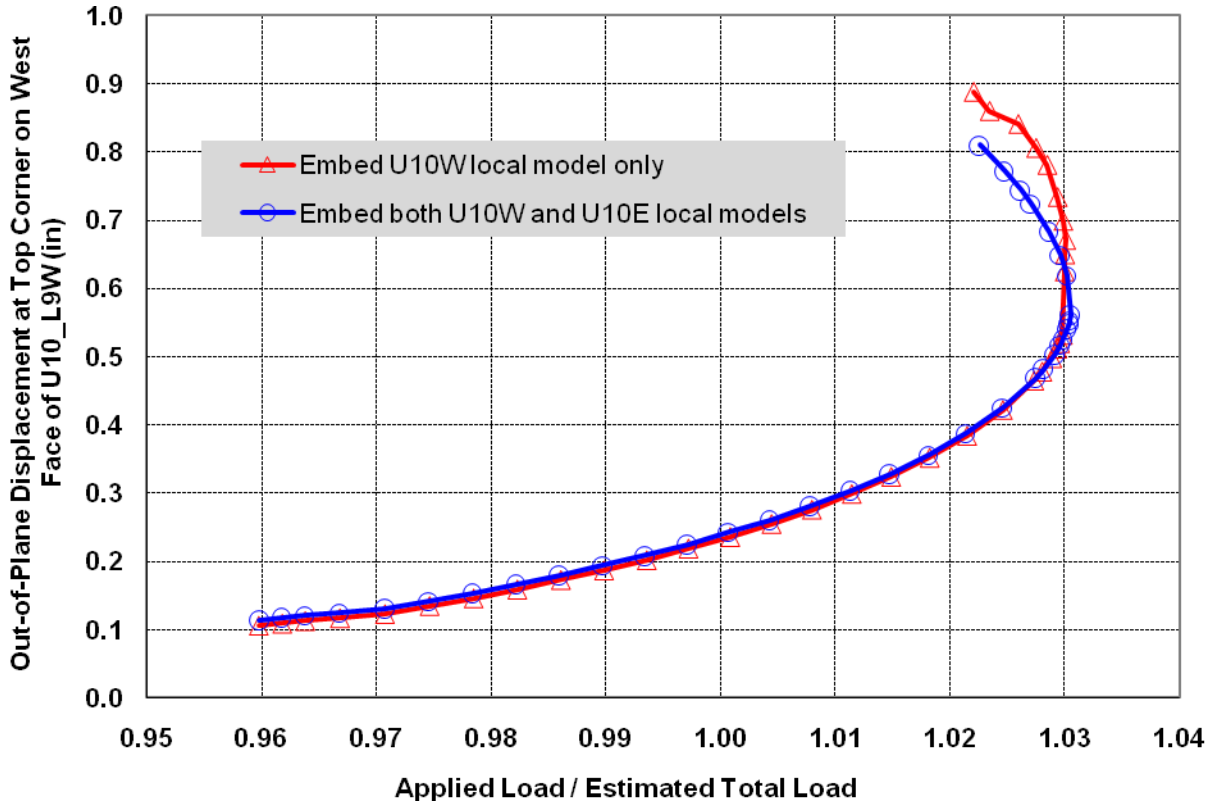
Figure 7.8: Comparison of normalized total load versus displacement in Riks step between embedding U10W local model only and embedding both U10W and U10E local models

Riks step: Under a total load of 25,212 kips

Figure 7.9: Von Mises stress distribution in the east gusset plate at the U10W joint in Riks step when only the U10W joint was embedded

U, U3
- 0.67
- 0.62
- 0.56
- 0.51
- 0.46
- 0.41
- 0.35
- 0.30
- 0.25
- 0.20
- 0.15
- 0.09
- 0.04

Max: 0.67
Node: U10_L9W_SOLID-1.9724

Max: 0.67

U10_L9E

U10_L9W

Positive out-of-plane displacement indicated that nodes moved towards west direction.
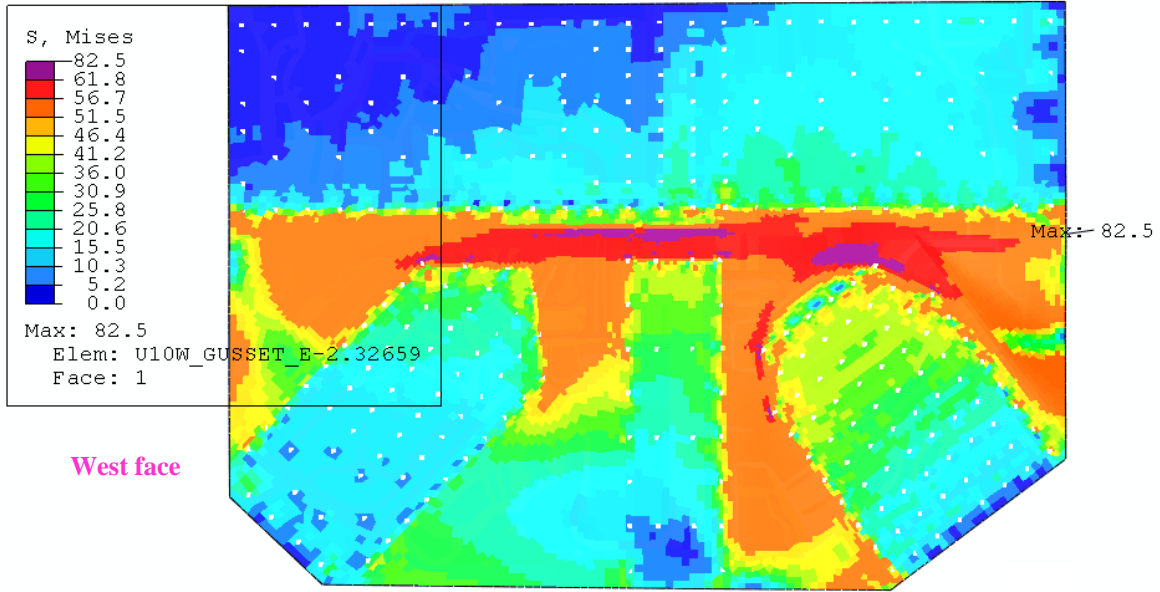
Step: Riks, Apply traffic/consturction load using Riks method
Increment   30: Arc Length =   1.977
Primary Var: U, U3
Deformed Var: U   Deformation Scale Factor: +1.00e+00
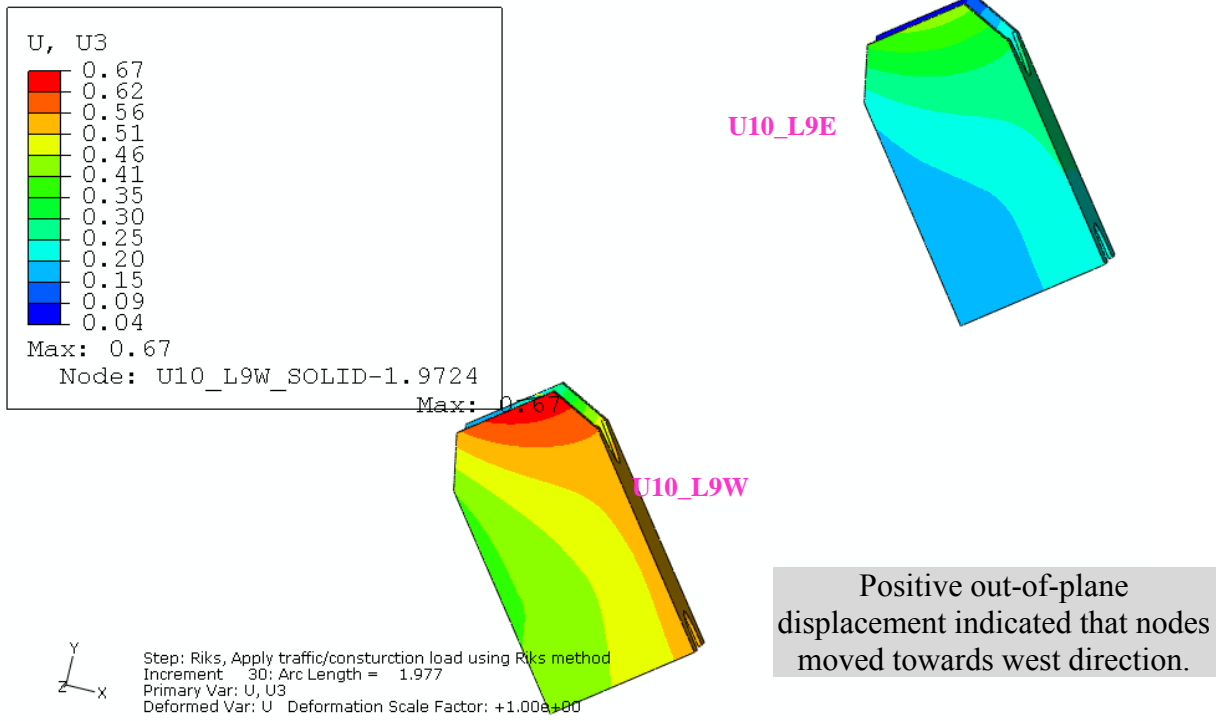
Riks step: Under a total load of 25,207 kips

Figure 7.10: Out-of-plane displacement in diagonal truss members U10_L9W and U10_L9E after the maximum load in Riks step when both U10W and U10E local models were embedded
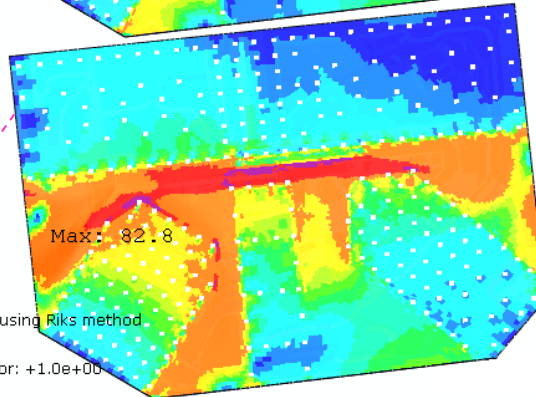
Riks step: Under a total load of 25,221 kips

Figure 7.11: Von Mises stress distribution in the east gusset plates at the U10W and U10E joints in Riks step when both the U10W and U10E joints were embedded
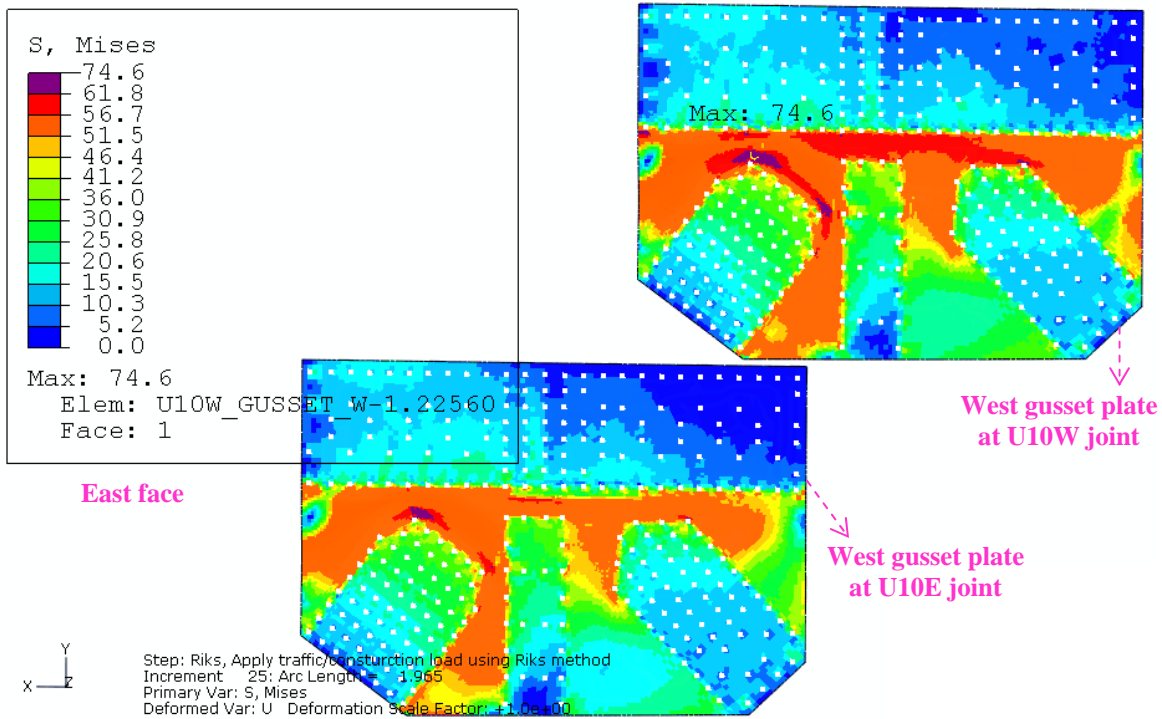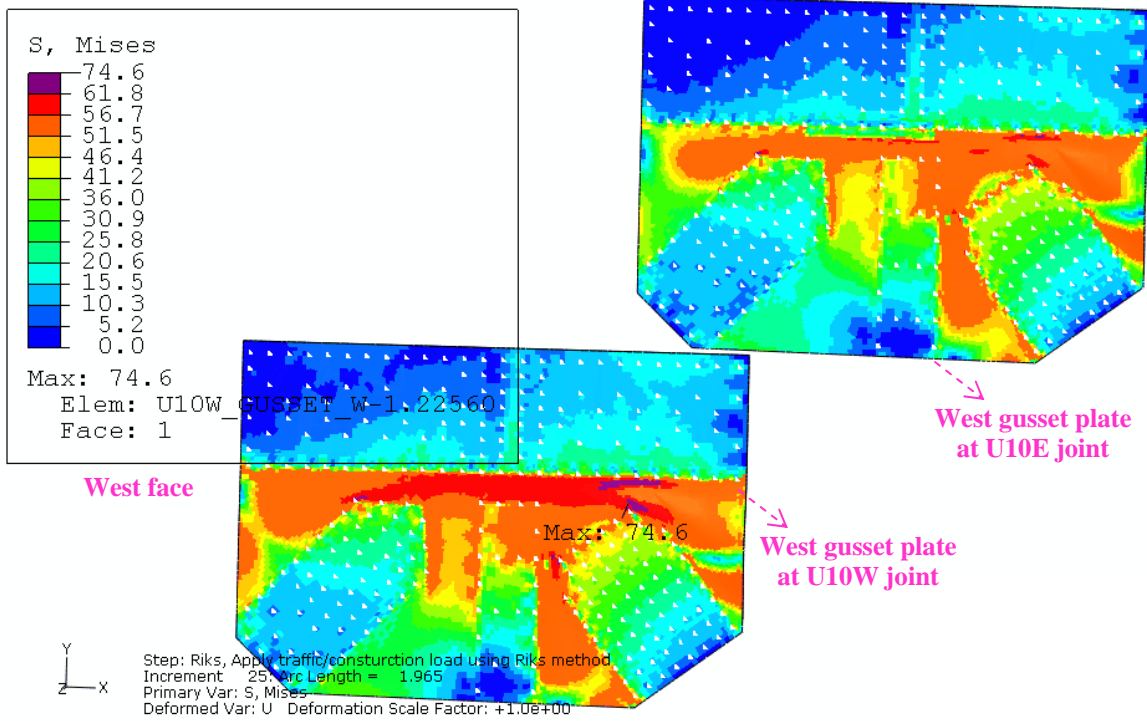
Riks step: Under a total load of 25,221 kips

Figure 7.12: Von Mises stress distribution in the west gusset plates at the U10W and U10E joints in Riks step when both the U10W and U10E joints were embedded

8   Embedding an L11W 3D Local Model into the FHWA Structural Element Bridge Model

Analyses were conducted to investigate the effect of embedding L11W 3D local models into the FHWA structural element bridge model. Corroded gusset plates at the L11W joint were observed in the field [3, 4] and the effect of the corrosion on the stress distribution in the gusset plates was studied. Four mixed models were investigated, as listed in Table 8.1. The first mixed model embedded an L11W 3D local model into the seventh FHWA structural element bridge model, where no corrosion was included in the gusset plates at the L11W joint. The second mixed model was the same as the first one except that corrosion was included in the gusset plates. The third mixed model embedded the L11W 3D local model with the corroded gusset plates and the U10W 3D local model with the bowed gusset plates into the eighth FHWA structural element bridge model. The L11W local model in the second mixed model was exactly the same as that in the third mixed model. The fourth mixed model embedded only the U10W 3D local model with the bowed gusset plates into the sixth FHWA structural element bridge model. The U10W local model in the third mixed model was exactly the same as that in the fourth mixed model. As stated in Section 2 of this report, the seventh and eighth FHWA structural element bridge models were the same as the sixth FHWA structural element bridge model except that the beam elements around the U10W and L11W joints had different mesh sizes. All four mixed models used load condition B, as described previously in Table 7.2.

Table 8.1
Mixed Models Investigated in the Current Section

Mixed Model	Local Models Embedded	Typical Mesh Size (inch)	Loading Condition	FHWA Structural Element Bridge Model
1	L11W joint with flat gusset plates	0.5	B	7
2	L11W joint with corroded gusset plates	0.5	B	7
3	L11W joint with corroded gusset plates and U10W joint with bowed gusset plates	0.5	B	8
4	U10W joint with bowed gusset plates	0.5	B	6

8.1   Description of the U10W 3D Local Model

Three major differences existed between the U10W 3D local model in the current section and the U10W 3D local models in Section 4 of this report, as listed below.

1. Initial bowing geometry of the two gusset plates
2. Meshing of the gusset plates
3. Material of the main truss upper chord member U10_U11W

In the models described in this section, gusset bowing was assumed to initiate along the outer rivet lines. This is in contrast to the bowing conditions described in Section 4, which defined the bowing to initiate at the outer edges of the truss members. The effects of different choices for the initial bowing geometry were also being investigated as discussed below in section 10 of this report, but in this section the bowing geometry is held fixed for the U10W node. Figure 8.1 shows the bowing region defined in the current studies, indicated by the red triangle. Figure 8.1 can be compared to Figure 3.6 to visualize the difference in bowing regions between the current studies and studies discussed previously. Comparison of the two figures indicates that the initial bowing region in the current models was larger than that in the prior models described in Section 4. Figure 8.2 compares the out-of-plane bowing deflections along the vertical edge AB of the gusset plates when the plates bowed along the member outer edges and along the outer rivet lines. The red curve in the figure shows the deflection when the plates bowed along the member outer edges. When the plates bowed along the outer rivet lines, the blue curve shows the deflection of the west plate, and the green curve shows the deflection of the east plate. The two gusset plates initially bowed along the rivet lines had different initial bowing geometry since some bowing portion of the west face of the east gusset plate was in contact with the east face of the truss member U10_L9W, which prevented the westward bowing of the east gusset plate, while the west gusset plate was free to bow towards the west. A cosine curve was assumed for the out-of-plane bowing deflection along the vertical edge of the west plate. The deflection along the vertical edge of the east plate consisted of three curves, a negative cosine curve, a positive cosine curve, and another negative cosine curve. These deflections tapered to zero at the upper left corner of the triangle; the decay to zero was assumed to be linear. Initial maximum out-of-plane deflection was assumed to be 0.5 inches, the same as that presented in Section 4. Figure 8.3 shows the contour plot of the initial relative Z-coordinates of the bowed region of the east gusset plate at the U10W joint.

The gusset plates were represented with C3D8R elements using total stiffness hourglass control [11]. An in-plane mesh size of 0.5 inches was typical in the highly stressed region of the gusset plates. The largest in-plane element size was about 1.0 inch. The east gusset plate contained 56,080 elements, and the west gusset plate contained 55,840 elements. Four elements were used through the thickness of the gusset plates.

The main truss upper chord member U10_U11W was represented by the 50 ksi steel, the same as the other components in the local models. Although the upper chord member U10_U11W should have been modeled with 36 ksi steel, only a few localized elements in that member had von Mises stress exceeding 36 ksi. The effect of this discrepancy was considered to be negligible.

8.2 Description of the L11W 3D Local Models

8.2.1 Geometry and Meshing at the L11W Joint

The NTSB provided original drawings of gusset plates, truss members, lateral braces, fasteners and their positions, and additional details as summarized in Table 8.2. Also provided were two CAD models, in Abaqus/CAE format, of the gusset joint at the L11W node. As stated previously, corrosion was observed in the two gusset plates at the L11W joint in the field, and the corrosion geometry was provided by NTSB, based on field measurements [3, 4].

Table 8.2
CAD Data of the Gusset Joint at the L11 Node

File Type	File Name	Note	Date Received
Drawing	1510 from BR9340 Steel Details (1965)_4.pdf	L11	05-01-08
Drawing	1515 from BR9340 Steel Details (1965)_4.pdf	L11	05-01-08
Drawing	1517 from BR9340 Steel Details (1965)_4.pdf	L11	05-01-08
Drawing	1526 from BR9340 Steel Details (1965)_5.pdf	L11	05-01-08
Drawing	1603 from BR9340 Steel Details (1965)_5.pdf	L11	05-01-08
Drawing	1606 from BR9340 Steel Details (1965)_5.pdf	L11	05-01-08
Drawing	1608 from BR9340 Steel Details (1965)_5.pdf	L11	05-01-08
Drawing	1612 from BR9340 Steel Details (1965)_5.pdf	L11	05-01-08
Abaqus CAE model	L11W.cae, L11W.jnl	L11W	05-01-08
Drawing	Corrosion input.pdf	L11W with corrosion	05-02-08
Abaqus CAE model	L11W_corrosion.cae, L11W_corrosion.jnl	L11W with corrosion	05-02-08

Figure 8.4 and Figure 8.5 show the CAD models of the gusset joint at the L11W node, where corrosion was not included in the gusset plates. The CAD model consisted of two identical gusset plates, five main truss members, one lateral brace, one strut, and other secondary structure, including filler plates, splice plates, and plates supporting the lateral brace and strut. Table 8.3 summarizes these components.

Table 8.3
Components in CAD Model L11W.cae

Type	Component 1	Component 2	Component 3
Gusset plate (0.5 inches thick)	L11W_Gusset_W	L11W_Gusset_E	---
Main truss member	L11_U9W	L11_U10W	L11_U11W
	L11_L9W	L11_L13W	---
Lateral brace	L11W_Lateral_brace	---	---
Strut	L11W_Strut	---	---
Internal filler plate	L11W_L9_fill_W	L11W_L9_fill_E	---
Internal splice plate	L11W_inner_splice_W	L11W_inner_splice_E	---
External splice plate	L11W_top_splice	L11W_bot_splice	---
Plate supporting lateral brace	L11W_strut_lateral_gusset	L11W_lateral_bot_fill	---
	L11W_angle	L11W_bot_gusset	---
Plate supporting strut	L11W_top_angle_north	L11W_top_angle_south	L11W_strut_top
	L11W_strut_top_gusset	L11W_strut_top_bevel	---
	L11W_strut_bot_bevel	L11W_strut_angle	---

The 3D local model of the L11W joint included all the components listed in Table 8.3 and shown in Figure 8.6 and Figure 8.7. The five main truss members, lateral brace, and strut in the local model were cut through the members in the FHWA structural element bridge model, as shown in Figure 8.6. The distances from these cutting planes to the L11W node were two fifths of the lengths of their bridge members. The gusset plates were represented with the C3D8R elements with total stiffness hourglass control [11]. An in-plane mesh size of 0.5 inches was typical in the highly stressed region of the gusset plates. The largest in-plane element size was about 1.0 inch. Four elements were used through the thickness of the gusset plates and each gusset plate contained 48,908 elements. The five main truss members were represented with the C3D8R and S4R elements, where the C3D8R elements were used in the portions of the truss members in contact with the gusset plates. Four C3D8R elements were used through the thickness of the main truss members. An in-plane mesh size of the solid representation of the truss members ranged from 0.5 inches to 1.5 inch. The mesh size of truss shell representation ranged from 1.5 inch to 3.0 inches. All other parts in the 3D local model were represented with S4R shell elements. The connecting plate L11W_strut_top had an element size of 1.5 inches. All other secondary structure had an average element size of 0.6 inch.

8.2.2   Corrosion of the Gusset Plates at the L11W Joint

Corrosion was observed by the NTSB in both gusset plates at the L11W joint and both gusset plates at the L11E joint [3, 4]. The top sketch in Figure 8.8 illustrates the area of corrosion in the

west gusset plate along the top edges of the lower chord members, where the plate was positioned as in shop drawing 1517B (Table 8.2). Vertices of the plate and the corroded region were labeled in the figure and their coordinates are listed in Table 8.4. The origin of these coordinates was at the center of the L11 node, where the centerlines of all of the truss members met. The modeled corrosion was based on measurements, which indicated an average plate thickness of 0.4 inch in the areas that were corroded. As modeled, the area of corrosion was 1 inch tall and 0.1 inch deep at its maximum, and it was blended smoothly into the un-corroded area. The section loss of the corroded region was assumed to follow a cosine curve. The bottom edge of the corroded region was along the top edge of the side plate of the lower chord of the main truss where the truss members came into contact with the gusset plate, as illustrated in the bottom sketch in Figure 8.8.

Table 8.4
Coordinates (inches) of the Labeled Vertices in Figure 8.8

Point	A	B	C	D	E	F	G
X Position	-45.25	-0.6998	49.3489	53.6438	36.5038	-32.1807	-45.25
Y Position	-14	-14	-19.0179	23.8194	45.9616	58.9594	49.7956
Point	H	I	J	K	L	M	---
X Position	-45.25	0.7	52.1422	-45.25	0.75	52.242	---
Y Position	14	14	8.8424	15	15	9.8374	---

Figure 8.9 shows the west gusset plate with corrosion in the local model. Figure 8.10 shows the meshing of the plate. The meshing of the gusset plates with corrosion was similar to that of the gusset plates without corrosion, except that an in-plane mesh size of 0.2 inches was typical in the corroded region. Figure 8.11 shows the position of the corroded region, relative to the two lower main truss members in the local model.

8.2.3 Material Properties

The 50 ksi steel was used to represent all components at the L11W joint. Although lower chord member L11_L9W should have been modeled with 36 ksi steel, the von Mises stress in that member never exceeded 36 ksi, so this discrepancy did not introduce any error.

8.2.4 Constraints, Rivets, Contacts and Boundary Conditions

The cut planes of the five main truss members, lateral brace, and strut passed through seven member nodes in the FHWA structural element bridge model. These bridge nodes were coupled to the cut planes of the shell representations of the seven members, as shown in Figure 8.12. All seven couplings were surface-based kinematic couplings. As modeled, the entire 3D local model was embedded into, and driven by, the FHWA structural element bridge model.

As stated previously, the five main truss members in the local 3D model were represented with both solid elements and shell elements. The transition from the shell element portion to the solid element portion was implemented using surface-based shell-to-solid coupling constraints.

All rivets connecting the two gusset plates and the five main truss members were represented by Abaqus fasteners. Figure 8.13 shows the locations of the fasteners related to the vertical faces, and Figure 8.14 shows the locations of the fasteners related to the top and bottom faces. In the local 3D model, the fasteners were defined to have a radius of influence of 0.5 inches. Both surfaces normal to the rivet axis of a solid component were involved in the fastener definition. The red dots in Figure 8.15 indicate the fastened nodes in the west gusset plate. All other connections between the components in Table 8.3 were represented by surface-based tie constraints. Contact pairs were defined between the components wherever the fasteners were employed to connect them. A Coulomb friction model with a friction coefficient of 0.1 was used to define the contact pairs. No translational or rotational boundary conditions were defined in the local 3D model. Figure 8.16 shows the embedded L11W joint and the U10W joint that incorporated the corrosion, bowing, fasteners, constraints, and contacts described above.

8.3 Analysis Results when the L11W 3D Local Models were Embedded into the FHWA Structural Element Bridge Model: with both Flat and Corroded Gusset Plates

Figure 8.17 shows the von Mises stress and equivalent plastic strain (PEEQ) distributions at the L11 joint under the bridge design weight for the L11W local model with flat gusset plates embedded into the seventh FHWA structural element bridge model. Figure 8.18 shows the von Mises stress and equivalent plastic strain (PEEQ) distributions in the east gusset plate at the L11 joint under the as-designed bridge weight. The two figures indicate that the gusset material between the five main truss members was predicted to yield under the as-designed bridge weight.

The Riks method was used to investigate the possibility of an instability by proportionally increasing the live load while other loads were maintained at the estimated values. As stated previously, for load condition B, the estimated live load was 984 kip, which includes the traffic load of 379 kip, the construction load of 576 kip, and the corresponding approach span force increment of 29 kip.

When the L11W local model with the flat gusset plates was embedded into the seventh FHWA structural element bridge model, the live load in the Riks step increased monotonically until the analysis was terminated because the applied live load had exceeded 3 times the estimated value. At the termination point the applied live load was 2,971 kip, or 3.02 times the estimated value. The total load at the termination point was 26,470 kip, or 1.081 times the estimated value of the total bridge load. The displacement along the vertical direction at one node of the west gusset plate was predicted to be -8.99 inches under the load at termination point. Figure 8.19 shows the von Mises stress and equivalent plastic strain distributions at the L11W joint under the load at the termination point. The maximum stress was predicted to be 65 ksi on the edge of the lower corner fastener connecting the west gusset and the diagonal truss member L11_U9W, which corresponded to an equivalent plastic strain of 2.0%.

When the L11W local model with the corroded gusset plates was embedded into the seventh FHWA structural element bridge model, the live load in the Riks step increased monotonically

until the analysis was terminated because the live load exceeded 3 times the estimated value. At the termination point the live load was 2,966 kip, or 3.02 times the estimated value. The total load at the termination point was 26,465 kip, or 1.081 times the estimated value of the total bridge load. The displacement along the vertical direction at one node of the west gusset plate was predicted to be -8.98 inches under the load at termination point. Figure 8.20 shows the von Mises stress and equivalent plastic strain distributions at the L11W joint under the load at the termination point. The maximum stress was predicted to be 72 ksi in the corroded region of the west gusset, which corresponded to an equivalent plastic strain of 3.2%.

Figure 8.21 compares the load displacement curves in the Riks step between the two mixed models, with the flat gusset plates and with the corroded gusset plates. The horizontal axis in this figure represents the normalized total load. The vertical axis represents the displacement along vertical direction (negative Y-direction) at one node of the west gusset plate at the L11W joint. The two curves were almost identical. The von Mises stress and equivalent plastic strain distributions were similar to each other between the two mixed models, except that the stress and strain in the corroded region were raised by the change in geometry defined by corrosion. Table 8.5 summarizes the loads, the displacement along the vertical direction, the maximum von Mises stress, and the maximum equivalent plastic strain at the termination point of the Riks step for the two models.

Table 8.5
Effect of the Corroded Gusset Plates at the L11W Joint on Results of Interest at the Termination Point of the Riks Step

	Without Corrosion	With Corrosion
Total Load at Termination Point of Riks Step (kip)	26,470	26,465
Traffic/Construction/Approach Span Force Increment (Live Load) (kip)	2,971	2,966
Displacement along Y-Direction at One West Gusset Node (inch)	-8.99	-8.98
Maximum von Mises Stress at L11W Joint (ksi)	65	72
Maximum Equivalent Plastic Strain at L11W Joint	2.0%	3.2%

8.4 Comparison between Embedding the U10W 3D Local Model Only and Embedding Both U10W and L11W 3D Local Models

The Riks method was used to predict the maximum live load at instability by proportionally increasing the live load while other loads were maintained at the estimated values. When the U10W local model with the bowed gusset plates was embedded into the FHWA structural element bridge model, the Riks analysis predicted a maximum live load of 1,506 kip, or 1.53 times the estimated value. The total load along the vertical direction was predicted to be 25,004 kip, or 1.021 times the estimated total bridge load, as shown by the red curve in Figure 8.22. The out-of-plane displacement at the top corner of the diagonal truss member U10_L9W was

predicted to be 0.591 inches under the maximum total load. After the maximum total load, the out-of-plane displacement continued to increase with reduced live load, indicating that the maximum in the load was associated with a geometric instability. The axial force and bending moment at the lower end of the diagonal truss member U10_L9W were predicted to be -2,557 kip and 1,639 kip-inch under the total load of 24,997 kip. Significant plastic deformation occurred in the two U10W gusset plates under this load, as shown in Figure 8.23. The maximum von Mises stress was predicted to be 77 ksi in the vicinity of the upper corner rivet in the east gusset plate. The maximum equivalent plastic strain was predicted to be 4.2%.

When both the U10W local model with the bowed gusset plates and the L11W local model with the corroded gusset plates were embedded into the FHWA structural element bridge model, the Riks analysis terminated before the live load decreased. Termination was driven by the fact that the maximum number of analysis increments allowed (50) had been reached. The total load had remained constant for 19 analysis increments prior to termination and the time increment size at termination was 2.6×10^{-6} seconds. As shown by the blue curve in Figure 8.22, the Riks analysis indicated that the maximum total load necessary to trigger the instability would be very close to the value at termination.

The live load at termination was 1,519 kip, or 1.54 times the estimated value. The total load along the vertical direction at the termination point was predicted to be 25,020 kip, or 1.022 times the estimated total bridge load. The out-of-plane displacement at the top corner of the diagonal truss member U10_L9W was predicted to be 0.6 inches at the termination point. The axial force and bending moment at the lower end of the diagonal truss member U10_L9W were predicted to be -2,557 kip and 1,683 kip-inch at the termination point. Significant plastic deformation occurred in the two U10W gusset plates under the applied load, as shown in Figure 8.24. The maximum von Mises stress was predicted to be 78 ksi in the vicinity of the upper corner rivet in the east gusset plate. The maximum equivalent plastic strain was predicted to be 4.7%.

Figure 8.25 shows the von Mises stress and the equivalent plastic strain distributions at the L11W joint at the termination point. The maximum von Mises stress was predicted to be 66 ksi in the corroded region of the west gusset plate. The maximum equivalent plastic strain was predicted to be 2.1%. The maximum von Mises stress at the L11W joint were significantly smaller than that at the U10W joint. The maximum and minimum out-of-plane displacements at the L11W joint were predicted to be 0.073 inches and -0.188 inches at the L11W joint.

Table 8.6 compares the loads, axial force and bending moment at the lower end of the diagonal truss member U10_L9W, out-of-plane displacement at the top corner of the diagonal truss member, the maximum von Mises stress in the east gusset at the U10W joint, and the maximum von Mises stress at the L11W joint. Comparisons are provided for the cases when only the U10W local model was embedded and when both the U10W and L11W (including corrosion) local models were embedded into the FHWA structural element bridge model. It shows that for the results of interest, the effect of embedding the L11W local model into the FHWA structural element bridge model was negligible.

Table 8.6
Effect of Embedding the L11W Local Model with U10W Local Model on Results of Interest,
Load Condition B

	Without L11W Embedded	With L11W Embedded (including corrosion)
Embedded L11W Local Model	No	Yes
Predicted Maximum Total Load at Instability (kip)	25,004	25,020
Traffic/Construction/Approach Span Force Increment (Live Load) at Predicted Maximum Load at Instability (kip)	1,506	1,519
Axial Force at Lower End Node of Truss Member U10_L9W (kip) *	-2,557	-2,557
Bending Moment at Lower End Node of U10_L9W (kip-inch) *	1,639	1,683
Out-of-Plane Displacement at Top Corner of U10_L9W (inch) *	0.591	0.600
Maximum Mises Stress in East Gusset at U10W (ksi) *	77	78
Maximum Mises Stress in West Gusset at L11W (ksi) *	N/A	66

* Values under load of 24,997 kip if only the U10W local model was embedded or under load of 25,020 kip if both the U10W and the L11W local models were embedded.

8.5 Summary: Embedding L11W 3D Local Model into the FHWA Structural Element Bridge Model with U10W 3D Local Model

Four mixed models with typical in-plane mesh sizes of 0.5 inches in the highly stressed region of the gusset plates were analyzed to investigate the effect of embedding the L11W 3D local model into the FHWA structural element bridge model with and without a U10W 3D local model. Load condition B was used, where the traffic load, construction load, and the approach span force increment were proportionally increased in the Riks step.

When only the L11W local models were embedded into the FHWA structural element bridge model, no instability was predicted before the Riks analyses were terminated. The analyses were terminated in these cases because the total load had exceeded the maximum value specified: 26,470 kip for the flat gusset plates or 26,465 kip for the corroded gusset plates.

When both the L11W and U10W local models were embedded into the FHWA structural element bridge model, the analyses indicated that the incorporation of the L11W 3D local model had negligible effect on the maximum load at instability and other results of interest. The mixed model with only the U10W local model embedded predicted a maximum total load of 25,004 kip, and the mixed model with both the U10W and the L11W local models embedded predicted a maximum total load of 25,020 kip. The local instability occurred at the U10W joint even if the L11W local model was embedded.

Analyses predicted that the unfastened central portion of the un-corroded gusset plates located at the L11W joint yielded under the bridge design weight. The corrosion in the gusset plates at the L11W joint slightly raised the von Mises stress in the corroded region. However, the maximum von Mises stress at the L11W joint at the maximum predicted load was predicted to be significantly smaller than that at the U10W joint when both local models were embedded into the FHWA structural element bridge model.

Figure 8.1: Initial bowing region of gusset plates along rivet lines at the U10W joint

Figure 8.2: Initial out-of-plane bowing deflection along vertical edge AB of gusset plates at the U10W joint
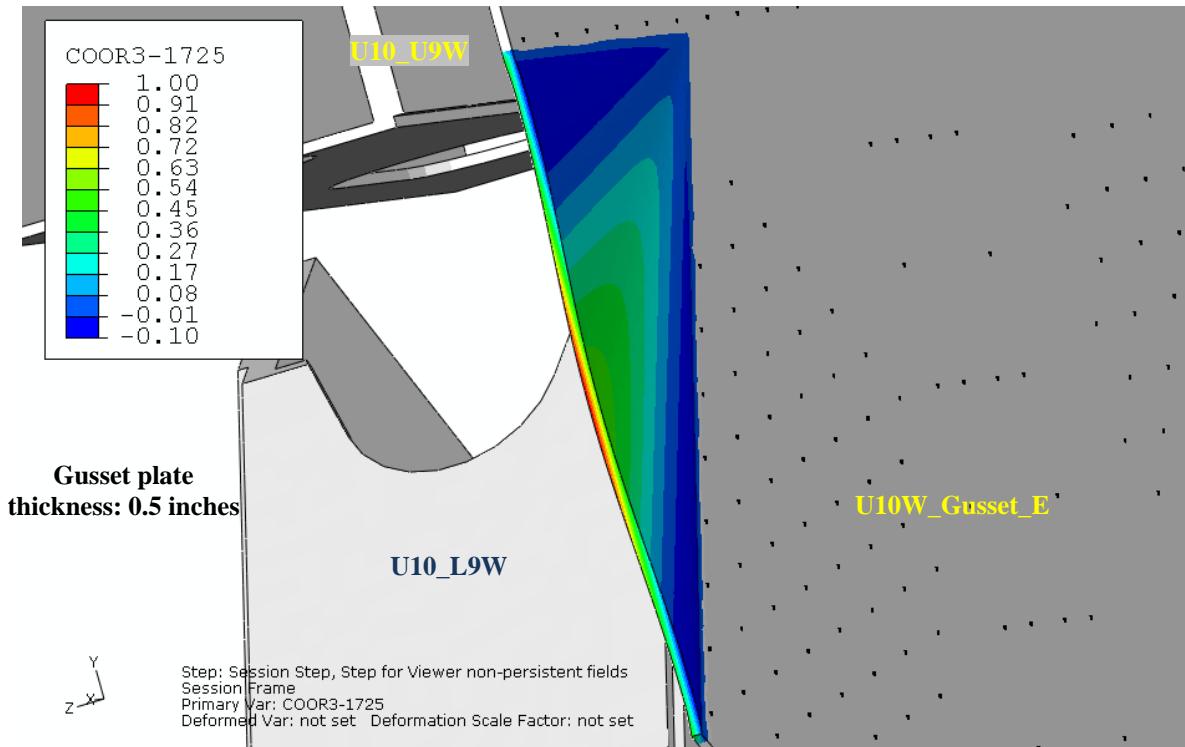
Figure 8.3: Initial Relative Z-coordinates of the bowed region at the east gusset plate of the U10W joint
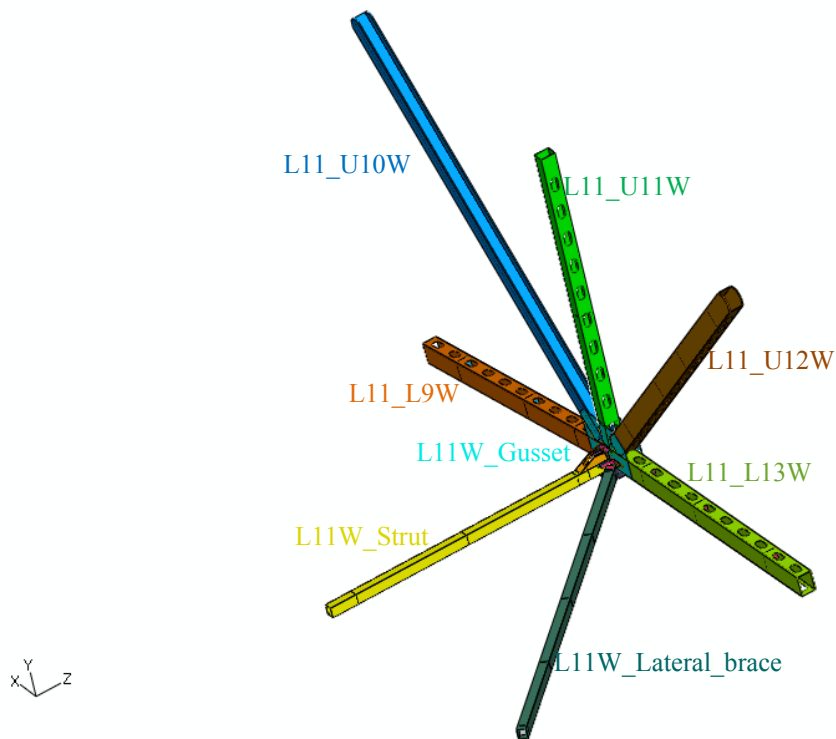
Figure 8.4: CAD model of the L11W joint provided by NTSB
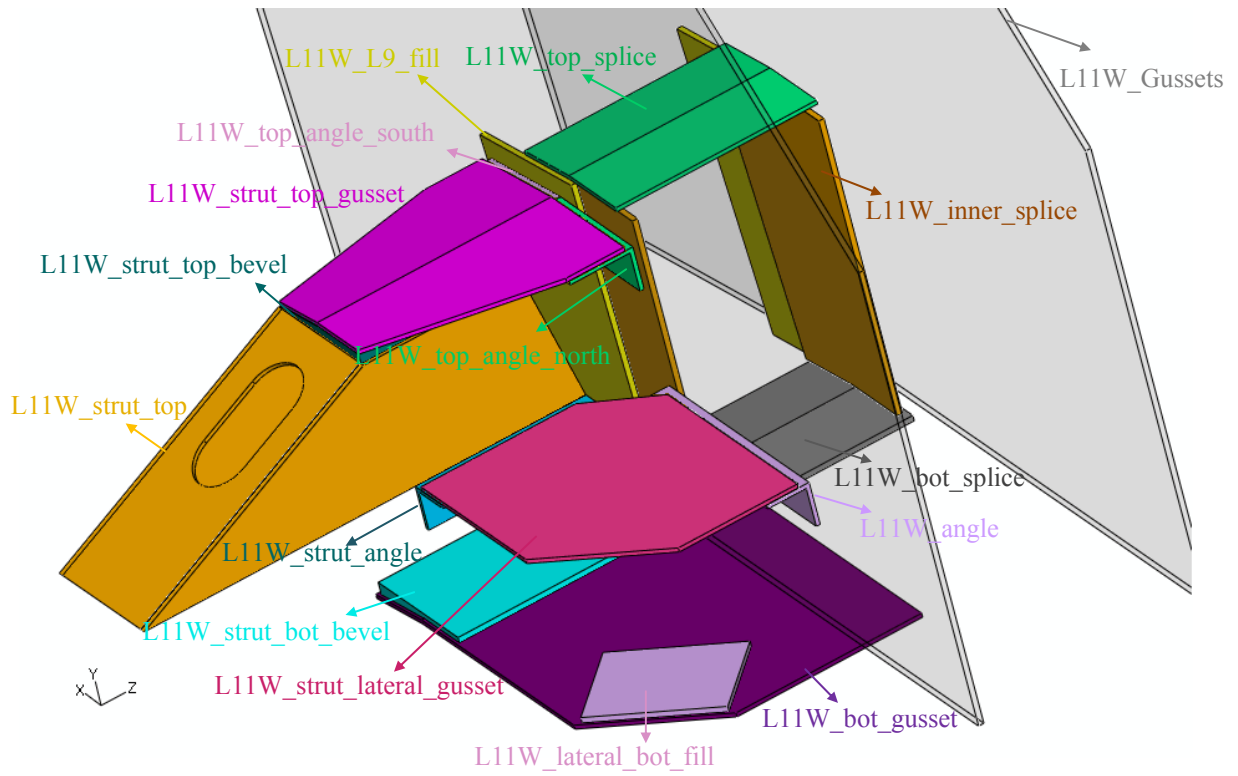
Figure 8.5: CAD model of connecting plates at the L11W joint provided by NTSB

Truss represented with B33
beam elements in FHWA
structural element model

Element
S4R

Element
C3D8R

Mesh 0.5 inch
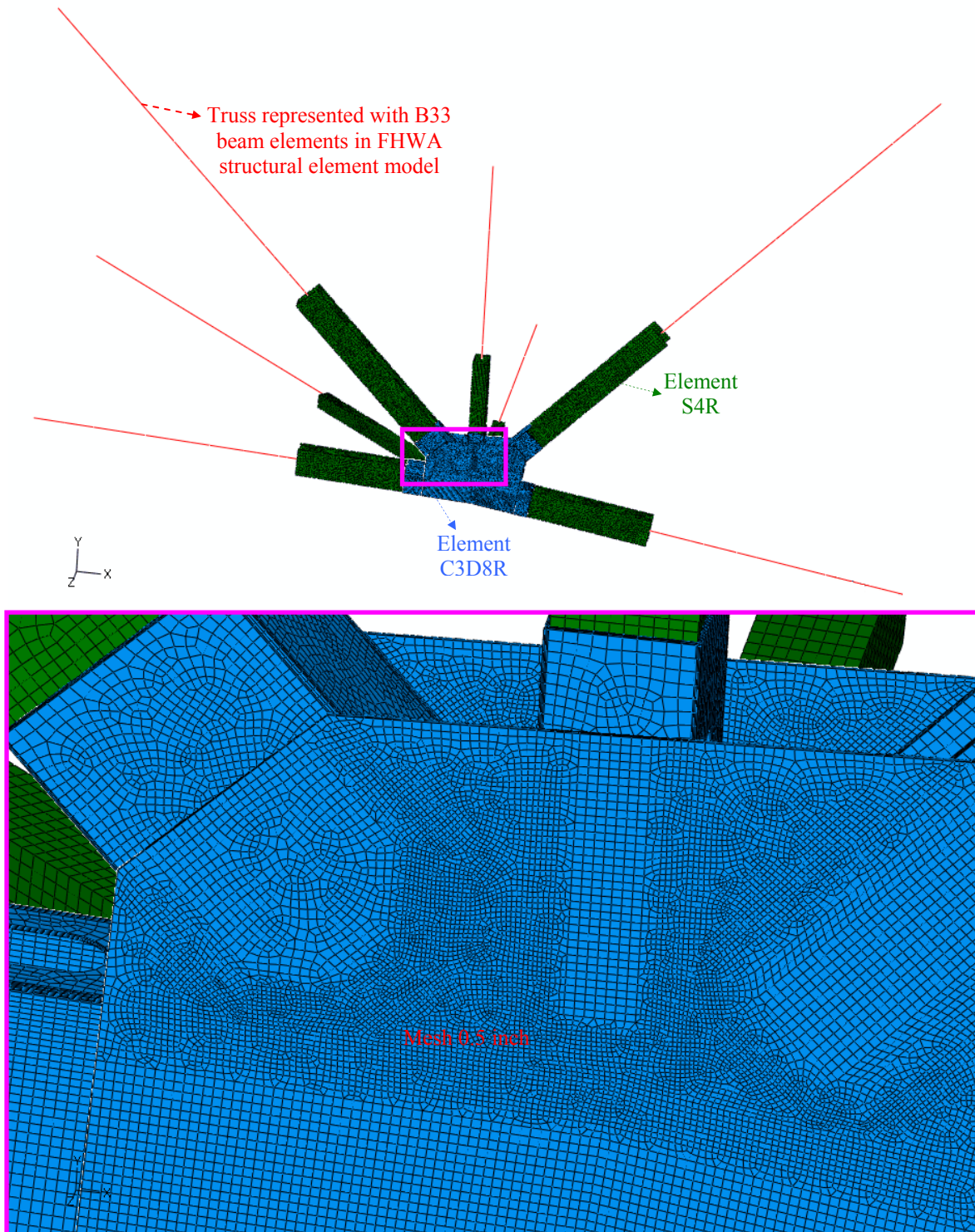
Figure 8.6: CAE model of the L11W joint without corrosion
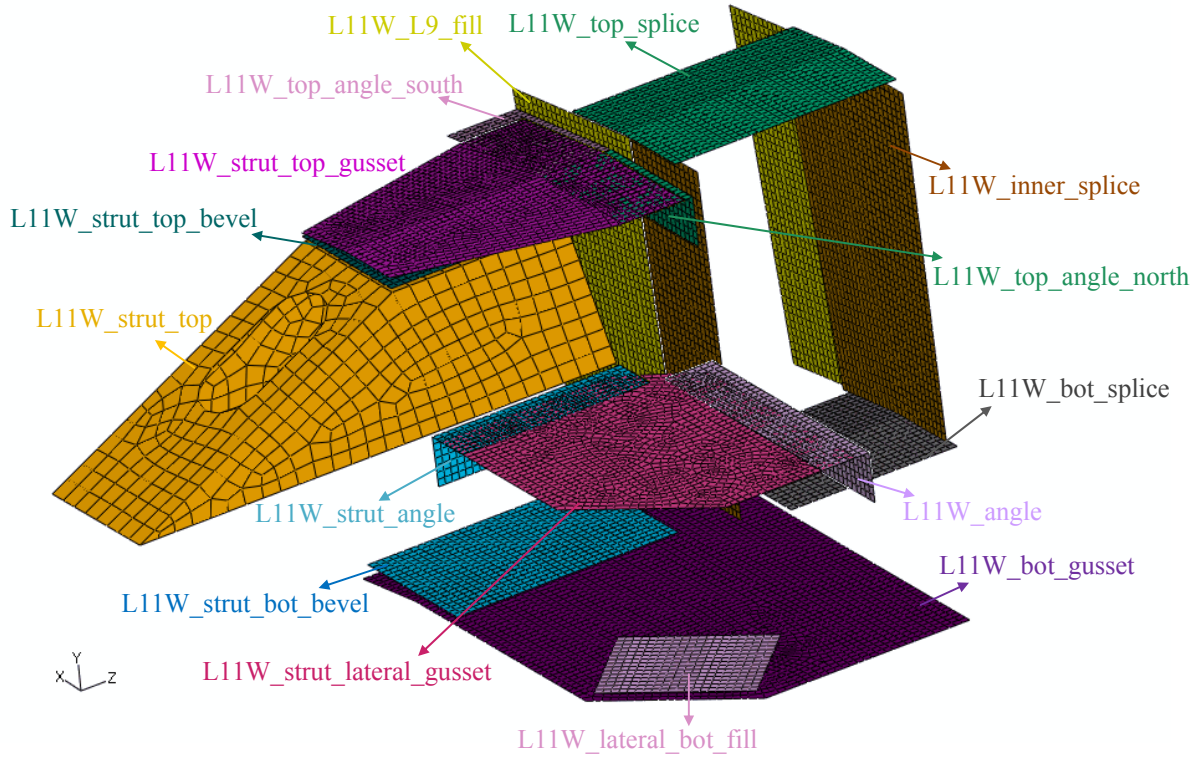
Figure 8.7: CAE model of connecting plates at the L11W joint: 0.6 inch mesh except L11W_strut_top
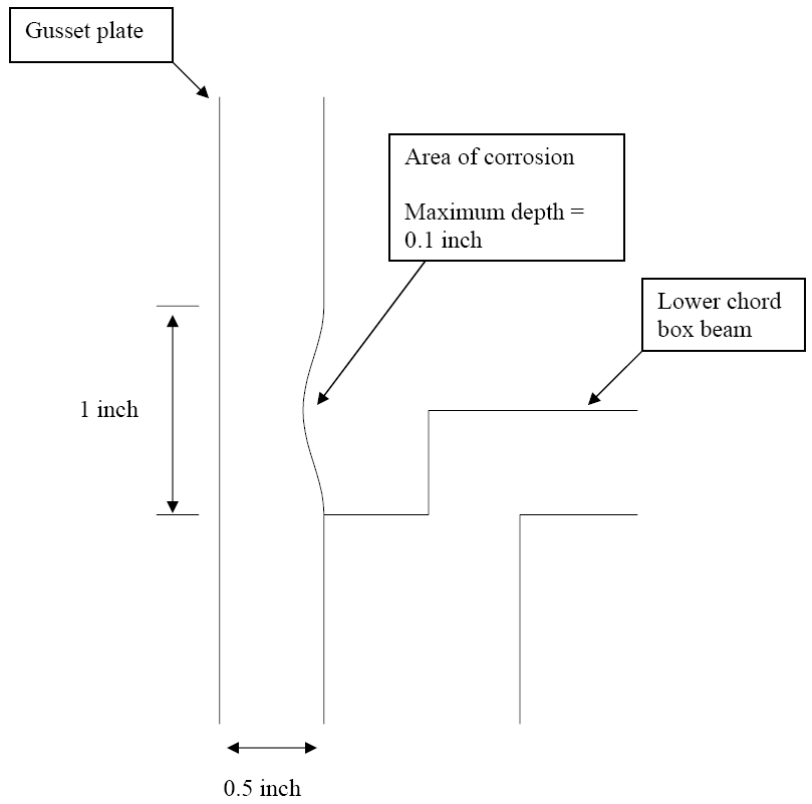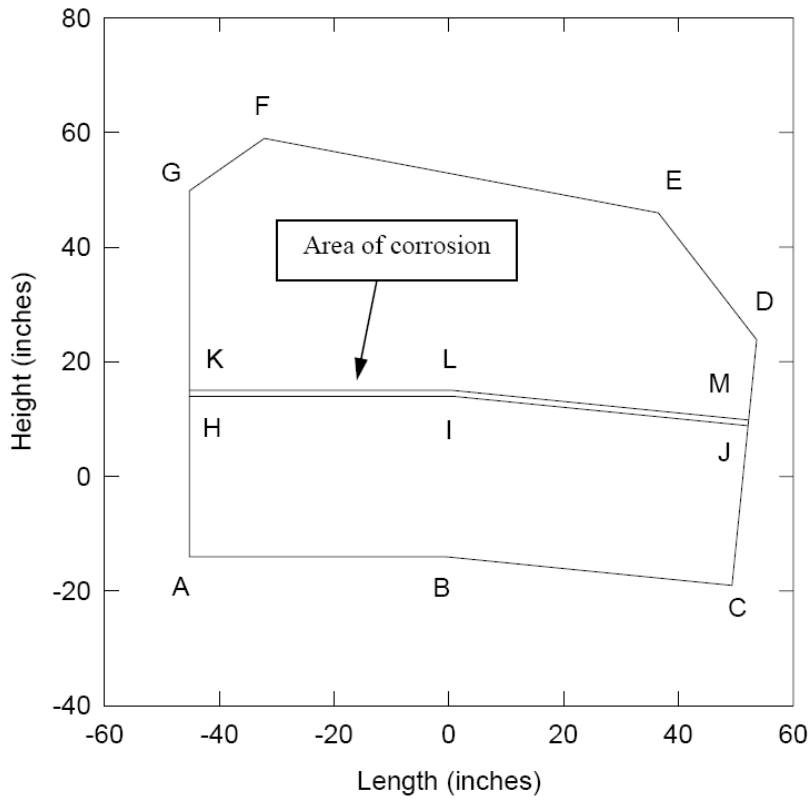
Figure 8.8: Illustration of corroded area in the west gusset plate at the L11W joint; provided by NTSB [3, 4] (gusset, side plate and cover plate of the lower chord box beam without fillet weld)
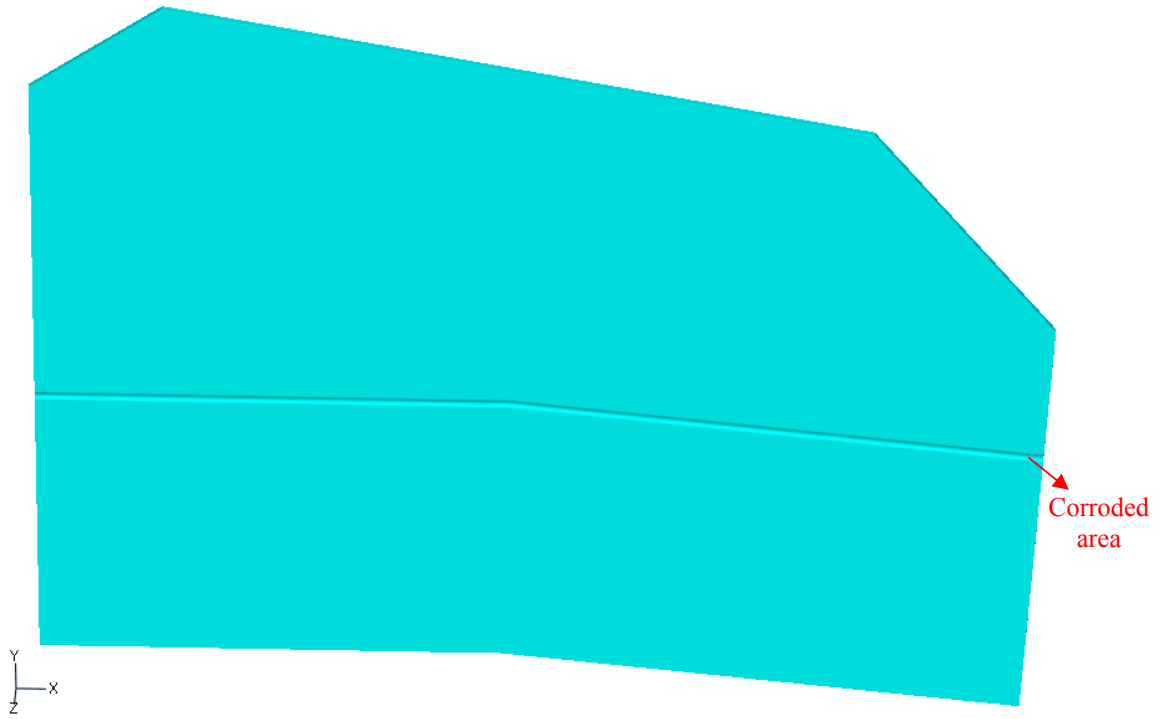
Figure 8.9: Corroded area in the west gusset plate at the L11W joint
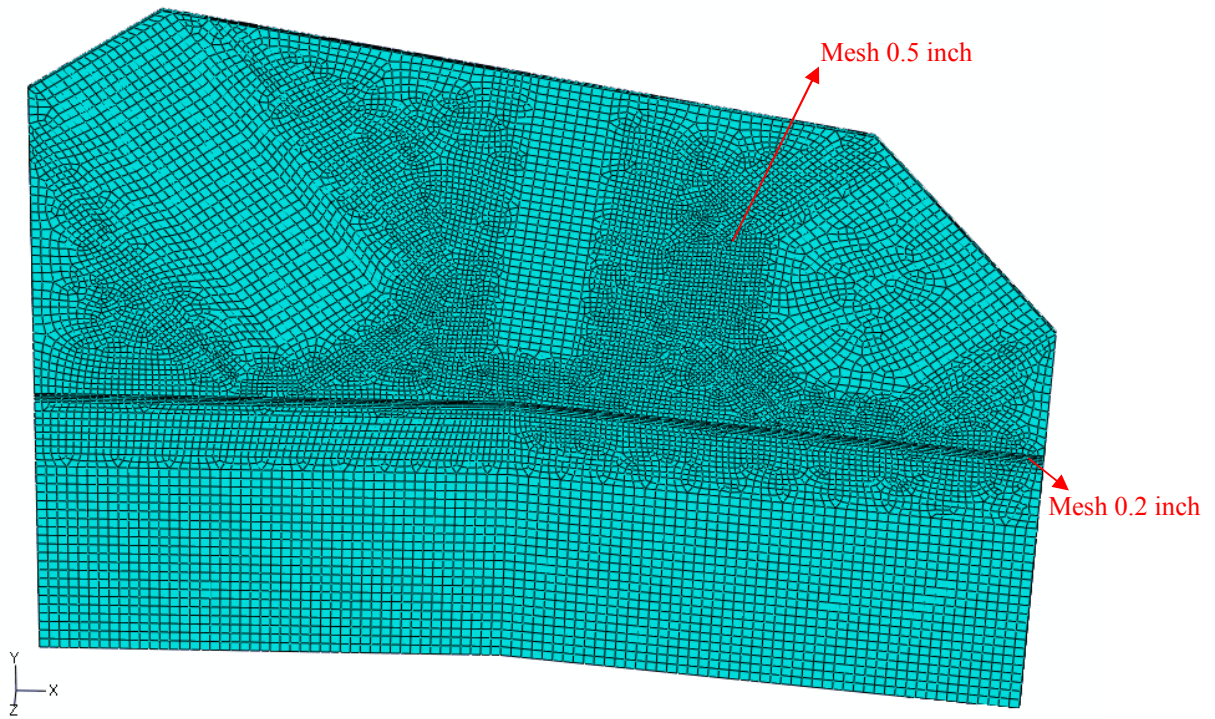
Figure 8.10: Meshing in the corroded west gusset plate at the L11W joint
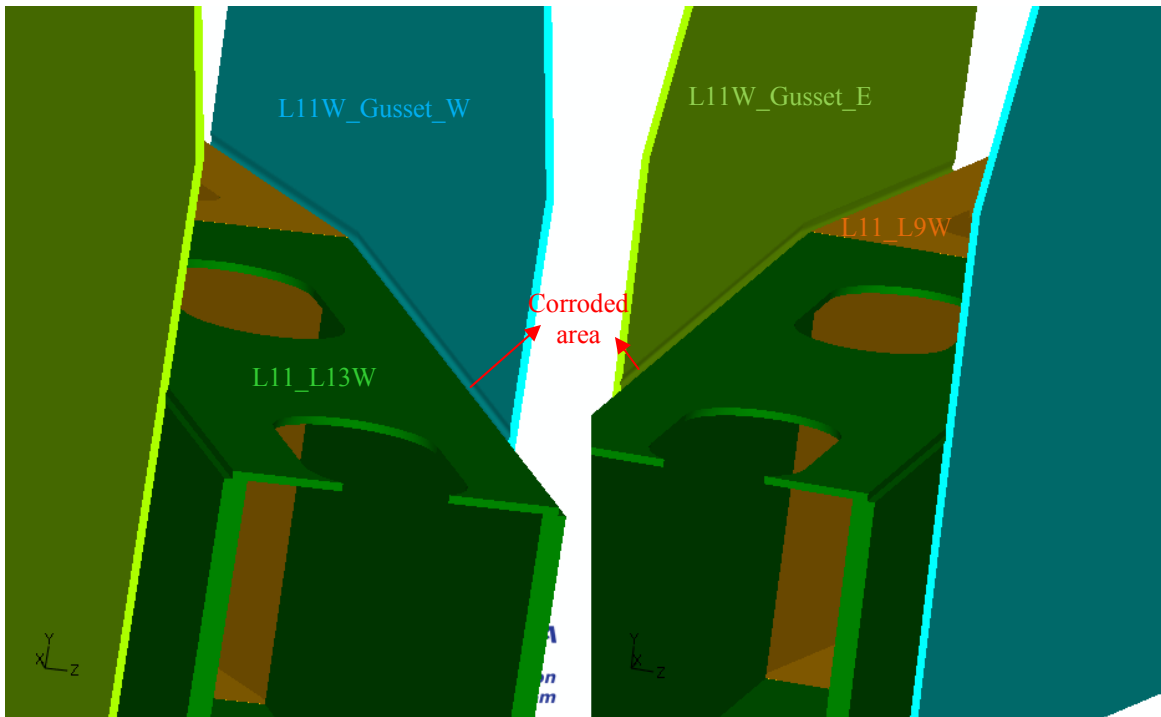
Figure 8.11: Position of the corroded area in the gusset plates at the L11W joint
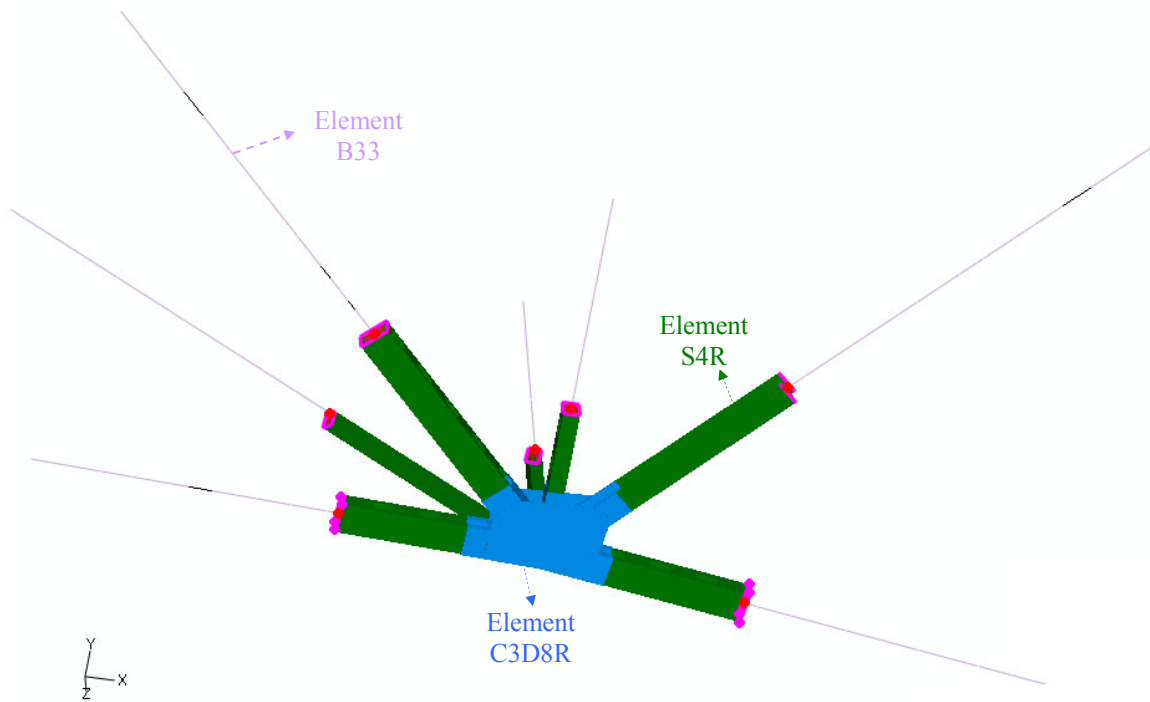
Figure 8.12: Seven couplings between the bridge nodes and shell cut planes at the L11W joint
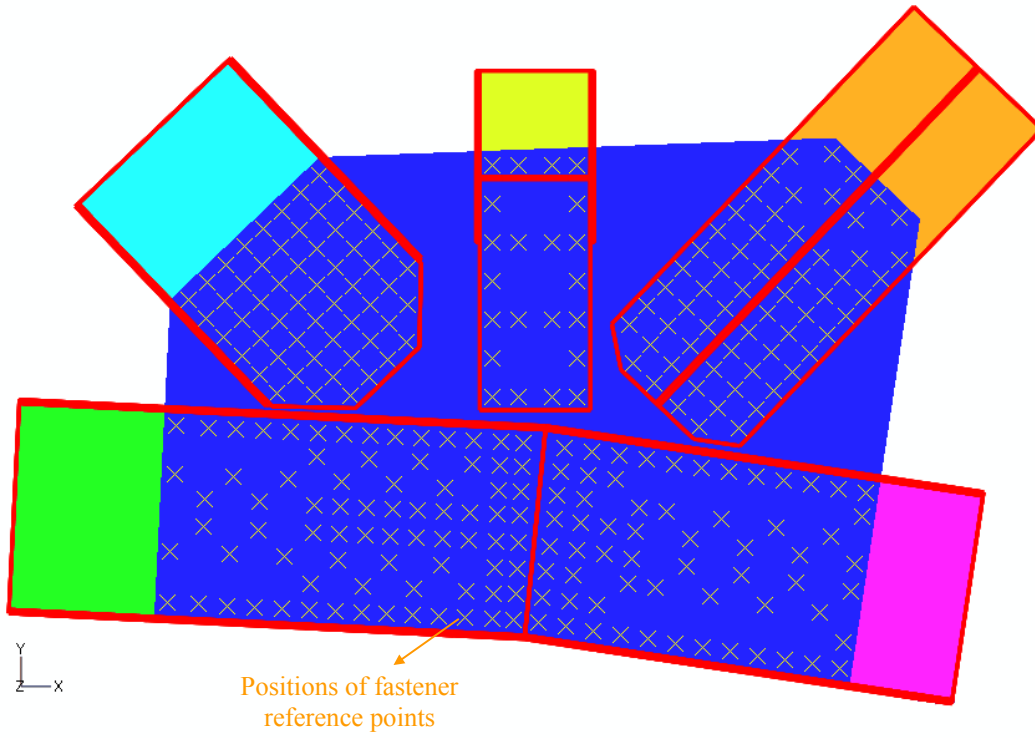
Figure 8.13: Reference points of fasteners related to the vertical faces at the L11W joint
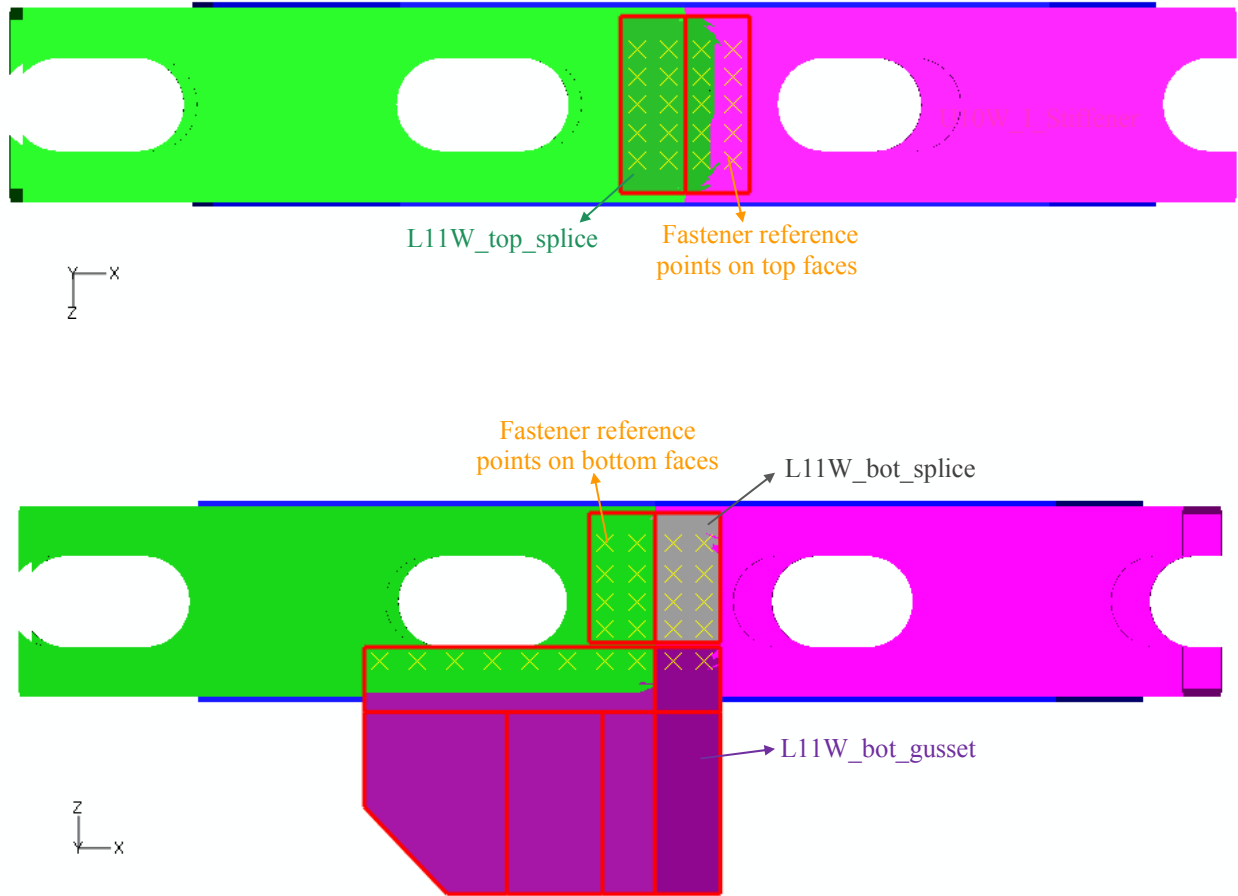
Figure 8.14: Reference points of fasteners related to the top and bottom faces at the L11W joint
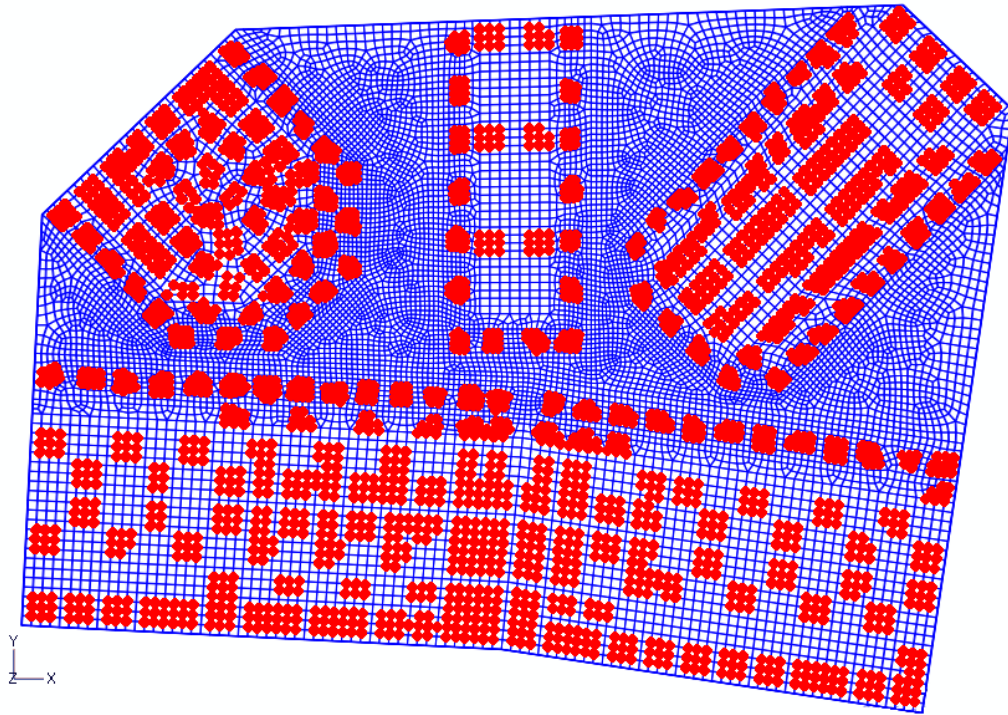
Figure 8.15: Fastened nodes of the west gusset plate at the L11W joint; 0.5 inch mesh
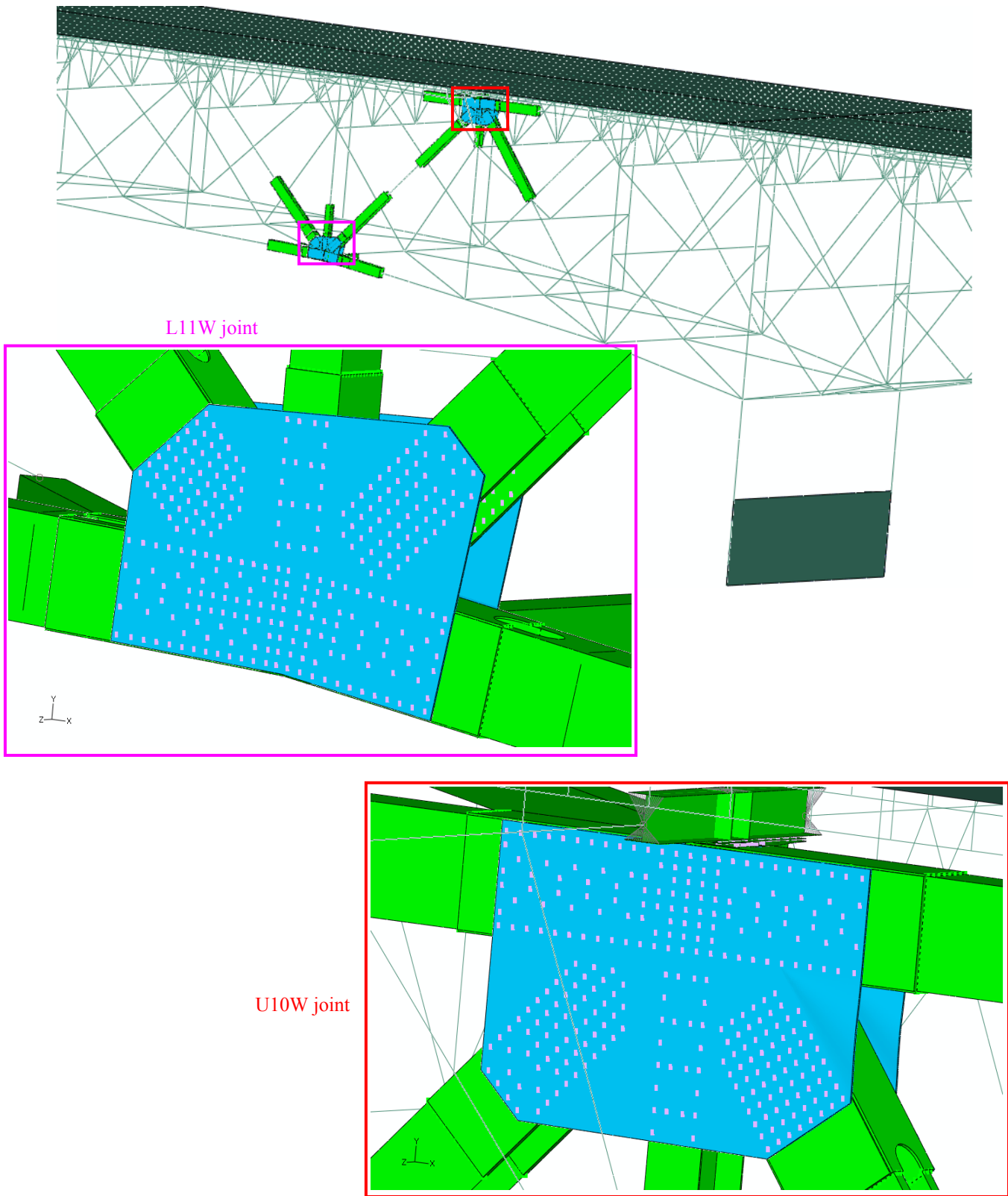
Figure 8.16: The L11W and U10W joints embedded in the FHWA structural element bridge model
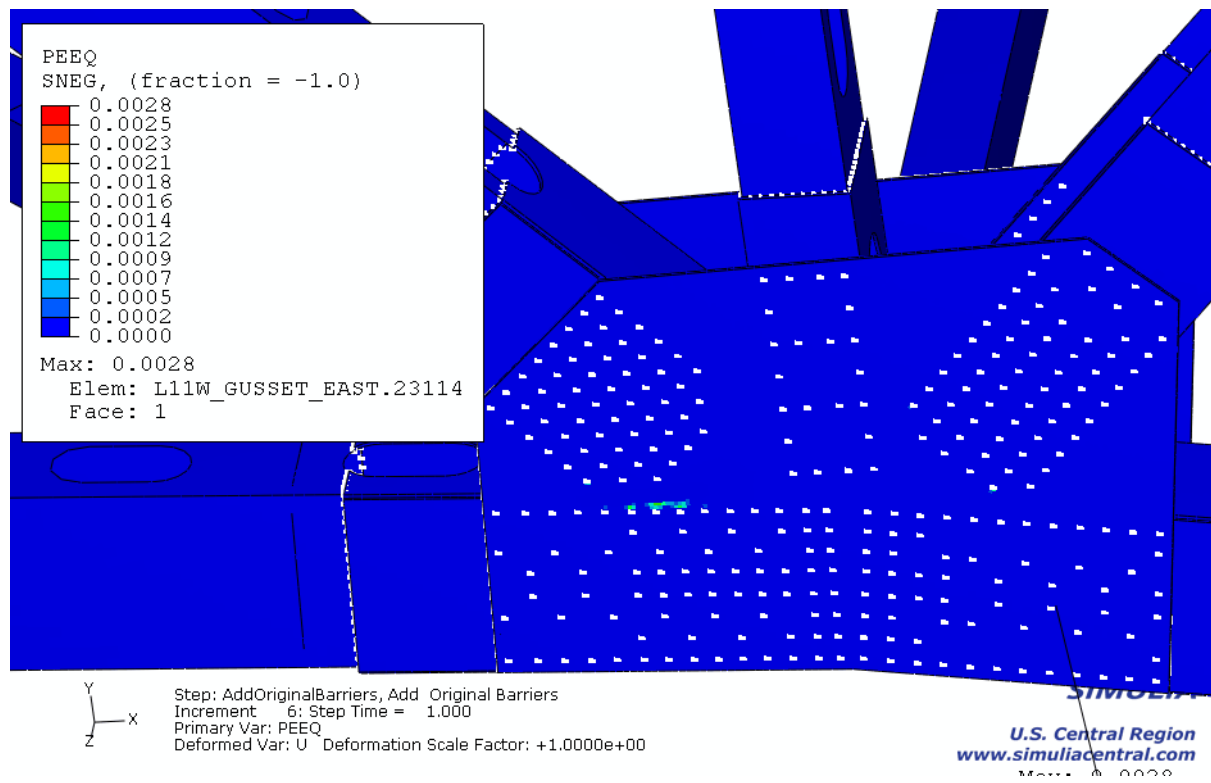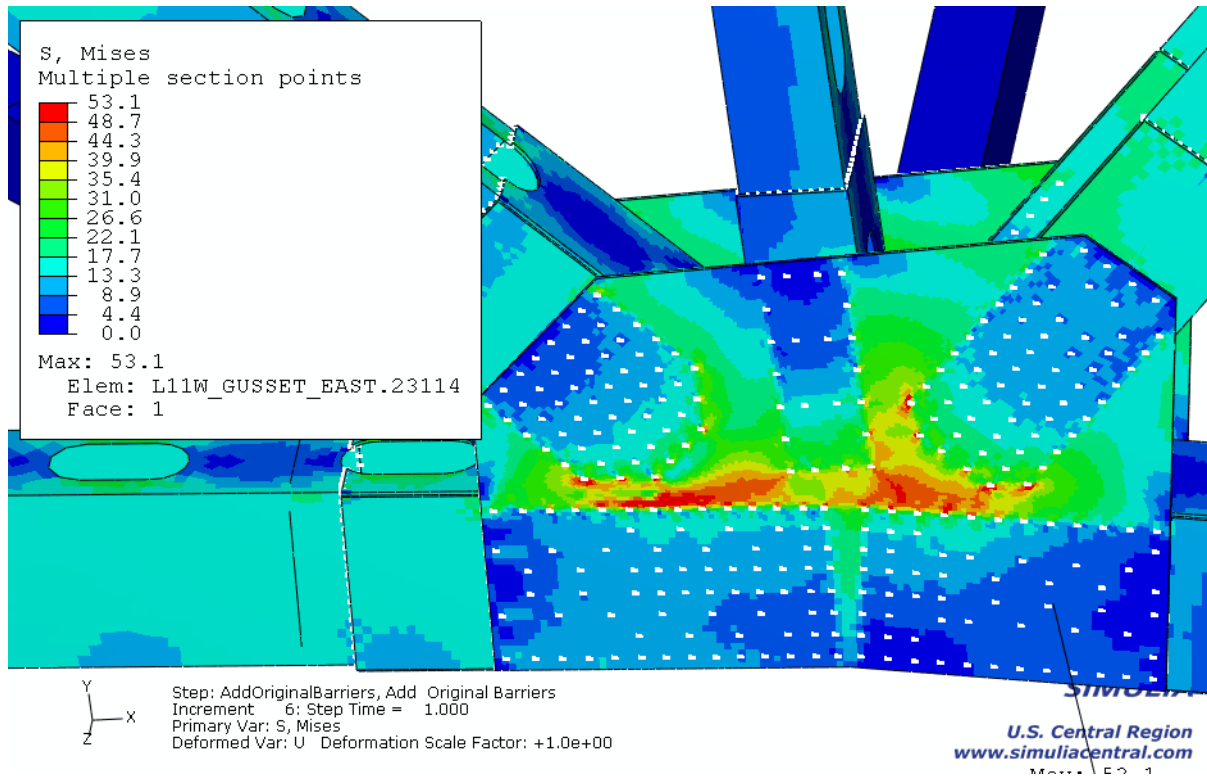
Figure 8.17: Von Mises stress and equivalent plastic strain (PEEQ) distribution at the L11W joint under the bridge design weight when only L11W joint with flat gusset plates were embedded
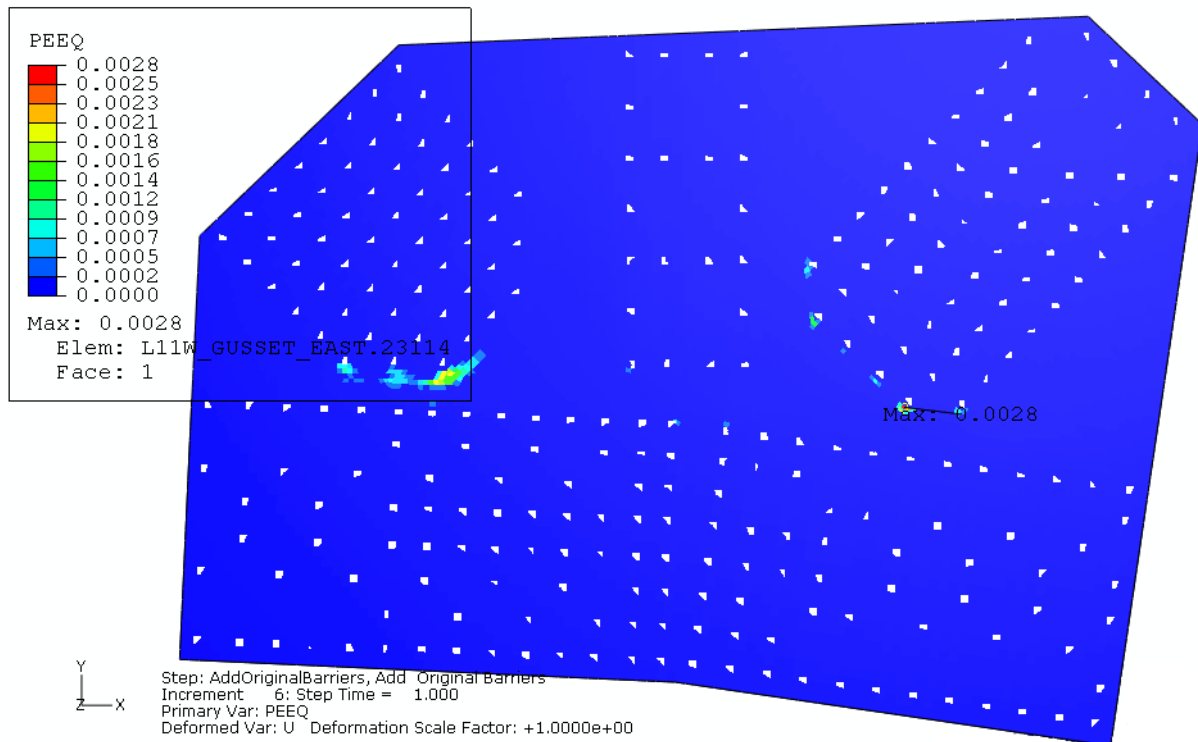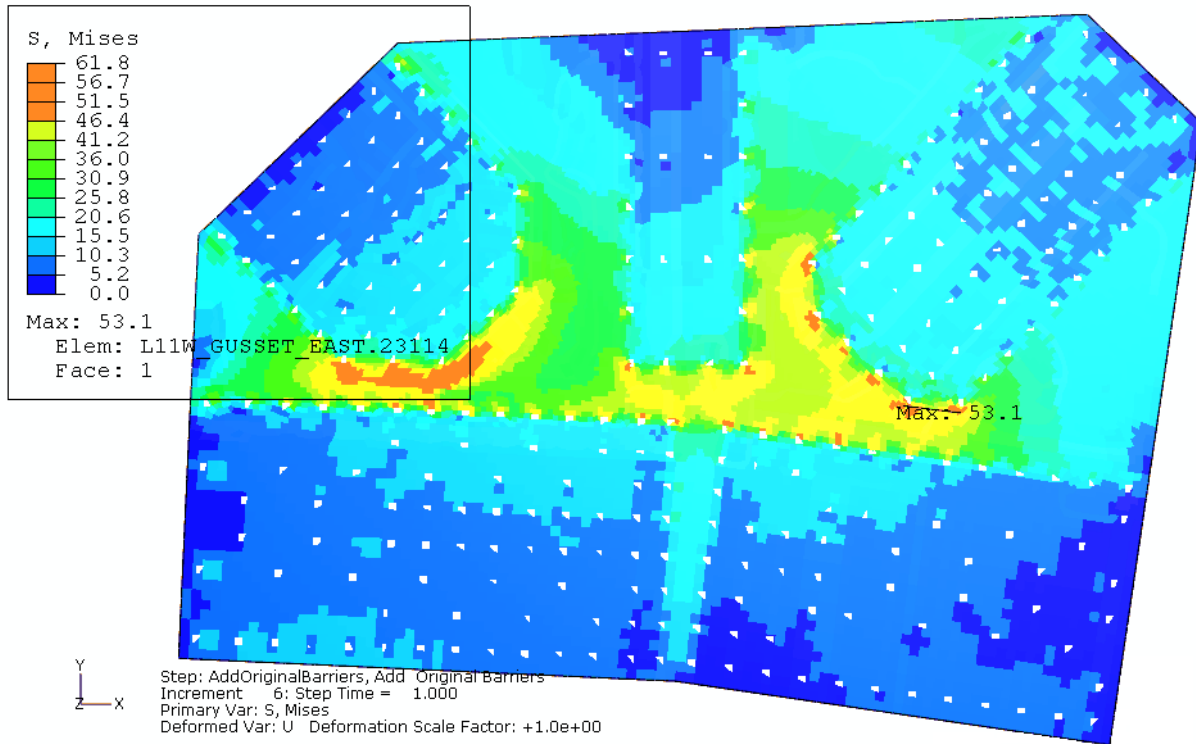
Figure 8.18: Von Mises stress and equivalent plastic strain (PEEQ) distribution in flat east gusset plate at L11W joint under the bridge design weight when only L11W joint was embedded
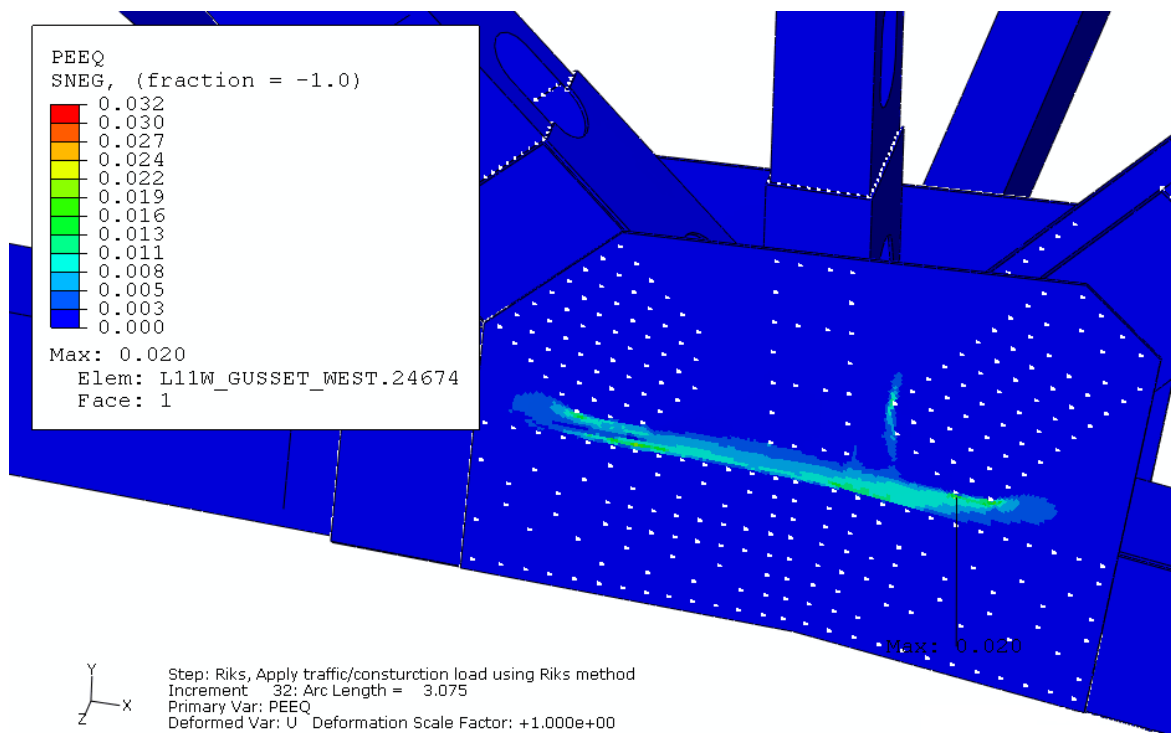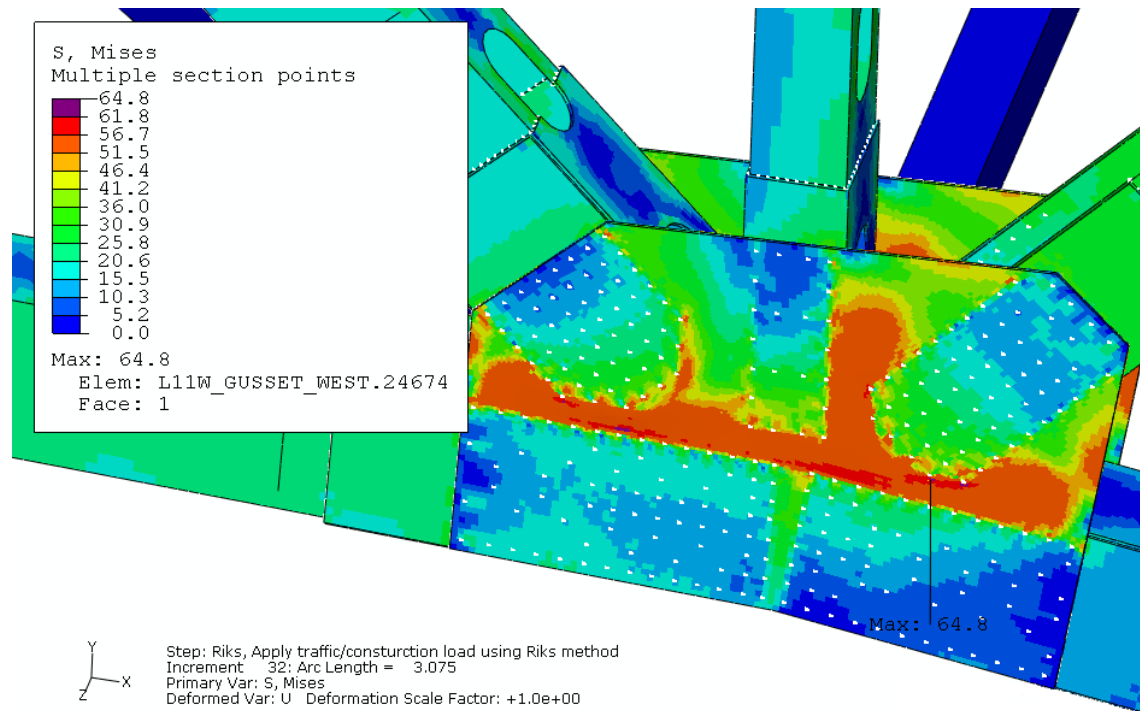
Riks step: Total load of 26,470 kips

Figure 8.19: Von Mises stress and equivalent plastic strain (PEEQ) distribution at L11W joint in Riks step at termination without instability when only L11W joint was embedded; Flat gusset plates were included
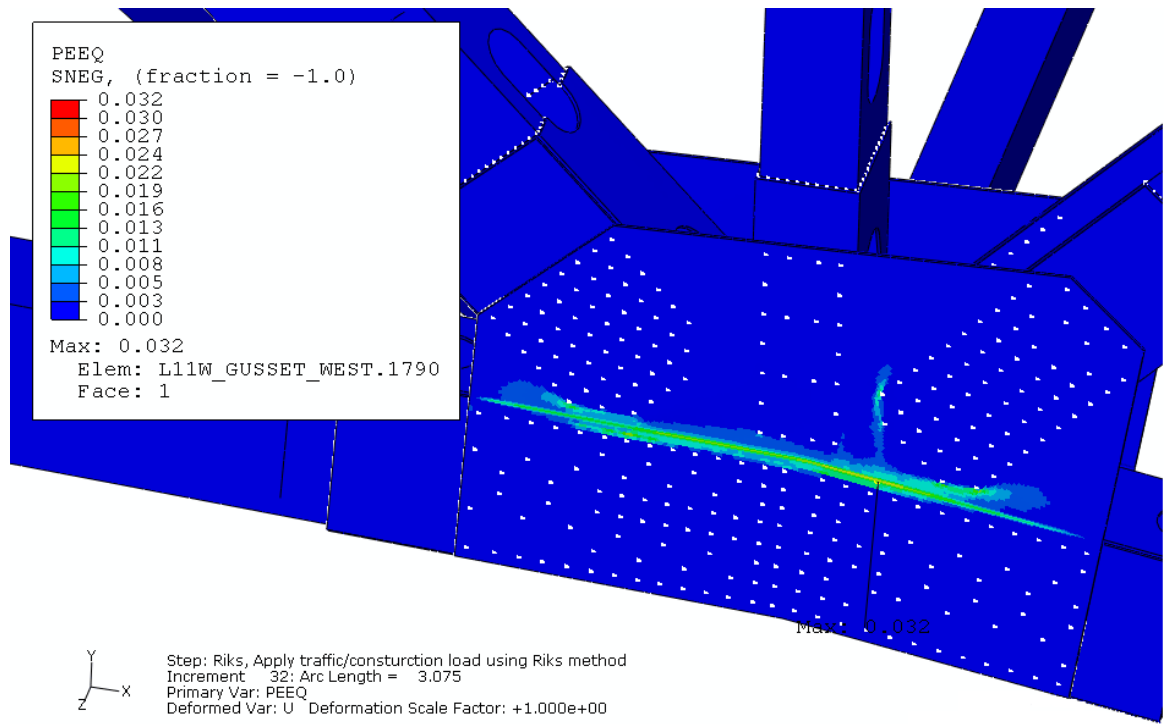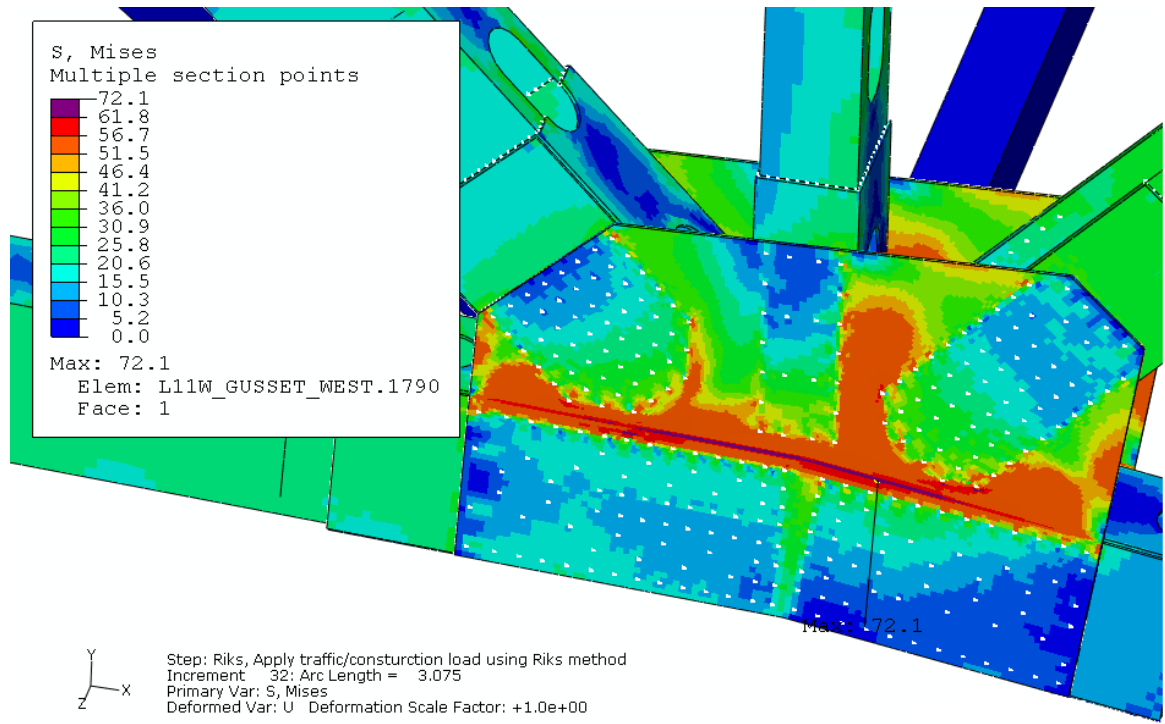
Riks step: Total load of 26,465 kips

Figure 8.20: Von Mises stress and equivalent plastic strain (PEEQ) distribution at L11W joint in Riks step at termination without instability when only L11W joint was embedded; Corroded gusset plates were included
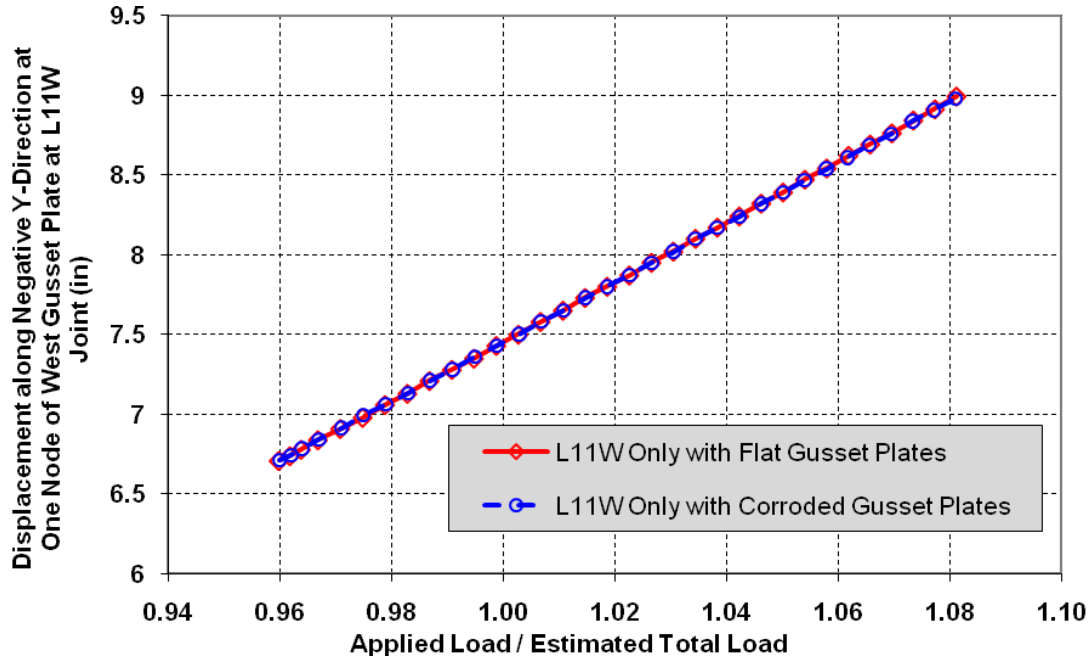
Figure 8.21: Comparison of normalized total load versus displacement in Riks loading step when only L11W local model was embedded between with flat and corroded gusset plates
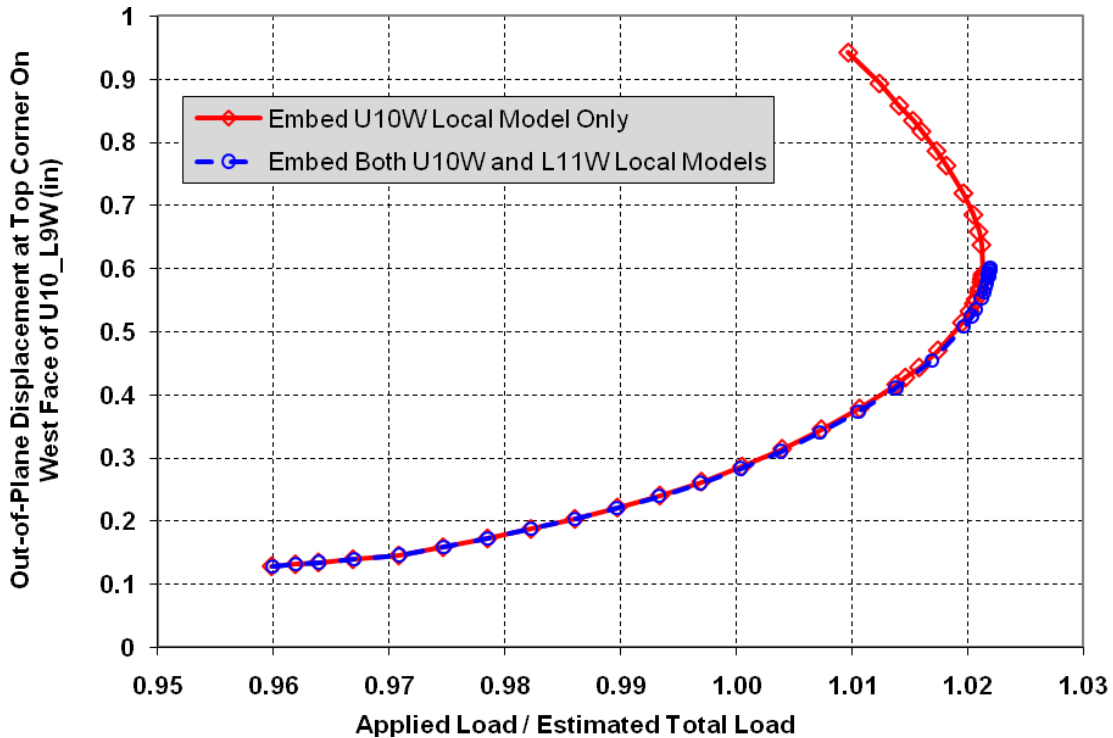
Figure 8.22: Comparison of normalized total load versus displacement in Riks loading step between embedding U10W local model only and embedding both U10W and L11W local models; Corroded gusset plates were included in the L11W local model

- 183 -
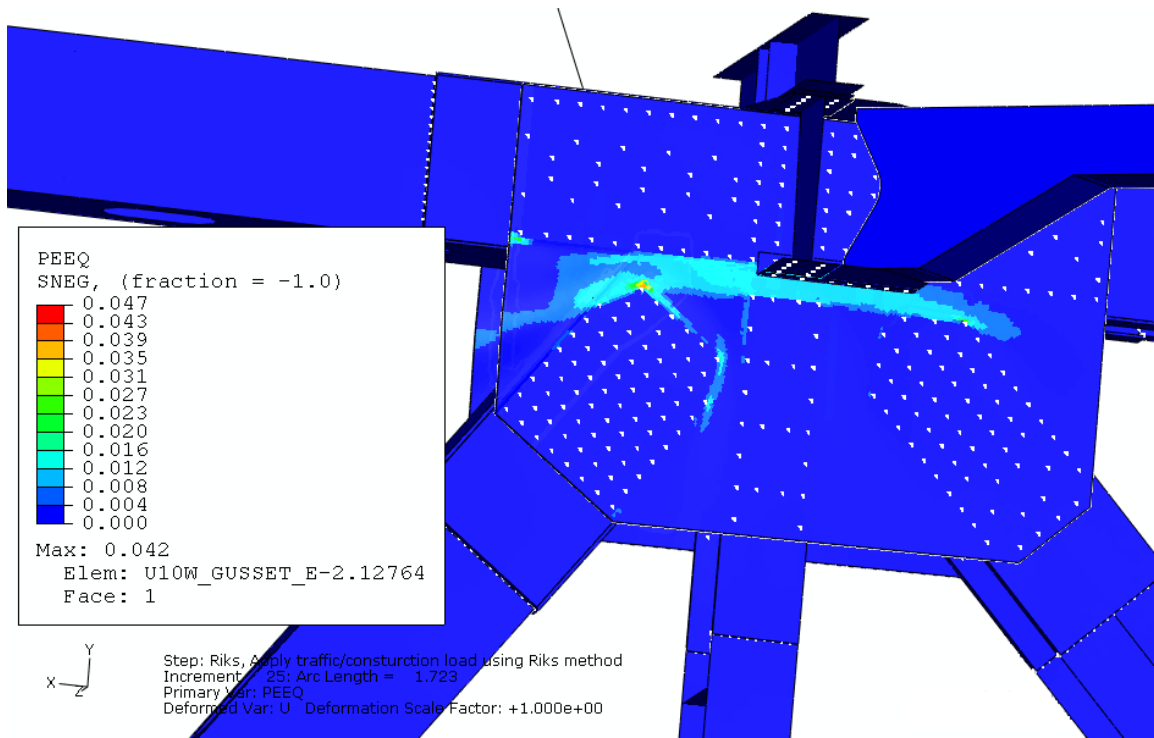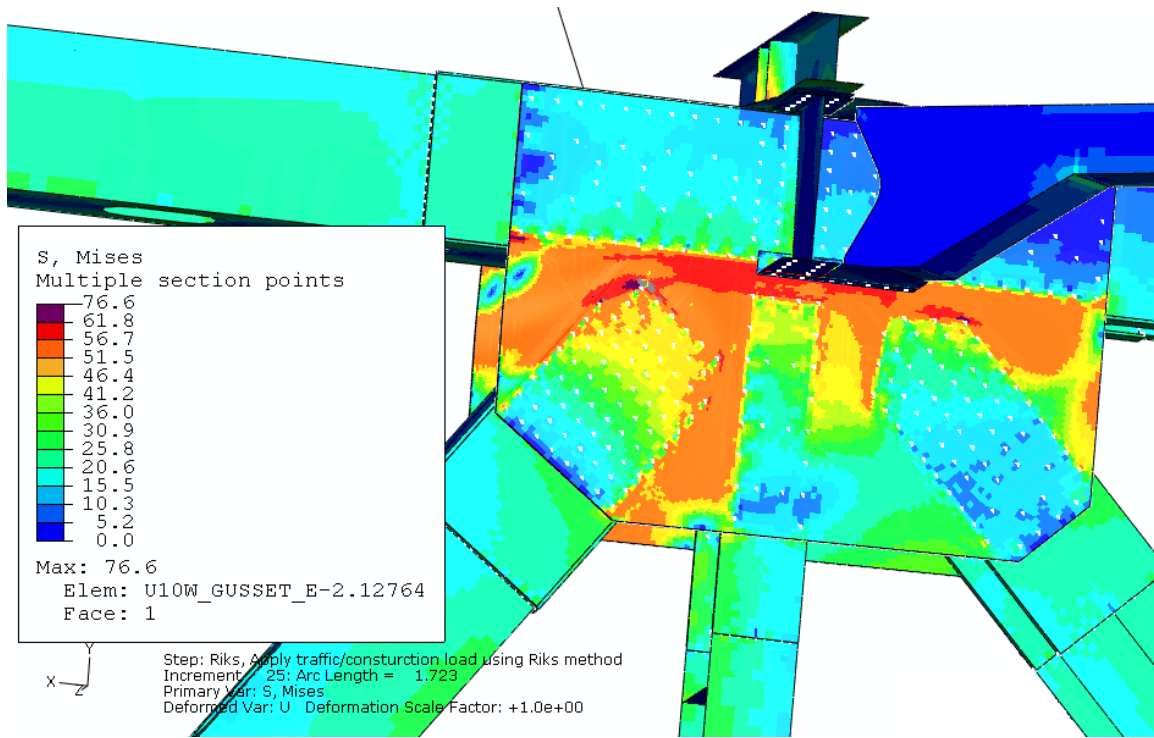
Riks step: Total load of 24,997 kips

Figure 8.23: Von Mises stress and equivalent plastic strain distribution under the load close to the predicted maximum load at instability at the U10W joint when only the U10W local model was embedded
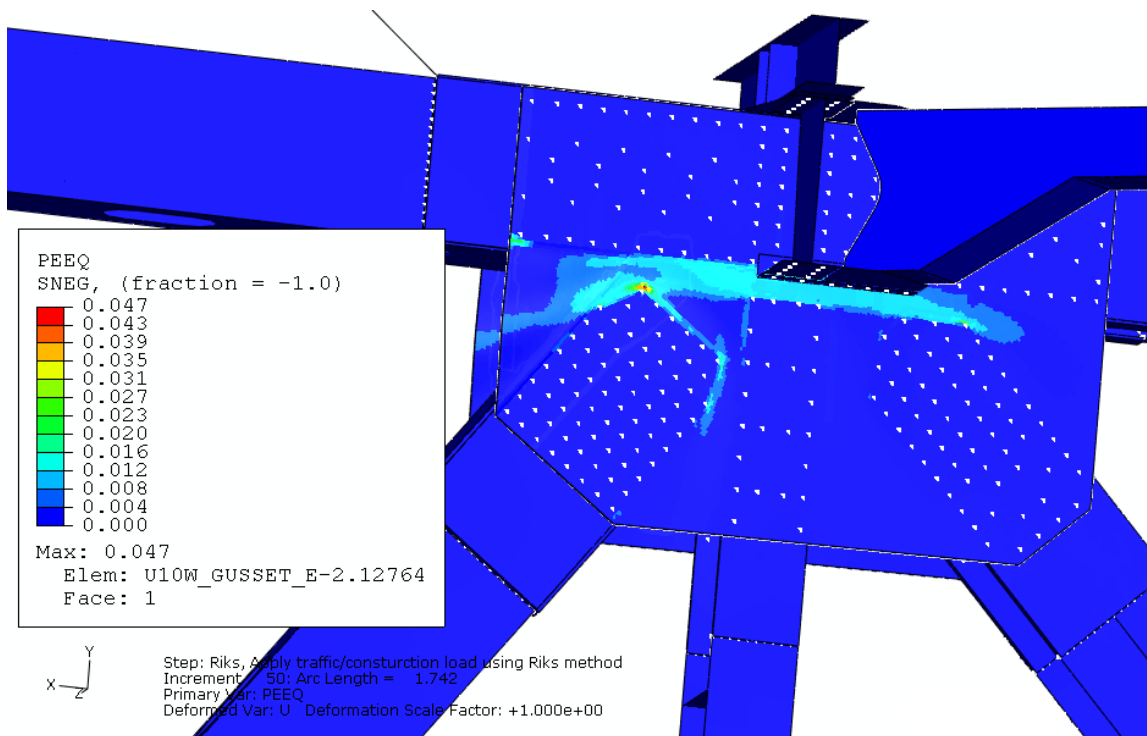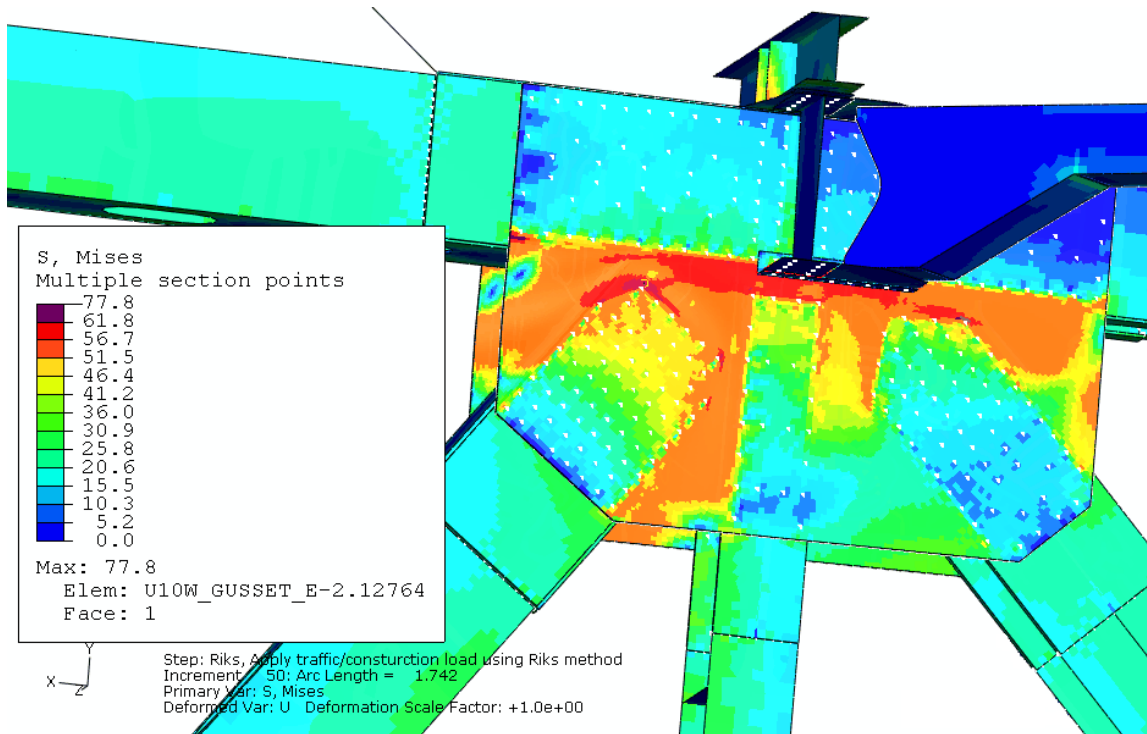
Riks step: Total load of 25,020 kips

Figure 8.24: Von Mises stress and equivalent plastic strain distribution under the load close to the predicted maximum load at instability at the U10W joint when both the U10W and L11W local models were embedded; Corroded gusset plates were included in the L11W local model
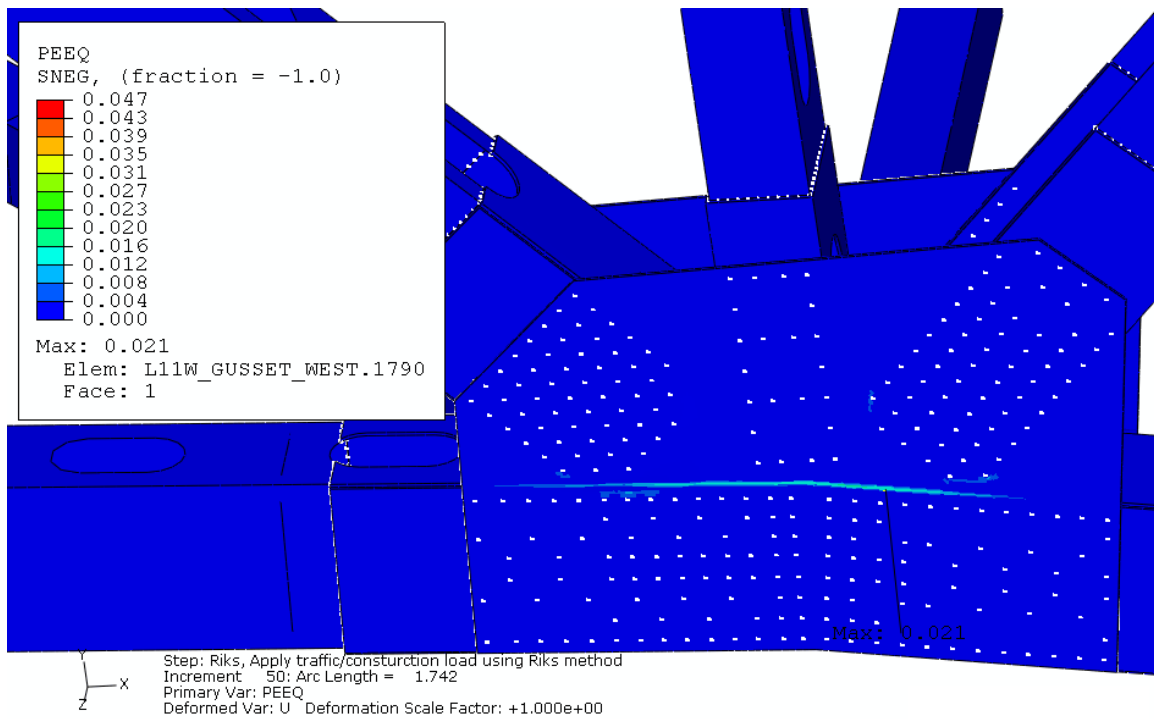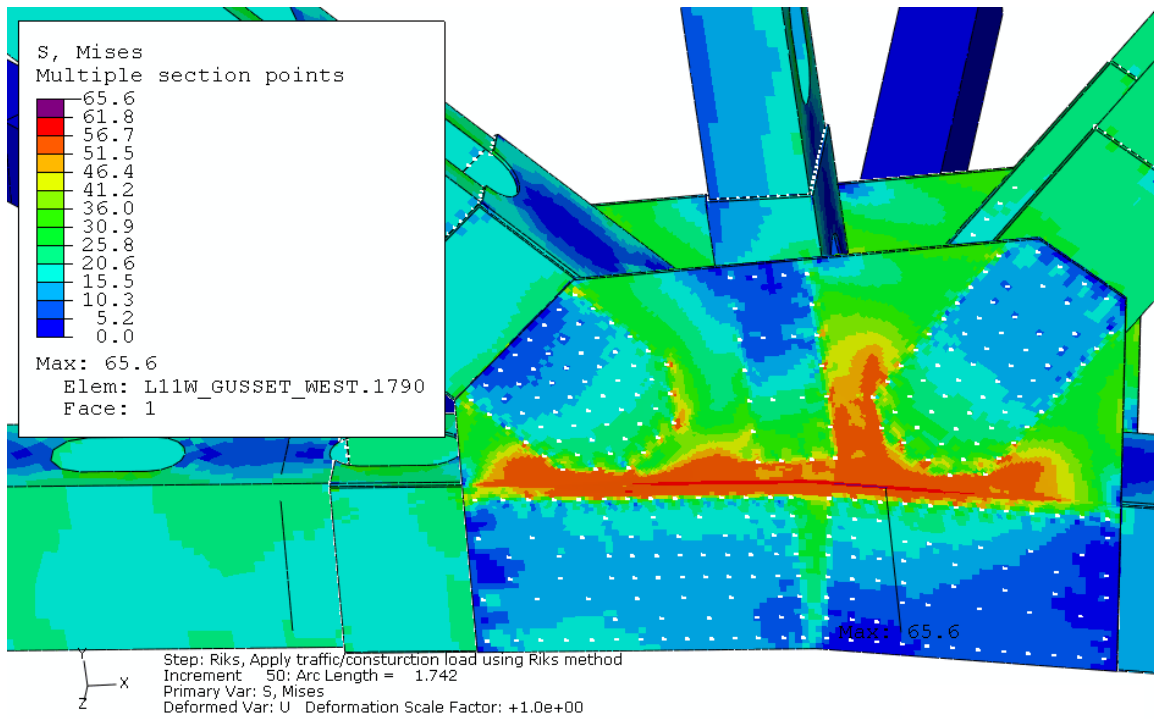
Riks step: Total load of 25,020 kips

Figure 8.25: Von Mises stress and equivalent plastic strain distribution under the load close to the predicted maximum load at instability at the L11W joint when both the U10W and L11W local models were embedded; Corroded gusset plates were included in the L11W local model

9   Effect of Gusset Plate Thickness in the U10W 3D Local Model

9.1   Description of the U10W 3D Local Model

Analyses were performed to investigate the effect of the gusset plate thickness in the U10W 3D local model. Two mixed models were investigated, as listed in Table 9.1. The first mixed model embedded a U10W 3D local model with bowed gusset plates of 0.5 inches thick. The second mixed model embedded a U10W 3D local model with bowed gusset plates of 1.0 inch thick. The two mixed models were exactly the same except for the thickness of the gusset plates. Both mixed models used load condition B. The U10W local model in the first mixed model was the same as that described in Section 7, except that no contact was defined in the current model.

Table 9.1
Mixed Models Used to Investigate Gusset Plate Thickness Effects

Local Model Embedded	Typical Mesh Size (inch)	Loading Condition	FHWA Structural Element Bridge Model
U10W joint with bowed gusset plates of 0.5 inches thick	0.5	B	6
U10W joint with bowed gusset plates of 1.0 inch thick	0.5	B	6

Figure 9.1 shows the two 1.0 inch thick gusset plates and the solid representation of the five main truss members at the U10W joint. Initial bowing was included in the gusset plates, and an initial maximum out-of-plane deflection of 0.5 inches was used. The gusset plates were represented with the C3D8R elements and used total stiffness hourglass control [11]. An in-plane mesh size of 0.5 inches was typical in the highly stressed region of the gusset plates. Four elements were used through the thickness of the gusset plates, resulting in 53,588 elements in each plate. The gusset plates were represented with 50 ksi steel.

9.2   Comparison between the 0.5 Inch and 1.0 Inch Thick Gusset Plates

The Riks method was used to investigate the possibility of an instability by proportionally increasing the live load while other loads were maintained at the estimated values. As stated previously, for load condition B, the estimated total live load was 984 kip, including the traffic load of 379 kip, the construction load of 576 kip, and the corresponding approach span force increment of 29 kip. When the U10W local model with the 0.5 inch thick bowed gusset plates and without contact defined was embedded into the sixth FHWA structural element bridge model, the Riks analysis predicted a maximum live load at instability of 1,143 kip, or 1.16 times the estimated value. The lack of a contact condition between the gusset plates and the truss members allowed for more deformation of the gusset plate, significantly reducing the load necessary to trigger the instability compared to the models that included contact. The total load along the vertical direction was predicted to be 24,641 kip, or 1.006 times the estimated total load. The out-of-plane displacement at top corner on the west face of the diagonal truss member U10_L9W was predicted to be 0.470 inches under the predicted maximum total load. Significant plastic deformation occurred in the two gusset plates when subjected to a load near the predicted

maximum, as shown in Figure 9.2. The maximum von Mises stress was predicted to be 81 ksi in the vicinity of the upper corner rivet in the east gusset plate. The maximum equivalent plastic strain was predicted to be 5.8%.

When the U10W local model with the 1.0 inch thick bowed gusset plates was embedded into the sixth FHWA structural element bridge model, the live load in the Riks step increased monotonically until the analysis was terminated. The analysis was terminated because the live load exceeded 3 times the estimated value, or 3,004 kip, which was 3.05 times the estimated value. This termination of the Riks analysis did not represent the occurrence of divergence or instability. The total load at the termination point was 26,504 kip, or 1.083 times the estimated value. The out-of-plane displacement at top corner on the west face of the diagonal truss member U10_L9W was predicted to be 0.144 inches under the load at termination point. Figure 9.3 shows the von Mises stress and equivalent plastic strain distributions at the U10W joint under the load at the termination point. The maximum stress was predicted to be 58 ksi on the edge of the top corner fastener connecting the west gusset and the diagonal truss member U10_L9W, which corresponded to an equivalent plastic strain of 1.0%.

Figure 9.4 compares the load displacement curves in the Riks step between the two mixed models. The blue curve in the figure was from the model with 0.5 inch thick gusset plates and the red curve was from the model with 1.0 inch thick gusset plates. This figure demonstrates that the bowed 1-inch thick 50 ksi gusset plates were predicted to support loads well above the predicted maximum load at instability for the 0.5-inch thick gusset plates.

Figure 9.5 a) and b) compares the von Mises stress distribution at the U10W joint under the estimated total load between the 0.5-inch thick gusset plates and the 1-inch thick gusset plates. Figure 9.5 a) shows the von Mises stress distribution for the 0.5-inch thick gusset plates, and Figure 9.5 b) shows the von Mises stress distribution for the 1-inch thick gusset plates. The figures indicate that a significant region of the 0.5-inch gusset plates yielded under the estimated load, but only a few spots in the 1-inch gusset plates yielded. The maximum von Mises stress for the 0.5-inch thick gusset plates was predicted to be 74 ksi, and for the 1-inch thick gusset plates it was 54 ksi. With the 0.5-inch thick gusset plates the axial force and bending moment at the lower end of the diagonal truss member U10_L9W were predicted to be -2,409 kip and 1,085 kip-inch under the estimated total load. With the 1-inch thick gusset plates the axial force and bending moment were predicted to be -2,428 kip and 768 kip-inch under the estimated total load. The axial forces in the two models were predicted to be similar to each other. However, the bending moment for the 0.5-inch thick gusset plates was predicted to be significantly larger than that for the 1-inch thick gusset plates, with a 40 percent difference. Table 9.2 summarizes the loads, the maximum von Mises stress, and the axial force and bending moment under the estimated total load for the two models.

Table 9.2
Effect of Gusset Plate Thickness on Load, Force, Stress, and Displacement

	0.5 Inch Thick Gusset	1.0 Inch Thick Gusset
Predicted Maximum Total Load at Instability (kip)	24,641	>26,504
Traffic/Construction/Approach Span Force Increment (Live Load) at Predicted Maximum Load at Instability (kip)	1,143	>3,004
Maximum von Mises Stress under Estimated Total Load (ksi)	74	54
Out-of-Plane Displacement at Top Corner on West Face of Truss Member U10_L9W at Instability or at Termination Point (inch)	0.470	0.144
Axial Force at Lower End of U10_L9W under Estimated Total Load (kip)	-2,409	-2,428
Bending Moment at Lower End of U10_L9W under Estimated Total Load (kip-inch)	1,085	768

9.3   Summary: Gusset Plate Thickness Investigation

Two mixed models, one with 0.5-inch thick bowed gusset plates and the other with 1-inch thick bowed gusset plates at the U10W joint, were analyzed to investigate the effect of gusset plate thickness. Load condition B was used, where the traffic load, construction load, and the approach span force increment proportionally increased in the Riks step. No contact was defined in either model. Analyses showed that the bowed 1-inch thick 50 ksi gusset plates would support loads well above the predicted maximum load at instability of the 0.5-inch thick gusset plate models. When the 0.5-inch thick gusset plates were used, the Riks method predicted a maximum total load of 24,641 kip. When the 1-inch thick gusset plates were used, no instability was predicted before the Riks analysis was terminated because the total load had exceeded the maximum value specified, 26,504 kip.
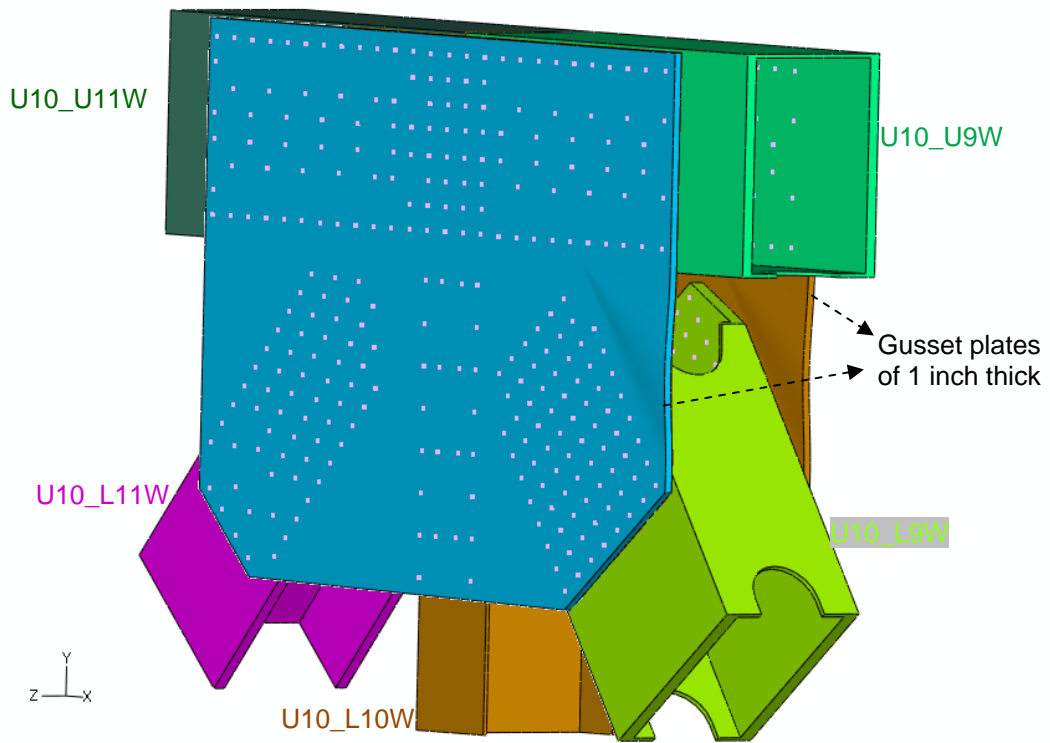
Figure 9.1: Gusset plates of 1.0 inch thick and solid representation of the main truss members at the U10W joint
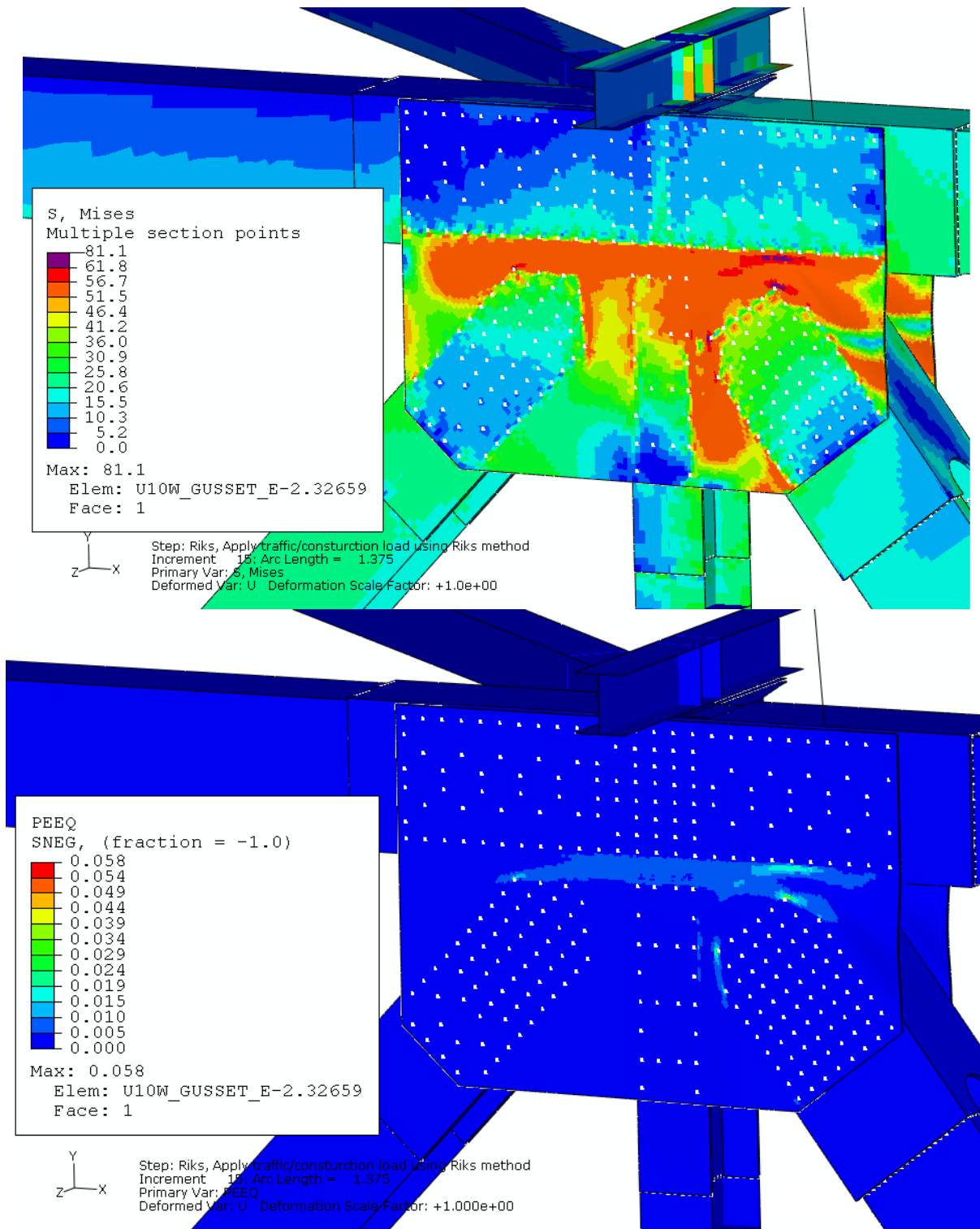
Riks step: Total load of 24,615 kips

Figure 9.2: Von Mises stress and equivalent plastic strain (PEEQ) distribution at the U10W joint
in Riks step at instability when the gusset plates of 0.5 inch thick were used
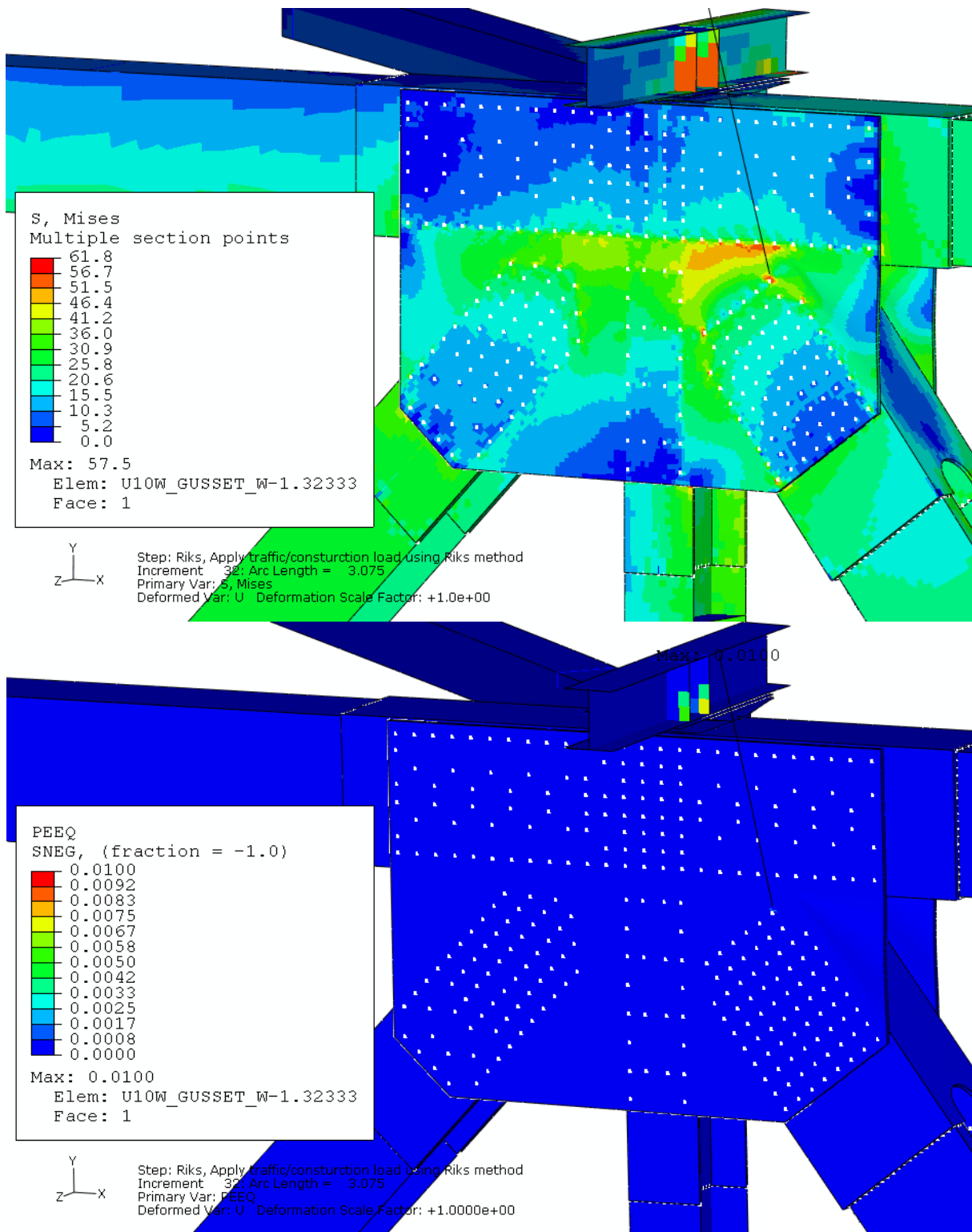
Riks step: Total load of 26,504 kips

Figure 9.3: Von Mises stress and equivalent plastic strain (PEEQ) distribution at the U10W joint in Riks step at termination without instability when the gusset plates of 1.0 inch thick were used
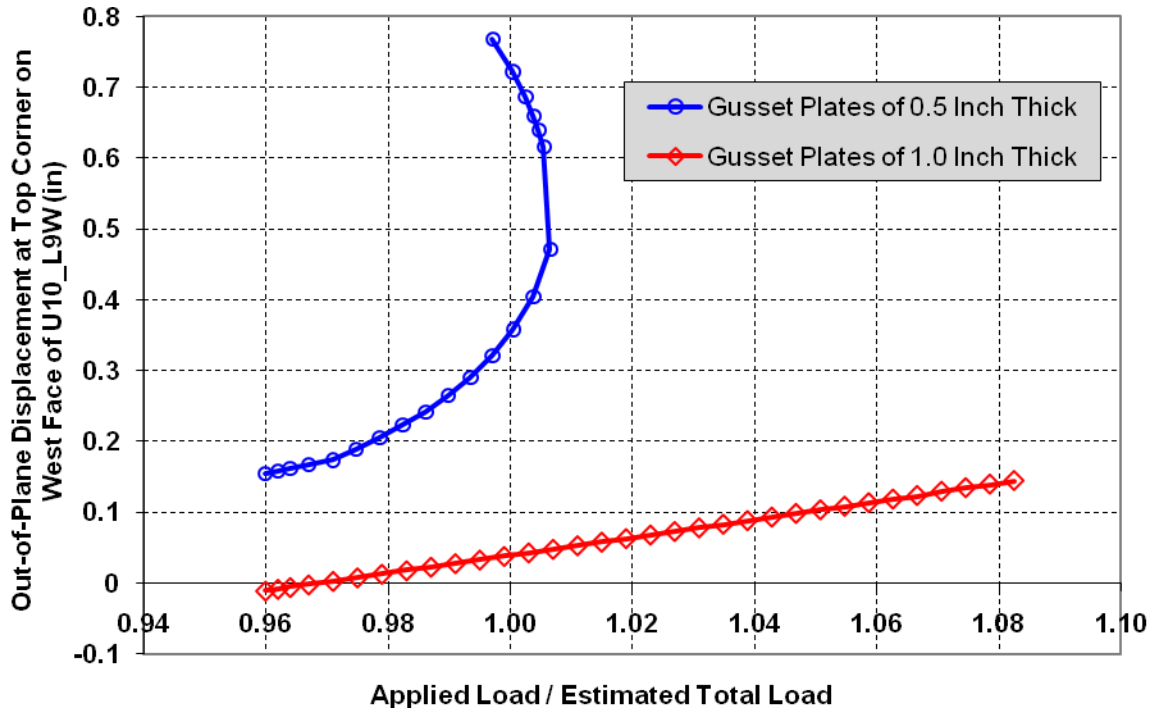
Figure 9.4: Comparison of normalized total load versus displacement in Riks loading step when embedding U10W local model between with bowed gusset plates of 0.5 inches thick and 1.0 inch thick
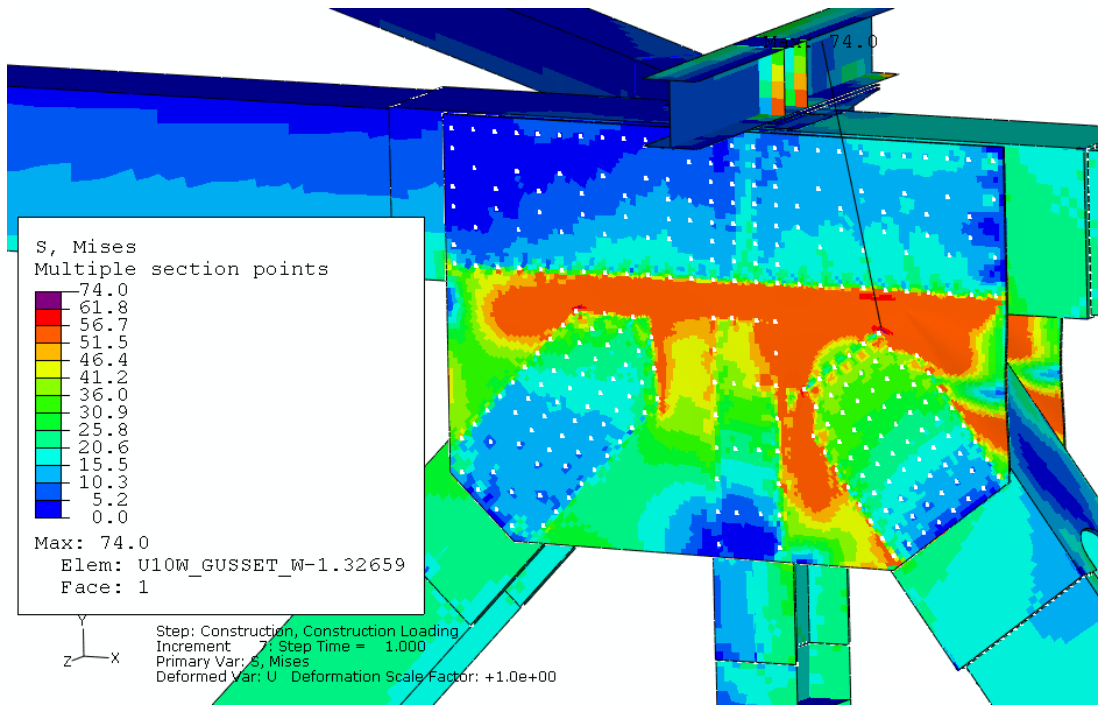
a) Gusset plates of 0.5 inches thick
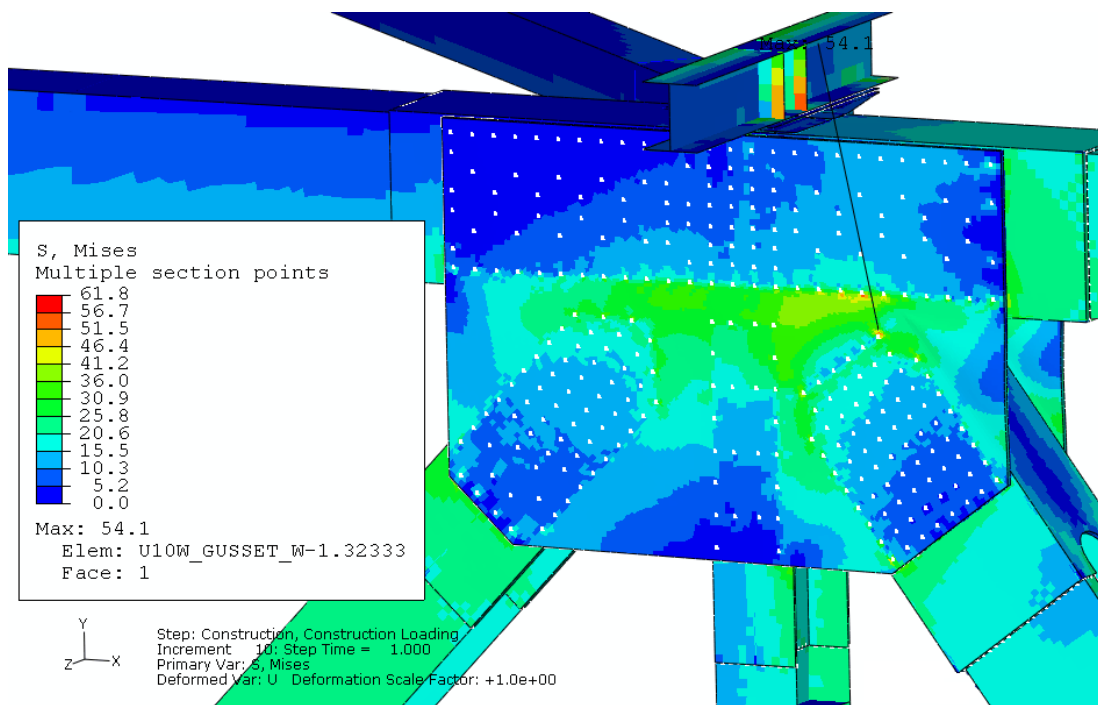
b) Gusset plates of 1.0 inch thick

Figure 9.5: Comparison of von Mises stress distribution at the U10W joint under the estimated total load between 0.5-inch gusset plates and 1-inch gusset plates

10 Effect of Initial Bowing Geometry in the U10W 3D Local Model

10.1 Description of the U10W 3D Local Models

Analyses were conducted to investigate the effect of the initial bowing geometry of the gusset plates in the U10W 3D local model. Two mixed models were investigated, as listed in Table 10.1. The two mixed models were exactly the same except for the initial bowing geometry of the gusset plates. In both models, the bowing was input as a stress-free initial imperfection before any loads were applied. The first mixed model embedded a U10W 3D local model with the gusset plates bowing along member outer edges, as previously described in Figure 3.6. The initial maximum out-of-plane deflection was 0.5 inches. The second mixed model embedded a U10W 3D local model with the gusset plates bowing along rivet lines, as shown in Figure 8.1. One possible source for initiating the bowing of the gusset plates is forces exerted during fabrication to line up the fastener holes in the gusset plates with the corresponding holes in the truss members. These forces would show up as loads transmitted between the gusset plates and the truss members through the rivets. Under such conditions, the bowing would develop along the rivet lines at the force application points. The initial maximum out-of-plane deflection was 0.45 inches. This value was smaller than the initial deflection for the bowing along member outer edges, in order to match the deflection of the two cases to the measured deflection after the loads through the 1998 modifications were made (the conditions when the photographs were taken). Both mixed models used load condition A1. The gusset plates bowing along the rivet lines had a larger region with non-zero initial out-of-plane displacement than the gusset plates bowing along truss member outer edges. The U10W local model in the first mixed model was the same as that in Section 4 of this report, except that four elements were used through the thickness of the gusset plates in the current model. Each gusset plate in the current model contained 76,865 elements.

Table 10.1
Mixed Models Used to Investigate Gusset Plate Bowing

Local Model Embedded	Typical Mesh Size (inch)	Loading Condition	FHWA Structural Element Bridge Model
U10W with gusset plates bowing along member outer edges	0.5	A1	6
U10W with gusset plates bowing along rivet lines	0.5	A1	6

10.2 Comparison between the Gusset Plates Bowing Along Member Outer Edges and Bowing Along Rivet Lines

10.2.1 Deformed Shape of Bowed Gusset Plates Prior to Applying the Construction Load

With the gusset plates at the U10W joint bowing along member outer edges and before the construction load was applied, the deformed maximum out-of-plane deflection was 0.665 inches in the east gusset plate, and 0.669 inches in the west gusset plate. With the gusset plates bowing along rivet lines and before the construction load was applied, the deformed maximum out-of-

plane deflection was 0.665 inches in the east gusset plate, and 0.618 inches in the west gusset plate. The model with the gusset plates bowing along the member outer edges had larger maximum out-of-plane deflection in the west gusset plate, but the maximum out-of-plane deflections in the east gusset plates were comparable between the two models. However, note that the model with the gusset plates bowing along the member outer edges had larger initial maximum out-of-plane deflection.

10.2.2 Load and Stress Predicted by the Riks Method

The Riks method was used to predict the maximum construction load at the onset of instability by proportionally increasing the construction load while other loads were maintained at the estimated values.

When the gusset plates bowed along the member outer edges, the Riks analysis predicted a maximum construction load of 1,057 kip, or 1.83 times the estimated value. The total load along the vertical direction was predicted to be 24,961 kip, or 1.020 times the estimated total load. The out-of-plane displacement at the top corner of the diagonal truss member U10_L9W was predicted to be 0.549 inches under the maximum total load. Under a load of 24,954 kip, just before the maximum predicted load occurred, the axial force and bending moment at the lower end of the diagonal truss member U10_L9W were predicted to be -2,611 kip and 1,653 kip-inch. Significant plastic deformation occurred in the two gusset plates, as shown in Figure 10.1. The maximum von Mises stress was predicted to be 75 ksi in the vicinity of the upper corner rivet in the east gusset plate. The maximum equivalent plastic strain was predicted to be 3.9%.

When the gusset plates bowed along the rivet lines, the Riks analysis diverged at a construction load of 983 kip, or 1.70 times the estimated value. The total load along the vertical direction was predicted to be 24,887 kip, or 1.017 times the estimated total load. The out-of-plane displacement at the top corner of the diagonal truss member U10_L9W was predicted to be 0.556 inches at the divergence point. The axial force and bending moment at the lower end of the diagonal truss member U10_L9W were predicted to be -2,581 kip and 1,669 kip-inch. Significant plastic deformation occurred in the two gusset plates, as shown in Figure 10.2. The maximum von Mises stress was predicted to be 76 ksi in the vicinity of the upper corner rivet in the east gusset plate. The maximum equivalent plastic strain was predicted to be 4.2%.

Figure 10.3 compares the load displacement curves in the Riks step between the two mixed models. The red curve in the figure was from the model with the gusset plates bowing along the member outer edges, and the blue curve was from the model with the gusset plates bowing along the rivet lines. The data suggest that the load at divergence for the model with initial bowing between rivet lines was close to the load necessary to trigger the geometric instability. The figure shows that the predicted total maximum load at instability with the gusset plates bowing along the rivet lines was 0.3% lower than the total maximum load at instability predicted for the gusset plates bowing along the member outer edges. Table 10.2 summarizes the loads, the maximum von Mises stress, and the axial force and bending moment at or near the maximum predicted load at instability of the two models.

Table 10.2
Effect of Initial Bowing Geometry on Results of Interest

Initial Bowing Geometry of Gusset Plates	Bowing Along Member Outer Edges	Bowing Along Rivet Lines
Predicted Maximum Total Load at Instability (kip)	24,961	24,887
Construction Load at Predicted Maximum Load at Instability (kip)	1,057	983
Maximum von Mises Stress (ksi)	75	76
Out-of-Plane Displacement at Top Corner of Truss Member U10_L9W (inch)	0.549	0.556
Axial Force at Lower End of U10_L9W (kip)	-2,611	-2,581
Bending Moment at Lower End of U10_L9W (kip-inch)	1,653	1669

10.3 Summary: Initial Bowing Geometry Study

Two mixed models with different initial bowing geometries in the gusset plates at the U10W joint were analyzed with load condition A1. One model had initial bowing along the member outer edges, and the other model had initial bowing along the rivet lines. The analyses indicated that the predicted maximum total load at instability decreased by 0.3 percent, or 13 percent of the estimated construction load, when the gusset plates bowed along the rivet lines compared to bowing along the truss member edges.
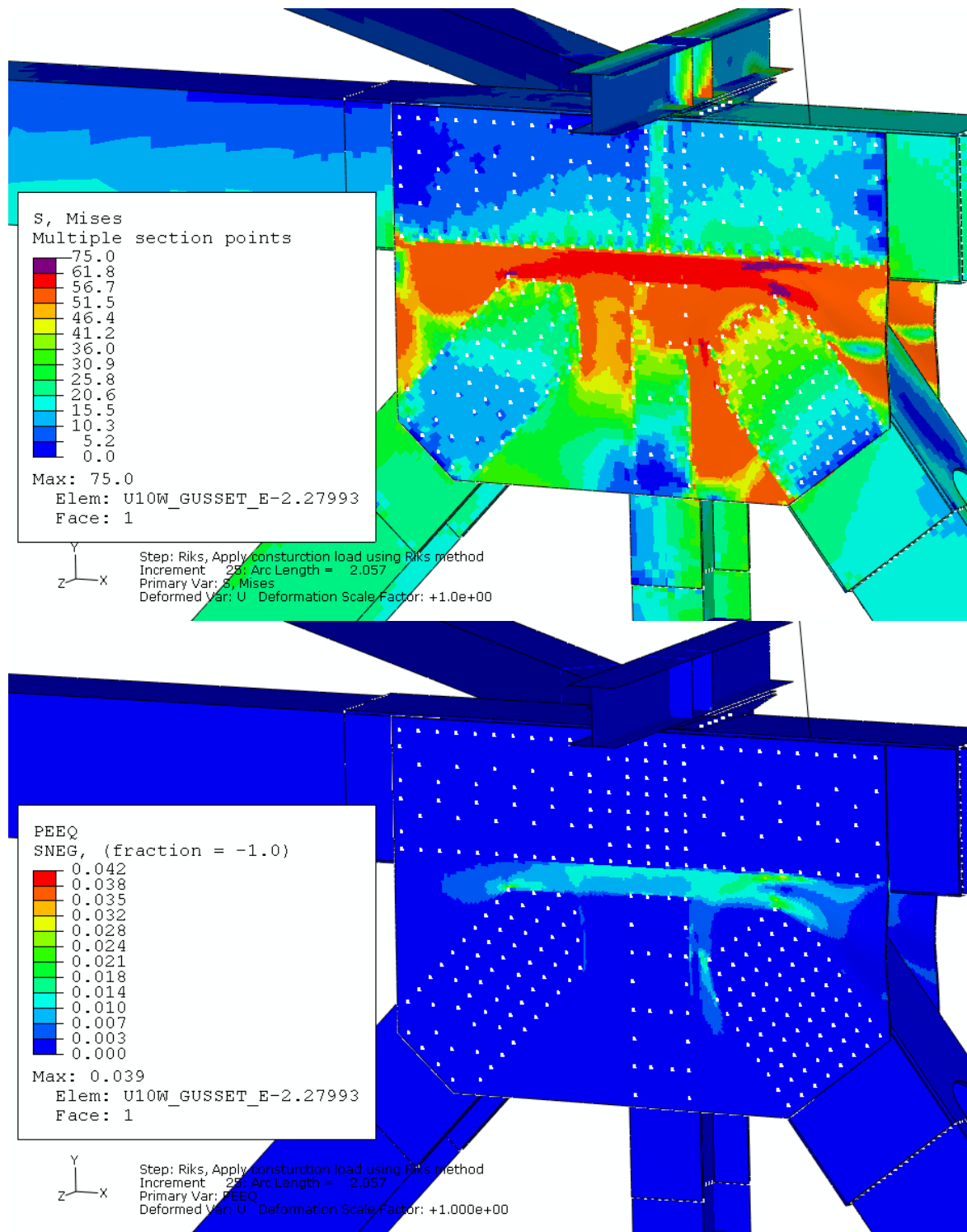
Riks step: Total load of 24,954 kips

Figure 10.1: Von Mises stress and equivalent plastic strain (PEEQ) distribution at the U10W joint in Riks step near instability when the gusset plates bowed along the member outer edges
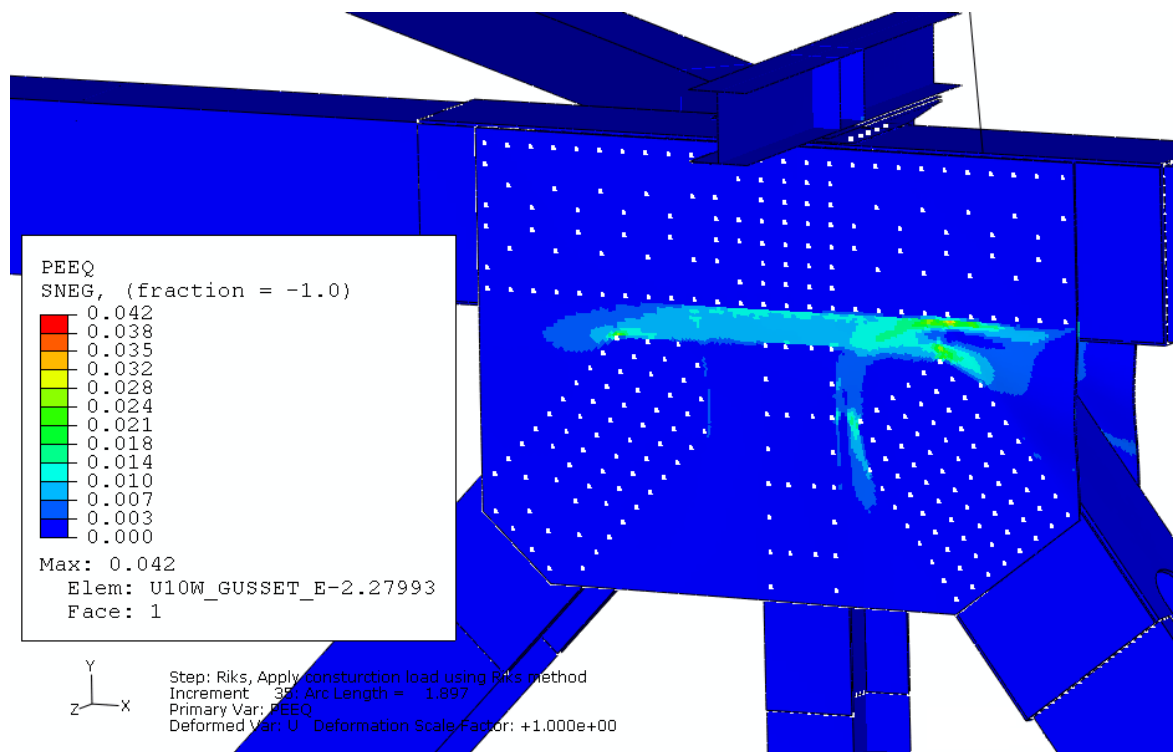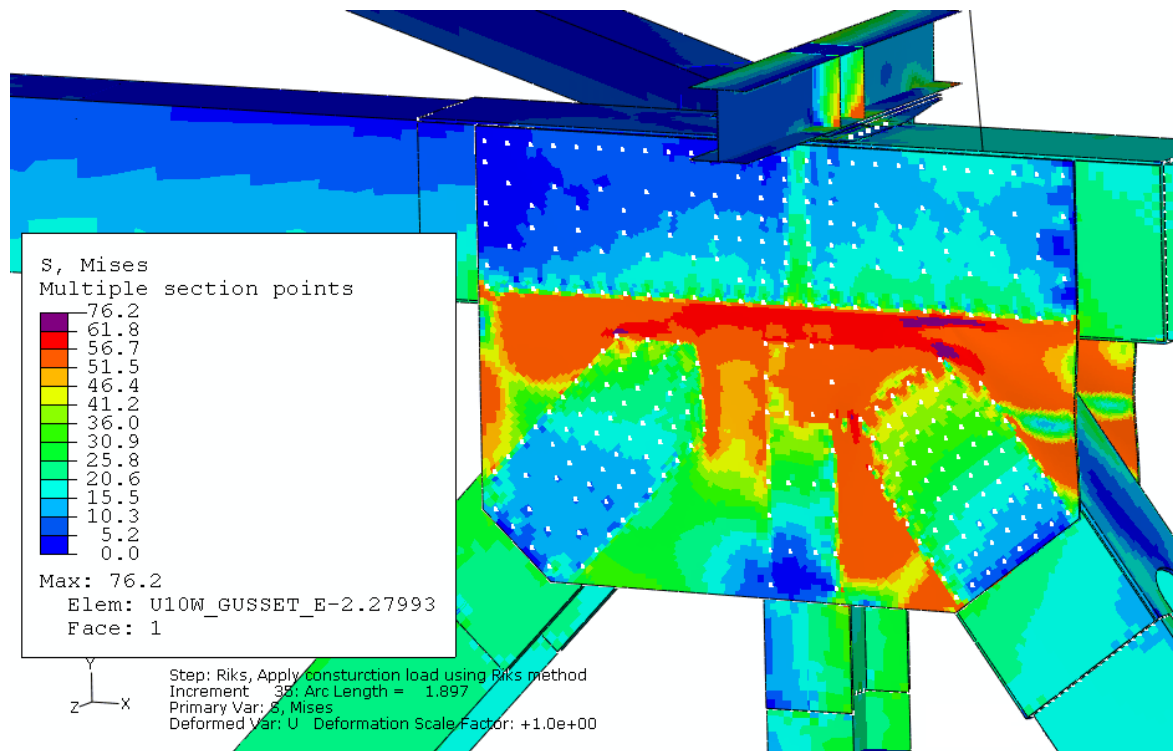
Riks step: Total load of 24,887 kips

Figure 10.2: Von Mises stress and equivalent plastic strain (PEEQ) distribution at the U10W
joint in Riks step at divergence when the gusset plates bowed along the rivet lines
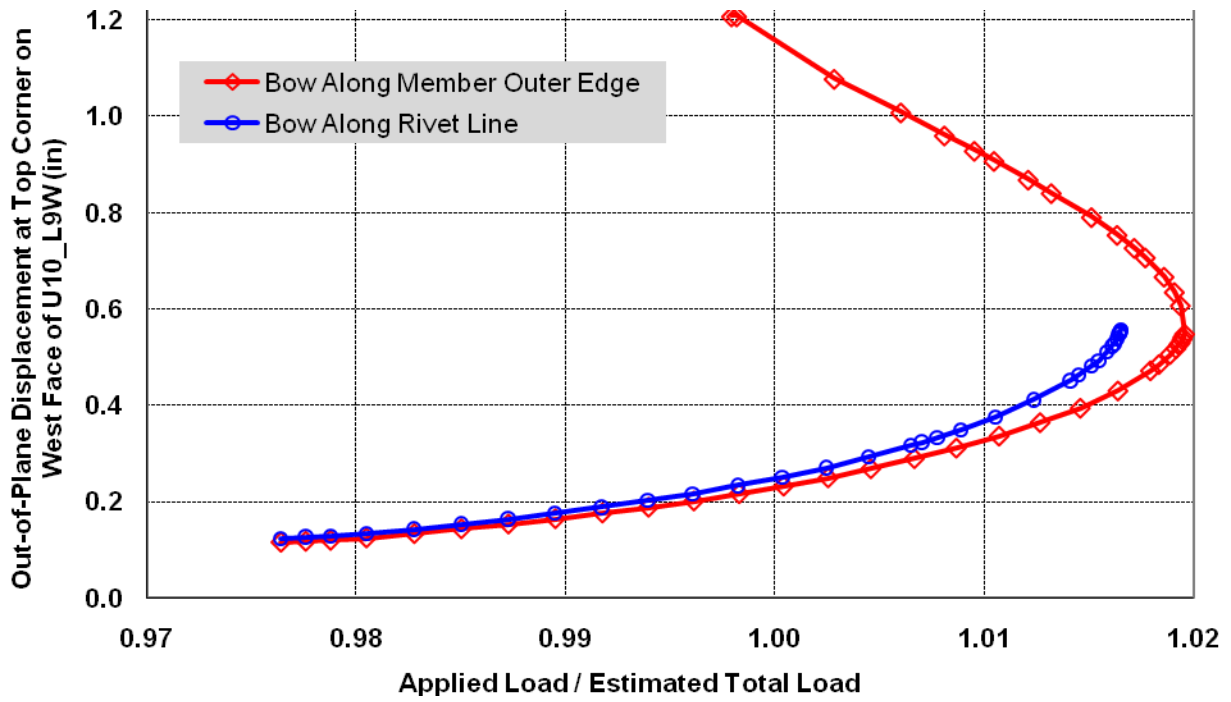
Figure 10.3: Comparison of normalized total load versus displacement in Riks loading step between when gusset plates bowed along member outer edges and along rivet lines at the U10W joint

11 Effect of a Uniform Temperature Increase Applied to the Whole Bridge

11.1 Model Description

The two mixed models listed in Table 11.1 were analyzed to investigate the effect of temperature increase on the maximum predicted load at instability. The first mixed model was described previously in Section 4 of this report, where load condition A1 was used. The second mixed model was exactly the same as the first model except that a uniform temperature increase of 20°F was applied to the entire bridge, in step 6 with the traffic load and the approach span force increment applied. The boundary conditions in the FHWA structural element models are described in Section 2. Those boundary conditions are equivalent to assuming that the roller bearings at piers 5, 6 and 8 were frozen, which would allow temperature changes to introduce stress in the structure [1]. If the bearings moved freely, changes in temperature would introduce very little additional stress. Measurements suggested that the bearings were not moving freely but were working intermittently (seasonally). Over the course of the day of the collapse, the temperature increased approximately 20 °F [5], but the zero-stress temperature of the bridge on the day of the collapse is unknown, so this investigation is somewhat qualitative. The linear coefficient of thermal expansion was 5.2 x 10^{-6} [1] for concrete and 6.5 x 10^{-6} for steel [1].

Table 11.1
Mixed Models Used to Investigate Temperature Effects

Local Model Embedded	Typical Mesh Size (inch)	Loading Condition	FHWA Structural Element Bridge Model	Uniform Temperature Increase (°F)
U10W joint with bowed gusset plates	0.5	A1	6	0
U10W joint with bowed gusset plates	0.5	A1	6	20

11.2 Comparison of Analysis Results with and without a Uniform Temperature Increase

11.2.1 Deformed Shape of Bowed Gusset Plates Prior to Applying the Construction Load

As stated previously in Section 4 of this report, when a temperature increase was not considered and before the construction load was applied, the deformed maximum out-of-plane deflection was 0.667 inches in the east gusset plate, and 0.671 inches in the west gusset plate. When a uniform temperature increase of 20°F was applied in step 6 with the traffic load and the approach span force increment, the entire U10W joint shifted to the west direction by 0.05 inches. The deformed maximum out-of-plane deflection was 0.667 inches in the east gusset plate, and 0.670 inches in the west gusset plate. Figure 11.1 shows the initial and deformed out-of-plane deflection along the vertical edge in the east gusset plate with and without the temperature increase, after correcting for the 0.05-inch shift of the entire joint to the west. The figure shows that the deformed out-of-plane deflection with the temperature increase was similar to that without the temperature increase.

11.2.2 Load and Stress Predicted by the Riks Method

The Riks method was used to predict the maximum construction load at the onset of instability by proportionally increasing the construction load while the other loads were maintained at their estimated values. When the temperature increase was applied, divergence in the Riks analysis predicted a maximum construction load of 1,144 kip, or 1.98 times the estimated value. The total load along the vertical direction was predicted to be 25,051 kip, or 1.023 times the estimated total load. The out-of-plane displacement at the top corner of the diagonal truss member U10_L9W was predicted to be 0.628 inches under the maximum total load. The axial force and bending moment at the lower end of the diagonal truss member U10_L9W were predicted to be -2,624 kip and 1,842 kip-inch. Significant plastic deformation occurred in the two gusset plates, as shown in Figure 11.2. The maximum von Mises stress was predicted to be 78 ksi in the vicinity of the upper corner rivet in the east gusset plate, as shown in Figure 11.3. The maximum equivalent plastic strain was predicted to be 4.6%.

Figure 11.4 compares the load displacement curves in the Riks step between the two mixed models. The blue curve in the figure was from the model with the temperature increase, and the red curve was from the model without the temperature increase. With the temperature increase, the maximum predicted total load increased by 0.3 percent, or increased from 24,973 kips to 25,051 kips. Table 11.2 summarizes the loads, the out-of-plane displacement, the maximum von Mises stress, the axial force, and bending moment at or near the maximum predicted load at instability of the two models. The von Mises stress distributions in the east gusset plate under maximum predicted load at instability were similar to each other, as shown in Figure 4.6 and Figure 11.3.

Table 11.2
Effect of Temperature Increase on Results of Interest

	No Temperature Increase	20°F Uniform Temperature Increase
Predicted Maximum Total Load at Instability (kip)	24,973	25,051
Construction Load at Predicted Maximum Load at Instability (kip)	1,069	1,144
Maximum von Mises Stress (ksi)	77	78
Out-of-Plane Displacement at Top Corner of Truss Member U10_L9W (inch)	0.572	0.628
Axial Force at Lower End of U10_L9W (kip)	-2,618	-2,624
Bending Moment at Lower End of U10_L9W (kip-inch)	1,738	1842

11.3 Summary: Uniform Temperature Increase Study

To investigate the effects of temperature increase, a uniform temperature of +20°F was applied to the whole bridge in the traffic loading step. With the 20°F temperature increase, the maximum

total load at instability was predicted to increase from 24,973 kips to 25,051 kips, or 0.3 percent. The von Mises stress distributions in the east gusset plate were similar to the von Mises stress distributions predicted in the model without a uniform temperature increase.
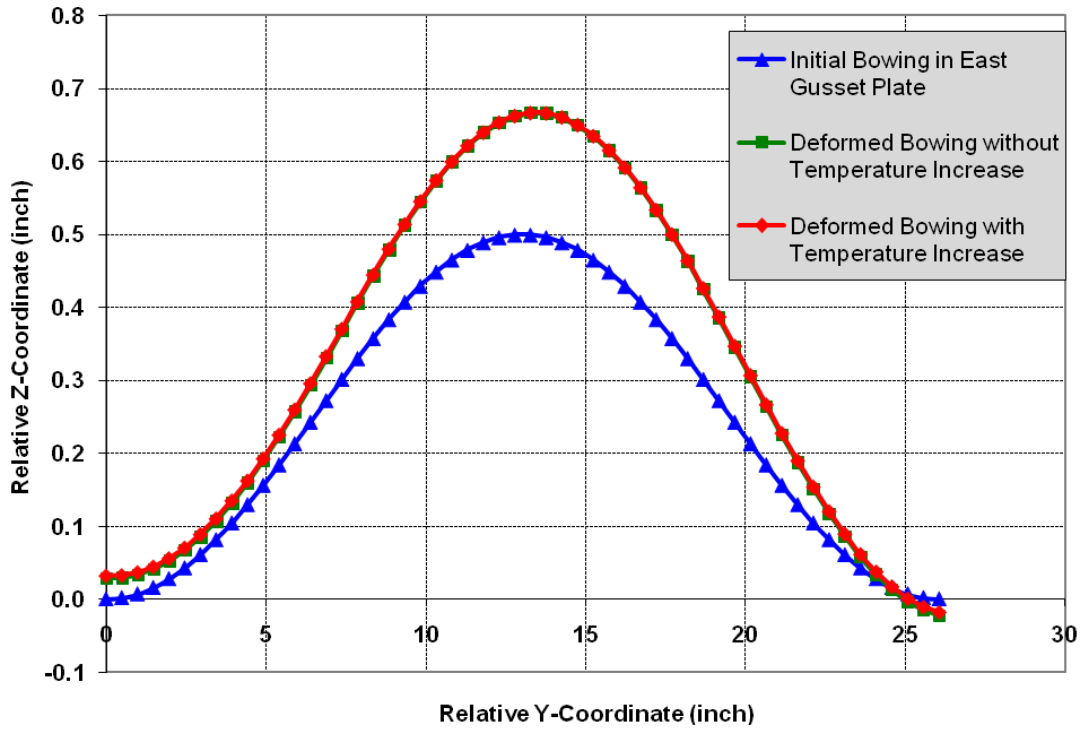
Figure 11.1: Initial and deformed out-of-plane bowing deflection along vertical edge AB of gusset plates at the U10W joint, after correcting for the 0.05-inch shift of the entire U10W joint to the west
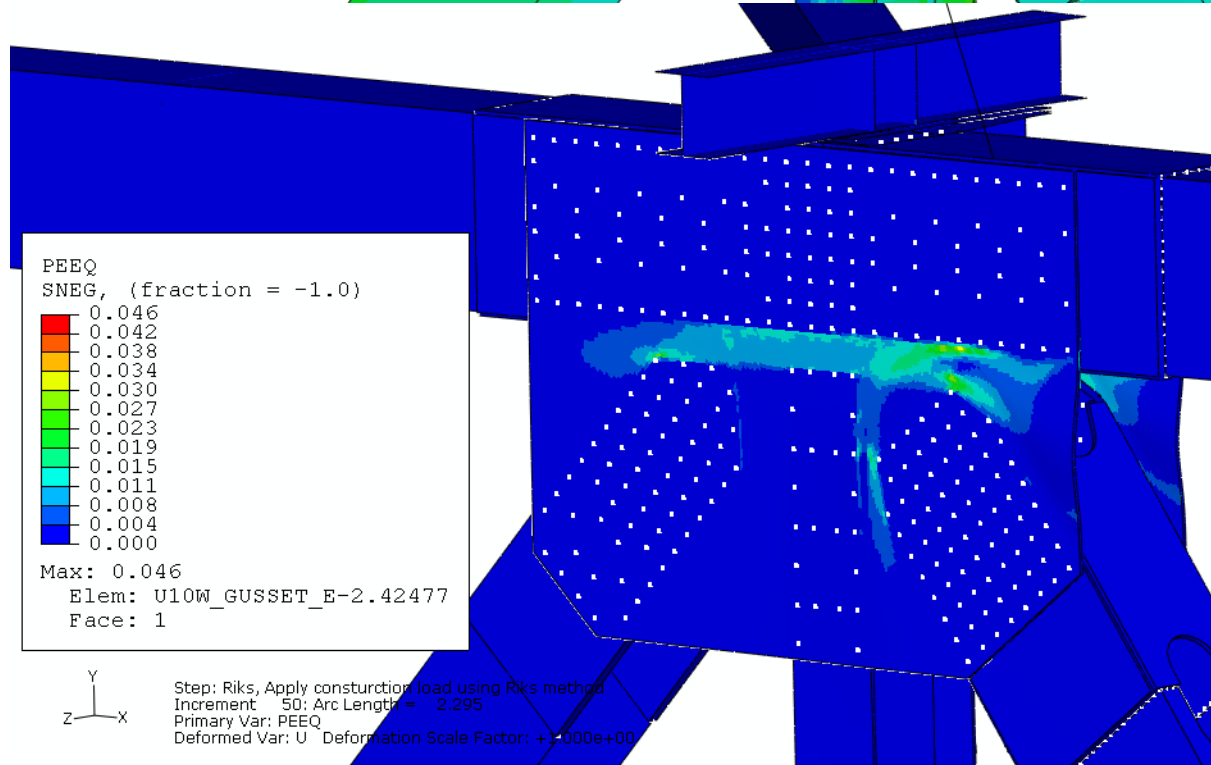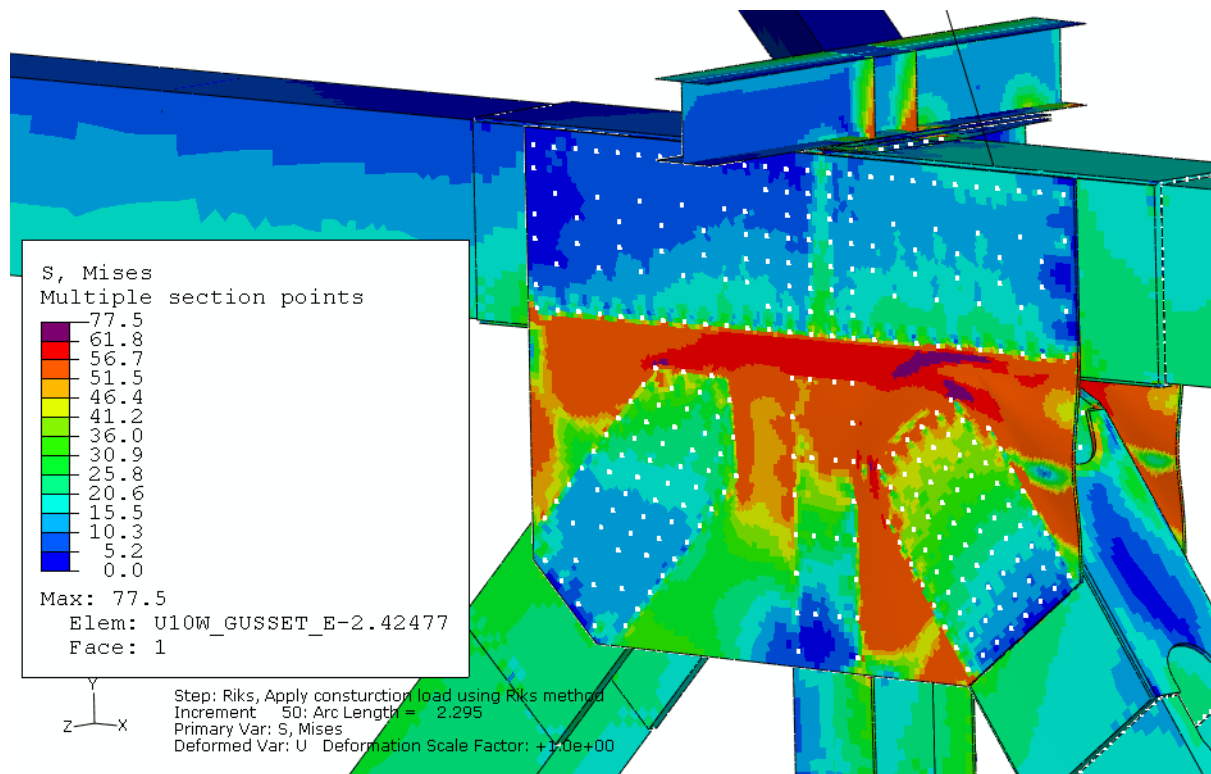
Riks step: Total load of 25,051 kips

Figure 11.2: Von Mises stress and equivalent plastic strain (PEEQ) distribution at the U10W joint in Riks step near divergence when the temperature increase was applied
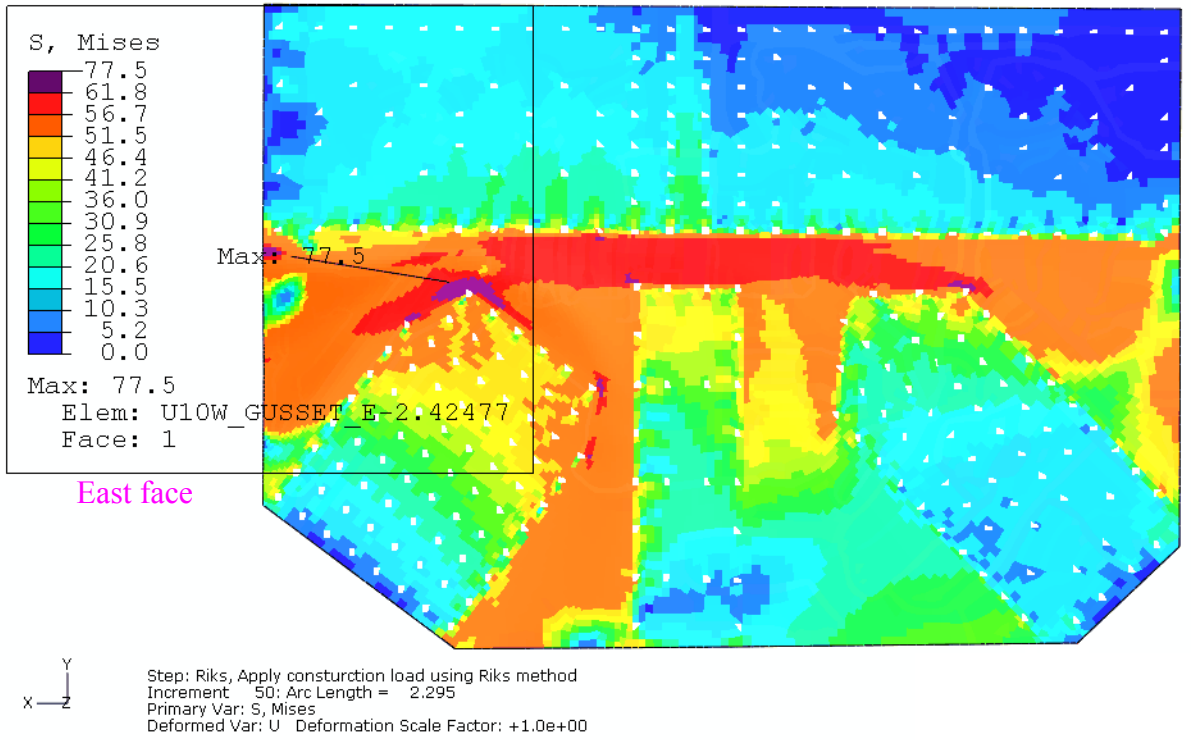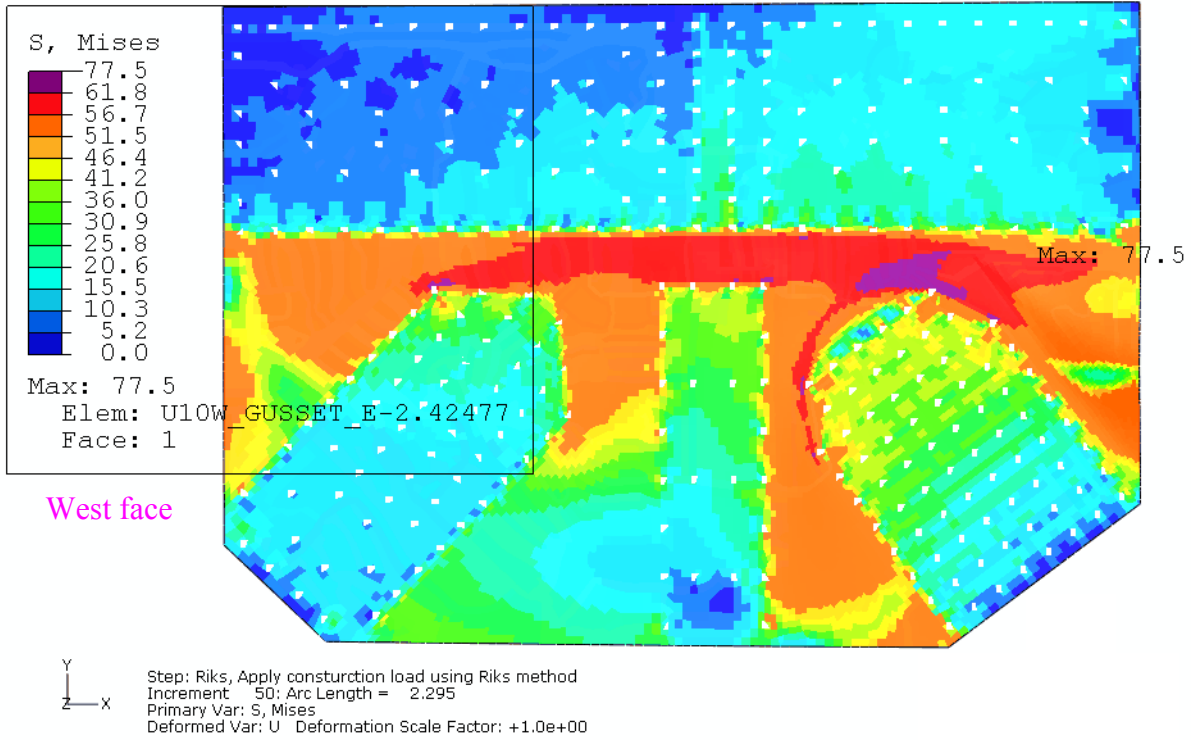
Riks step: Total load of 25,051 kips

Figure 11.3: Von Mises stress distribution in the east gusset plate at the U10W joint in Riks step near divergence when the temperature increase was applied
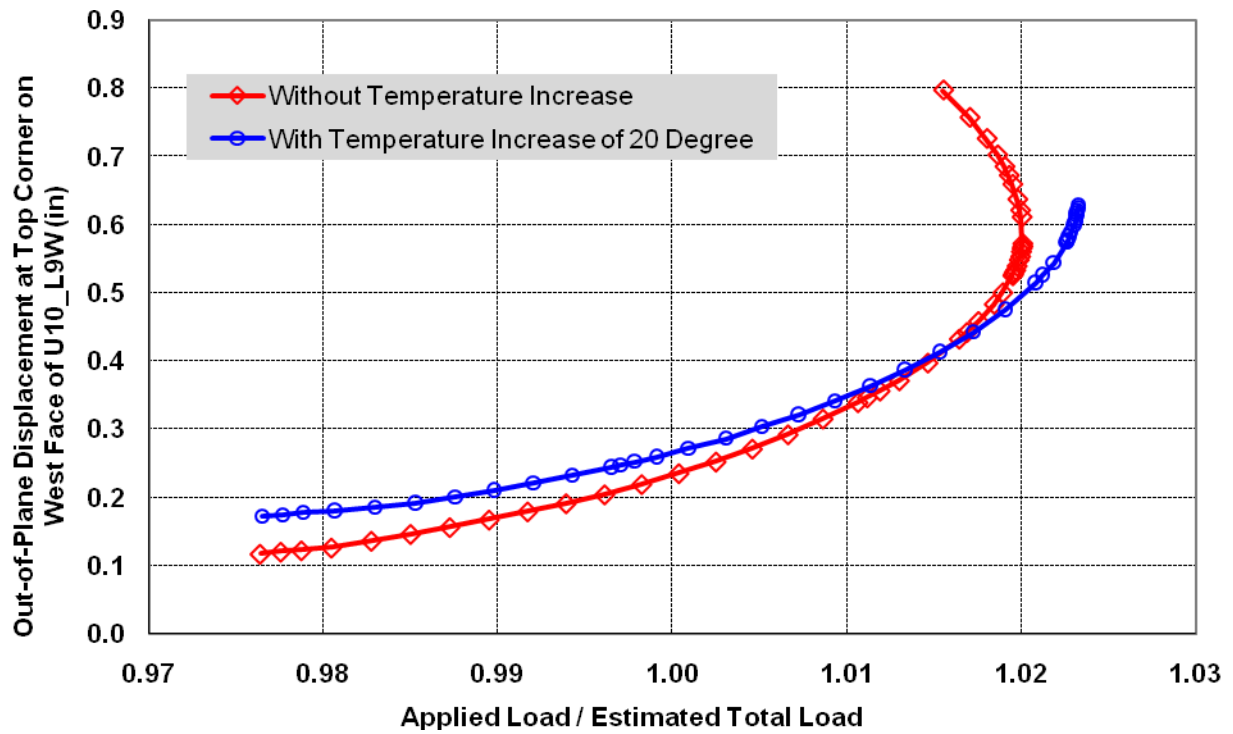
Figure 11.4: Comparison of normalized total load versus displacement between applying a uniform temperature increase of 20°F to the whole bridge and not applying the temperature increase

Appendices

A1 Axial Forces in Members Near U10W and U10E

The FHWA structural element model (Abaqus_Model_2_05142008.inp) was used to calculate the axial forces in the truss members near the U10 nodes at each loading step of the analysis. These axial forces are compared to the original design loads for the members shown on the drawings. One change was made to the FHWA structural element model, which was to split the original step 3 into two steps. The original step 3 in the model included loads to simulate the 1977 increase in deck thickness and the 1998 modifications to the median barrier and outside railings. For the model in this section of the report, step 3 now applies only the forces simulating the increase in deck thickness, and step 4 applies the forces simulating the modifications to the median barrier and outside railings. The approach span forces applied at the ends of the deck truss in the original step 3 were also separated; 73 % of the approach span force increment was applied in the new step 3, and the remaining 27 % of the approach span force increment was applied in the new step 4. The steps for the model used in this section are:

1. Original bridge weight (wet concrete was represented by forces)
2. Deck weight to replace the forces representing the wet concrete (model change), plus original barrier weight
3. Additional concrete weight from increase in deck thickness
4. Additional concrete weight from modifications to median barrier and outside railings
5. Reduced concrete weight (concrete removed for repaving on the day of the accident)
6. Traffic load at collapse
7. Construction load at collapse

The loads at the end of step 2 represent the dead load of the as-designed bridge.

Axial forces were calculated for members from node 9 to node 12 on both the east and west sides of the bridge. These forces are shown in the following tables. Also shown in the tables are the design loads for the members taken from the original design plans, and the forces at the point of instability calculated from the models described in section 3 with an in-plane mesh size of 0.2 inch in the highly stressed regions of the gusset plates, using load cases A1 and A2.

Figure A 1.1 plots the axial forces normalized by the design loads for the five truss members that connect at node U10W. The figure shows the data for load steps 1 through 7 that were calculated with the FHWA structural element model, as described above. The figure also plots the normalized member axial force at instability for load cases A1 and A2, calculated using the models in section 3 with an in-plane mesh size of 0.2 inch in the highly stressed regions of the gusset plates.

Table A 1.1

Axial Forces Calculated for Members from Node 9 to Node 12 on the West Side of Bridge

Member	U9/L9W Axial Force (kips)	U9/U10W Axial Force (kips)	L9/U10W Axial Force (kips)	L9/L10W Axial Force (kips)	U10/L10W Axial Force (kips)
Design Load	-600	2147	-2288	-919	540
Step					
1	-272	1424	-1600	-478	233
2	-303	1565	-1755	-527	263
3	-362	1839	-2062	-614	309
4	-383	1937	-2171	-647	329
5	-366	1895	-2092	-616	313
6	-371	1932	-2134	-647	320
7	-443	2011	-2401	-641	396
Instability Case A1	-506	2054	-2548	-646	436
Instability Case A2	-497	2117	-2544	-682	420

Member	U10/U11W Axial Force (kips)	U10/L11W Axial Force (kips)	L10/L11W Axial Force (kips)	U11/L11W Axial Force (kips)	U11/U12W Axial Force (kips)
Design Load	-924	1975	-919	-538	-924
Step					
1	-413	1334	-477	-247	-399
2	-444	1460	-527	-274	-421
3	-512	1712	-614	-327	-474
4	-535	1801	-647	-345	-491
5	-499	1740	-611	-331	-467
6	-505	1772	-644	-338	-467
7	-669	1942	-650	-416	-606
Instability Case A1	-767	2012	-661	-449	-683
Instability Case A2	-720	2029	-692	-433	-646

Member	L11/U12W Axial Force (kips)	L11/L12W Axial Force (kips)	U12/L12W Axial Force (kips)
Design Load	-1725	2011	539
Step			
1	-1127	1225	215
2	-1234	1337	244
3	-1447	1572	286
4	-1523	1654	305
5	-1470	1613	291
6	-1501	1623	296
7	-1576	1781	344
Instability Case A1	-1618	1854	371
Instability Case A2	-1661	1868	367

Table A 1.2

Axial Forces Calculated for Members from Node 9 to Node 12 on the East Side of Bridge

Member	U9/L9E Axial Force (kips)	U9/U10E Axial Force (kips)	L9/U10E Axial Force (kips)	L9/L10E Axial Force (kips)	U10/L10E Axial Force (kips)
Design Load	-600	2147	-2288	-919	540
Step					
1	-271	1421	-1596	-476	232
2	-302	1563	-1752	-526	262
3	-361	1835	-2059	-614	308
4	-383	1933	-2169	-646	329
5	-375	1910	-2127	-627	322
6	-377	1932	-2148	-648	324
7	-416	1968	-2298	-631	369
Instability Case A1	-445	1994	-2415	-617	400
Instability Case A2	-448	2077	-2461	-657	398

Member	U10/U11E Axial Force (kips)	U10/L11E Axial Force (kips)	L10/L11E Axial Force (kips)	U11/L11E Axial Force (kips)	U11/U12E Axial Force (kips)
Design Load	-924	1975	-919	-538	-924
Step					
1	-413	1331	-476	-246	-400
2	-444	1458	-526	-273	-422
3	-513	1709	-614	-326	-475
4	-536	1798	-646	-344	-493
5	-514	1764	-631	-337	-475
6	-516	1783	-650	-341	-475
7	-622	1875	-622	-384	-573
Instability Case A1	-687	1928	-601	-415	-631
Instability Case A2	-668	1978	-645	-414	-613

Member	L11/U12E Axial Force (kips)	L11/L12E Axial Force (kips)	U12/L12E Axial Force (kips)
Design Load	-1725	2011	539
Step			
1	-1125	1224	215
2	-1232	1336	243
3	-1445	1570	285
4	-1521	1651	304
5	-1492	1620	297
6	-1509	1627	300
7	-1544	1747	324
Instability Case A1	-1564	1825	339
Instability Case A2	-1624	1855	344
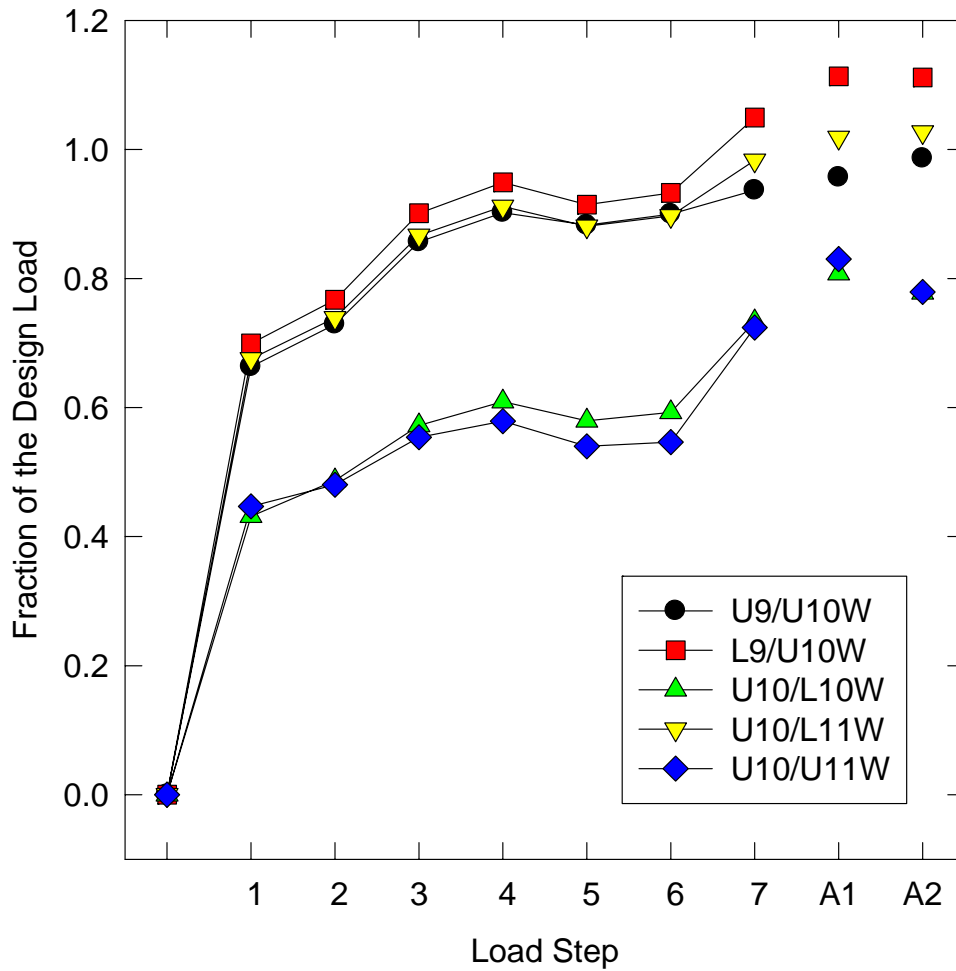
Figure A 1.1: Axial forces in the five truss members that connect at node U10W, normalized by their original design loads. The data for load steps 1 through 7 were calculated with the FHWA structural element model, as described in this appendix. The data for the steps labeled A1 and A2 represent the member axial force at instability calculated using the models in section 3, with detailed representations of U10 and an in-plane mesh size of 0.2 inch in the highly stressed regions of the gusset plates.

A2   Additional Modeling/Mesh Issues

A2.1   Coupling between Global and Local Models

The connections between beam elements and shell elements at the boundaries of global/local model may significantly influence the states of stress in the gusset plates. Two types of coupling conditions were considered, distributed load and kinematic as shown in Figure A 2.1. The former coupling resulted in large (self-equilibrating) local deformations of the truss members of the local model at their connecting locations. While the kinematic coupling may impose additional constraints (slightly increased stiffness of local model), this coupling was chosen at all the connecting locations to avoid the locally large deformations found with the distributed load coupling.

A2.2   Stiffness of Joint Region

In order to assess the discrepancy between the beam-only model and the solid/shell element model at U10W joint, the local stiff nesses of two models are compared by the load-point-deformation behaviors. In each calculation, a unit force/moment is applied at one degree of freedom (DOF) of a node and other DOF of all nodes are fixed to zero. Then resulting displacements/rotations are compared with those of the detailed 3D solid/shell model of the U10W joint as shown in Figure A 2.2. Here a total of 108 calculations (54 each for beam-only and solid/shell models) is carried out. Table A 2.1 shows the displacements and rotations of nine connecting points for "beam-only" model and "solid/shell/beam" model.

Table A 2.1. Stiffness comparison of beam-only and solid/shell models.

Beam Model

end nodes	Ux	Uy	Uz	Rx	Ry	Rz
1	9.01E-03	1.63E-03	2.22E-04	1.26E-06	6.05E-06	3.71E-03
2	7.08E-03	1.37E-03	2.16E-04	1.02E-06	3.63E-06	2.64E-03
3	1.52E-03	3.15E-01	1.67E-03	1.30E-05	7.23E-06	1.21E-05
4	1.92E-02	2.19E-04	3.96E-03	6.53E-07	6.86E-03	3.78E-06
5	4.72E-04	2.60E-04	3.57E-02	6.01E-07	1.02E-06	4.18E-07
6	2.02E-04	1.27E-02	1.26E-02	5.60E-06	4.17E-07	4.43E-07
7	1.75E-04	1.06E-02	1.05E-02	5.13E-06	3.21E-07	3.52E-07
8	4.19E-04	3.81E-04	3.10E-02	9.38E-07	1.03E-06	9.39E-07
9	3.11E-03	1.01E-04	2.22E-03	1.72E-05	1.75E-03	2.04E-05

Solid/Shell Model

end nodes	Ux	Uy	Uz	Rx	Ry	Rz
1	5.66E-03	2.12E-03	1.94E-04	1.61E-06	5.33E-06	1.30E-03
2	2.46E-03	1.30E-03	1.82E-04	1.29E-06	3.05E-06	9.12E-04
3	1.56E-03	2.40E-01	1.91E-03	1.21E-05	7.00E-06	1.05E-05
4	4.68E-03	1.67E-04	5.11E-03	9.31E-07	4.10E-05	2.53E-06
5	4.78E-04	2.64E-04	3.77E-02	6.61E-07	1.13E-06	3.88E-07
6	1.81E-04	8.69E-03	1.20E-02	4.27E-06	4.39E-07	3.99E-07
7	1.61E-04	7.76E-03	1.08E-02	3.94E-06	3.48E-07	3.23E-07
8	3.99E-04	3.64E-04	3.07E-02	1.00E-06	1.10E-06	8.33E-07
9	2.11E-03	1.12E-04	6.24E-04	1.18E-05	1.06E-03	1.90E-05

Normalized Differences bet Solid and Beam Models

end nodes	ΔUx	ΔUy	ΔUz	ΔRx	ΔRy	ΔRz
1	-0.37	0.05	0.00	0.00	0.00	-0.65
2	-0.64	-0.01	0.00	0.00	0.00	-0.65
3	0.00	-0.24	0.00	-0.04	-0.01	-0.08
4	-0.74	0.00	0.06	0.00	-0.99	0.00
5	0.00	0.00	0.06	0.05	0.08	-0.02
6	0.00	-0.22	-0.03	-0.24	0.00	-0.01
7	0.00	-0.19	0.02	-0.23	0.01	-0.01
8	0.00	0.00	-0.01	0.04	0.04	-0.06
9	-0.26	0.00	-0.42	0.00	-0.39	0.00

In the third table, a negative value indicates the DOF of solid/shell model is stiffer than the same DOF in the beam-only model. As shown in the tables, the solid/shell model is generally stiffer than that of the beam-only model although the stiffness differences at many DOF are less than 1% of the beam model displacements/rotations. The notable difference appears on the rotation about the vertical axis of end node 4 where nearly two orders of magnitudes stiffer response is observed in the solid/shell model. The torsional stiffness at this location may not be represented accurately since multiple members are joined together at this point in a global model.

To further estimate the significance of stiffness difference at each DOF in the present analysis, nodal forces and moments at the end nodes are obtained from the 'global model calculations' of beam-only model. Since the displacements/rotations are obtained via unit load applications, forces/moments are squared and multiplied with the corresponding displacement differences $F_i^2 \Delta u_i$ to obtain the energy differences as shown in Table A 2.2.

Table A 2.2 Product (energy) of force and displacement difference (klb·in)

nodes	Ex	Ey	Ez	Erx	Ery	Erz
1	0	0	0	0	0	0
2	-4	0	-1	0	0	-4
3	0	0	0	0	0	0
4 (L10)	0	0	2	1	-225	0
5 (L9)	10	15	0	0	0	0
6 (U11)	-11	-2	0	0	0	0
7 (U9)	-46	-1	0	0	0	0
8 (L11)	-32	-31	0	0	0	0
9	-4	0	0	0	0	0

At some DOF, large energy differences are observed but generally not where forces/moments are high. In overall, the differences between the detail shell/solid model and the beam only model are limited and they are not expected to make significant differences in the failure mode/load of U10W joint.

A2.3 Effects of Camber

To compensate the deflection due to the bridge weight itself, the orignial construction had a camber. The effects of such upward curvature were evaluated with independent models with initial camber. In the models, the middle-section of bridge was raised as shown in Figure A 2.3 with the maximum rise of 10" at the center.

Analyses were carried out to determine the change in forces transmitted to the U10W joint by the major beams. The computed results show less than 0.3% change in the axial loads as compared to those of models without camber. Thus such effects are considered to be minimal in the calculation of the load necessary to trigger instability.

A2.4 Modifications of Moment of Inertia

To investigate some variations in boundary and physical conditions, the moments of inertia of some members were adjusted. First modifications were made on vertical connectors (between bridge frame and deck) that were not embedded into the bridge frame. Their moment of inertia was set lower. The resulting effects on the estimated load to trigger instability were limited as it appears to reduce the value by about 0.4%. Second, to account for some flexibility of connections at joints, the moment of inertia of the U10_L9W member near the L9W joint was lowered. In the beam model, the joint itself is modeled as rigid. This adjustment was carried out to see if some flexibility at the L9W joint might accelerate the tilting instability of the U10_L9W member. The results predict up to 0.3% reduction in the load needed to trigger instability.
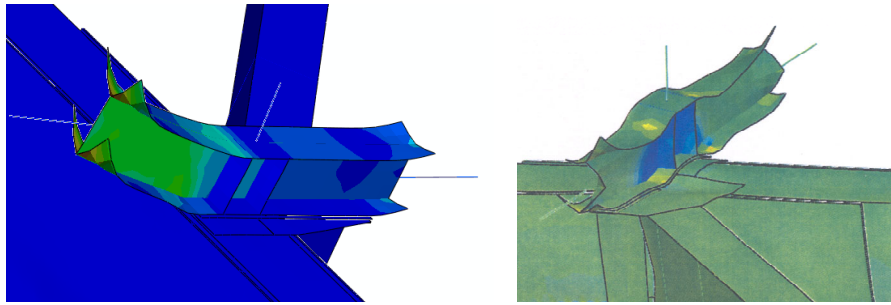
Figure A 2.1: Large local deformation of shell elements at ends with distributed coupling condition
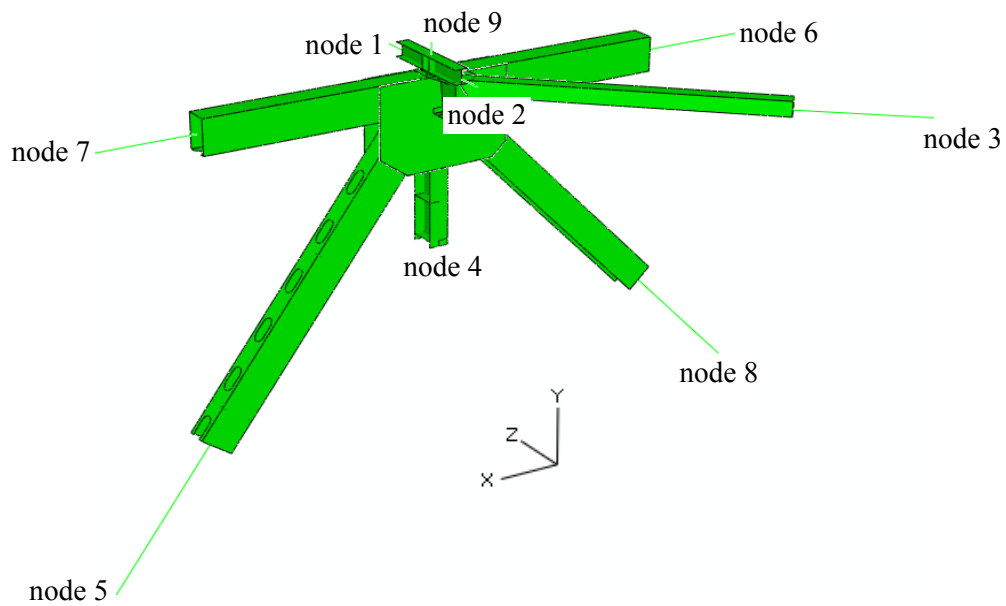
Figure A 2.2: Schematic of U10W joint solid/shell model and node labels for connections

$$y \Leftarrow y + \frac{D_{max}}{2}\left[\cos\left(\frac{2(x-x_m)\pi}{L}\right)+1\right] \quad \text{for} \quad x_A < x < x_B \quad \text{and} \quad y \leq 0.0$$

$$L = x_A - x_B = 5,472, \; h = y_0 - y_B = 720$$
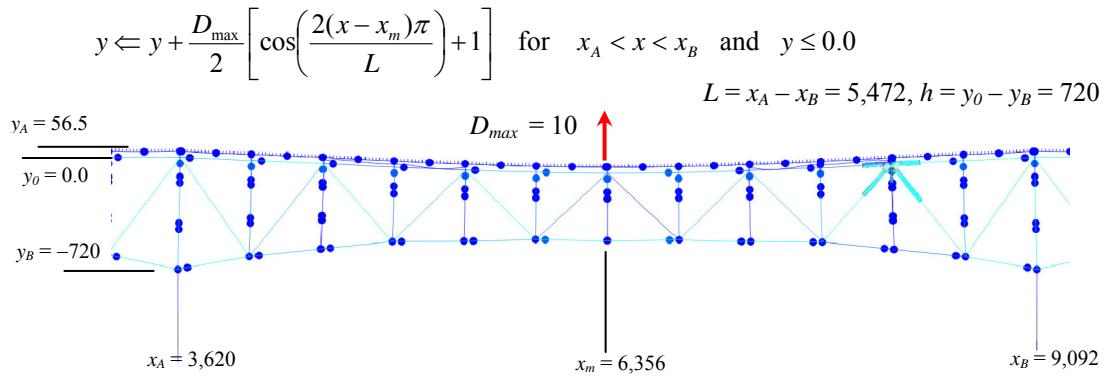
Figure A 2.3: Formula and schematic used to add camber

A3 Investigation of Connection Methods Between the Gusset Plates and the Main Truss Members

A3.1 Description of the U10W 3D Local Models

The three mixed models listed in Table A 3.1 were analyzed to investigate the effects of connection methods between the gusset plates and the main truss members in the U10W 3D local models. Each mixed model had a U10W 3D local model embedded into the sixth FHWA structural element bridge model. Tie constraints were used to connect all secondary structure. An in-plane mesh size of 0.5 inches was typical in the highly stressed region of the gusset plates. Load condition B was used. The three mixed models were the same, except for the connection methods between the gusset plates and the main truss members. Only fasteners were used to connect the main truss members to the gusset plates in the first mixed model, and no contact was defined between the truss members and the gusset plates. This model was described previously in Section 9 of this report, where the thickness of the gusset plates was 0.5 inches.

Table A 3.1
Mixed Models Used to Investigate Connection Methods

Local Model Embedded	Connection Methods Between Gusset Plates and Main Truss Members	Typical Mesh Size (inch)	Loading Condition	FHWA Structural Element Bridge Model
U10W joint with bowed gusset plates	Fastener + no contact	0.5	B	6
U10W joint with bowed gusset plates	Fastener + contact	0.5	B	6
U10W joint with bowed gusset plates	Fastener + contact for U10_L9W; tie for other four main truss members	0.5	B	6

In the second mixed model, fasteners and contact pairs were defined to connect the main truss members to the gusset plates. This model was described previously in Section 7 of this report, where only the U10W local model was incorporated. In the third mixed model, fasteners and two contact pairs were defined to connect the diagonal truss member U10_L9W to the gusset plates, and eight tie constraints were used to connect the other four main truss members to the gusset plates.

A3.2 Comparison Between the Three Connection Methods

The Riks method was used to predict the maximum live load at the onset of instability by proportionally increasing the live load while other loads were maintained at the estimated values. When the fasteners with contact were used to connect the diagonal truss member U10_L9W to the gusset plates, and tie constraints were used to connect the other four main truss members to the gusset plates, the live load in the Riks step increased monotonically until the analysis was terminated. The analysis was terminated because the live load of 2,956 kips was greater than three times the estimated live load. The total load at the termination point was 26,454 kips, or 1.081 times the estimated total load. The displacement along the vertical direction at the U10W

node was predicted to be -6.13 inches under the load at termination point. Figure A 3.1 shows the von Mises stress and equivalent plastic strain distributions at the U10W joint under the load at the termination point. The maximum von Mises stress was predicted to be 89 ksi on the edge of the top corner fastener connecting the east gusset and the diagonal truss member U10_L9W, which corresponded to an equivalent plastic strain of 11.0 percent.

Table A 3.2 compares the predicted maximum total load at instability and the maximum von Mises stress in the east gusset plate at the U10W joint in the three mixed models. The table shows that the model with tie constraints supported loads well above the predicted maximum load capacities of the models with fasteners. The table also shows that the model with contact supported heavier loads than the model without contact.

Table A 3.2
Effect of Connection Methods Between Gusset Plates and Main Truss Members on Load and Stress

Connection Methods between Gusset Plates and Main Truss Members	Fastener + no contact	Fastener + contact	Fastener + contact for U10_L9W; tie for other four main truss members
Predicted Maximum Total Load at Instability (kip)	24,641	25,219	>26,454
Traffic/Construction/Approach Span Force Increment (Live Load) at Predicted Maximum Load at Instability (kip)	1,143	1,721	>2,956
Maximum von Mises Stress in East Gusset at U10W Under Load at Instability (ksi)	81	83	89

A3.3   Summary: Connection Method Investigation

Three mixed models with different connection methods between the gusset plates and the main truss members in the 3D local models were analyzed with load condition B. In the first model, fasteners were used, and no contact was defined. In the second model, the fasteners and contact were used. In the third model, the fasteners and contact were used to connect the diagonal truss member U10_L9W to the gusset plates, and tie constraints were used to connect the other four main truss members to the gusset plates.

The analyses indicated that the model with tie constraints would support loads well above the predicted maximum total load at instability of the models with fasteners. The analyses also indicated that the model with contact supported more loads than the model without contact. When the fasteners were used and no contact was defined, the Riks method predicted a maximum total load at instability of 24,641 kips. When the fasteners were used and contact was defined, the Riks method predicted a maximum total load at instability of 25,219 kips. When the fasteners and contact were used to connect the diagonal truss member U10_L9W to the gusset plates and the tie constraints were used to connect the other four main truss members to the gusset plates, no instability was predicted before the Riks analysis was terminated, because the total load had exceeded the maximum value specified, 26,454 kips.
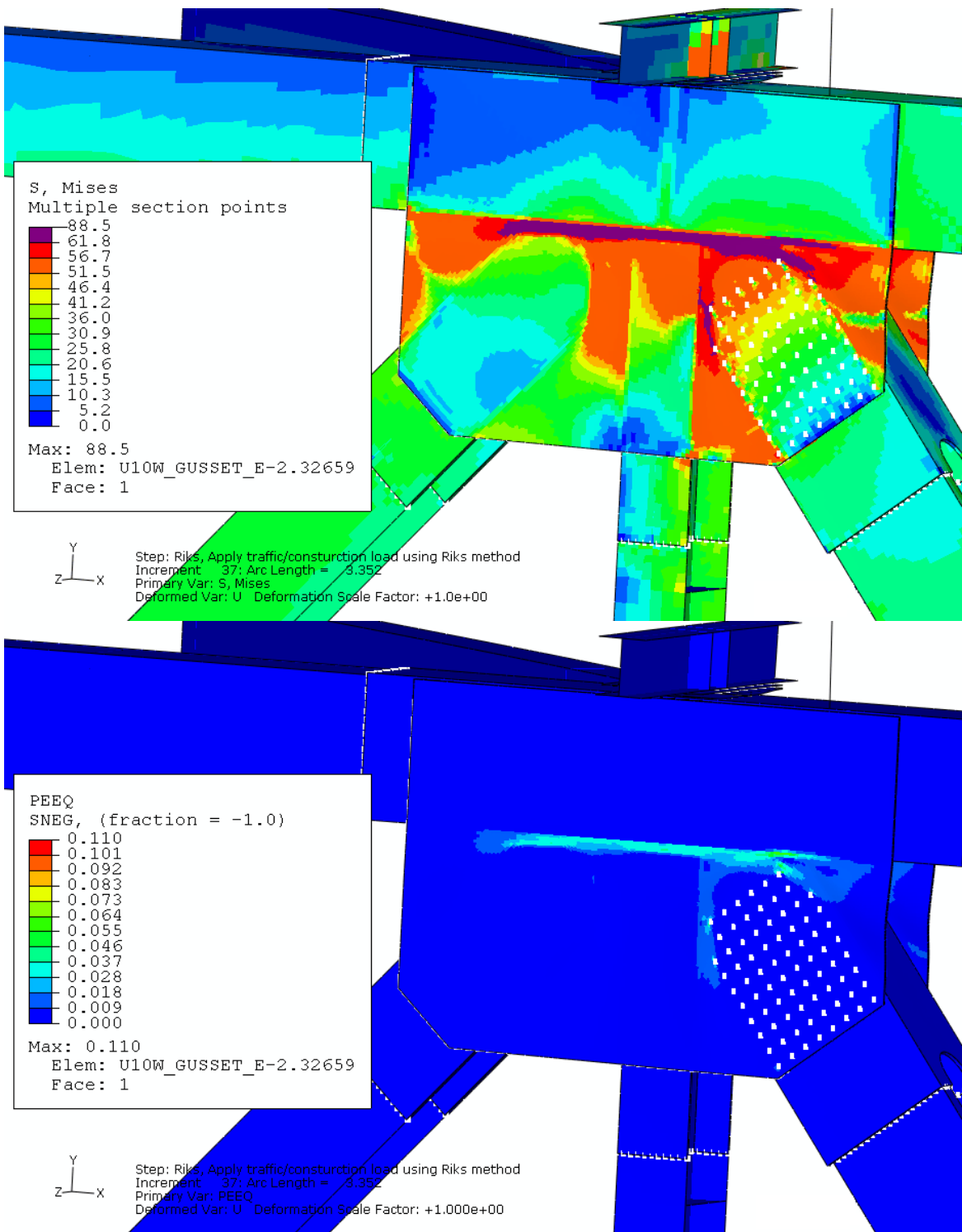
Riks step: Total load of 26,454 kips

Figure A 3.1: Von Mises stress and equivalent plastic strain (PEEQ) distribution at the U10W joint in Riks step when tie constraints were used to connect four main truss members to the gusset plates

A4 Comparison of Shell Representation and Solid Representation of the Main Truss Members

A4.1 Model Description

Analyses were conducted to investigate the effect of main truss representation on the stress distribution in the gusset plates at the U10W joint. Table A 4.1 lists the two mixed models used for the truss representation comparison. Each mixed model had a U10W 3D local model with flat gusset plates embedded into the fourth structural element bridge model provided in January 2008 by FHWA. An in-plane mesh size of 0.5 inches was typical in the highly stressed region of the gusset plates. Fasteners were used to connect the main truss members to the gusset plates, and no contact was defined in the two models. Tie constraints were used to connect all secondary structure. Load condition C, which will be discussed in detail later in this section, was used.

Table A 4.1
Mixed Models Used to Investigate Truss Representation

Local Model Embedded	Representation of Main Truss Members	Typical Mesh Size (inch)	Loading Condition	FHWA Structural Element Bridge Model
U10W joint with flat gusset plates	Shell	0.5	C	4
U10W joint with flat gusset plates	Shell + Solid	0.5	C	4

The two mixed models were the same, except for the representation of the gusset plates and the main truss members at the U10W joint. In the first mixed model, shell elements S4R were used to represent the five main truss members, and solid elements C3D20R were used to represent the two gusset plates. A C3D20R element is a twenty-node quadratic brick element using reduced integration. Two elements were used through the thickness of the gusset plates. Each gusset plate contained 26,950 elements. Figure A 4.1 shows the meshing of the gusset plates and the main truss members in the first mixed model.

The second mixed model was similar to the model described previously in Section 7 of this report, where only the U10W local model was incorporated. In the second mixed model, solid elements C3D8R were used to represent the truss member portion in contact with the gusset plates, and shell elements S4R were used to represent the remaining portion of the truss members. Solid elements C3D8R were used to represent the two gusset plates. Total stiffness hourglass control [11] was used for elements C3D8R. Four elements were used through the thickness of the gusset plates. Each gusset plate contained 53,824 elements.

Two other differences existed between the models described in this section of the report and the models described previously in this report:

- The models in this section used distributing couplings to connect the lateral brace and floor truss upper chord section in the local models to the FHWA structural element bridge model.

- The models in this section had only four load steps. In the first step, decks and expansion joint springs were removed from the model. The weight of steel and walkways, the forces representing wet deck concrete, and approach span reaction forces were then applied. In the second step, the weight of decks was applied to replace the forces representing the wet concrete, and the weight of the original barriers was applied. In the third step, expansion joint springs were added. The weight of the modified deck (increased deck thickness, less the deck milled off for the repaving operation) and the added barriers was then applied. The corresponding approach span force increment was also applied. In the fourth step, the live load, including traffic load, construction load, and corresponding approach span force increment, was applied. The combination of the four load steps was identified as load condition C. Table A 4.2 describes and summarizes load condition C. All four steps were regular static analysis steps.

Table A 4.2
Load Steps in Load Condition C

Step	Load Description	Model Change	Load Increment (kip)	Total Load (kip)	Normalized Total Load (kip)
1	Weight of steel and walkways, forces representing wet deck concrete, and approach span reaction forces	Remove decks and expansion joint springs	17,860	17,860	0.730
2	Weight of decks to replace the forces representing the wet concrete and weight of original barriers	Add decks	1,627	19,487	0.797
3	Weight of modified deck and added barriers through the life of the bridge and approach span reaction force increment	Add expansion joint springs	3,985	23,472	0.960
4	Live load, including traffic load and construction load at collapse and approach span reaction force increment	---	986	24,458	1.000

A4.2   Comparison of Element Types Used to Represent Truss Members

When the shell representation was used for the main truss members at the U10W joint, the maximum von Mises stress under the estimated total load of 24,458 kips with load condition C was predicted to be 66 ksi on the edge of the top corner fastener connecting the east gusset and the diagonal truss member U10_L9W, which corresponded to an equivalent plastic strain of 2.8

percent, as shown in Figure A 4.2 and Figure A 4.3. Figure A 4.2 shows the von Mises stress and equivalent plastic strain distributions at the U10W joint under the estimated total load. Figure A 4.3 shows the von Mises stress and equivalent plastic strain distributions in the east gusset plate.

When the shell plus solid representation was used for the main truss members, the maximum von Mises stress was predicted to be 65 ksi on the edge of the top corner fastener connecting the east gusset and the diagonal truss member U10_L9W, which corresponded to an equivalent plastic strain of 2.3 percent, as shown in Figure A 4.4 and Figure A 4.5. Figure A 4.4 shows the von Mises stress and equivalent plastic strain distributions at the U10W joint under the estimated total load. Figure A 4.5 shows the von Mises stress and equivalent plastic strain distributions in the east gusset plate. Comparison of the four figures indicated that the von Mises stress and equivalent plastic strain distributions at the U10W joint for the two models were similar.

A4.3   Summary: Element Types Used to Represent Truss Members

Two mixed models were analyzed to investigate the effect of truss member element type on stress and strain distributions. One mixed model used shell elements to represent truss members; the other mixed model used a combination of shell and solid elements to represent truss members. Similar von Mises stress and equivalent plastic strain distributions were obtained in the two models. Under the estimated total load of 24,458 kip, the maximum von Mises stress was predicted to be 66 ksi for the model with truss shell representation and 65 ksi for the model with truss shell plus solid representation.
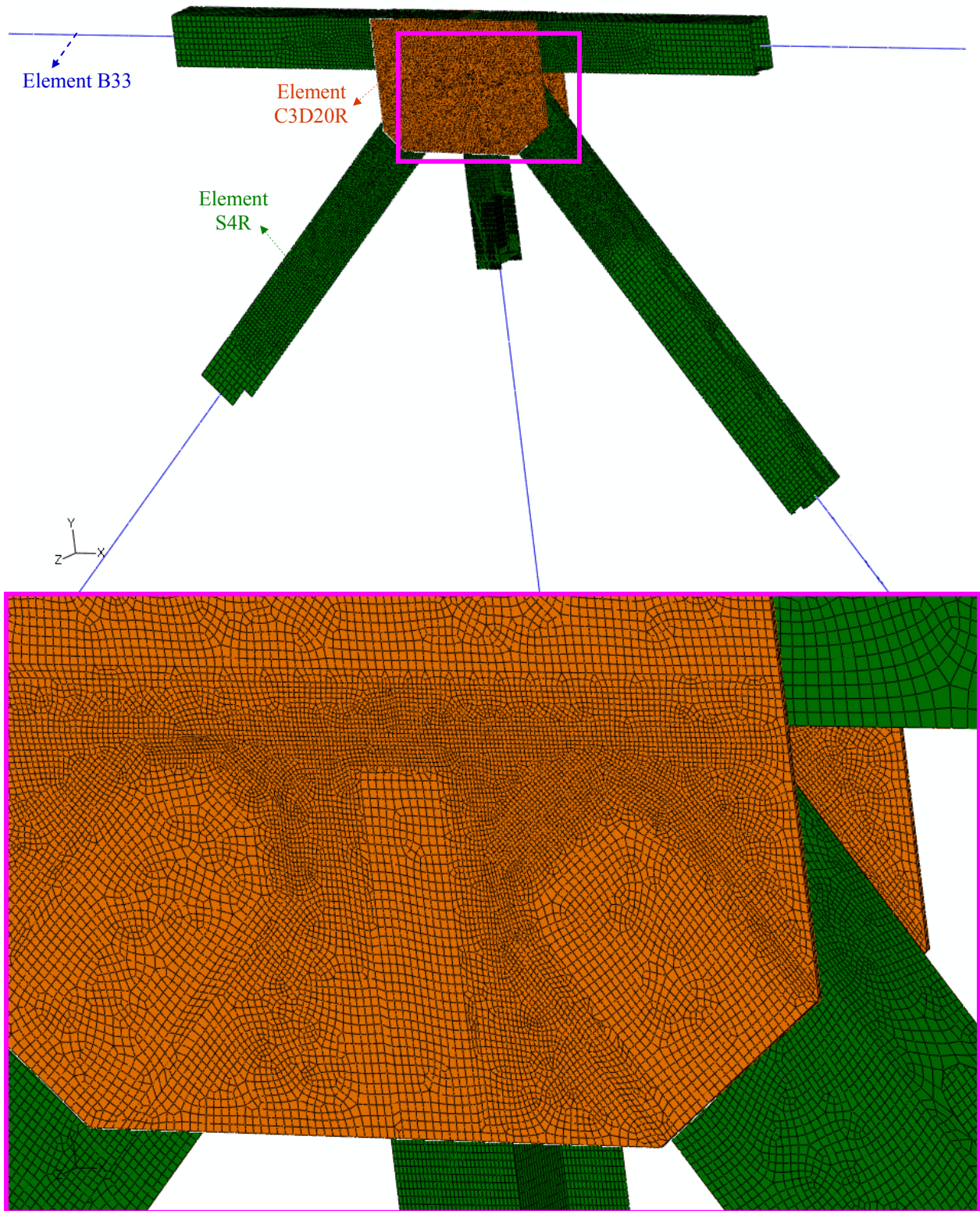
Figure A 4.1: Meshing of solid gusset plates and shell truss members at the U10W joint
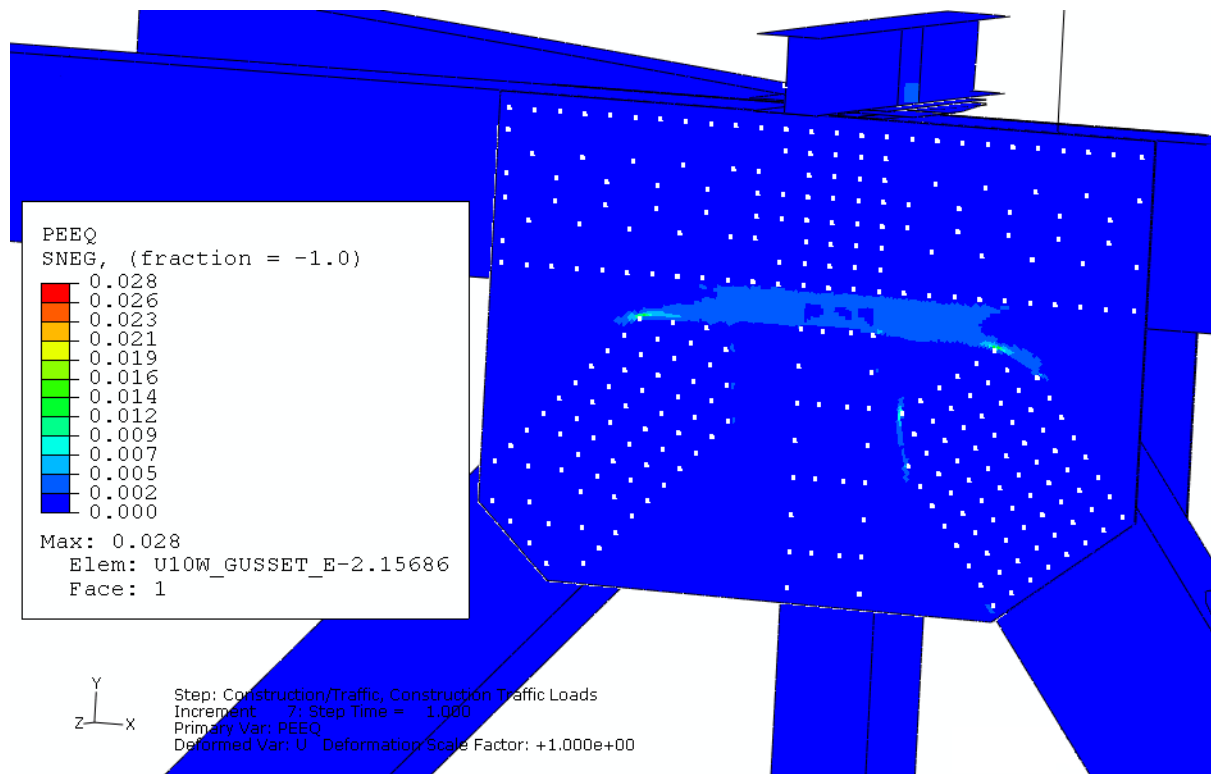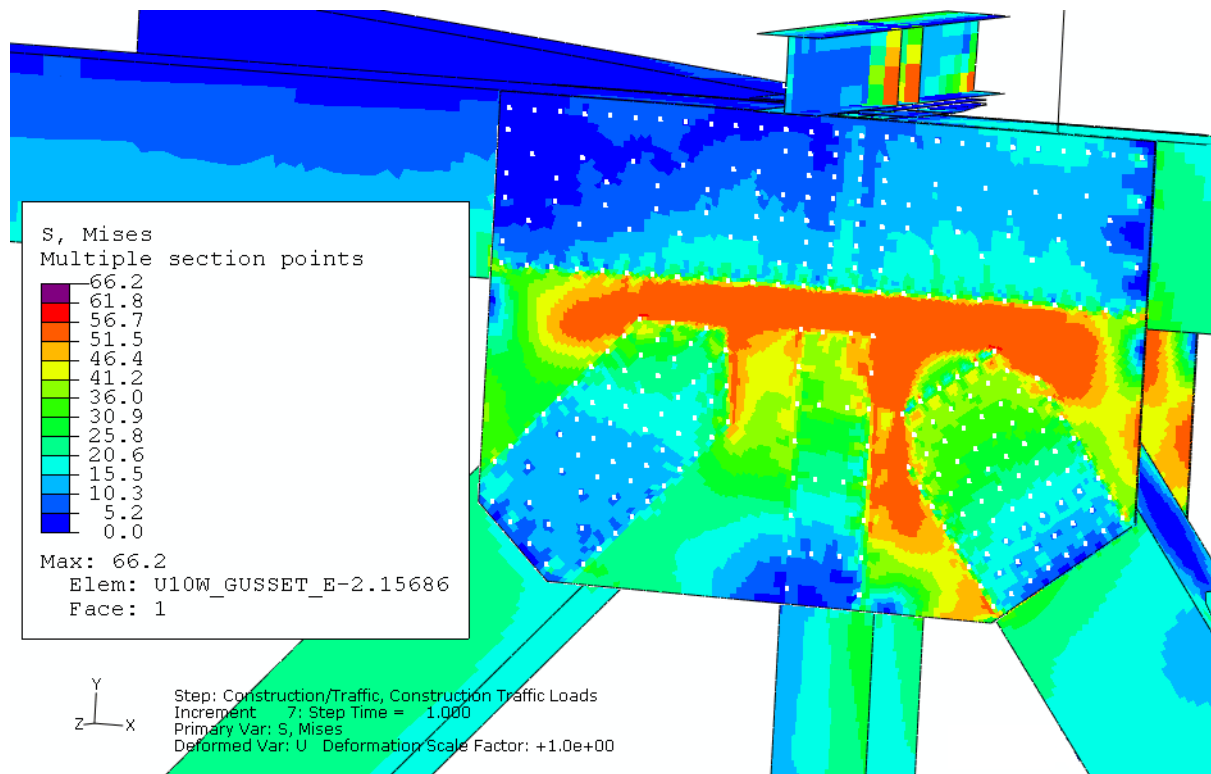
Figure A 4.2: Von Mises stress and equivalent plastic strain (PEEQ) distributions at the U10W joint under the estimated total load when shell representation was used for the main truss members

Figure A 4.3: Von Mises stress and equivalent plastic strain (PEEQ) distributions in the east gusset under the estimated total load when shell representation was used for the main truss members

Figure A 4.4: Von Mises stress and equivalent plastic strain (PEEQ) distributions at the U10W joint under the estimated total load when shell plus solid representation was used for the main truss members

S, Mises
- 64.7
- 61.8
- 56.7
- 51.5
- 46.4
- 41.2
- 36.0
- 30.9
- 25.8
- 20.6
- 15.5
- 10.3
- 5.2
- 0.0

Max: 64.7
 Elem: U10W_GUSSET_E-2.6408
 Face: 1

Max: 64.7

West face

Y
Z — X

Step: Construction/Traffic, Construction Traffic Loads
Increment   7: Step Time =   1.000
Primary Var: S, Mises
Deformed Var: U   Deformation Scale Factor: +1.0e+00

PEEQ
- 0.028
- 0.026
- 0.023
- 0.021
- 0.019
- 0.016
- 0.014
- 0.012
- 0.009
- 0.007
- 0.005
- 0.002
- 0.000

Max: 0.023
 Elem: U10W_GUSSET_E-2.6408
 Face: 1

Max: 0.023

West face

Y
Z — X
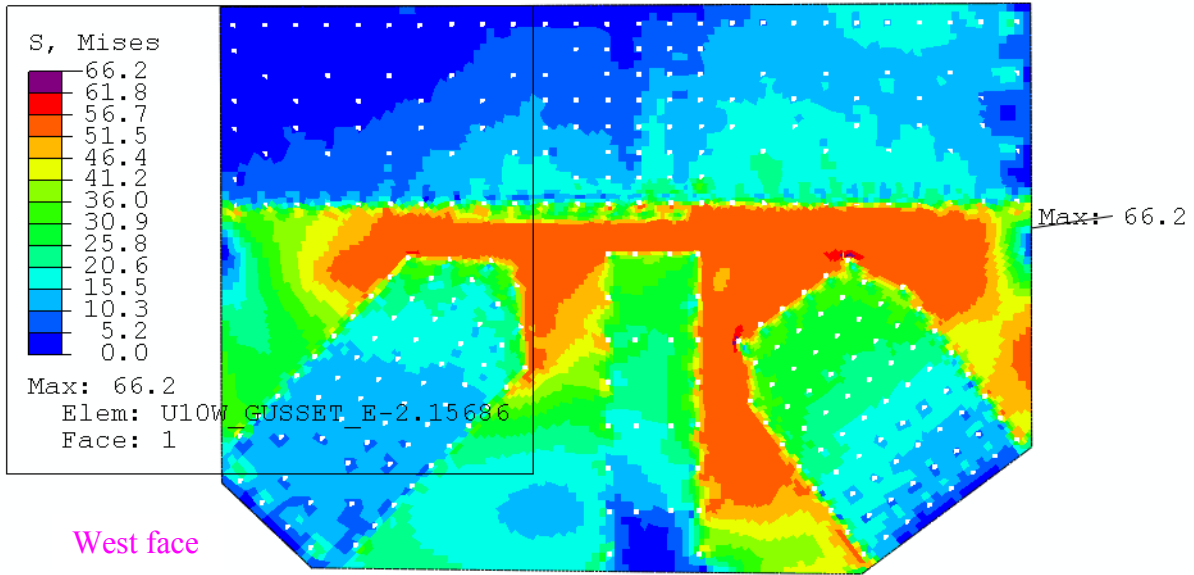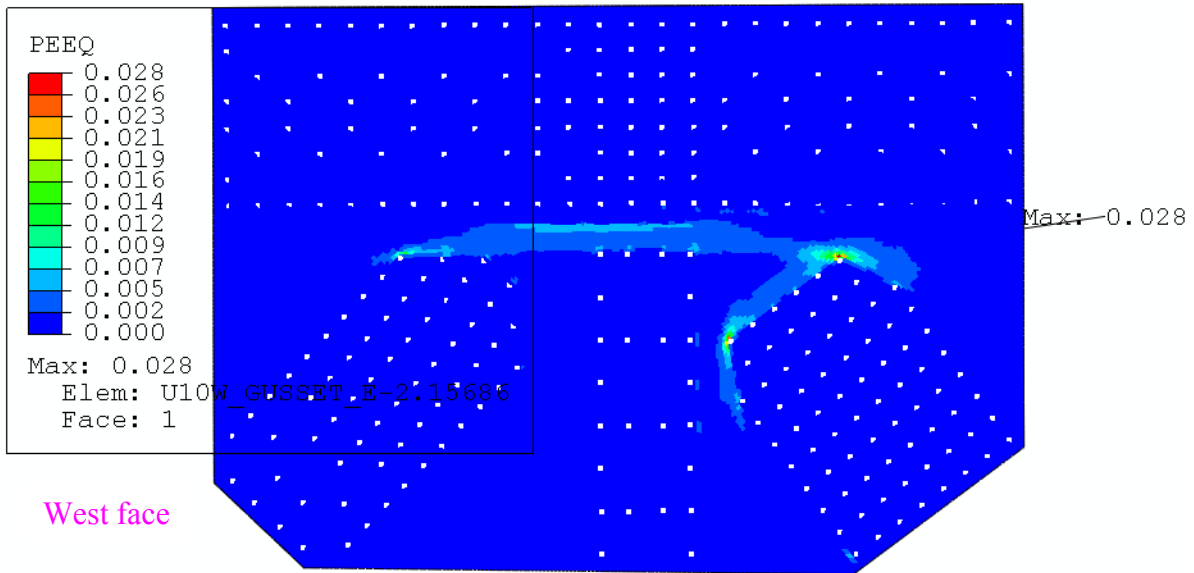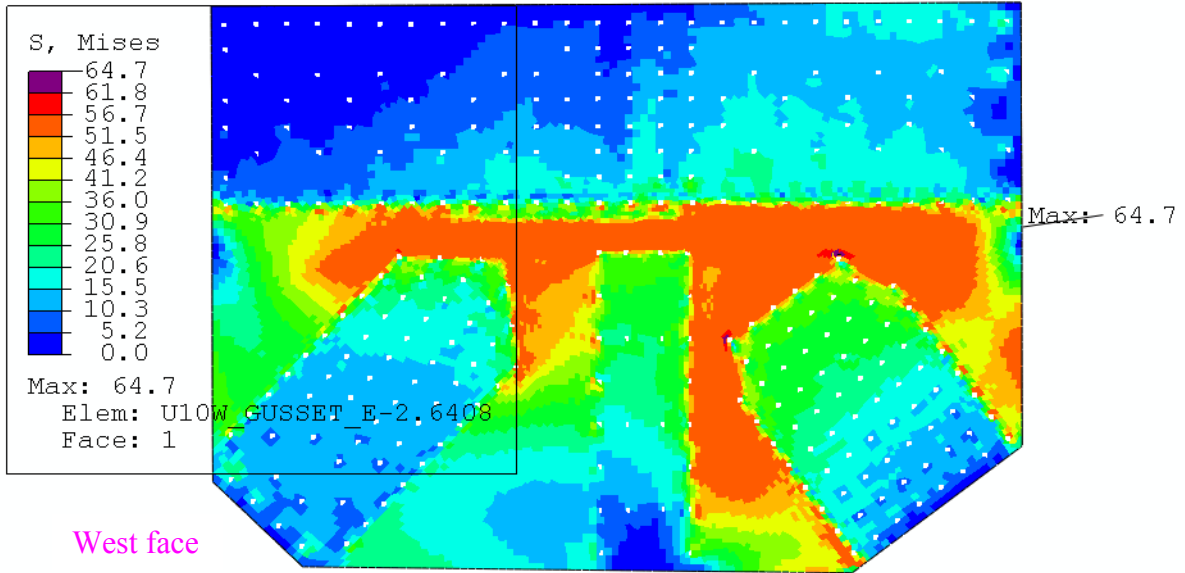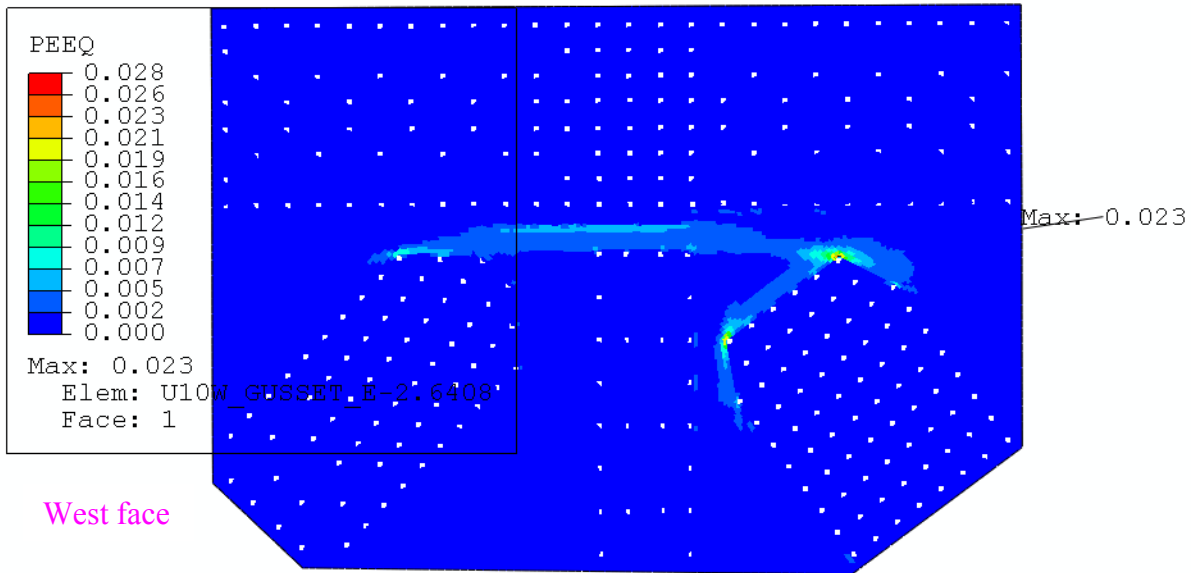
Step: Construction/Traffic, Construction Traffic Loads
Increment   7: Step Time =   1.000
Primary Var: PEEQ
Deformed Var: U   Deformation Scale Factor: +1.000e+00

Figure A 4.5: Von Mises stress and equivalent plastic strain (PEEQ) distributions in the east gusset under the estimated total load when shell plus solid representation was used for the main truss members

A5 Investigation of Methods Used to Model the Deck and Apply Bridge Deadweight

A5.1 Model Description

Four mixed models were analyzed to investigate the effects of changing the method used to model the deck and apply the bridge deadweight. Each mixed model had a U10W 3D local model embedded into the sixth FHWA structural element bridge model. In the four mixed models, fasteners were used to connect the main truss members to the gusset plates at the U10W joint, and no contact was defined. Tie constraints were used to connect all secondary structure. An in-plane mesh size of 0.5 inches was typical in the highly stressed region of the gusset plates.

The four mixed models were the same, except for the methods used to model the deck and apply the bridge deadweight, as described in Table A 5.1. The first mixed model was described previously in Section 9 of this report, where the gusset plate thickness was 0.5 inches. Loading condition B was used, as described in Table 7.2. Six load steps were used, and the first five steps were used to apply the bridge deadweight. The estimated total load was 24,482 kips. Decks and deck offsets were removed from the model in the first step and added back into the second step.

Table A 5.1
Mixed Models Analyzed for Bridge Deadweight Application Comparison

Local Model Embedded	Methods Used to Apply Bridge Deadweight	Typical Mesh Size (inch)	Loading Condition	FHWA Structural Element Bridge Model
U10W joint with bowed gusset plates	With model change of decks and deck offsets	0.5	B	6
U10W joint with bowed gusset plates	With model change of decks; without model change of deck offsets	0.5	D	6
U10W joint with bowed gusset plates	Without model change of decks and deck offsets; bridge deadweight was applied in four steps	0.5	E	6
U10W joint with bowed gusset plates	Without model change of decks and deck offsets; bridge deadweight was applied in two steps	0.5	F	6

The second mixed model also had six load steps. However, the deck offsets were excluded from the model change. Table A 5.2 describes the six load steps used in the second mixed model. The combination of these six load steps was identified as load condition D. The total load in load condition D was 24,532 kips.

In the third mixed model, decks were included in the model from the beginning of the analysis, and the first four steps were used to apply the bridge deadweight. Table A 5.3 describes the five

load steps used in the third mixed model. The combination of the five load steps was identified as load condition E. The total load in load condition E was 24,484 kips.

In the fourth mixed model, decks were included in the model from the beginning of the analysis, and all the bridge deadweight, except for the weight reduction due to milling, was applied in the first step. Table A 5.4 summarizes the three load steps used in the fourth mixed model. The combination of the three load steps was identified as load condition F. The total load in load condition F was 24,484 kips. For ease of comparison, the total load in the four mixed models was normalized with respect to the estimated total load in the first mixed model in the results sections below.

Table A 5.2
Load Steps in the Second Mixed Model with Load Condition D

Step	Load Description	Model Change	Load Increment (kip)	Total Load (kip)	Normalized Total Load (kip)
1	Weight of steel and walkways, forces representing wet deck concrete, and approach span reaction forces	Remove decks (deck offsets are still in the model) and expansion joint springs	17,900	17,900	0.731
2	Weight of decks to replace the forces representing the wet concrete	Add decks	60	17,960	0.734
3	Weight of original barriers	---	1,623	19,583	0.800
4	Weight of added deck and barriers through the life of the bridge and approach span reaction force increment	---	4,550	24,133	0.986
5	Reduced weight of deck concrete due to milling	Add expansion joint springs	-585	23,548	0.962
6	Live load, including traffic load and construction load at collapse and approach span reaction force increment	---	984	24,532	1.002

Table A 5.3
Load Steps in the Third Mixed Model with Load Condition E

Step	Load Description	Model Change	Load Increment (kip)	Total Load (kip)	Normalized Total Load (kip)
1	Weight of steel, deck, and walkways and approach span reaction forces	Remove expansion joint springs	17,902	17,902	0.731
2	Weight of original barriers	---	1,628	19,530	0.798
3	Weight of added deck and barriers through the life of the bridge and approach span reaction force increment	---	4,555	24,085	0.984
4	Reduced weight of deck concrete due to milling	Add expansion joint springs	-585	23,500	0.960
5	Live load, including traffic load and construction load at collapse and approach span reaction force increment	---	984	24,484	1.000

Table A 5.4
Load Steps in the Fourth Mixed Model with Load Condition F

Step	Load Description	Model Change	Load Increment (kip)	Total Load (kip)	Normalized Total Load (kip)
1	Weight of steel, original deck and added deck, walkways, original barriers, and added barriers and approach span reaction forces	Remove expansion joint springs	24,085	24,085	0.984
2	Reduced weight of deck concrete due to milling	Add expansion joint springs	-585	23,500	0.960
3	Live load, including traffic load and construction load at collapse and approach span reaction force increment	---	984	24,484	1.000

A5.2 Comparison Among the Four Methods Used to Model the Deck and Apply the Bridge Deadweight

A5.2.1 Bridge Deadweight and Deformed Shape Comparison

The bridge deadweights of the first, third, and fourth mixed models were similar at 23,498 kips for the first model and 23,500 kips for the third and fourth models. The bridge deadweight of the second mixed model, 23,548 kip, was slightly different from the other three models. This was caused by the zig-zag shape of the deformed decks when the deck offsets were excluded from the model change of the decks.

When the deck offsets were included in the model change of the decks, the decks were flat, but the deck offsets were elongated under the bridge weight, as shown in Figure A 5.1. This was caused by the model change of the decks and deck offsets. The decks were entirely removed from the model in the first step. When they were added back into the model in the second step, the deck nodes took their initial positions and the decks remained flat. In contrast, the lower end nodes of the deck offsets were retained in the model to deform with other bridge portions in the first step, although the upper end nodes of the deck offsets were removed from the model. When the upper end nodes were added back into the model in the second step, they took their initial positions and the deck offsets became elongated.

When the deck offsets were excluded from the model change of the decks, the resulting decks had a zig-zag shape, as shown in Figure A 5.2, deformation magnified by a factor of 20. This was caused by the model change of the decks. Although the deck elements were removed from the model in the first step, the deck nodes connected to the deck offsets were included in the model, because the deck offsets were retained in the model. These deck nodes underwent deformation in the first step. However, the deck nodes not connected to the deck offsets took their initial undeformed position when they were added back into the model in the second step. When the decks were included in the model from the beginning of the analysis, the decks sagged due to the bridge weight, as shown in Figure A 5.3.

A5.2.2 Load and Stress at Predicted Maximum Load at Instability, Riks Method

The Riks method was used to predict the maximum live load at the onset of instability by proportionally increasing the live load while maintaining the other loads at their estimated values. Table A 5.5 summarizes the predicted maximum load at instability and other results of interest for the four models. The table indicates that the results of interest were similar in the four models except for the out-of-plane displacement at the top corner of truss member U10_L9W.

Table A 5.5
Effect of Methods Used to Apply Bridge Deadweight on Results of Interest

	With model change of decks and deck offsets	With deck model change; without deck offset model change	Without deck model change; four steps to apply bridge deadweight	Without deck model change; two steps to apply bridge deadweight
Predicted Maximum Total Load at Instability (kip)	24,641	24,653	24,631	24,615
Traffic/Construction/Approach Span Force Increment (Live Load) at Instability (kip)	1,143	1,105	1,131	1,115
Maximum von Mises Stress in Gusset Plates at U10W Joint (ksi)	81	80	79	79
Maximum Equivalent Plastic Strain in Gusset Plates at U10W Joint	5.8%	5.4%	5.1%	5.2%
Out-of-Plane Displacement at Top Corner of Truss Member U10_L9W (inch)	0.470	0.539	0.560	0.554

Figure A 5.4 compares the load-displacement curves in the Riks step in the four models. The horizontal axis in the graph represents the normalized total load with respect to the estimated total load of the first model. The vertical axis represents the out-of-plane displacement at the top corner of truss member U10_L9W. The figure shows that the predicted maximum total load at instability of the four models was similar.

For the second mixed model, Figure A 5.5 shows the von Mises stress and equivalent plastic strain distributions at the U10W joint under a total load of 24,652 kips after the maximum total load was attained. For the third model, Figure A 5.6 shows the von Mises stress and equivalent plastic strain distributions at the U10W joint under a total load of 24,631 kips prior to the predicted maximum. For the fourth mixed model, Figure A 5.7 shows the von Mises stress and equivalent plastic strain distributions at the U10W joint under the predicted maximum load at instability. The three figures show that significant plastic deformation occurred in the two gusset plates and the maximum von Mises stress occurred in the vicinity of the upper corner rivet in the east gusset plate.

A5.3   Summary: Bridge Deadweight Application Comparison

Four mixed models were analyzed to investigate the effect of changing methods used to apply the deadweight of the bridge. Analyses showed that the predicted maximum load at instability was similar in the four models. When the deck offsets were included in the model change of the decks, the Riks analysis predicted a maximum total load at instability of 24,641 kip. When the deck offsets were excluded from the model change of the decks, the Riks analysis predicted a maximum total load at instability of 24,653 kip. When the bridge deadweight was applied in four

steps and no deck model change was included, the Riks method predicted a maximum total load at instability of 24,631 kip. When the bridge deadweight was applied in two steps and no deck model change was included, the predicted maximum total load at instability was 24,615 kip.
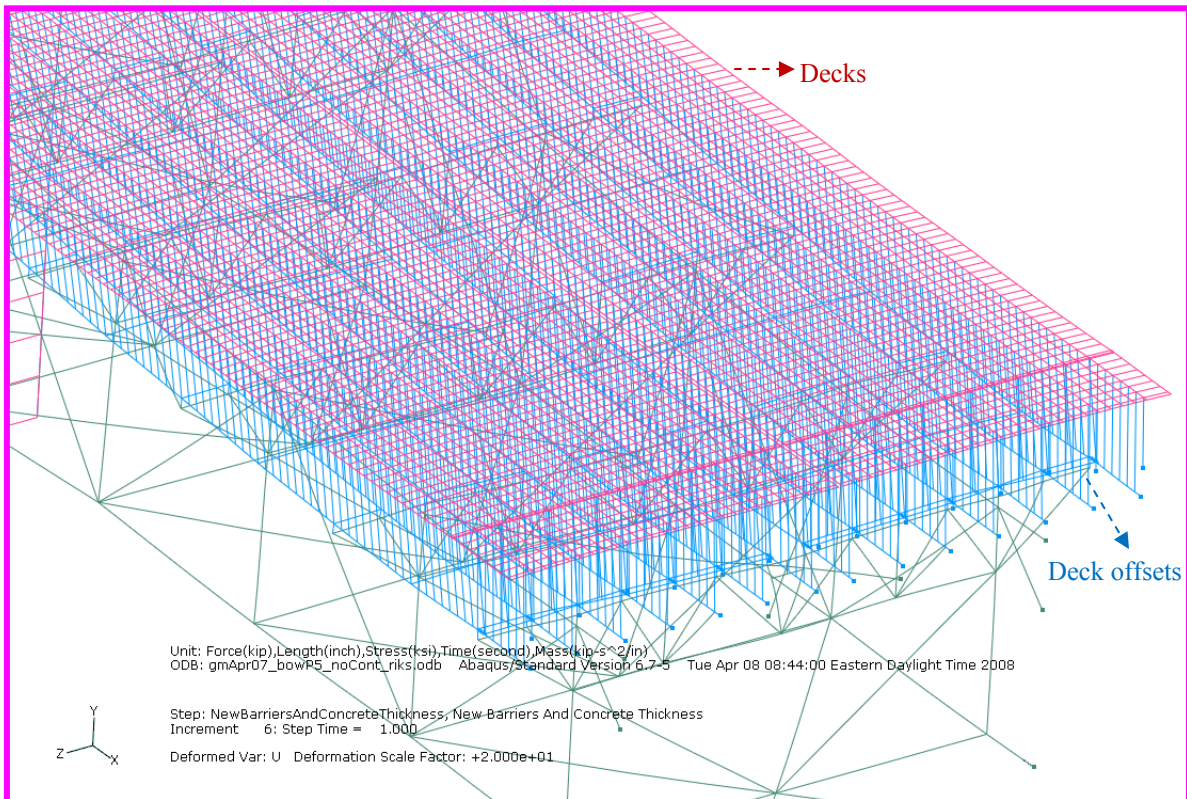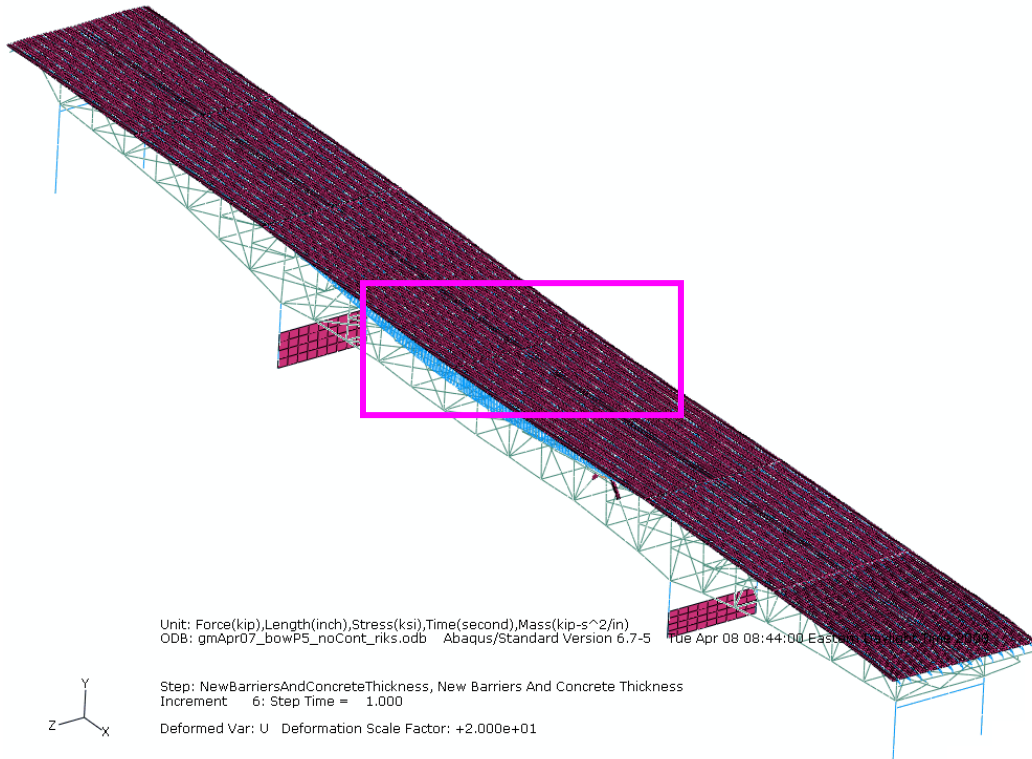
Figure A 5.1: Flat decks and elongated deck offsets under the bridge deadweight when the decks and deck offsets were included in the model change; first mixed model with load condition B (deformation magnified 20x)
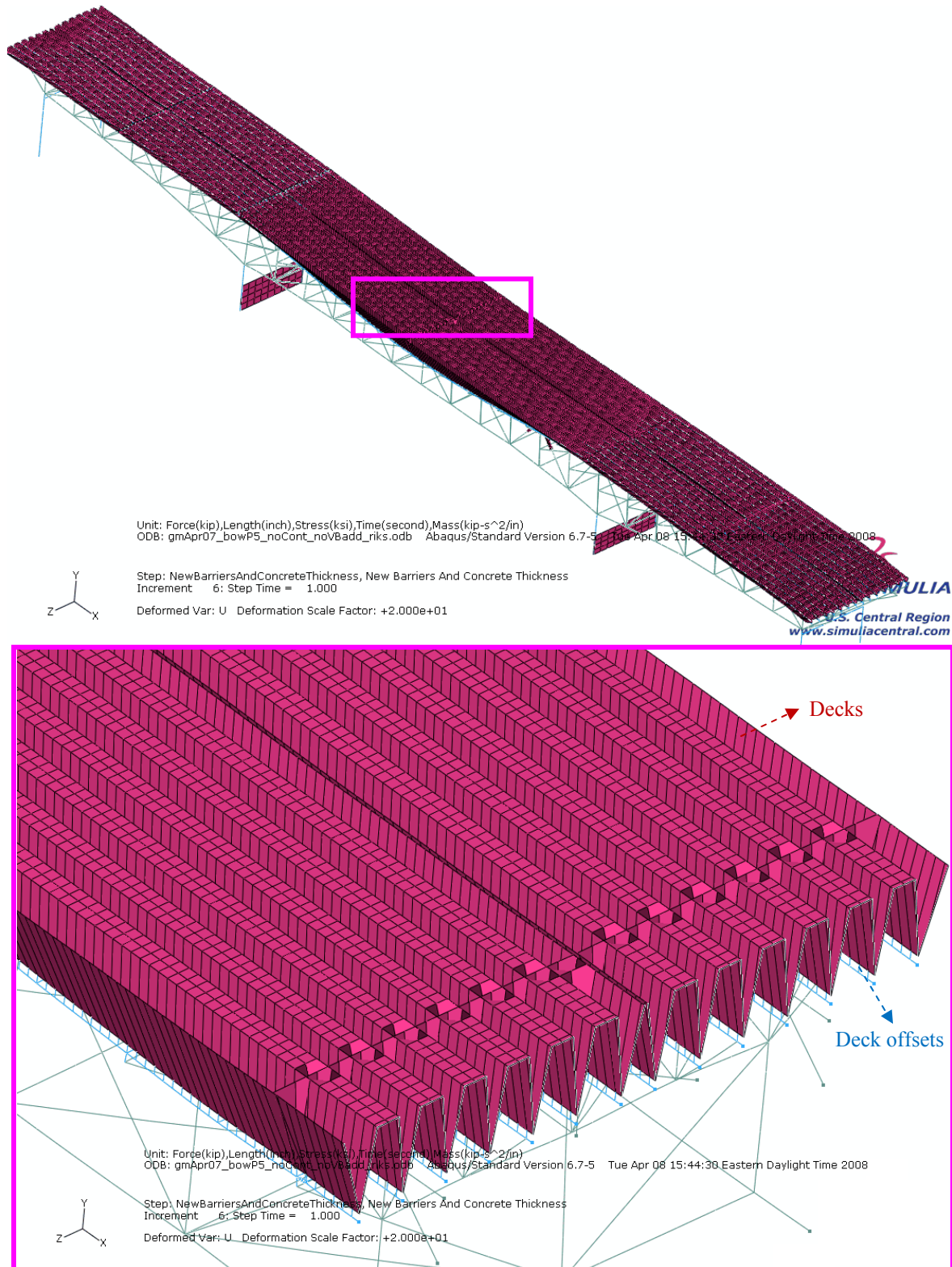
Figure A 5.2: Zig-zag shaped decks under the bridge deadweight when the deck offsets were excluded from the model change of the decks; second mixed model with load condition D (deformation magnified 20x)
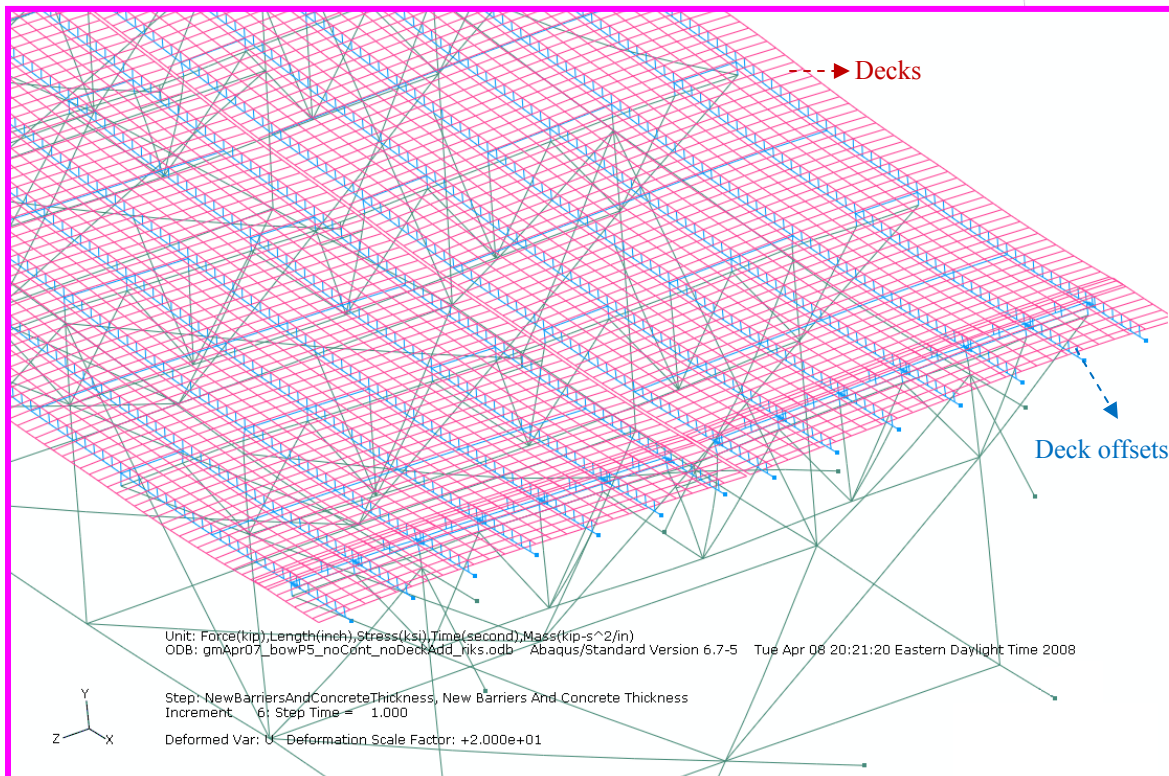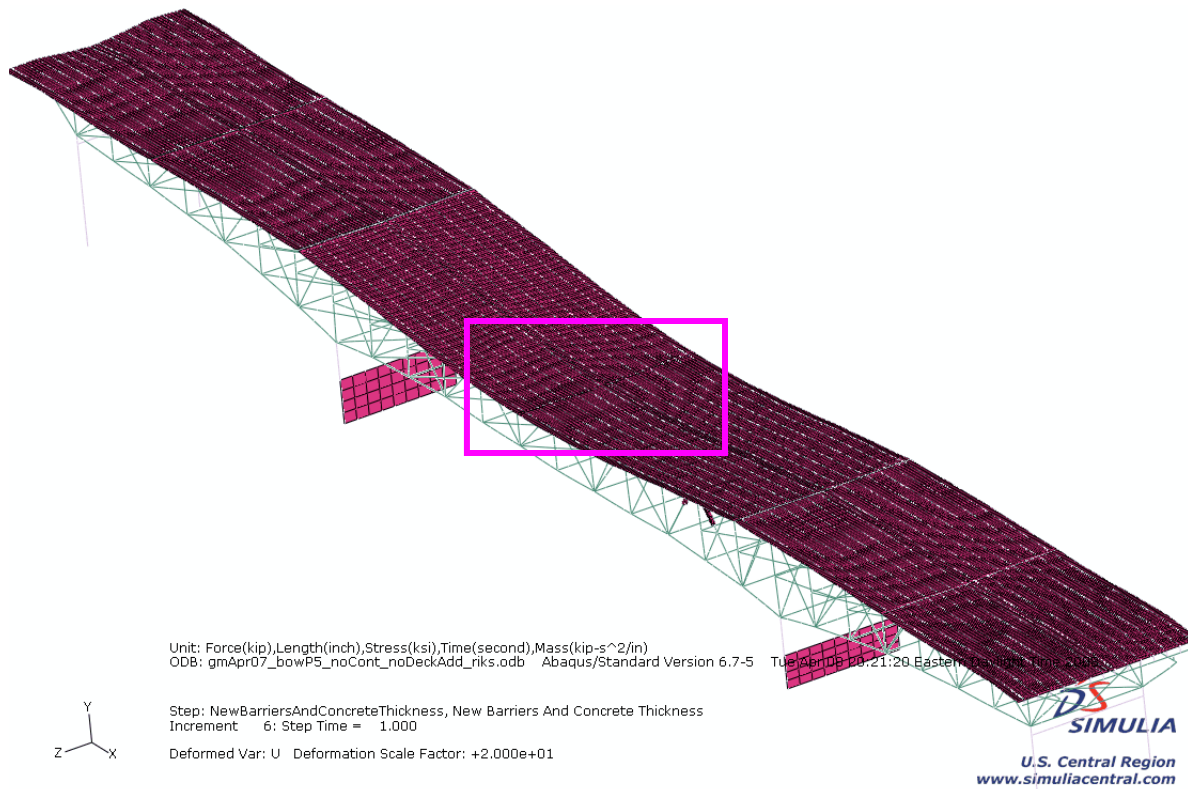
Figure A 5.3: Sagged decks under the bridge deadweight when the decks were included in the model from the beginning of the analysis; third mixed model with load condition E (deformation magnified 20x)
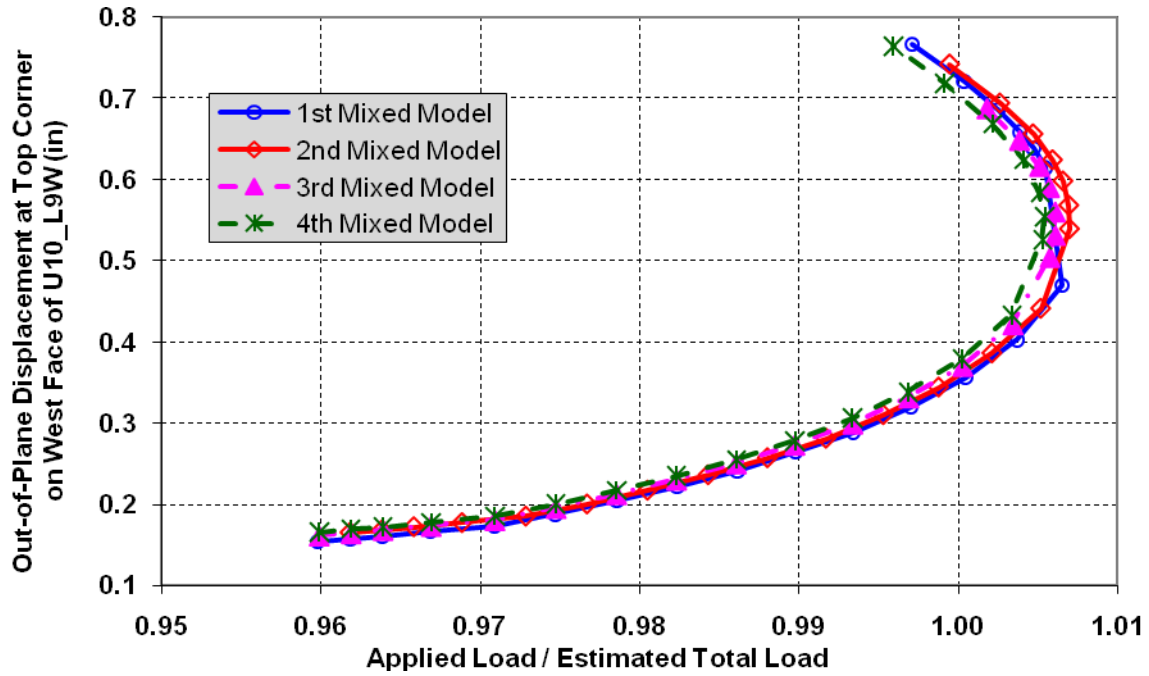
Figure A 5.4: Comparison of normalized total load versus displacement in Riks loading step when U10W local model was embedded for four methods used to apply the deadweight of the bridge
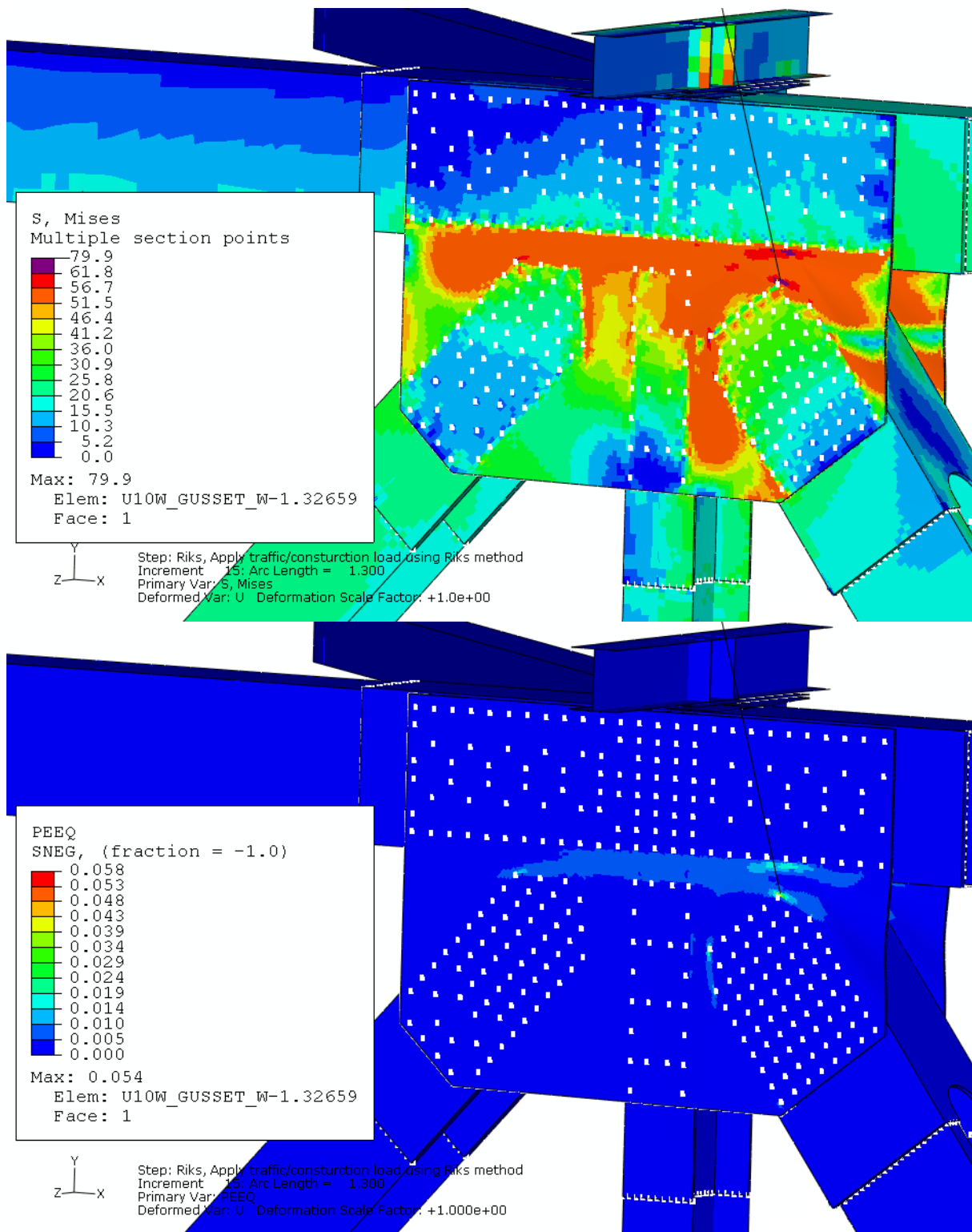
Riks step: Total load of 24,652 kips

Figure A 5.5: Von Mises stress and equivalent plastic strain (PEEQ) distributions at the U10W joint in Riks step in the second mixed model with load condition D
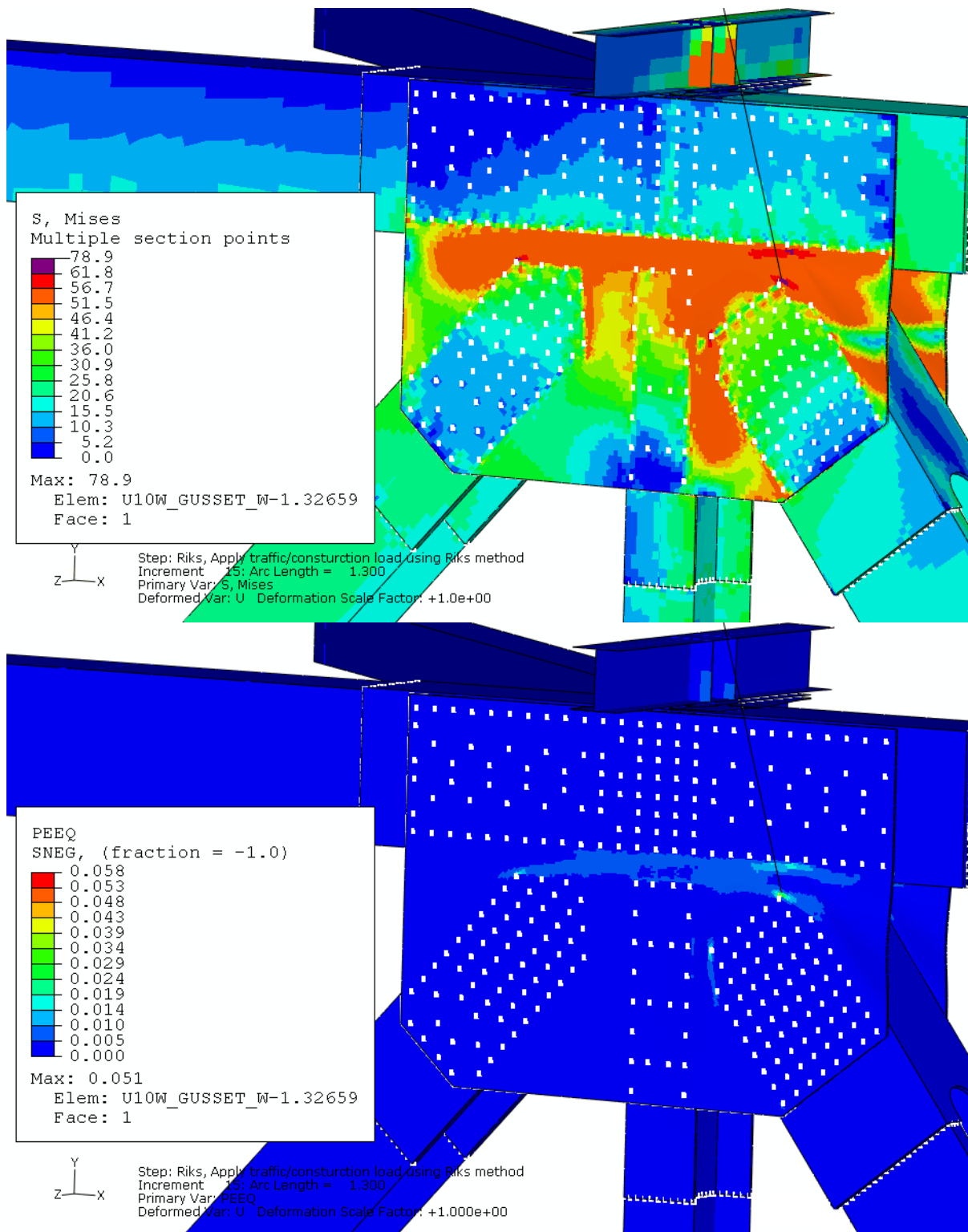
Riks step: Total load of 24,631 kips

Figure A 5.6: Von Mises stress and equivalent plastic strain (PEEQ) distributions at the U10W joint in Riks step in the third mixed model with load condition E
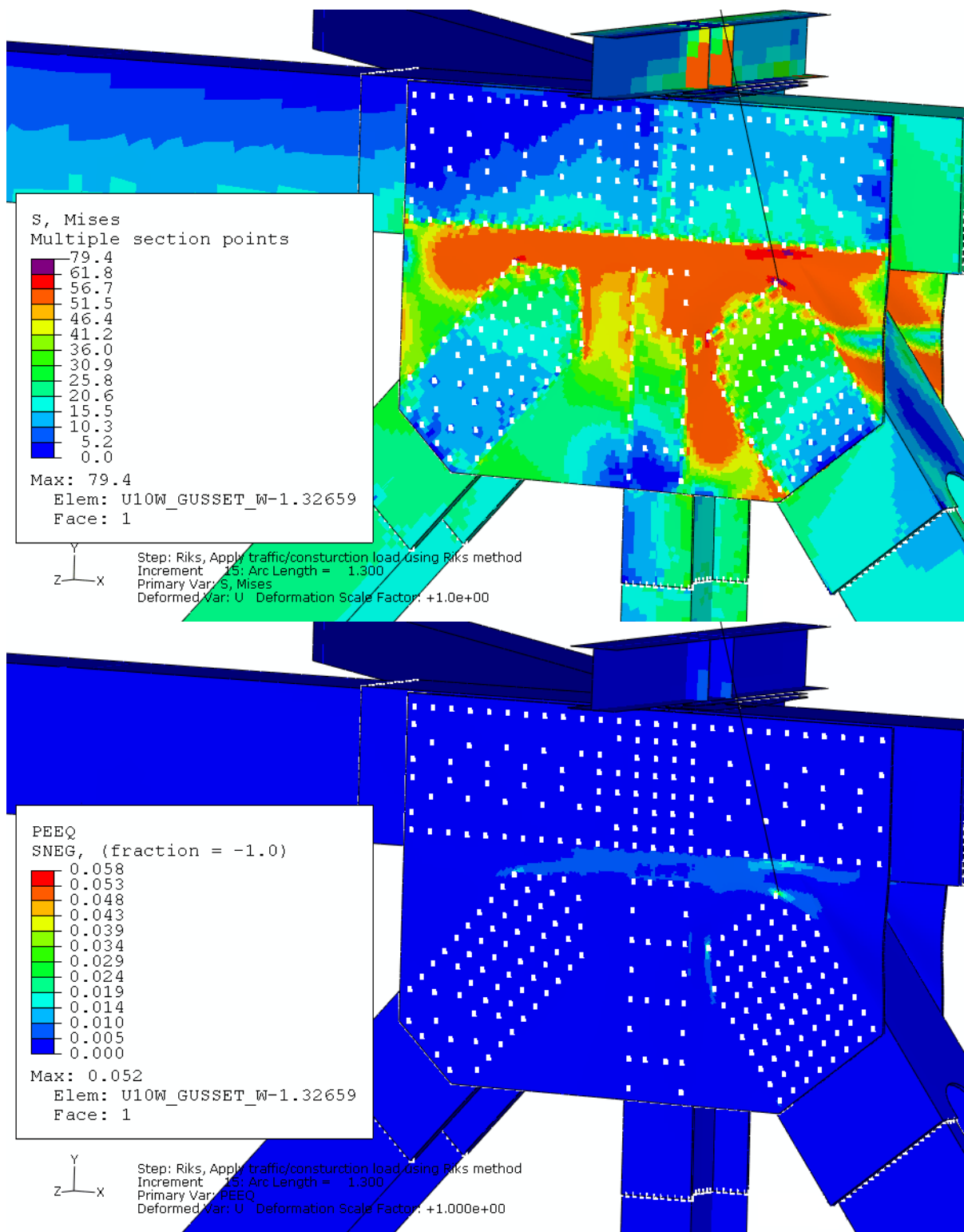
Riks step: Total load of 24,631 kips

Figure A 5.7: Von Mises stress and equivalent plastic strain (PEEQ) distributions at the U10W joint in Riks step in the fourth mixed model with load condition F

A6   Investigation of Gusset Plate Element Type

A6.1   Model Description

Three mixed models were analyzed to investigate the effect of the gusset plate element type in the U10W 3D local model. Each mixed model had a U10W 3D local model embedded into the sixth FHWA structural element bridge model. Load condition A1 was used in the three mixed models. Tie constraints were used to represent all connections related to the lateral brace, the floor truss upper chord section, and the floor truss support. All other connections in the U10W local model were represented with fasteners and contact. An in-plane mesh size of 0.5 inches was typical in the highly stressed region of the gusset plates. Four elements were used through the thickness of the gusset plates.

The three mixed models were identical except for the gusset plate element type, as listed in Table A 6.1. C3D8R elements with enhanced hourglass control approach [11] were used to represent the gusset plates in the first mixed model. The stiffness coefficients in the enhanced hourglass control approach are based on the enhanced assumed strain method. This approach gives more accurate displacement solutions for coarse meshes with linear elastic materials as compared to other hourglass control methods. It also provides increased resistance to hourglassing for nonlinear materials. Although generally beneficial, this may give overly stiff response in problems displaying plastic yielding under bending. The first mixed model was described previously in Section 10 of this report, where the gusset plates bowed along truss member outer edges. C3D8R elements with total stiffness hourglass control [11] were used to represent the gusset plates in the second mixed model. The hourglass stiffness factors in the total stiffness approach depend on the shear modulus for the C3D8R elements. The hourglass stiffness factors are constant for the entire model. A scale factor can be applied to these stiffness factors to increase or decrease the hourglass stiffness. A scale factor of one was used. C3D8I elements were used to represent the gusset plates in the third mixed model. A C3D8I element is an eight-node linear brick element with incompatible modes [11].

Table A 6.1
Mixed Models Used to Investigate Gusset Plate Representation

Local Model Embedded	Element Type of Gusset Plate	Typical Mesh Size (inch)	Loading Condition	FHWA Structural Element Bridge Model
U10W joint with bowed gusset plates	C3D8R with enhanced hourglass control [11]	0.5	A1	6
U10W joint with bowed gusset plates	C3D8R with total stiffness hourglass control [11]	0.5	A1	6
U10W joint with bowed gusset plates	C3D8I	0.5	A1	6

A6.2   Comparison Between Three Gusset Plate Element Types

The Riks method was used to predict the maximum bridge load at instability by proportionally increasing the construction load while maintaining the other loads at their estimated values. When the C3D8R elements with total stiffness hourglass control were used for the gusset plates, the Riks analysis predicted a maximum construction load of 1,052 kips, or 1.82 times the estimated construction load. The total load along the vertical direction was predicted to be 24,956 kips, or 1.019 times the estimated total load. The out-of-plane displacement at the top corner of the diagonal truss member U10_L9W was predicted to be 0.579 inches under the maximum total load. Under a total load of 24,953 kips prior to the predicted maximum, the axial force and bending moment at the lower end of the diagonal truss member U10_L9W were predicted to be -2,609 kips and 1,710 kip-inch. Significant plastic deformation occurred in the two gusset plates under this load, as shown in Figure A 6.1. The maximum von Mises stress was predicted to be 77 ksi in the vicinity of the upper corner rivet in the east gusset plate. The maximum equivalent plastic strain was predicted to be 4.5 percent.

When the C3D8I elements were used for the gusset plates, the Riks analysis diverged due to severe contact overclosures. The load in the Riks step had not decreased prior to the divergence point. At the divergence point, the construction load was predicted to be 1,039 kip, or 1.80 times the estimated construction load. The total load along the vertical direction was predicted to be 24,943 kips, or 1.019 times the estimated total load. The out-of-plane displacement at the top corner of the diagonal truss member U10_L9W was predicted to be 0.519 inches at the divergence point. The axial force and bending moment at the lower end of the diagonal truss member U10_L9W were predicted to be -2,607 kips and 1,638 kip-inch. Large plastic deformation occurred in the two gusset plates, as shown in Figure A 6.2. The maximum von Mises stress was predicted to be 81 ksi in the vicinity of the upper corner rivet in the east gusset plate. The maximum equivalent plastic strain was predicted to be 5.0 percent.

Figure A 6.3 compares the load displacement curves in the Riks step for the three models. The horizontal axis in the graph represents the normalized total load with respect to the estimated total load. The vertical axis represents the out-of-plane displacement at the top corner of the diagonal truss member U10_L9W. The figure shows that the three curves were similar before their maximum loads were reached. Table A 6.2 summarizes the results of interest in the three models. The table shows that the predicted maximum load capacities were similar. However, the model with the C3D8I elements predicted a larger maximum von Mises stress in the gusset plates at the U10W joint.

Table A 6.2
Effect of Gusset Plate Representation on Results of Interest

Gusset Plate Element Types ⇨	C3D8R with enhanced hourglass control	C3D8R with total stiffness hourglass control	C3D8I (prior to load instability)
Predicted Maximum Total Load at Instability (kip)	24,961	24,956	24,943*
Construction Load at Instability (kip)	1,057	1,052	1,039
Out-of-Plane Displacement at Top Corner of U10_L9W (inch)	0.549	0.579	0.519
Axial Force at Lower End of U10_L9W (kip)	-2,611	-2,609	-2,607
Bending Moment at Lower End of U10_L9W (kip-inch)	1,653	1,710	1,638
Maximum von Mises Stress in Gusset Plates at U10W Joint (ksi)	75	77	81

* Total load at the divergence point of the Riks step

A6.3   Summary: Gusset Plate Element Type Investigation

Three mixed models were analyzed to investigate the effect of gusset plate element types. Analyses showed that the predicted maximum load at instability was similar in the three models. When the C3D8R elements with enhanced hourglass control were used for the gusset plates, the Riks analysis predicted a maximum total load at instability of 24,961 kip. When the C3D8R elements with total stiffness hourglass control were used for the gusset plates, the Riks analysis predicted a maximum total load at instability of 24,956 kip. When the C3D8I elements were used for the gusset plates, the Riks analysis diverged at a total load of 24,943 kip.
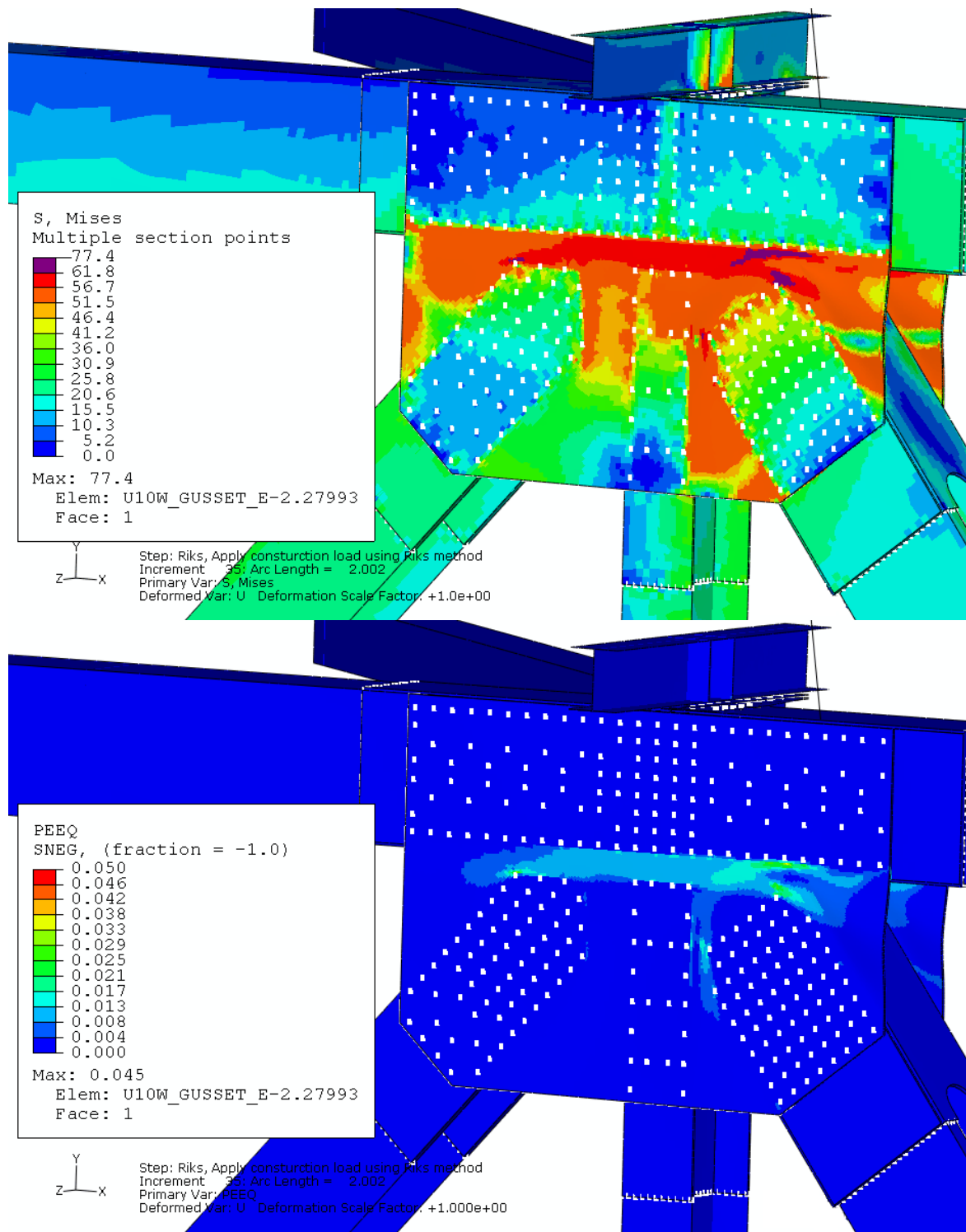
Riks step: Total load of 24,953 kip

Figure A 6.1: Von Mises stress and equivalent plastic strain (PEEQ) distribution at the U10W joint in Riks step when C3D8R elements with total stiffness hourglass control were used for the gusset plates
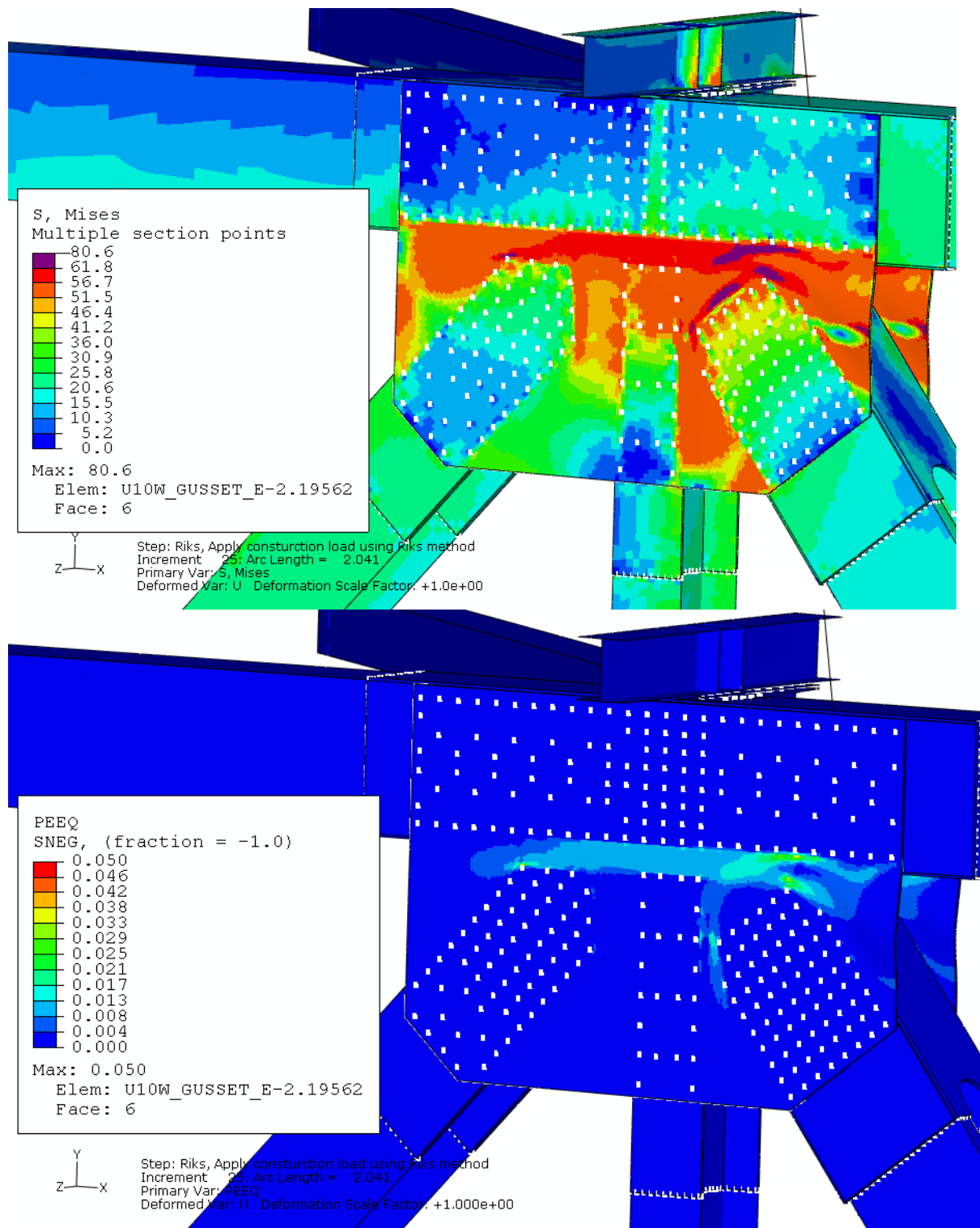
Riks step: Total load of 24,943kip

Figure A 6.2: Von Mises stress and equivalent plastic strain (PEEQ) distribution at the U10W joint in Riks step when C3D8I elements were used for the gusset plates
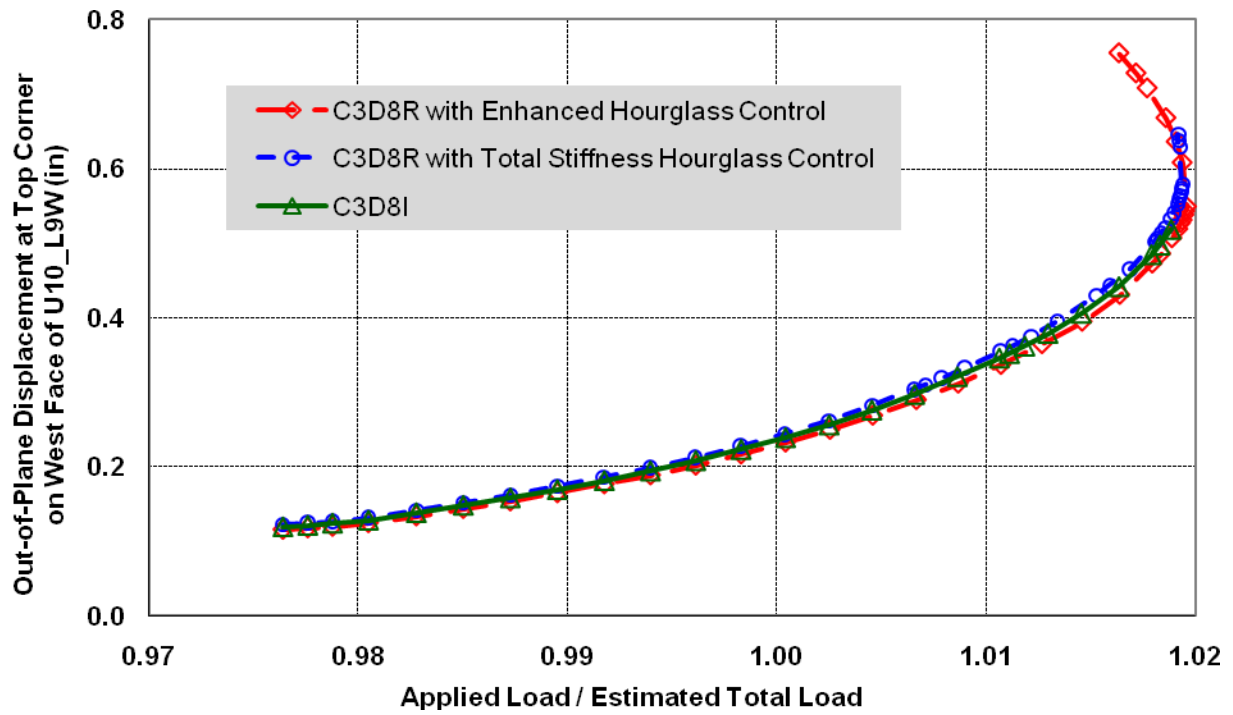
Figure A 6.3: Normalized total load versus displacement in Riks loading step when the U10W local model was embedded; three representations were used for the gusset plates

A7   Investigation of Gusset Plate Through-Thickness Mesh Density

A7.1   Model Description

Nine mixed models were analyzed to investigate the effect of gusset plate through-thickness mesh density in a U10W 3D local model. Each mixed model had a U10W 3D local model embedded into the sixth FHWA structural element bridge model. Loading condition A1 was used in the nine mixed models. Tie constraints were used to represent all connections related to the lateral brace, the floor truss upper chord section, and the floor truss support. All other connections in the U10W local model were represented with fasteners and contact. An in-plane mesh size of 0.5 inches was typical in the highly stressed region of the gusset plates.

The nine mixed models were the same except for the gusset plate representation. Table A 7.1 summarizes the nine models. These models were divided into three groups. The models in each group had the same element type for the gusset plates but had different numbers of elements through the gusset plate thickness.

1. C3D8R elements with enhanced hourglass control were used to represent the gusset plates in the four models in the first group. The number of elements through the gusset plate thickness in the four models was 4, 6, 8, and 12, respectively.

2. C3D8R elements with total stiffness hourglass control were used to represent the gusset plates in the three models in the second group. The number of elements through the gusset plate thickness in the three models was 4, 8, and 12, respectively.

3. C3D8I elements were used to represent the gusset plates in the two models of the third group. The number of elements through the gusset plate thickness in the two models was 4 and 8, respectively.

The first mixed model in the first group was described previously in Section 10 of this report, where the gusset plates bowed along truss member outer edges. The second mixed model in the first group was described previously in Section 4 of this report. The first mixed model in the second group and the first mixed model in the third group were described previously in Section A6 of this report.

Table A 7.1

Mixed Models Used to Investigate Element Number Through Gusset Plate Thickness

Local Model Embedded	Gusset Plate Element Type	Number of Elements Through Gusset Plate Thickness	Typical Mesh Size (inch)	Loading Condition	FHWA Structural Element Bridge Model
U10W joint with bowed gusset plates	C3D8R with enhanced hourglass control [11]	4	0.5	A1	6
		6			
		8			
		12			
U10W joint with bowed gusset plates	C3D8R with total stiffness hourglass control [11]	4	0.5	A1	6
		8			
		12			
U10W joint with bowed gusset plates	C3D8I [11]	4	0.5	A1	6
		8			

A7.2   Comparison Between Nine Gusset Plate Representations

The Riks method was used to predict the maximum bridge load at instability by proportionally increasing the construction load while maintaining other loads at their estimated values. Table A 7.2 summarizes the results of interest in the nine models. When the gusset plates were represented with C3D8R elements with enhanced hourglass control or represented with C3D8I elements, the effect of the gusset plate through-thickness mesh density on the predicted maximum load capacities and on the predicted maximum von Mises stress was negligible. However, when the gusset plates were represented with C3D8R elements with total stiffness hourglass control, the maximum load capacities were predicted to increase with increasing element number through gusset plate thickness.

When the number of elements through gusset plate thickness was 4, the predicted maximum load capacities were similar between the three element types, as described previously in Section A6 of this report. Also, the models with C3D8I elements predicted a larger maximum von Mises stress in the gusset plates at the U10W joint than the models with C3D8R elements.

Table A 7.2
Effect of Gusset Plate Through-Thickness Mesh Density on Results of Interest

Gusset Plate Element Type	Number of Elements Through Gusset Plate Thickness	Predicted Maximum Total Load at Instability (kip)	Construction Load at Instability (kip)	Maximum von Mises Stress in Gusset Plates at U10W Joint (ksi)
C3D8R with enhanced hourglass control	4	24,961	1,057	75
	6	24,973	1,069	77
	8	24,957*	1,053	75
	12	24,965	1,061	77
C3D8R with total stiffness hourglass control	4	24,956	1,052	77
	8	$25,272^{\#}$	1,368	84
	12	25,639	1,735	85
C3D8I	4	24,943*	1,039	81
	8	24,960	1,056	83

*: Load at divergence point of the Riks step
$^{\#}$: Load at termination point of the Riks step

A7.3 Summary: Gusset Plate Through-Thickness Mesh Density Investigation

Nine mixed models in three groups were analyzed to investigate the effect of gusset plate through-thickness mesh density. The only difference in the models in each group was the element number through gusset plate thickness. Four models in the first group had gusset plates represented with C3D8R elements with enhanced hourglass control. Three models in the second group had gusset plates represented with C3D8R elements with total stiffness hourglass control. Two models in the third group had gusset plates represented with C3D8I elements.

Analyses indicated that the effect of gusset plate through-thickness mesh density on the predicted maximum load capacities and on the predicted maximum von Mises stress was negligible for the six models in the first and third groups. However, analyses indicated that the maximum load capacities were predicted to increase with increasing element number through gusset plate thickness for the three models in the second group, which used the total stiffness hourglass control.

A8 Investigation of Divergence and Instability

A8.1 Model Description

Analyses were performed to investigate the relationship between the divergence point in a regular static analysis and the maximum load point in a Riks analysis. The two mixed models listed in Table A 8.1 were investigated. Each mixed model had a U10W 3D local model embedded into the sixth FHWA structural element bridge model. The first mixed model was described previously in Section 4 of this report, where load condition A1 was used. The two models were the same except for the methods used to apply the construction load. In the first mixed model, a Riks analysis was used to predict the maximum construction load at instability by proportionally increasing the construction load while maintaining other loads at their estimated values. In the second mixed model, a regular static analysis was used to proportionally increase the construction load while maintaining other loads at their estimated values.

Table A 8.1
Mixed Models Used to Investigate Divergence and Instability

Local Model Embedded	Method Used to Apply Construction Load	Typical Mesh Size (inch)	Loading Condition	FHWA Structural Element Bridge Model
U10W joint with bowed gusset plates	Riks	0.5	A1	6
U10W joint with bowed gusset plates	Regular static	0.5	A1	6

A8.2 Comparison Between Riks Analysis and Regular Static Analysis

The Riks analysis predicted a maximum construction load of 1,069 kips, or 1.85 times the estimated construction load. The total load along the vertical direction was predicted to be 24,973 kips, or 1.020 times the estimated total load. The out-of-plane displacement at the top corner of the diagonal truss member U10_L9W was predicted to be 0.572 inches under the maximum total load. The axial force and bending moment at the lower end of the diagonal truss member U10_L9W were predicted to be -2,618 kips and 1,738 kip-inch. Significant plastic deformation occurred in the two gusset plates when subjected to a load near the predicted maximum, as shown in Figure 4.5 and Figure 4.6. The maximum von Mises stress was predicted to be 77 ksi in the vicinity of the upper corner rivet in the east gusset plate. The maximum equivalent plastic strain was predicted to be 4.5 percent.

When the regular static analysis was used to apply the construction load, the analysis diverged at a construction load of 1,061 kips, or 1.84 times the estimated construction load. The total load at the divergence point was 24,965 kips, or 1.020 times the estimated total load. The out-of-plane displacement at the top corner of the diagonal truss member U10_L9W was predicted to be 0.576 inches at the divergence point. The axial force and bending moment at the lower end of the diagonal truss member U10_L9W were predicted to be -2,614 kips and 1,756 kip-inch. Significant plastic deformation occurred in the two gusset plates at the divergence point, as shown in Figure A 8.1 and Figure A 8.2. The maximum von Mises stress was predicted to be 78

ksi in the vicinity of the upper corner rivet in the east gusset plate. The maximum equivalent plastic strain was predicted to be 4.7 percent.

Figure A 8.3 compares the predicted load-displacement curves for two analyses as the construction load was increased. The red curve in the figure is from the Riks analysis and the blue curve is from the regular static analysis. This figure demonstrates that the predicted load displacement curves of the two analyses were almost identical until the regular static analysis diverged. The total load at the divergence point in the regular static analysis was almost identical to the maximum total load predicted by the Riks analysis. Figure 4.5, Figure 4.6, Figure A 8.1, and Figure A 8.2 show that the von Mises stress and equivalent plastic strain distributions at the U10W joint were similar for the two analyses. Table A 8.2 summarizes the results of interest at the divergence point in the regular static analysis and at the maximum load point in the Riks analysis. The stress, force, moment and displacements were almost identical between the two analyses.

Table A 8.2
Comparison of Results at Divergence Point and Maximum Load Point

	Riks analysis	Regular static analysis
Total Load at Divergence Point or at Maximum Load Point (kip)	24,973	24,965
Construction Load at Divergence Point or at Maximum Load Point (kip)	1,069	1,061
Maximum von Mises Stress in Gusset Plates at U10W Joint (ksi)	77	78
Axial Force at Lower End of U10_L9W (kip)	-2,618	-2,614
Bending Moment at Lower End of U10_L9W (kip-inch)	1,738	1,756
Out-of-Plane Displacement at Top Corner of U10_L9W (inch)	0.572	0.576

A8.3   Summary: Divergence and Instability Investigation

Two mixed models, one using a Riks analysis to apply a construction load and the other using a regular static analysis to apply a construction load, were analyzed to investigate the relationship between the divergence point in a regular static analysis and the maximum load point in a Riks analysis. Load condition A1 was used. Analyses showed that the total load at the divergence point was almost equal to the maximum load at instability predicted by the Riks analysis. The regular static analysis diverged at a total load of 24,965 kips, and the Riks analysis predicted a maximum total load of 24,973 kips.
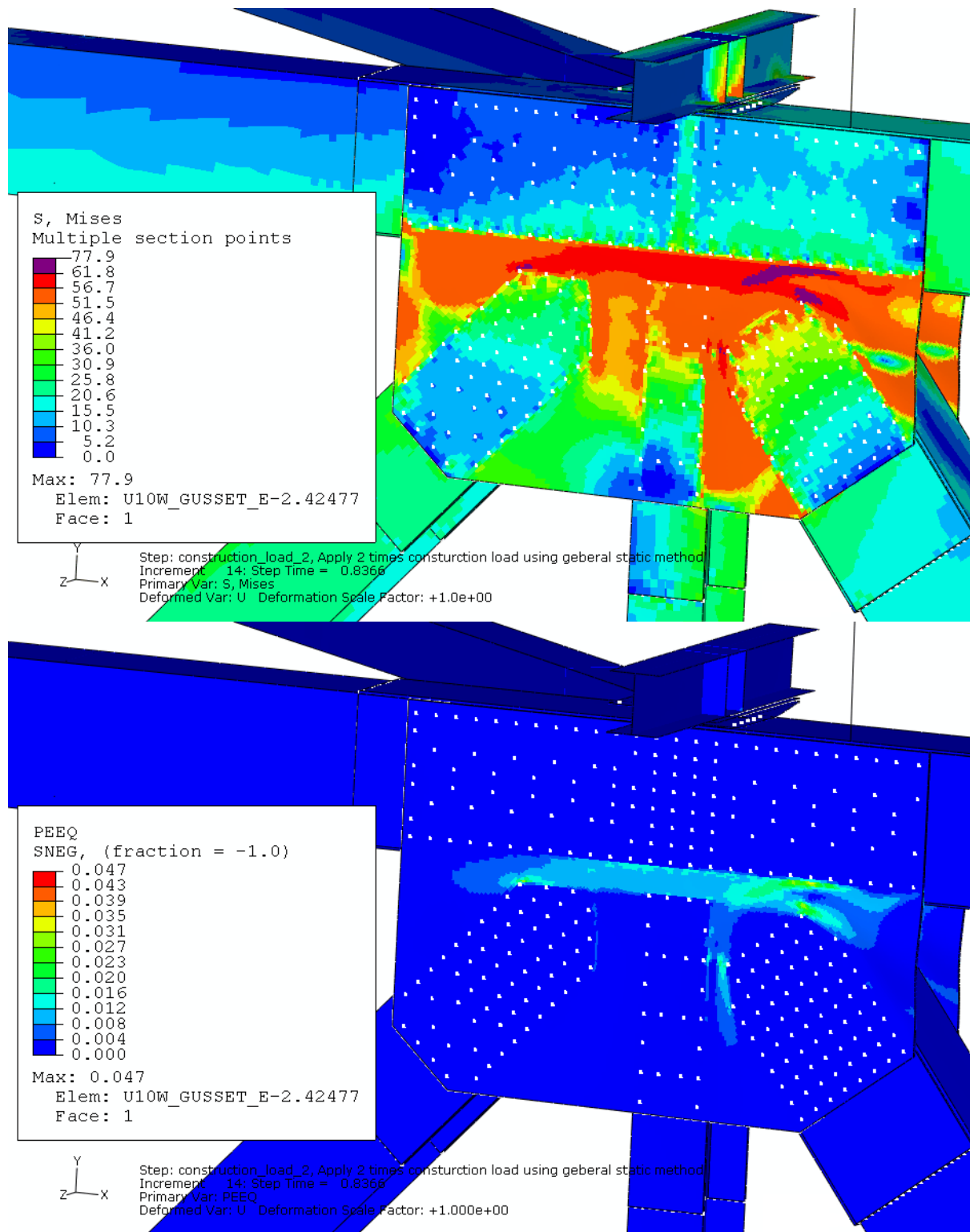
Regular static step: Total load of 24,965 kips

Figure A 8.1: Von Mises stress and equivalent plastic strain (PEEQ) distributions at the U10W joint in regular static analysis
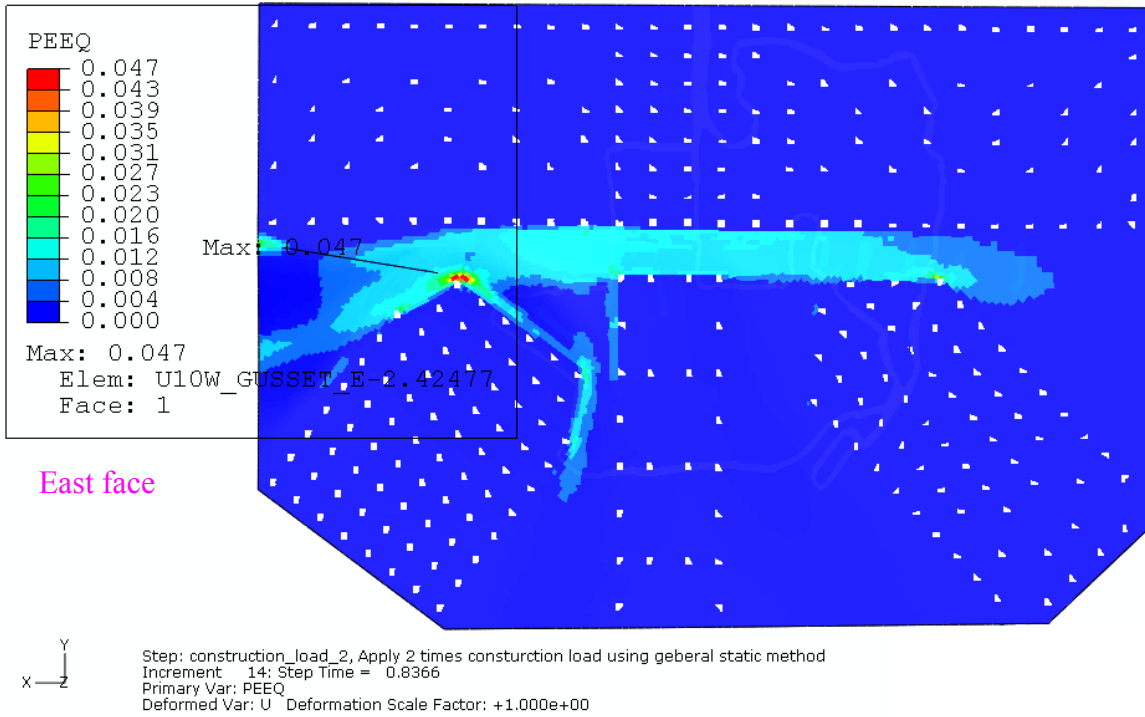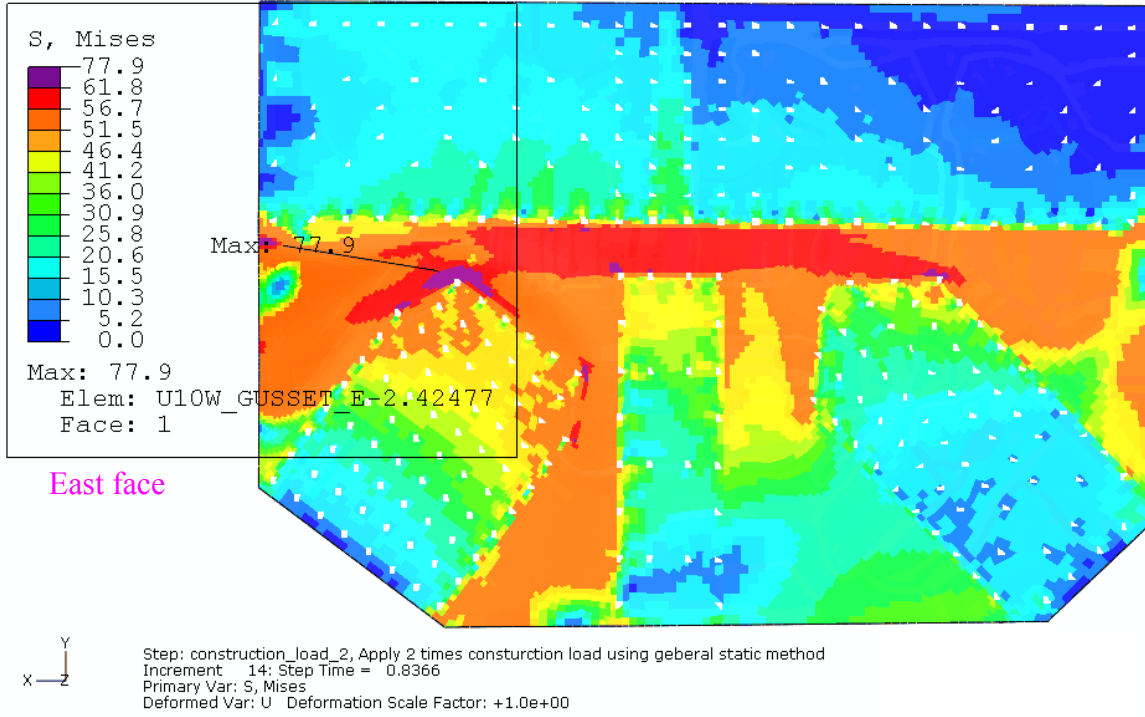
Regular static step: Total load of 24,965 kips

Figure A 8.2: Von Mises stress and equivalent plastic strain (PEEQ) distributions in the east gusset plate at the U10W joint in regular static analysis
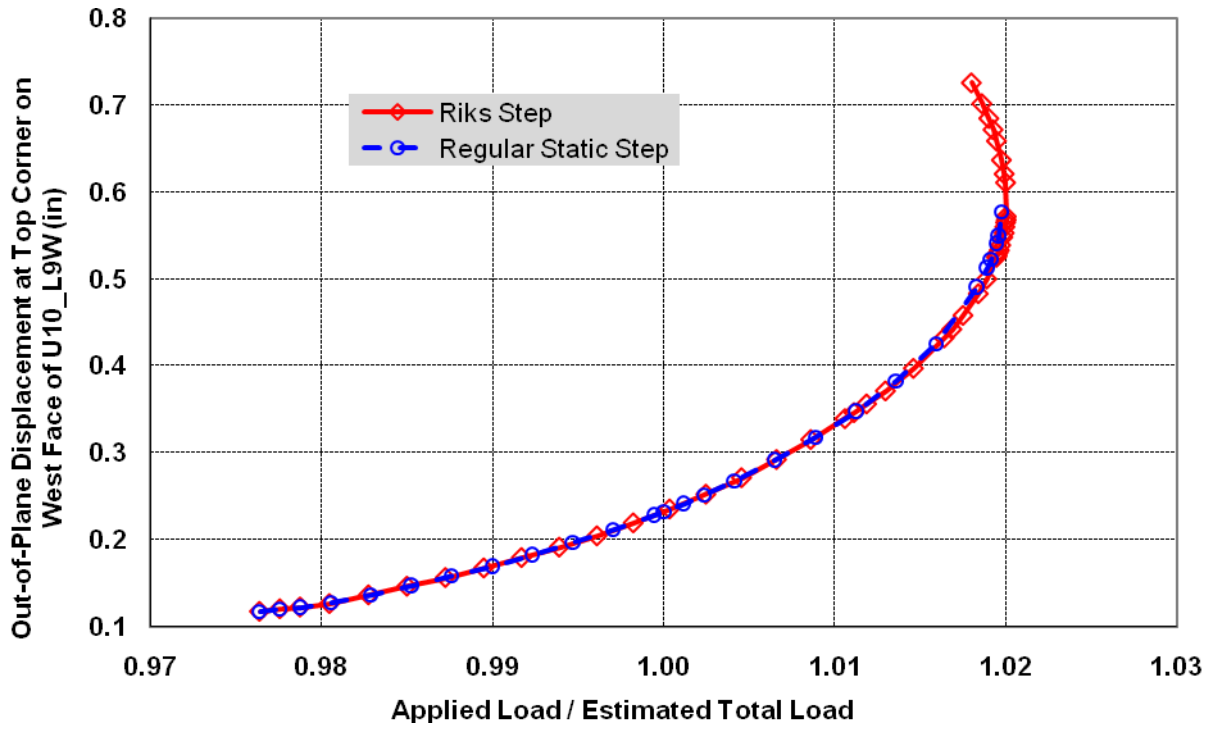
Figure A 8.3: Normalized total load versus displacement as construction load was increased in Riks analysis and regular static analysis

12 References

1. Ocel, J.M., and Wright, W.J., "Finite element Modeling of I-35W Bridge Collapse Final Report," Federal Highway Administration Turner-Fairbank Highway Research Center Report, October 2008.

2. "Structural and Local Failure Study of Gusset Plate in Minneapolis Bridge Collapse," Modeling Group Contractor Interim Report, National Transportation Safety Board, Washington, D.C., February 14, 2008.

3. Materials Laboratory Factual Report 08-096, "Laser scans of gusset plates from nodes L11E and L11W to assess corrosion," National Transportation Safety Board, Washington, D.C., October 24, 2008.

4. Structural Investigation Group Chairman Factual Report 08-015, National Transportation Safety Board, Washington, D.C., March 5, 2008.

5. Modeling Group Study Report 07-115, "Loads on the bridge at the time of the accident," National Transportation Safety Board, Washington, D.C., November 8, 2007.

6. Beshah, F., Wright, W.J., and Graybeal, B., "Mechanical Property Test Report (I-35W over the Mississippi River)," Federal Highway Administration Turner-Fairbank Highway Research Center Report, October 15, 2008.

7. Hertzberg, R.W., *Deformation and Fracture Mechanics of Engineering Materials*, Third Edition, John Wiley and Sons, New York, 1989.

8. Materials Laboratory Factual Report 08-006, "Rivet and bolt hardness," National Transportation Safety Board, Washington, D.C., January 8, 2008.

9. Materials Laboratory Factual Report 08-053, "Gusset plate hardness," National Transportation Safety Board, Washington, D.C., May 5, 2008.

10. "Gusset Plate Photographs – Measurement Study Report," National Transportation Safety Board, Vehicle Recorder Division, Washington, D.C., July 16, 2008.

11. Dassault Systemes Simulia Corp., "Abaqus Version 6.7 Documentation", June, 2007.

13 List of Figures